

March, 2014

# Control of Macrophage Homeostasis


A thesis presented for the degree of Doctor of Philosophy

**Luke Cynlais Davies**




## **DECLARATION**

This work has not been submitted in substance for any other degree or award at this or any other university or place of learning, nor is being submitted concurrently in candidature for any degree or other award.

Signed .......... (candidate)     Date: **24/03/2014**


## **STATEMENT 1**

This thesis is being submitted in partial fulfilment of the requirements for the degree of PhD.

Signed .......... (candidate)     Date: **24/03/2014**


## **STATEMENT 2**

This thesis is the result of my own independent work/investigation, except where otherwise stated. Other sources are acknowledged by explicit references. The views expressed are my own.

Signed .......... (candidate)     Date: **24/03/2014**


## **STATEMENT 3**

I hereby give consent for my thesis, if accepted, to be available for photocopying and for inter-library loan, and for the title and summary to be made available to outside organisations.

Signed .......... (candidate)     Date: **24/03/2014**

## **STATEMENT 4: PREVIOUSLY APPROVED BAR ON ACCESS**

I hereby give consent for my thesis, if accepted, to be available for photocopying and for inter-library loans after expiry of a bar on access previously approved by the Academic Standards & Quality Committee.

Signed .......... (candidate)     Date: **24/03/2014**

## Acknowledgements

First and foremost, I would like to thank Phil Taylor for his fantastic supervision, excellent support, ongoing contribution to and original conception of this thesis. I would also like to express my gratitude to Marcela Rosas whose initial work helped construct this project; and for her additional supporting work, which is critical for the overall message of this thesis. I would also like to acknowledge the rest of the Taylor group, particularly Nicola Dierkes and Dina Fathalla for their technical support, and Bashar Kharfan (Masters student) for his aid in production of lentiviral vectors.

Of course, I would not have achieved anything in this thesis without the constant support of my friends, family and Xbox; which played no small part in the maintenance of my sanity. Six Nations weekends (especially Super Saturday) and excellently hosted events by Christopher Rice and Helen Brook helped make the time during my PhD enjoyable. The quantity and quality of drinking games constructed during my PhD far outstripped any experiences in undergrad. And, in particular, I enjoyed the weeks 'wasted' on the design of an intriguingly complex game of thrones board game, that nearly resulted in murders and/ or suicides.

Additionally, I would like to thank beer in all its splendour. Principally, I would like to express my appreciation to the Banterstreet brewery, for the expertly crafted real ales, which were full of exceptional character. The long hours brewing and designing new beer labels were one of the escapes from a macrophage driven world, and I thank Christopher Rice and Matthew White for all those steamy evenings... basking in the glory of the boiling wort in the Banterstreet kitchens.

I would like to express my appreciation to the Cardiff Blues rugby team for having a few terrible seasons in a row, which really allowed me to concentrate on my work. I would also like to thank Tristan Ardley and Matthew White for keeping me humble, by repeatedly destroying my soul in countless squash matches. The numerous curses used in squash, were critical for relieving the constant pressures of postgraduate research.

Schließlich, möchte ich mich herzlich bedanken bei meine Freundin Anja Bloom, vor allem für ihre tagtägliche Unterstützung und ihrem Beistand. Sie hat mich zu einem besseren Mensch und Wissenschaftler gemacht. Danke schön mein Liebling.

# Contents

<b>Summary</b> .....	12
<b>Abbreviations</b> .....	13
<b>Chapter 1 – General Introduction</b> .....	17
1.1 – Macrophages: discovery, origins and heterogeneity .....	18
1.1.1 – Discovery of macrophages .....	18
1.1.2 – Tissue resident MØ heterogeneity .....	18
1.1.3 – Origins of ResMØs .....	21
1.2 – MØs in inflammation.....	24
1.2.1 – The peritoneal acute immune response .....	24
1.2.2 – Role of MØs in acute inflammation.....	28
1.3 – Work leading up to this thesis.....	31
1.3.1 – Microarray analysis of MØ populations .....	31
1.3.2 – The GATA family of transcription factors .....	34
1.4 – General hypothesis.....	35
1.5 – Aims.....	35
<b>Chapter 2 – Methods</b> .....	36
2.1 – Notes .....	37
2.2 – Health and safety .....	37
2.3 – Antibodies and dyes .....	38
2.4 – Cell counting.....	40
2.4.1 – Haemocytometer.....	40
2.4.2 – Millipore Muse .....	40
2.4.3 – Haemacolor staining.....	41
2.5 – Cell Culture .....	42
2.5.1 – General cell culture .....	42

2.5.2 – Culture of primary peritoneal cells.....	43
2.5.3 – Culture of bone marrow (BM) MØs .....	43
2.5.4 – Culture of 293-T cells.....	44
2.5.5 – Culture of MØ precursor cells .....	44
2.5.6 – Culture of Jurkat-Eb.1 cells.....	45
2.6 – Animal work .....	46
2.6.1 – Animals used in this study .....	46
2.6.2 – Intra-peritoneal (i.p.) injection.....	46
2.6.3 – Sub-cutaneous (s.c.) injection .....	47
2.6.4 – Genotyping .....	47
2.6.5 – Peritoneal lavage .....	48
2.6.6 – Pleural lavage .....	49
2.6.7 – Adoptive transfer.....	50
2.6.8 – Femur extraction .....	50
2.7 – Flow Cytometry .....	52
2.7.1 – Total cell staining.....	52
2.7.2 – Use of nuclear isolation media (NIM)-DAPI for flow cytometry .....	53
2.7.3 – Flow cytometric cell sorting .....	53
2.8 – Lentiviral vector cloning .....	55
2.8.1 – Primer design.....	55
2.8.2 – Restriction endonuclease digestions.....	57
2.8.3 – Agarose gel electrophoresis (AGE) .....	57
2.8.4 – Gel extraction and DNA purification .....	58
2.8.5 – Polymerase chain reaction (PCR) .....	58
2.8.6 – In-fusion cloning .....	59
2.8.7 – <i>E. coli</i> transformation via heat shock .....	60
2.8.8 – <i>E. coli</i> culture .....	61

2.8.9 – Plasmid DNA extraction.....	61
2.8.10 – DNA sequencing and validation .....	62
2.9 – Viral particle production .....	63
2.9.1 – Transfection.....	63
2.9.2 – Viral particle concentration.....	63
2.9.3 – Multiplicity of infection (MOI) calculations.....	64
2.9.4 – Use of lentiviral particles in culture.....	65
2.10 – Real-time PCR.....	66
2.10.1 – RNA extraction.....	66
2.10.2 – Reverse transcription .....	66
2.10.3 – Primer design.....	66
2.10.4 – Real-time PCR .....	67
2.11 – Immunocytochemistry .....	71
2.11.1 – Cytospins, fixation and permeabilisation .....	71
2.11.2 – Staining .....	71
2.11.3 – Slide mounting.....	72
2.11.4 – Fluorescence microscopy .....	72
2.11.5 – Image processing.....	72
2.12 – Statistics .....	72
<b>Chapter 3 - ResMØs self-renew by <i>in situ</i> proliferation.</b> .....	<b>73</b>
3.1 – Introduction.....	74
3.1.1 – Zymosan peritonitis .....	74
3.1.2 –Proliferation.....	75
3.1.3 – Hypothesis .....	76
3.1.4 – Aims .....	76
3.2 – Results .....	77
3.2.1 – Doublet discrimination in complex polychromatic flow cytometry.....	77

3.2.2 – Definition of ResMØs in complex inflammatory environments.....	78
3.2.3 – Identification of non cell cycle-associated DNA content and ResMØs in cell cycle.....	80
3.2.4 – ResMØs expand by proliferation during the neonatal period .....	83
3.2.5 – ResMØs recover from acute inflammation by proliferation.....	86
3.2.6 – ResMØs in the naïve tissue survive inflammation and proliferate .....	92
3.2.7 – A significant proportion of ResMØs are generated by proliferation during inflammation .....	96
3.3 – Discussion.....	99
3.3.1 – Flow cytometric analysis of MØ populations .....	99
3.3.2 – Nuclear profile of ResMØs .....	100
3.3.3 – ResMØs proliferate in homeostasis and neonatal growth .....	101
3.3.4 – ResMØs proliferate during acute inflammation to restore depleted numbers .....	102
3.3.5 – ResMØs renew <i>in situ</i> , without the need for blood monocyte precursors ..	102
3.3.6 – Conclusion .....	103
<b>Chapter 4 – InfMØs proliferate <i>in situ</i> during inflammation.....</b>	<b>104</b>
4.1 – Introduction.....	105
4.1.1 – Ly-6B <sup>+</sup> InMØ persistence .....	105
4.1.2 – Prospect of Ly-6B <sup>+</sup> InfMØ proliferation.....	107
4.1.3 – Hypothesis .....	109
4.1.4 – Aims .....	109
4.2 – Results .....	110
4.2.1 – Definition of Ly-6B <sup>+</sup> InfMØs in complex inflammatory environments.....	110
4.2.2 – Ly-6B <sup>+</sup> InfMØs proliferate during the resolution of zymosan induced peritonitis .....	111
4.2.3 – Proliferation of Ly-6B <sup>+</sup> InfMØs is not restricted to zymosan peritonitis.....	114



4.2.4 – Both Ly-6B <sup>+</sup> and Ly-6B <sup>-</sup> InfMØs are derived from the bone marrow.....	117
4.2.5 – M-CSF is required but not sufficient for substantial ResMØ proliferation ...	120
4.2.6 – IL-4 is not essential for MØ proliferation during acute inflammation .....	127
4.3 – Discussion.....	131
4.3.1 – Ly-6B <sup>+</sup> InfMØs .....	131
4.3.2 – Ly-6B <sup>+</sup> InfMØs proliferate during inflammation.....	132
4.3.3 – Ly-6B <sup>+</sup> InfMØ and ResMØ proliferation is a general phenomenon in inflammation .....	132
4.3.4 – Ly-6B <sup>+</sup> InfMØs are bone marrow-derived .....	133
4.3.5 – M-CSF dependency of MØs .....	133
4.3.6 – MØ proliferation is not dependent upon IL-4 .....	136
4.3.7 – Conclusion .....	137
<b>Chapter 5 – Lentiviral modification of MØ gene expression .....</b>	<b>138</b>
5.1 – Introduction.....	139
5.1.1 – Lentiviral vectors .....	139
5.1.2 – RNA interference .....	140
5.1.3 – Markers used to identify infected cells .....	140
5.1.4 – Hypothesis .....	141
5.1.5 – Aims .....	141
5.2 – Results .....	142
5.2.1 – Lentiviral titre calculations <i>in vitro</i> .....	142
5.2.2 – Lentiviral infection of BMMØs and ResMØs <i>in vitro</i> .....	143
5.2.3 – Specific lentiviral infection of ResMØs <i>in vivo</i> .....	145
5.2.4 – Lentiviral knockdown of target gene expression in ResMØs <i>in vivo</i> .....	146
5.2.5 – Validation of a lentiviral expression vector .....	147
5.2.6 – Lentiviral vectors constructed for this thesis .....	148
5.2.7 – Preferential inflammatory loss of infected ResMØs <i>in vivo</i> .....	149

5.3 – Discussion .....	153
5.3.1 – Viral titre .....	153
5.3.2 – Selective infection of ResMØs .....	154
5.3.3 – Immune rejection of infected ResMØs .....	154
5.3.4 – Conclusion .....	155
<b>Chapter 6 – Gata6 controls ResMØ renewal .....</b>	<b>156</b>
6.1 – Introduction.....	157
6.1.1 – Pleural ResMØs.....	157
6.1.2 – Hypothesis .....	158
6.1.3 – Aims .....	158
6.2 – Results .....	159
6.2.1 – Gata6 is expressed selectively by peritoneal ResMØ.....	159
6.2.2 – Knockdown of Gata6 expression results in a reduction in F4/80 protein.....	161
6.2.3 – Knockout of the Gata6 gene causes a marked reduction in the F4/80 phenotype of adult ResMØ .....	162
6.2.4 – Gata6 knockout in the myeloid lineage gives viable ResMØs with an altered F4/80 phenotype .....	164
6.2.5 – Knockout of Gata6 has a cell-intrinsic effect on peritoneal ResMØ proliferation and polyploidy .....	168
6.2.6 – Knockout of Gata6 has a cell-intrinsic effect on pleural ResMØ proliferation, polyploidy and phenotype.....	171
6.2.7 – Absence of Gata6 results in a reduced ability of ResMØs to recover after inflammation by proliferation .....	174
6.2.8 – Myeloid Gata6 deficiency is associated with delayed clearance of neutrophils from the peritoneal cavity during inflammation.....	182
6.2.9 – Enforced expression of Gata6 in adoptively transferred BMMØs alters their phenotype and peritoneal retention .....	183
6.3 – Discussion.....	185

6.3.1 – Selective expression of Gata6 in peritoneal and pleural ResMØ	185
6.3.2 – Phenotypic changes in ResMØ after Gata6-depletion	185
6.3.3 – Identification of ‘WT’ F4/80 <sup>high</sup> ResMØs in <i>Gata6</i> -KO <sup>mye</sup> mice	187
6.3.4 – Gata6 effects cell proliferation and euploidy in a cell-intrinsic manner	187
6.3.5 – Conditional myeloid knockout of Gata6 results in altered homeostatic cell numbers	188
6.3.6 – Absence of Gata6 results in a reduced ability of ResMØs to recover after inflammation by proliferation	188
6.3.7 – Potential mechanism for altered ResMØ proliferation	190
6.3.8 – The absence of Gata6 is associated with alterations in inflammatory resolution	190
6.3.9 – Gata6 imparts a peritoneal-like phenotype and increases the tissue retention of BMMØs	191
6.3.10 – Microarray analysis of Gata6-deficient ResMØs	191
6.3.11 – Conclusion	192
<b>Chapter 7 – General Discussion</b>	<b>193</b>
7.1 – MØ origins and self-renewal	194
7.1.1 – Past reflection	194
7.1.2 – Current paradigms	195
7.2 – MØ tissue specific phenotype and function	199
7.2.1 – Gata6 as a transcriptional regulator of ResMØ phenotype and renewal	199
7.2.2 – Other examples of MØ transcriptional regulation	200
7.3 – Conclusion	202
7.3.1 – Conclusions	202
7.3.2 – Future perspectives	202
<b>Supplemental appendix figures</b>	<b>204</b>
<b>Bibliography</b>	<b>204</b>

## Summary

Tissue resident macrophages are extremely heterogeneous, which reflects their unique microenvironments and tissue specific functions. They are a constituent of all tissues, and are involved in homeostatic processes and inflammatory disease. Recent studies have shown that select tissue resident macrophage populations, such as Langerhans cells of the skin and microglia of the brain, are able to self-renew independently from the bone marrow. This is contrary to the prevailing model macrophage origins, the 'mononuclear phagocyte system', which dictates that all macrophages are derived from bone marrow monocytes. The work carried out in this thesis investigated the self-renewing potential of peritoneal tissue resident macrophages, and its control. Several novel discoveries were made: i) peritoneal resident macrophages proliferate at low levels to maintain their numbers during homeostasis, at higher levels during neonatal growth, and undergo a burst in proliferation during acute inflammation to restore their depleted population; ii) renewal of peritoneal resident macrophages during an acute inflammatory episode was found to be independent from the bone marrow, and dependent upon macrophage colony stimulating factor, but importantly, not interleukin-4; iii) Monocyte-derived macrophages could also proliferate within an inflammatory lesion. Collectively, these observations challenge the dogma of the mononuclear phagocyte system: they demonstrate that in vascular tissues, tissue resident macrophages could self-renew independently of monocytes, and that monocyte-derived cells are not terminally-differentiated. Additional work leading up to these studies implicated Gata6 as a peritoneal macrophage-specific transcription factor. In this thesis, Gata6 was found to be necessary for peritoneal macrophage phenotype, normal proliferation, euploidy, and normal responses to inflammation. In summary, these studies demonstrate not only are macrophages capable of self-renewal, but this is dependent upon discrete transcriptional control. Understanding the molecular controls of tissue macrophage heterogeneity and renewal could provide novel avenues for the therapeutic manipulation of their activities.

## Abbreviations

A (as in A488, 647 etc.) – AlexaFluor

AGE – agarose gel electrophoresis

AIDS – acquired immunodeficiency syndrome

APC – allophycocyanin

B2m –  $\beta$ -2 microglobulin

BLAST – basic local alignment search tool

BM – bone marrow

bp – base pair

BrdU – 5-bromo-2'-deoxyuridine

BSA – bovine serum albumin

CBS – Cardiff University Central Biotechnology Services

CD – cluster of differentiation

C/EBP $\alpha$  – CCAAT-enhancer-binding protein  $\alpha$

CNS – central nervous system

cPPT – central polypurine tract

Cre – Cre recombinase

CR1g – Complement receptor of the immunoglobulin superfamily

Cy – cyanine

DAPI – 4',6-diamino-2-phenylindole

DAVID – the database for annotation, visualization and integrated discovery

DC – dendritic cells

dH<sub>2</sub>O – deionised H<sub>2</sub>O

DMEM – Dulbecco's Modified Eagle Medium

DMSO – dimethylsulphoxide

DNA – deoxyribonucleic acid

ds – double stranded

EDTA – Ethylenediaminetetraacetic acid

EdU – 5-ethynyl-2'-deoxyuridine

eGFP – enhanced green fluorescent protein

EGF-TM7 – epidermal growth factor receptor 7 pass trans-membrane

env – envelope protein

*E. coli* – *Escherichia coli*  
FDR – false discovery rate  
FITC – fluorescein isothiocyanate  
FSc – forward scatter  
g – gauge  
G (phase) – gap  
GM-CSF – granulocyte/MØ colony stimulating factor  
HIV – human immunodeficiency virus  
ICAM – intercellular adhesion molecule  
Id2 – inhibitor of DNA binding 2  
IFN – interferon  
IL – interleukin  
Inf – inflammation associated  
JBIOS – Cardiff University Joint Biological Services  
kB – kilo base pair (1000 base pairs)  
KC – keratinocyte-derived chemokine  
LB – lysogeny broth  
LED – light emitting diode  
LXR $\alpha$  – liver X receptor  $\alpha$   
M1 – ‘classically activated’ MØ  
M2 – ‘alternatively activated’ MØ  
MARCO – MØ receptor with a collagenous structure  
MASPs – MBL associated serine proteases  
MBL – mannose-binding-lectin  
M-CSF – MØ colony stimulating factor  
MFI – median fluorescent intensity  
M (phase) – Mitosis  
mU6 – mouse U6  
MØ – macrophage  
nef – negative factor  
*op* – osteopetrotic mutant allele  
PAMPs – pathogen associated molecular patterns  
PBS – phosphate buffered saline

PCR – polymerase chain reaction  
PCT- Peltier thermal cycler  
PE – phycoerythrin  
PEG – polyethylene glycol  
PerCP – peridinin chlorophyll  
pH3 – phospho-histone H3  
PPAR – peroxisome proliferator-activated receptor  
rCD2 – rat CD2  
Res – tissue resident  
rev – regulator of expression of viron proteins  
RISC – RNA induced silencing complex  
RNA – ribonucleic acid  
RPMI – Roswell Park Memorial Institute medium  
ROX – 6-carboxyl-x-rhodamine  
rpm – revolutions per minute  
RT – room temperature  
Runx3 – Runt-related transcription factor 3  
SignR1 – Sign related 1  
SDS – sodium dodecyl-sulphate  
SEM – standard error of mean  
SES – *Staphylococcus epidermidis* supernatant  
SEW – pHR'SIN-cPPT-SEW  
sh – short hairpin  
SOC – super optimal broth with catabolite repression  
S (phase) – synthesis  
Spi – SFFV proviral integration oncogene  
Sq – semi-quantitative  
SSc – side scatter  
SXW - pHR'SIN-cPPT-SXW  
T – Nunclon delta-treated tissue culture flask  
tat – trans-activator of transcription  
TBE – Tris-Borate EDTA  
TGF-  $\beta$  – transforming growth factor  $\beta$

T<sub>h</sub>2 – type 2 helper

Tip – TNF and iNOS producing

TNF – tumour necrosis factor

Tpl2 – tumour progression locus 2

trCD2 – truncated rat CD2

UV – ultraviolet

VEGF – vascular endothelial growth factor

*vif* – viral infectivity factor

VLA – very late antigens

*vpr* – viral protein R

*vpu* – viral protein unique

Wnt – wingless-type MMTV integration site family member



## **Chapter 1 – General Introduction**

## **1.1 – Macrophages: discovery, origins and heterogeneity**

### **1.1.1 – Discovery of macrophages**

The word macrophage (M $\emptyset$ ) is derived from the Greek words for large/ big (macro) and devourer/ eater (phage). M $\emptyset$ s are phagocytic (Greek: devouring cell) cells which engulf apoptotic cells, debris or pathogens to help maintain the function of body tissues. The Russian/ Ukrainian zoologist Ilya Ilyich Mechnikov (Elie Metchnikoff) was one of the first to describe phagocytosis as an active, purposeful event by a 'professional' cell (Metchnikoff, 1880, Metchnikoff, 1883). Metchnikoff described phagocytic cell activity during inflammation (Metchnikoff, 1892), and formulated the beginnings of the M $\emptyset$  system of innate immunity. However, phagocytosis itself was reported to have been discovered a few years before Metchnikoff's publications (Ambrose, 2006, Osler, 1875). These studies were unrefined at the time, and therefore Metchnikoff was accredited the discovery of phagocytosis due to his extensive body of research (Gordon, 2007). Metchnikoff is considered to be the father of natural immunity (Gordon, 2008), and was awarded the Nobel Prize in Medicine along with Paul Ehrlich (adaptive immunity) in 1908. M $\emptyset$  biology has been continually refined since these discoveries (Gordon, 2007), and remains an active area of research to date.

### **1.1.2 – Tissue resident M $\emptyset$ heterogeneity**

Before blood monocytes were identified as a source of phagocytic cells (Sabin, 1925), tissue histocytes formed part of the reticuloendothelial system (Aschoff, 1924). These histocytes were phagocytic cells which existed within the tissues (endothelia) themselves and were known to play a major role in tissue regulation. These cells are now known as tissue resident (Res) M $\emptyset$ s; the origin of which still remains a current and controversial issue (discussed below 1.1.3). M $\emptyset$ s are often classified functionally into one of two main categories: the 'M1/M2' M $\emptyset$  activation nomenclature (Mantovani *et al.*, 2004). This was based on the initial observations of 'classical' (M1) M $\emptyset$  activation by interferon (IFN)  $\gamma$  (Nathan *et al.*, 1983), and 'alternative activation' by interleukin (IL) 4 (Stein *et al.*, 1992) and IL-13 (de Waal Malefyt *et al.*, 1993). This paradigm has been extended to include M1 activation states induced by granulocyte/M $\emptyset$  colony stimulating factor (GM-CSF); and M2 activation states induced by M $\emptyset$  colony

stimulating factor (M-CSF)/ IL-10/ transforming growth factor  $\beta$  (TGF $\beta$ ) and steroids (Gordon, 2003). M1 'classically' activated M $\phi$ s are associated with inflammation, while M2 'alternatively activated' M $\phi$ s are linked with tissue repair (anti-inflammatory) (Gordon, 2003). ResM $\phi$ s are sometimes termed M2-like cells (Sato *et al.*, 2013). However, the M1/M2 paradigm was intended as a 'simplified conceptual framework' (Mantovani *et al.*, 2005) and is an oversimplification, given the complexity of ResM $\phi$  heterogeneity and activation. Therefore, cells originating in the tissue will be referred to as ResM $\phi$ s in this thesis, even during inflammation where these cells are likely activated (or 'polarised'). Monocyte-derived M $\phi$ s which are recruited to the tissue during inflammation are discussed below (1.2), but the same principle is followed, in that these cells will be termed 'inflammation-associated' (Inf) M $\phi$ s.

Different tissues have diverse physiological environments and micro-environments, which require distinct homeostatic functions. As an integral part of the tissue, ResM $\phi$ s are appropriately placed to both shape and be shaped by the tissue physiology. M $\phi$ s are most commonly known for their principal ability to phagocytose pathogens during infection (Metchnikoff, 1892). However, the roles of ResM $\phi$ s include: the phagocytosis of apoptotic cells, presentation of antigens to lymphocytes, regulation of immune responses, maintenance of stem cell populations, and control of physiological metabolism (Davies *et al.*, 2013a). These processes are not a feature of all ResM $\phi$ , and some are restricted to specific tissue niches. However, the role of phagocytosis, specifically with the removal of apoptotic cells, is considered to be common to all M $\phi$ s whether tissue resident or monocyte derived (Gordon, 2007).

ResM $\phi$ s in different tissues are often given unique nomenclature, and have differential expression of clusters of differentiation (CD) antigens and additional surface receptors, which are often used as markers to define cellular subsets. A few examples of such specialised ResM $\phi$ s subsets are osteoclasts, Langerhans cells and microglia (Gordon and Taylor, 2005). Osteoclasts are multinucleated M $\phi$ s (formed from cell fusion) which reside in and resorb bone matrices during homeostasis (Pollard, 2009). These cells are usually separated from other M $\phi$ s by their multinuclear phenotype and expression of the calcitonin receptor (Quinn *et al.*, 1999). Langerhans cells were discovered by Paul Langerhans in 1868, and were originally described as neurones due to their dendritic appearance (Langerhans, 1868). These cells reside in the epidermal layer of the skin

and are usually differentiated from dendritic cells (DCs) by their expression of Langerin (CD207), and high expression of F4/80 (Chorro *et al.*, 2009). Langerhans cells are well known for their roles in immunosurveillance and have the ability to present antigens to T-lymphocytes of the adaptive immune system (Merad *et al.*, 2008). For this role, Langerhans cells have been traditionally viewed as DCs. However their resemblance to ResM $\emptyset$  populations, such as microglia, and their dependence on M-CSF means they can be considered as ResM $\emptyset$ s (Satpathy *et al.*, 2012). Microglia are ResM $\emptyset$ s which reside in brain tissues and play a major role in promoting neuronal survival and synaptic remodelling (Paolicelli *et al.*, 2011, London *et al.*, 2013). These cells are usually described as being CD45<sup>low</sup>, CD11b<sup>+</sup> and F4/80<sup>+</sup> in the brain (Prinz *et al.*, 2011), however these antigens are common to most M $\emptyset$  populations (Davies *et al.*, 2013a).

F4/80 is a common antigen found on numerous M $\emptyset$  populations, it was first discovered by the creation of a monoclonal antibody (the 80<sup>th</sup> hybridoma in the 4<sup>th</sup> attempted fusion) which bound to an antigen expressed by M $\emptyset$ s (Austyn and Gordon, 1981). This antigen was found to be a G-protein coupled receptor and a member of the epidermal growth factor receptor 7 pass trans-membrane (EGF-TM7) family (McKnight *et al.*, 1996). F4/80 shares structural identity with growth factors, suggesting it is involved in cell adherence and signalling. There has been some evidence to suggest that F4/80 plays a role in the generation of immune tolerance (van den Berg and Kraal, 2005). However, the specific function of the F4/80 protein has been poorly categorised.

CD11b is the  $\alpha_M$  subunit of the integrin  $\alpha_M\beta_2$  complex, also known as Mac-1 and complement receptor 3. It was originally identified as a surface receptor on neutrophils (Hickstein *et al.*, 1987), but is now used as a common pan-myeloid cell marker for the identification of neutrophils, eosinophils and M $\emptyset$ s. However, it is also expressed on B1 cells (Morabito *et al.*, 1987).

The specific expression patterns of both F4/80 and CD11b can help distinguish M $\emptyset$ s from eosinophils and neutrophils, particularly when using physical parameters such as light scatter in flow cytometry. M $\emptyset$ s of the peritoneal cavity can be used as an example, as they consist of two major populations that are commonly separated by CD11b and F4/80 expression: F4/80<sup>high</sup> CD11b<sup>high</sup> ResM $\emptyset$ s and F4/80<sup>low</sup> CD11b<sup>+</sup> MHCII<sup>high</sup> ResDCs/M $\emptyset$ s (Dioszeghy *et al.*, 2008), the latter is most likely a mix of cells. Eosinophils and neutrophils can also be distinguished using these markers; which is

explained in more detail in chapter 3 of this thesis. However, additional markers can be used to subdivide the major ResMØs populations.

The peritoneal ResMØ population can be further divided into multiple sub-populations using a few additional markers, such as: Tim4 (Miyanishi *et al.*, 2007), CD73 (Petrovic-Djergovic *et al.*, 2012), SignR1 (Taylor *et al.*, 2004), and CR1g (Gorgani *et al.*, 2008). Tim4 is a phosphatidylserine receptor which is selectively expressed on the vast majority (95 %) of peritoneal ResMØ, but is also seen in CD11b<sup>+</sup> cell populations in other tissues (Miyanishi *et al.*, 2007). CD73 (ecto-5'-nucleotidase) is involved (along with CD39) in the direct extracellular production of adenosine from exported cyclic AMP or ATP. Adenosine, ATP and cyclic AMP are important modulators of inflammation, and adenosine can additionally modulate neurotransmission (Cohen *et al.*, 2013, Latini and Pedata, 2001, Petrovic-Djergovic *et al.*, 2012). SignR1 (Sign related 1) is a mannose receptor found on MØ, and is involved in the recognition of fungal carbohydrates (Taylor *et al.*, 2004). CR1g (complement receptor of the immunoglobulin superfamily) is a complement receptor which binds to C3b on opsonised apoptotic cells and microbes (Kim *et al.*, 2008), but inhibits activation of the alternative complement pathway, preventing autoimmunity (He *et al.*, 2008). These surface receptors can be used purely as markers; however, as shown above, they have defined functions which will provide this heterogeneous ResMØ population with a broad spectrum of functional characteristics. This likely equips the population with a diversity of responses, which are needed to efficiently survey the tissue for potential pathogenic threats and maintain tissue homeostasis.

### **1.1.3 – Origins of ResMØs**

The MØ system was first introduced by Elie Metchnikoff in the late 19<sup>th</sup> century, and described phagocytic activity during inflammation (Metchnikoff, 1892). This system was refined in 1924 by Aschoff and formed part of the reticuloendothelial system (Aschoff, 1924); a tissue system comprised of reticuloendothelia (histocytes/ ResMØs) and endothelial cells. These cells were proposed to have a common tissue origin and regulated their numbers through the local expansion of cells. However, this system was flawed due to the false assumption that phagocytosis was the only mechanism which lithium carmine (the tracer used in these studies) could be absorbed into cells.

The discovery of pinocytosis (cell drinking) (Lewis, 1931) cast doubts over the phagocytic ability of reticuloendothelia. At the same time as the reticuloendothelial system was formulated, blood monocytes were identified as a source of phagocytic cells (Sabin, 1925), with the others considered to be of tissue origin. These two populations (tissue and monocyte exudate) were investigated during later years, and with the aid of technological advances, more increasing differences were observed, such as the differential peroxidase activity of these cells (Daems, 1971).

In 1968 van Furth and Cohn showed that major populations of MØs were derived from blood monocytes (van Furth and Cohn, 1968) and this concept was extended to the broader range of phagocytes including ResMØs, establishing the mononuclear phagocyte system (MPS) (van Furth *et al.*, 1972). These results were disputed at the time due to evidence of proliferation (Parwaresch and Wacker, 1984, Sawyer *et al.*, 1982, Czernielewski and Demarchez, 1987), the apparent longevity of ResMØs (Melnicoff *et al.*, 1988), and the fact that MØ populations were present in the yolk sac before primitive haematopoiesis (Naito *et al.*, 1996). However, due to the limited technology of the time these observations could not be validated as representing a divergence from the MPS. One example is an experiment using aliphatic dye labelling of peritoneal ResMØs (Melnicoff *et al.*, 1989). Naïve ResMØs were labelled with a dye *in vivo*, and then inflammation was initiated with thioglycollate broth. The number of dyed MØs was found to be nearly double the number seen in naïve mice. The authors attributed this to either ResMØs or their precursors expanding by *in situ* proliferation during the recovery from inflammation. This experimental approach was later applied to homeostatic renewal over a period of 49 days, and found that dyed cells persisted in the peritoneal cavity (Melnicoff *et al.*, 1988). However, these dyes can be transferred by membrane transfer (Harvey *et al.*, 2008) or via phagocytosis of apoptotic cells (Soehnlein and Lindbom, 2010), and are not readily degraded. This cast doubts over the conclusions made in these reports. Another example is the incorporation of tritiated thymidine into ResMØs (Parwaresch and Wacker, 1984). The authors explained that this was evidence of ResMØ proliferation. However this was also disputed, because this proliferation could have occurred either in monocytes or other MØ precursors.

Work on M $\emptyset$  heterogeneity carried on through to the end of the twentieth century and more deficiencies were detected in the absolutes of the MPS (Takahashi, 2000, Naito *et al.*, 1996). In 2000, Ovchinnikov and colleagues concluded that embryonic phagocytes were of a separate lineage and this raised the possibility of their persistence into adulthood (Ovchinnikov, 2008, Lichanska and Hume, 2000). This theory was cemented with the breakthrough work on Langerhans cells and microglia. Langerhans cells were originally thought of as bone-marrow derived DCs, but their proliferative capacity has been known in humans for some time (Czernielewski and Demarchez, 1987). More recent data revealed that human Langerhans cells were still donor derived 4.5 years after a double hand allograft (Kanitakis *et al.*, 2004). The self-renewing capacity was confirmed in mice (Merad *et al.*, 2002) and similar observations were made in the brain, with microglia also renewing their population via local proliferation (Ajami *et al.*, 2007). Both microglia and Langerhans cells could be derived from blood monocytes, but only under certain conditions (Mildner *et al.*, 2007, Merad *et al.*, 2002). M $\emptyset$  proliferation has also been observed in many other tissues (Gordon and Taylor, 2005). So it was becoming clear that the MPS was too limited to answer the questions of M $\emptyset$  origins, fate, function and control of heterogeneity. In response to this, Chorro *et al.* investigated the origins of Langerhans cells and showed that the adult population was created by the local expansion of Langerhans cells in the neonate (Chorro *et al.*, 2009). This contradicts the basic principles of the MPS, but may as the authors suggested, be a special case and restricted to tissues with limited vasculature.

## **1.2 – MØs in inflammation**

### **1.2.1 – The peritoneal acute immune response**

A major tool used in this thesis is a murine model of acute peritonitis (peritoneal inflammation). This involves the intra-peritoneal transfer of an inflammation-inducing agent (e.g. live pathogens, pathogen derived materials or irritants) into the peritoneal cavity which triggers an acute, innate immune response. During this response the cellular kinetics are altered in order to eliminate potential pathogens and restrict tissue damage. An example of a typical cellular change during an acute inflammatory episode is depicted in figure 1.1; this figure depicts that these cellular changes are occurring simultaneously, and conveys that this is a fluid system. The acute inflammatory response is initiated by interaction of an inflammatory agent (e.g. a pathogen) with various recognition systems, such as complement components, immunoglobulins (Ig) and receptors on tissue resident cells, such as mast cells and MØs.



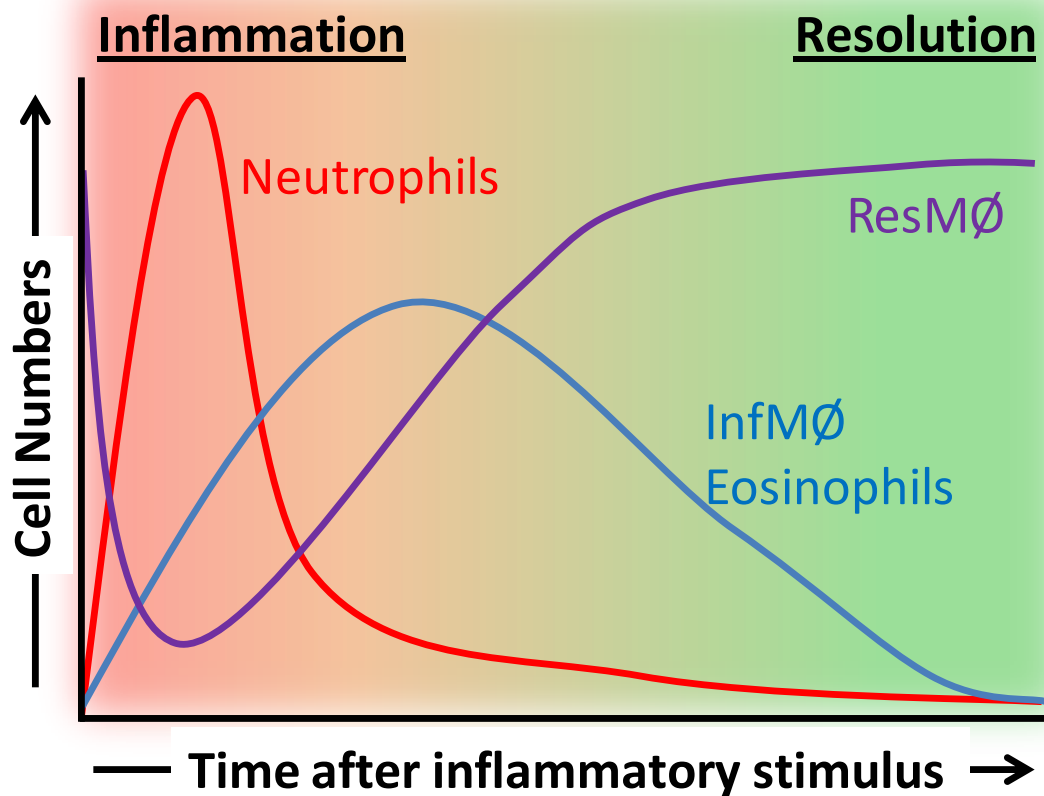


**Figure 1.1. The acute peritoneal immune response**

Schematic showing changes in the number of different cell populations after an acute inflammatory stimulus. Note the 'disappearance' of ResMØs early in the inflammatory response, when neutrophil numbers are at their peak; followed by the return of ResMØs with declining neutrophil numbers.

Complement activation can occur via the classical, alternative or mannose-binding-lectin (MBL) or lectin pathway (Muller-Eberhard, 1988, Matsushita, 1996). The classical pathway involves binding of C1 (via C1q) either to pre-bound Ig or directly to antigens. IgG molecules are produced by plasma B lymphocytes to recognise foreign antigens; however this usually requires adaptive immunity. Alternatively, 'natural' IgM can bind to specific antigens, such as carbohydrate without requirement for pre-immunisation (Bos *et al.*, 1989). The binding of the C1 complex leads to the first stage of the complement cascade and the sequential cleavage of C4, C2, and C3 (the latter into C3a and C3b). In the alternative complement pathway: C3a and C3b are generated directly from C3 via activated factors B and D. Alternatively, in the lectin pathway: MBL forms a complex with MBL associated serine proteases (MASPs), which leads to cleavages similar to the classical pathway. All pathways converge on the cleavage of C3 and the

generation of the opsonin C3b. The cleavage of C3 leads to the assembly of a C5 convertase and the generation of the potent anaphylotoxin C5a, and the first part of the membrane attack complex: C5b, which initiates the 'terminal' complement pathway. The peritoneal cavity contains basal levels of complement that are able to effectively opsonise microbial material (Tsoni *et al.*, 2009). However, it is likely that all pathways will be activated during inflammation, such as that seen with pathogenic fungal infections (Ip and Lau, 2004, Kozel, 1996, Speth *et al.*, 2004). Complement activation liberates the C3a and C5a anaphylatoxins, which bind to their respective receptors on immune cells to activate their chemotaxis and/ or expression of pro-inflammatory mediators (Sacks, 2010).

In addition to complement receptors, resident peritoneal cells including mast cells, ResM $\phi$ s, DCs and mesothelial cells, have a broad range of pattern recognition and Fc receptors. In the peritoneal cavity these receptors include: toll-like receptors, such as TLR4 (Kato *et al.*, 2004, Iwasaki and Medzhitov, 2004); scavenger receptors, such as M $\phi$  receptor with a collagenous structure (MARCO) (Peiser *et al.*, 2002); and carbohydrate receptors, such as SignR1 and mannose receptor (Taylor *et al.*, 2004). These receptors are heterogeneously expressed in different tissues and discrete tissue niches (Taylor *et al.*, 2005a).

These pattern recognition receptors bind specific motifs, referred to as pathogen associated molecular patterns (PAMPs). The binding of certain receptors during infection/ inflammation triggers downstream signalling cascades, such as the myeloid differentiation primary response gene 88 (MyD88) – nuclear factor- $\kappa$  light chain enhancer of activated B cells (NF $\kappa$ B) pathway; which leads to cellular activation and production of inflammatory mediators. In addition, mast cells secrete pro-inflammatory granules upon their activation. These granules contain histamine, platelet activating factor, and inflammatory cytokines such as IL-6 and tumour necrosis factor  $\alpha$  (TNF $\alpha$ ) (St John and Abraham, 2013). These inflammatory regulators trigger the release of further inflammatory mediators via positive feedback loops, but will also produce specific neutrophil chemo-attractants such as CXCL1 and CXCL2 (Soehnlein and Lindbom, 2010).

An increase in these chemo-attractants leads to neutrophil infiltration from the blood, which is aided by an increase in vascular permeability (Davis *et al.*, 2004). Neutrophils

phagocytose and destroy invading pathogens using oxidative burst (Nathan, 2006), secretion of biocidal granules (Borregaard *et al.*, 2007) and neutrophil extracellular traps (NETs) (Brinkmann *et al.*, 2004). However the cytotoxic effects of neutrophils can cause collateral damage to the tissue (Weiss, 1989). At the same time as neutrophil recruitment, MØs, mast cells, mesothelial cells and neutrophils produce chemo-attractants such as CCL2-4; which leads to an influx of monocytes into the peritoneal cavity. These monocytes quickly differentiate into phagocytic MØs, and will aid in the clearance of pathogens (Soehnlein and Lindbom, 2010). Eosinophils are also recruited to the inflammatory lesion via chemo-attractants such as CCL11 (Ganzalo *et al.*, 1996), which also restricts neutrophil recruitment (Cheng *et al.*, 2002).

The neutrophils recruited during inflammation eventually become apoptotic, and are subsequently cleared from the peritoneal cavity by MØs. This decline in neutrophil numbers is associated with the resolution of inflammation. During this resolution phase, the total number of inflammation-associated cells decline and tissue homeostasis is restored. Neutrophil-mediated damage is repaired, and this is usually attributed to a shift in the cytokine balance in the tissue from pro-inflammatory to anti-inflammatory, with the associated repair mechanisms.

This process known as wound healing can be categorised into three stages: inflammation, tissue formation and remodelling (Gurtner *et al.*, 2008). Tissue formation overlaps with the resolution of inflammation. Damaged tissue must first be cleared, and then new cells migrate and proliferate to form new granulation tissue and blood vessels; this is usually followed by collagen deposition by fibroblasts. This deposition can lead to fibrosis, which is a rapid process to aid the restoration of tissue homeostasis, but can lead to later complications and impairment of proper tissue function. This type of repair is usually restricted to chronic inflammation, and in the peritoneal cavity this is known to be driven by cytokines such as IL-6 (Fielding *et al.*, 2014). However, in many tissues, this is considered to be associated with a T<sub>h</sub>2-mediated environment and the growth factor TGFβ (Leask and Abraham, 2004). Tissue remodelling by fibroblasts, MØs and endothelial cells works to remove the collagen core from the fibrotic lesion restoring normal tissue structure; however this can take years (Gurtner *et al.*, 2008).

### 1.2.2 – Role of MØs in acute inflammation

MØs have an integral role in the initiation, modulation and resolution of inflammation. ResMØs initially play a role in the recruitment of neutrophils to the peritoneal cavity following the initial inflammatory insult. Depletion of peritoneal MØs before inflammatory stimulus can result in the loss of CXCL1 and CXCL2 neutrophil chemo-attractants, and a substantial reduction in neutrophil numbers (Cailhier *et al.*, 2005). In the case of zymosan induced peritonitis (as seen in Cailhier *et al.* and described in 3.1.1), this could be attributed to lack of MØ specific recognition of zymosan particles with molecules such as dectin-1 (Brown and Gordon, 2001); as mesothelial cells alone are known to respond to endotoxin and secrete CXCL2 (Kato *et al.*, 2004). Consistent with this, Dectin-1 KO mice exhibit significantly reduced neutrophil recruitment in response to a fungal pathogen (Taylor *et al.*, 2007).

After the initial inflammatory stimulus, the number of recoverable ResMØs decreases, at the same time as neutrophil influx. This fall in ResMØ numbers is termed ‘the disappearance reaction’ (see *figure 1.1*). In the peritoneal cavity this is defined as an experiential failure to recover the cells by lavage. This could be due to increased adherence to the mesothelial tissues, cell migration to draining lymph nodes, or cell death (Barth *et al.*, 1995). Tissue adherence is a likely contributor, as adhesion molecules such as intercellular adhesion molecule (ICAM) 1 are known to be regulated upon MØ activation (Hubbard and Giardina, 2000); and additionally, ResMØ adhesion has been observed in the peritoneal cavity during inflammation (Bellingan *et al.*, 2002).

As the inflammation progresses, ResMØs along with recruited neutrophils and mesothelial cells produce monocytic chemo-attractants, such as CCL2-4. This results in the invasion of the tissue by peripherally recruited monocytes (Soehnlein and Lindbom, 2010). Two subsets of monocyte are recruited to the inflammatory lesion, and are separated by expression of Ly-6C (Geissmann *et al.*, 2003): Ly-6C<sup>low</sup> and Ly-6C<sup>high</sup>. These monocytes differentiate into InfMØs, and are initially distinguishable from ResMØs by their expression of F4/80 and CD11b. InfMØs are also frequently termed ‘M1 polarised’ MØs in the early stage of acute inflammation (Mantovani *et al.*, 2004). The immediate role of InfMØs in acute models is to aid neutrophils in the phagocytic clearance of pathogens and secrete pro-inflammatory cytokines (Soehnlein and Lindbom, 2010). However, these InfMØs also play a key role in the resolution of

inflammation. For example, Ly-6C<sup>low</sup> InfMØs limit leukocyte recruitment and aid in tissue recovery (Gautier *et al.*, 2012a). However, the number of InfMØs slowly decreases after inflammation, while ResMØs return to their normal numbers (Rosas *et al.*, 2010).

Some of these InfMØs are lost during these late stages of inflammatory resolution possibly through emigration to draining lymph nodes (Bellingan *et al.*, 1996). This is a process which is dependent upon regulation of the very late antigens (VLA) 4 and 5 (Bellingan *et al.*, 2002). Therefore, these InfMØs (which could include 'TNF and iNOS producing (Tip) DCs') could present pathogenic antigens to the T-cells within the lymphatics. However, it has recently been reported that the majority of InfMØs are cleared from the lesion via apoptosis and subsequent phagocytosis by ResMØs (Gautier *et al.*, 2013, Janssen *et al.*, 2011).

During the resolution of inflammation, apoptotic neutrophils are preferentially cleared by ResMØs, but InfMØs which are usually in the majority, can also phagocytose them. ResMØs have been suggested to actively inhibit the ability of InfMØs to phagocytose apoptotic neutrophils; potentially preventing autoimmunity (Uderhardt *et al.*, 2012). In addition to this, extracellular adenosine (a product of ResMØ CD73 and CD39) can inhibit the respiratory burst of neutrophils, therefore preventing excess tissue damage (de la Harpe and Nathan, 1989). Hence, not only are specific subsets of MØs present during inflammation, but they also have distinct functions.

MØs are also essential for tissue remodelling and repair after injury, by producing factors such as TGFβ and wingless-type MMTV integration site family members (Wnts). Vascular endothelial growth factor (VEGF) and angiopoietin are up-regulated by MØ produced Wnts and promote vascular regeneration at the site of injury (Rao *et al.*, 2007). The TGFβ pathway has been studied extensively during wound healing, TGFβ1 and TGFβ2 contribute to scarring whilst TGFβ3 can promote scar free healing (Beanes *et al.*, 2003). During wound healing it is generally considered that most MØs are derived from circulating monocytes (Brancato and Albina, 2011). These monocytes are recruited to wounds where they appear to play differential roles producing pro-inflammatory mediators such as TNF in the early phase, and anti-inflammatory repair roles in the later phases (Nahrendorf *et al.*, 2007). A specific role of ResMØs in wound healing has been largely neglected. However, time-dependent conditional depletion of

MØs in mice revealed differential MØ functions throughout the wound healing process (Lucas *et al.*, 2010). Depletion in the inflammatory phase demonstrated roles for MØs in the formation of vascularised granulation tissue, impaired epithelialisation, and minimised scar formation. Depletion during the tissue formation stage led to haemorrhage and a failure of wound closure and transition to the remodelling stage. MØ depletion during the remodelling stage had less impact on the natural healing progress.

### **1.3 – Work leading up to this thesis**

In 2005, Siamon Gordon and Phil Taylor reviewed monocyte and MØ heterogeneity (Gordon and Taylor, 2005). This review emphasised the vast heterogeneity seen in MØs within and between tissues in both the human and mouse. Additionally, the authors highlighted evidence of ResMØ proliferation, such as that seen in Langerhans cells (Merad *et al.*, 2002), microglia (Lawson *et al.*, 1992) and alveolar ResMØs (Tarling *et al.*, 1987). The lessons learnt from this review were combined with studies carried out in Prof. Phil Taylor's laboratory on MØ heterogeneity during inflammation, to formulate the working hypothesis of this thesis (see 1.4). Marcela Rosas identified that the unknown antigen 7/4 was synonymous with Ly-6B (Rosas *et al.*, 2010), and showed heterogeneous expression of Ly-6B, F4/80 and CD11b on MØs during inflammation. Her observations provided a basis on which cell populations could be separated for further analysis, enabling detection of differential functions and genetic programming. These subsequent experiments were to form the foundations of this thesis, and some of which are described below.

#### **1.3.1 – Microarray analysis of MØ populations**

In 2007, Dr. Marcela Rosas carried out microarray analysis of monocyte and MØ populations during peritoneal inflammation, based upon cell populations identified in her previous work (Rosas *et al.*, 2010). The results of this microarray are currently within a manuscript that is in submission (Rosas *et al.*, 2014). The primary objective of this microarray study was to investigate the differences in the transcriptional profiles of ResMØs and InfMØs. Peritonitis was induced with  $2 \times 10^6$  particles of zymosan, and target cell populations were purified by flow cytometric cell sorting using select markers, including Ly-6B, F4/80 and CD11b (table 1.1). Monocytes from the bone marrow were additionally purified as a reference population. The populations used in this microarray were selected as they represent a typical model of ResMØs and monocytes/ InfMØs with distinct lineage origins (Rosas *et al.*, 2010). The RNA was extracted from the cells, then amplified, labelled and hybridised to Affymetrix MOE430 2.0 GeneChips. Expression data was calculated and probe-sets were annotated using

the database for annotation, visualization and integrated discovery (DAVID) (Dennis *et al.*, 2003).

Cell type	Zymosan	Purification Criteria	Simplification (Population Number)
Bone marrow monocytes	0 hours	Ly-6B <sup>high</sup> , Ly-6G <sup>-</sup>	Naïve bone marrow <b>monocytes</b> (1)
Inflammatory monocytes	4 hours	Ly-6B <sup>high</sup> , Ly-6G <sup>-</sup>	Early recruited <b>monocytes</b> (2)
Inflammatory monocytes/MØ	18 hours	Ly-6B <sup>+</sup> , Ly-6G <sup>-</sup>	Late recruited <b>monocytes</b> / InfMØs (3)
MØ	3 days	F4/80 <sup>+/high</sup> , CD11b <sup>+/hi</sup>	Mixed <b>ResMØs</b> / InfMØs (4)
Ly-6B <sup>+</sup> MØ	7 days	F4/80 <sup>high</sup> , Ly-6B <sup>+</sup>	Ly-6B <sup>+</sup> InfMØs (5)
Ly-6B <sup>-</sup> MØ	7 days	F4/80 <sup>high</sup> , Ly-6B <sup>-</sup>	Predominantly <b>ResMØs</b> (6)
ResMØ	0 hours	F4/80 <sup>high</sup> , CD11b <sup>high</sup>	Naïve <b>ResMØs</b> (7)

**Table 1.1. Purification criteria for monocyte and MØ populations**

Table showing the different cell populations, which were purified by flow cytometric cell sorting and used for microarray analysis. Inflammation was induced with  $2 \times 10^6$  particles of zymosan and cell populations extracted at the indicated time after zymosan. Purification criteria shows the antibody targets used to label the cells for sorting. These cells are heterogeneous phenotypes that are reminiscent of ResMØs and InfMØs/ monocytes. The simplification column separates the cells into these categories, but this was not known until after microarray analysis and subsequent hierarchical clustering. The bold lettering in the simplified column shows a broad separation into monocyte and ResMØ groupings.

Differentially-expressed probe-sets were identified using a one-way ANOVA with the *P*-values corrected for false discovery and multiple testing with the false discovery rate (FDR) methodology. Hierarchical clustering of these differentially-regulated probe-sets separated the 7 subsets broadly into a ‘monocytic-like’ and ‘ResMØ-like’ groupings (*figure 1.2a*) and emphasized the relationship between the three ResMØ enriched populations (*table 1.1*). ResMØ-like groupings were labelled as such because the majority of cells shared the same CD11b<sup>high</sup> F4/80<sup>high</sup> phenotype as naïve ResMØ. Probe-sets with ANOVA *P*-values of  $<0.001$  were subject to K means clustering using *Genesis* (Sturn *et al.*, 2002), generating 15 distinct gene expression clusters. ‘Cluster 15’ consisted of  $\approx 800$  genes and was highly expressed only in the ResMØ enriched preparations. Within this cluster, 215 individual probe-sets exhibited 10-fold higher expression than the mean expression in the ‘monocytic’ hierarchical cluster. ‘Cluster



15' was validated by transcripts that are suggested to be restricted to ResMØs in C57BL/6 mice: SignR1, CRlg and Tim4 (*figure 1.2b*). The cluster was further authenticated by assessment of the surface expression of these proteins (*figure 1.2c*).

The 215 individual probe-sets in 'cluster 15' defined a ResMØ-restricted gene profile, which allowed identification of novel ResMØ-restricted probe-sets. Among these was the zinc finger transcription factor *Gata6* (*figure 1.2b*).

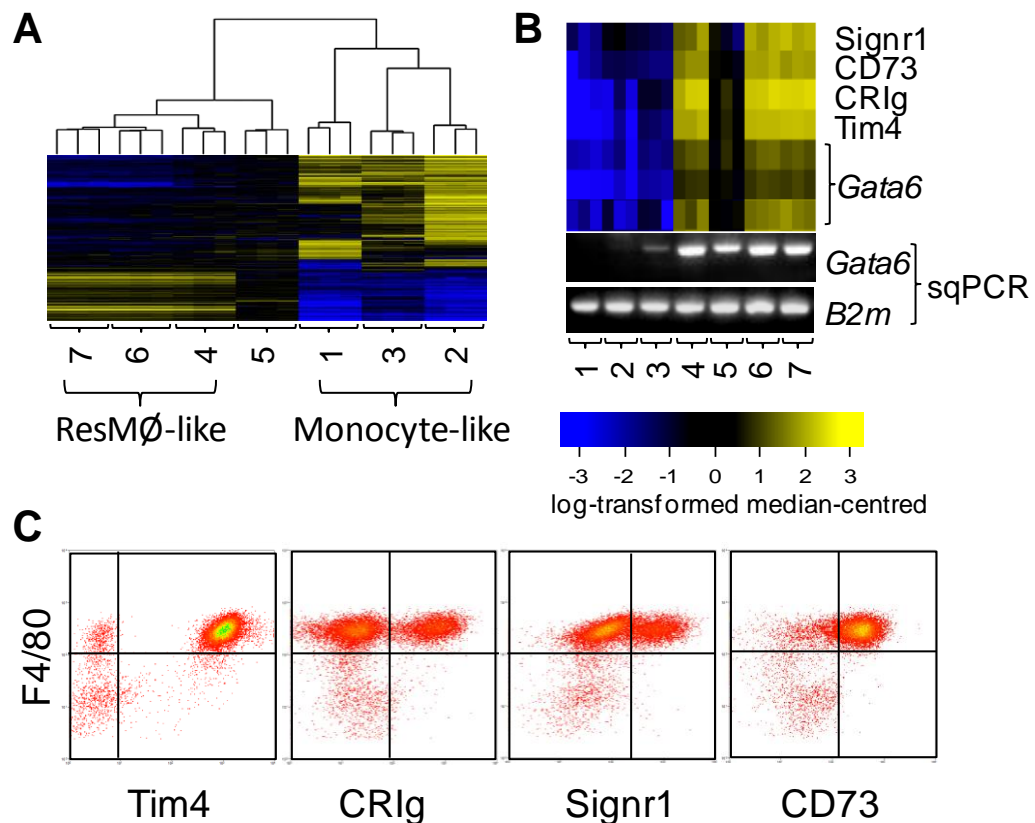


**Figure 1.2. Clustering of monocyte and MØ populations by microarray analysis**

**A)** Heat map depicting the hierarchical clustering into 'monocytic-like' and 'ResMØ-like' groupings. Population numbers 1-7 (A-B) are shown in table 1.1. **B)** Heat map showing the enriched expression of SignR1, CD73, CRlg, Tim4 and *Gata6* in the MØ-like cluster. *Gata6* expression was validated by semi-quantitative (sq) PCR using the endogenous control *B2m* ( $\beta$ 2 microglobulin). **C.** Representative density plots showing the expression of SignR1, CD73, CRlg and Tim4 restricted to the F4/80<sup>high</sup> ResMØs from the peritoneal cavity of naïve C57BL/6 mice. Plots were pre-gated to remove doublets and eosinophils, and gated on F4/80<sup>+</sup> CD11b<sup>+</sup> MØ.

### 1.3.2 – The GATA family of transcription factors

The Gata family of class IV zinc finger transcription factors is separated into two main groups: Gata1-3 function in haematopoietic cells, while Gata4-6 are considered restricted to mesoderm/ endoderm derived tissues (Maeda *et al.*, 2005). The latter group has been implicated in the control of tissue specific genes in these mesoderm/ endoderm-derived tissues, such as the heart and gastrointestinal tract (Molkentin, 2000). The Gata6 gene encodes a single transcript which contains two potential translational initiation sites. Translation at the first site encodes a long Gata6 isoform, while the second gives rise to a shorter isoform. The skipping of the first site has been attributed to 'leaky scanning' by ribosomes, and occurs in all tissues containing Gata6. The short length Gata6 is similar to the other Gata factors 4 and 5, while the long version contains an extra 146 amino acids at the N-terminus (Takeda *et al.*, 2004). The short version of Gata6 is reported to have lower activity than the long version of Gata6 (Takeda *et al.*, 2004). This has been attributed to the lack of a PEST sequence (Obayashi *et al.*, 2012), that is usually associated with protein degradation (Rogers *et al.*, 1986). Therefore, although short Gata6 has lower activity, it is likely to be more stable, due to the lack of this PEST sequence. However, additional protein interactions with the PEST sequence itself, or the other missing amino acids could have an impact on additional DNA binding activity.

Gata6 itself binds to the (A/T/C)GAT(A/T)(A) consensus sequence in regulatory elements of target genes, with the AGAT(A/T)A sequence giving the strongest binding. It is normally associated with the embryonic mesoderm/ endoderm (Morrisey *et al.*, 1996); or organs derived from these, such as the heart and gastrointestinal tract (Maeda *et al.*, 1996). Gata6 is vital for the development of these organs (Morrisey *et al.*, 1996), but has also been shown to regulate proliferation and differentiation in cells of the small intestine of adult mice (Beuling *et al.*, 2011).

Gata6 is one target among many which were linked to proliferation and enriched in ResMØs. Additional genes associated with proliferation were identified and enriched in ResMØs and interestingly, in Ly-6B<sup>+</sup> InfMØs. The sum of data revealed by this microarray lead to the formation of the hypothesis tested in this thesis (below).

## **1.4 – General hypothesis**

The hypothesis tested in this thesis is that MØs have the capacity to proliferate in homeostasis and inflammation. This proliferation is under the control of specific mediators, which includes the ResMØ enriched zinc finger transcription factor Gata6.

## **1.5 – Aims**

- To determine whether ResMØs have the capacity to self-renew by proliferation
- To examine whether InfMØs can proliferate during inflammation
- To determine the role of Gata6 in ResMØs

## **Chapter 2 – Methods**

## **2.1 – Notes**

All concentrations given are final reaction concentrations (working concentrations) unless specifically stated.

Autoclaving was carried out at 120°C and 100 kPa for 15 minutes to sterilise equipment.

All lab equipment, e.g. centrifuge tubes, conical flasks and tissue culture plates was from Thermo-Fisher Scientific, unless otherwise stated. All reagents were from Sigma Aldrich unless otherwise stated.

## **2.2 – Health and safety**

The appropriate risk assessments were adhered to when using all reagents and equipment.

## 2.3 – Antibodies and dyes

Antibody/Dye	Clone	Company	Final Conc.
<b>Flow cytometry</b>			
CD45.1 FITC	A20	Biologend	10 µg/ ml
GFP AlexaFluor647	FM264G	Biologend	4 µg/ ml
B220 PerCP-Cy5.5	RA3-6B2	Becton Dickinson	2 µg/ ml
B220 eFluor450	RA3-6B2	eBioscience	2 µg/ ml
CD43 FITC	S7	Becton Dickinson	5 µg/ ml
ICAM-1 PE	3E2	Becton Dickinson	2 µg/ ml
ICAM-1 Biotin	YN1/1.7.4	Caltag Laboratories	1 in 50
CD3 PerCP-Cy5.5	17A2	Biologend	2 µg/ ml
CD19 APC	1D3	eBioscience	2 µg/ ml
CD23 PE	B3B4	Becton Dickinson	2µg/ ml
CCR2 PE	475301	Research&Development	0.625 µg/ ml
CD226 APC	10E5	eBioscience	2 µg/ ml
IgM PE-Cy5	II/41	eBioscience	2 µg/ ml
CD5 PE-Cy7	53-7.3	eBioscience	2 µg/ ml
Siglec F PE	E50-2440	Becton Dickinson	1 µg/ ml
Myc-tag AlexaFluor647	9B11	New England Biolabs	1.5 µg/ ml
SignR1 AlexaFluor647	22D1	eBioscience	2 µg/ ml
CRlg FITC	MBI4	In House (Gift from Dr. Claire Harris)	9.2 µg/ ml
rCD2 AlexaFluor647	OX-34	ABD Serotec	1 in 100
rCD2 AlexaFluor488	OX-34	ABD Serotec	1 in 100
CRlg Biotin	MBI4	In House (Gift from Dr. Clair Harris)	6.2 µg/ ml
CD45.2 APC-Cy7	104	Biologend	2 µg/ ml
CD45.1 APC	A20	eBioscience	2 µg/ ml
Tim 4 PE	RMT4-54	Biologend	0.4 µg/ ml
Tim 4 AlexaFluor647	RMT4-54	Biologend	0.25 µg/ ml
CD45.2 PerCP-Cy5.5	104	Becton Dickinson	4 µg/ ml
Rabbit IgG1	DA1E	New England Biolabs	0.25 µg/ ml
pHH3 AlexaFluor488	D2C8	New England Biolabs	0.25 µg/ ml
Ki67 PE Kit	B56	Becton Dickinson	1 in 5
Ki67 FITC Kit	B56	Becton Dickinson	1 in 5
Ly6G Pe-Cy7	1A8	Becton Dickinson	2 µg/ ml
Ly-6B.2 PerCP	7/4	In House	12 µg/ ml
F4/80 APC	Cl:A3-1	ABD Serotec	1 in 100
F4/80 Pacific Blue	Cl:A3-1	ABD Serotec	1in 10 - 1 in 100
F4/80 Pacific Blue	BM8	Biologend	5 µg/ ml
F4/80 V405	Cl:A3-1	ABD Serotec	1 in 100
F4/80 PE-Cy7	BM8	Biologend	4 µg/ ml
F480 PerCP	Cl:A3-1	In House	10.8 µg/ ml

F4/80 PE	Cl:A3-1	ABD Serotec	1 in 100
F4/80 PE-AlexaFluor750	Cl:A3-1	ABD Serotec	1 in 100
F4/80 PE-Texas Red	BM8	Life Technologies	1 in 50
F4/80 Biotin	Cl:A3-1	In House	20 µg/ ml
CD11b FITC	5C6	In House	8 µg/ ml
MHCII PerCP-Cy5.5	M5/114.15.2	Biologend	1 µg/ ml
CD11b PerCP-Cy5.5	M1/70	Becton Dickinson	2 µg/ ml
CD11b APC-Cy7	M1/70	Becton Dickinson	0.2 µg/ ml
FcγRII/III	2.4G2	In House	4 µg/ ml
CD11c PeCy7	HL3	Becton Dickinson	4 µg/ ml
CD73 Biotin	TY/11.8	Biologend	5 µg/ ml
CD73 PE-eFluor710	TY/11.8	eBiosciences	4 µg/ ml
<b>Dyes</b>			
DAPI	N/A	Life Technologies	25 ng/ ml
Draq5	N/A	Biostatus	25 µg/ ml
Propidium Iodide	N/A	Life Technologies	125 ng/ ml
LDS 751	N/A	Life Technologies	100 ng/ ml
<b>Streptavidin linked fluorochromes</b>			
-PE-Texas Red	N/A	Becton Dickinson	2 µg/ ml
-Pacific Blue	N/A	Becton Dickinson	2 µg/ ml
-APC	N/A	Becton Dickinson	2 µg/ ml
-PE	N/A	Becton Dickinson	2 µg/ ml
-AlexaFluor488	N/A	Becton Dickinson	2 µg/ ml
-Dylight594	N/A	Biologend	2 µg/ ml
<b>Immunocytochemistry</b>			
Gata6 Biotin	Polyclonal	R&D Systems	40 µg/ ml

**Table 2.1. Antibodies and dyes**

Table showing the antibodies, dyes and streptavidin linked fluorochromes used in this thesis. Antibody concentrations are a rough guide for flow cytometry. New antibody lots were tested/ titrated before use due to variability in production; some companies do not disclose the antibody concentration. Abbreviations: FITC= fluorescein isothiocyanate, PE= phycoerythrin, Cy= cyanine, PerCP= peridinin chlorophyll, APC= Allophycocyanin, DAPI= 4',6-diamino-2-phenylindole.

## **2.4 – Cell counting**

Most of the cell counting carried out in this thesis was performed using a haemocytometer. However, the Muse cell counter was used in chapter 6 of this thesis, and gave more accurate, objective results than the haemocytometer. The cell counter showed lower coefficients of variation than the haemocytometer, which is mainly attributed to the higher number of events counted (nominally 1000 in the Muse, compared with  $\approx 200$  on the haemocytometer).

### **2.4.1 – Haemocytometer**

Cells were counted with a Neubauer bright line haemocytometer (depth: 0.1mm, small square area:  $0.0025\text{mm}^2$ ). The cells in four large squares ( $20\times 20$  small squares) were counted and the number divided by 4 to gain an average number of cells in  $0.0001\text{cm}^3$  ( $20\times 20\times 0.0025\text{mm}^2\times 0.1\text{mm}$ ). This cell number was multiplied by 10,000 to give the number of cells per ml ( $1\text{cm}^3$ ).

### **2.4.2 – Millipore Muse**

The Millipore Muse cell counter contains a 532 nm green laser which stimulates the fluorescence of two deoxyribonucleic acid (DNA) dyes. One is LDS 751, and the other is propidium iodide (both from Life Technologies). LDS 751 is cell permeant, binds to the DNA of live cells and becomes fluorescent (peak emission = 543nm). Propidium iodide (peak emission = 617 nm) is cell impermeant, so only binds exposed DNA; for example: dead/ dying cells, whose plasma membranes are permeant. Thus, when cells were labelled with these dyes, all cells were LDS 751<sup>+</sup>, but only dead cells were propidium iodide<sup>+</sup>. Debris and non-nucleated cells (e.g. erythrocytes) were negative for both dyes. This, along with the cell counting ability (events/  $\mu\text{l}$ ) allowed for accurate counts of both live and dead cells (to additionally gain viability %).

The short staining protocol was as follows:

A cell aliquot (20  $\mu\text{l}$ ) was added to 80  $\mu\text{l}$  of Muse staining solution (625 ng/ml Propidium iodide, 500 ng/ml LDS 751 in phosphate buffered saline (PBS)) within a screw-cap 1.5 ml microcentrifuge tube (VWR International), and incubated at room



temperature (RT) for 10 minutes. During this incubation the Muse cell counter was turned on and cleaned as per instrument instruction. The dyed cells were counted according to instrument instruction. The total number of cells was calculated using the dilution factor (this was 5 for 20:80  $\mu$ l), total volume, and number of LDS 751<sup>+</sup> events/ $\mu$ l. Viability counted was the percentage of propidium iodide<sup>+</sup> events within the LDS 751<sup>+</sup> population. If the cells were too concentrated (this was advised by the instrument), then a set volume of dyed cells was further diluted with PBS as required. If the cells were too dilute, a 50  $\mu$ l aliquot of fresh cells were added to 50  $\mu$ l staining solution, and recounted. Note: this was the limit of cell to staining solution mix (1:1 ratio) for this stock concentration (625 ng/ml Propidium iodide, 500 ng/ml LDS 751 in PBS). However, a more concentrated stock could be formulated for very dilute cells. After counting the instrument was cleaned as per instrument instruction and switched off.

#### **2.4.3 – Haemacolor staining**

Cells ( $0.4-1.2 \times 10^5$ ) in 100  $\mu$ l PBS were centrifuged onto polylysine-coated glass slides (Fisher Scientific) using a cytopspin 3 (Thermo Scientific). The cells were air-dried for a maximum of 5 minutes, and the cells stained using the Haemacolor staining kit (Millipore). This involved fixing the cells with methanol, and subsequent staining with eosin and haematoxylin (by immersion, 30-60 seconds per step). After staining, cells were covered with 10 mm thin glass cover slips (Fisher Scientific) using 5  $\mu$ l of DPX mountant (Sigma). Cells were viewed under a light microscope, and photographs were taken using the Leica DFC 490 camera.

## 2.5 – Cell Culture

### 2.5.1 – General cell culture

Canonical volumes of complete media (see individual cell sections below) used in Nunclon delta-treated tissue culture flasks (abbreviated as T) (Thermo-Fisher Scientific) are as follows: T25 (surface area – 25 cm<sup>2</sup>)= 5 ml; T75 (75 cm<sup>2</sup>)= 20 ml; T175 (175 cm<sup>2</sup>)= 40 ml.

Subculture: As an example, a 1 in 5 subculture translates as transferring  $\frac{1}{5}$  the cells from an old flask to a new flask, and restoring the volume to canonical levels (as mentioned above) with fresh complete media. All cells were incubated/ cultured at 37 °C in a humidified incubator with 5 % CO<sub>2</sub>. For subculture of adherent cells: excess media was removed from the cells via aspiration. The cells were lifted from the flask surface by a 3 minute incubation at 37 °C with 2-10 ml (depending on flask size, see below) 0.05 % trypsin – EDTA (Life Technologies). The trypsin was inactivated by adding an equal volume of complete media to the flask, and a suitable volume of cells removed to a new flask containing 5-40 ml (depending on flask size, see above) of fresh complete media. Trypsin volumes used for various flask sizes were as follows: T25 = 2 ml; T75 = 5 ml; T175 = 10 ml.

Freezing of cell lines: Viable cells were centrifuged at 350 × g for 5 minutes, the supernatant removed by aspiration and the pellet resuspended in foetal calf serum (FCS) supplemented with 10 % (v/v) dimethylsulfoxide (DMSO). The cells were aliquoted into 1 ml cryogenic vials (VWR), placed into a ‘Mr. Frosty’ freezing container (Thermo Scientific) filled with isopropanol (Sigma), and stored at -80 °C for 2 hours (assuming a -1 °C/ minute freezing time). The cells could then be removed from the ‘Mr. Frosty’ container and stored long-term in liquid nitrogen storage (< -196 °C) or at -80 °C for up to 1 year (lower levels of viability with time).

Revival of frozen cell lines: A 1 ml aliquot of frozen cells was thawed quickly in a 37 °C water bath until only a small frozen fragment remained. These cells were then aliquoted into a 50 ml centrifuge tube containing 10 ml complete media and centrifuged at 350 × g for 5 minutes. The supernatant containing DMSO was removed and the pellet resuspended gently in 1 ml complete media. The cells were transferred to a tissue culture flask containing 10-40 ml (depending on flask size, see above) pre-

warmed complete media, the flask was rocked gently to mix, and then placed horizontally in a humid 37 °C incubator (5 % CO<sub>2</sub>).

### **2.5.2 – Culture of primary peritoneal cells**

Lavaged murine peritoneal cells (lavaged with Aim-V instead of standard lavage solution, see 2.6.5) were centrifuged at 350 × g for 5 minutes, and the supernatant aspirated with an aspirator pump. The cells were resuspended in 1ml of Aim-V and counted. The cell solution was made up to 1 × 10<sup>6</sup> cells per ml of Aim-V, and 0.5ml (0.5 × 10<sup>6</sup> cells) was aliquoted into each well of a 48 well Nunc UpCell plate (Thermo-Fisher). Cells were washed and resuspended in Aim-V media on day 1 and were cultured as required before further analysis.

### **2.5.3 – Culture of bone marrow (BM) MØs**

Complete media: Roswell Park Memorial Institute medium (RPMI) (Life Technologies) supplemented with 10 % FCS, 0.2U/μl Penicillin and 100 μg/μl Streptomycin.

An extracted femur (2.6.8) was placed in a bacterial Petri dish, submerged with 70 % ethanol and left to sterilise/wash for 1 minute. The ethanol was aspirated and the femur re-submerged in PBS, to remove excess ethanol. One end of the femur was removed carefully (to avoid shattering the bone) using forceps and a pair of scissors. A 20 ml syringe (attached to a 23 G needle) filled with complete media was used to carefully flush out the bone marrow. The bone was held with a pair of forceps (exposed lumen up) over a 50 ml centrifuge tube and the needle tip was placed gently into the exposed bone lumen, whilst slowly pushing fluid through the needle. The needle was slowly pushed all the way into the bone lumen (still slowly ejecting fluid) and moved up and down through the lumen to remove all bone marrow. The previously dark red core of the bone looked white and semi-translucent after this procedure. If there was a substantial volume of bone marrow remaining near the closed end of the bone: this end was carefully removed and the procedure repeated to remove all the bone marrow. The 50ml centrifuge tube containing bone marrow was poured into a nylon membrane filter attached to a 50ml centrifuge tube. The new tube containing filtered bone marrow cells was centrifuged at 350 × g for 5 minutes. The

pellet was resuspended gently in 1 ml ACK red blood cell lysis buffer (Life Technologies) and 9 ml PBS was added. FCS (1 ml) was drawn into a 1 ml plastic Pasteur pipette, placed into the bottom of the tube containing the PBS/lysis solution and slowly ejected to create a layer of FCS at the bottom of the tube. This layer helped separation of debris from cells. The tube was centrifuged at  $350 \times g$  for 5 minutes and the pellet washed twice with complete media: the supernatant was removed and the pellet was resuspended in 1 ml of complete media and made up to 10 ml. The tube was centrifuged at  $350 \times g$  for 5 minutes. After the last wash, the cell pellet was resuspended in 1 ml complete media supplemented with 20 ng/  $\mu$ l M-CSF, and made up to 10 ml. The cells were counted and  $1 \times 10^7$  cells were plated onto a 145 mm Petri dish ( $4 \times 10^5$  cells per ml in 25 ml total volume) using complete media supplemented with 20 ng/  $\mu$ l M-CSF. Additional complete media supplemented with 20 ng/  $\mu$ l M-CSF (10 ml) was added every three days for up to 10 days, until the cells were confluent enough to re-seed for experimentation (as in 2.9.4).

#### **2.5.4 – Culture of 293-T cells**

Complete media: Dulbecco's Modified Eagle Medium (DMEM) supplemented with 10 % FCS, 0.2U/ $\mu$ l penicillin and 100  $\mu$ g/ $\mu$ l streptomycin.

These adherent cells were sub-cultured 1 in 10 roughly every 2 days to maintain cell health. The cells were sub-cultured 1 in 20 if left for more than 2 days. These cells were never allowed to reach 100 % confluency, due to the tendency of the cells to clump/fuse.

#### **2.5.5 – Culture of M $\emptyset$ precursor cells**

Complete media: RPMI supplemented with 10 % FCS, 400 $\mu$ M L-glutamine, 0.2U/ $\mu$ l penicillin, 1  $\mu$ M Oestrogen ( $\beta$ -estradiol), 10 ng/ml GM-CSF and 100  $\mu$ g/ $\mu$ l streptomycin.

Differentiation media: RPMI supplemented with 10 % FCS, 400 $\mu$ M L-glutamine, 0.2U/ $\mu$ l penicillin, 100  $\mu$ g/ $\mu$ l streptomycin, and 20 ng/  $\mu$ l M-CSF.

These non-adherent cells were sub-cultured 1 in 10 roughly every 3 days to maintain cell health.

These cells could be differentiated into MØ: The cells were washed with RPMI three times; this involved removing the cells to a 50 ml centrifuge tube, centrifuging at  $350 \times g$  for 5 minutes, removing the supernatant by aspiration and re-suspending the pellet in 10 ml RPMI. After the last wash, the pellet was resuspended in 1 ml differentiation media and the cells counted. The cell number was adjusted to  $0.64 \times 10^6$  cells per ml with differentiation media, and 1 ml was aliquoted into each well of a 6-well plate. The cells were incubated for 4 days, with the differentiation media topped up with an extra 1 ml on day 2.

#### **2.5.6 – Culture of Jurkat-Eb.1 cells**

Complete media: RPMI supplemented with 10 % FCS, 400µM L-glutamine, 0.2U/µl penicillin and 100 µg/µl streptomycin.

These non-adherent cells were sub-cultured 1 in 5 roughly every 2 days to maintain cell health. The cells were sub-cultured 1 in 10 if left for more than 2 days.

## 2.6 – Animal work

### 2.6.1 – Animals used in this study

Most animals were housed and maintained by Cardiff University's Joint Biological Services (JBIOS) unit. C57BL/6 female mice were obtained from Harlan Olac. 129S6/SvEv mice and 129S6/SvEv.*Clec7a*<sup>-/-</sup> (Dectin1-KO) (Taylor *et al.*, 2007) were from Prof. Phil Taylor's breeding colonies. The 129S6/SvEv.CD45.1 congenic mouse strain was bred from our own colonies (a kind gift from Prof. F. Powrie, Oxford). C57BL/6.*Il4ra*<sup>-/-</sup> mice were generated by backcrossing *Il4ra*<sup>-/-</sup> (Mohrs *et al.*, 1999) onto the C57BL/6 genetic background for at least 9 generations (kindly provided by Prof. Frank Brombacher), and maintained in Edinburgh (by Dr. Steve Jenkins and Prof. Judith Allen). FoxP3-DTR-eGFP mice (Kim *et al.*, 2007) were a kind gift from Prof. Alexander Rodensky (Memorial Sloan-Kettering Cancer Center, New York). Lysozyme M Cre recombinase (Cre) 'knock-in' congenic mice on the C57BL/6 background (*Lyz2*<sup>Cre</sup>, B6.129P2-*Lyz2*<sup>tm1(cre)lfo/J</sup>) (Clausen *et al.*, 1999) and conditional 'floxed' Gata6 deficient mice (*Gata6*<sup>Fl</sup>, *Gata6*<sup>tm2.1Sad/J</sup>) (Sodhi *et al.*, 2006) were obtained from the Jackson Laboratories. Gata6-myeloid knockout (KO<sup>mye</sup>) mice (*Lyz2*<sup>+Cre</sup>*Gata6*<sup>Fl/Fl</sup>), heterozygous KO<sup>mye</sup> mice ('Het', *Lyz2*<sup>+Cre</sup>*Gata6*<sup>+/Fl</sup>) and 'wild type' (WT) littermates (*Lyz2*<sup>+/+</sup>*Gata6*<sup>Fl/Fl</sup> or *Lyz2*<sup>+/+</sup>*Gata6*<sup>+/Fl</sup>) were generated from crosses of two double heterozygous KO animals or crosses of KO animals and *Lyz2*<sup>+/+</sup>*Gata6*<sup>Fl/Fl</sup> mice, as appropriate (see figure 6.5). All animal work was conducted in accordance with Institutional and UK Home Office guidelines under the project licenses 30/2401 (2010-2012) and 30/2938 (2012-2014). All experiments were age and sex matched, unless specifically stated. For *ex vivo* culture, different strains of mice were used depending on availability, however these experiments were usually internally controlled (e.g. ± growth factor).

### 2.6.2 – Intra-peritoneal (i.p.) injection

Mice were restrained by pinching the loose skin above the neck with the thumb and side of the index finger of the left hand, holding the loose skin of the back with the two middle fingers pressed toward the palm, and by using the right hand to place the tail under the little finger of the left hand. The syringe needle (usually a 31 G, 0.5 ml insulin syringe) containing up to 500 µl of fluid was inserted into the lower left (posterior-left)

quadrant of the ventral abdomen at a 45° angle along the dorsoventral axis, when the mouse was tilted with its anterior pointed toward the table (to move the organs away from the injection point). The syringe was depressed to full, the needle removed, and the mouse returned. In the case of 4 % thioglycollate broth, a 27 gauge (G) needle in conjunction with a 2 ml syringe was used.

Substances injected intra-peritoneally were: 100/ 200 µl zymosan in PBS ( $2 \times 10^{6-7}$  particles) (Life technologies); 1ml 4 % Brewer's thioglycollate broth (Sigma); 400 µl EdU in PBS (1 mg) (Life Technologies); αM-CSF, αIL-4 and IgG control (0.4 mg) in PBS (produced in house (no BSA) and from Bio X Cell (0.05 % BSA)); recombinant M-CSF (0.4 µg) in PBS containing 0.05 % BSA (Peprotech); and peritoneal/ BM cells (up to  $1 \times 10^6$  in up to 500 µl PBS). Additionally, lentiviral particles were injected; this was typically between 200-400 µl of 10-15 × concentrated lentivirus (see 2.9.2) in PBS or AimV media (Life Technologies).

### **2.6.3 – Sub-cutaneous (s.c.) injection**

Mice were restrained by pinching the loose skin above the neck with the thumb and side of the index finger of the left hand, holding the loose skin of the back with the two middle fingers pressed toward the palm, and by using the right hand to place the tail under the little finger of the left hand. The syringe needle (31 G, 0.5ml insulin syringe) containing 400 µl EdU (1 mg) (Life Technologies) was inserted inside the loose skin of the posterior left of the abdomen (above the hip joint) at a shallow <45° angle along the dorsoventral axis. The syringe was depressed to full, the needle removed, and the mouse returned.

### **2.6.4 – Genotyping**

A mouse ear disc (obtained using an ear punch – performed by JBIOS staff for genotyping purposes) was placed into a 1.5 ml microcentrifuge tube containing 50 µl of lysis buffer (100 mM Tris (pH 8.5), 5mM ethylenediaminetetraacetic acid (EDTA), 0.2 % sodium dodecylsulphate (SDS) (w/v), 200 mM NaCl, 100 µg/ ml proteinase K – all from Sigma). The ear disc was submerged and the tube incubated at 50 °C for 1 hour (h) at 1200 revolutions per minute (rpm) in a shaking microcentrifuge tube heat block

(or 50 °C overnight with no revolutions). The reaction was terminated by incubation at 72 °C for 15 minutes. The samples were diluted with 400 µl of clean deionised H<sub>2</sub>O (dH<sub>2</sub>O) to reduce the concentration of SDS. These samples could then be used in a polymerase chain reaction (PCR) (as in 2.8.5) at 0.8 µl per 20 µl reaction. The primers used are listed below.

Cre F: CAGGCATGCTTTCTCTAGTCAG, R: TGATCCTGGCAATTTCCGGCT.

Gata6-Loxp: F: GTGGTTGTAAGGCGGTTTGT, R: ACGCGAGCTCCAGAAAAAGT.

Lyz2-Cre: Cre-F: CCCAGAAATGCCAGATTACG,

Lyz2-F: TTACAGTCGGCCAGGCTGAC, R: CTTGGGCTGCCAGAATTTCTC.

Note: the Lyz2-Cre primer set was used for identification of *Lyz2*-Cre heterozygous/homozygous mice during early breeding (*figure 6.5*). However, the newer Cre primers were used to assess the presence of Cre in *Gata6*-KO<sup>mye</sup> mice. These new primers were more efficient than the old when identifying Cre in genomic PCR.

### **2.6.5 – Peritoneal lavage**

Mice were sacrificed in accordance with schedule one procedure (rising CO<sub>2</sub> concentration, followed by careful cervical dislocation to confirm death). The cadaver was turned upon its back, the loose skin of the abdomen was pinched together, and a sharp pair of scissors was used to cut a small incision in the skin at an upward 45° angle along the dorso-ventral axis (care was taken not to pierce the abdominal wall). The loose skin was then torn toward the hips (at a ≈45° angle along the left-right axis) on both sides to expose the abdominal wall (care was taken to avoid the navel, a weak point in the abdominal wall). A 5ml syringe containing 5ml of lavage solution (PBS + 5mM EDTA) was loaded with a 21 G hypodermic needle. The needle was inserted into the peritoneal cavity at a low (≈20°) angle along the dorso-ventral axis (the bevelled tip pointing up), care was taken to avoid the intestines and blood vessels in the peritoneal wall. The needle was then rotated around 180° so that the bevelled tip pointed down. A small volume of solution was injected to give the needle room, then the angle of the needle was increased to 45-75° and the syringe depressed quickly to mix the peritoneum with all the lavage solution. The needle-syringe joint was held while



depressing the syringe to avoid separation, care was taken to keep the tip of the needle in the cavity, but not contact organs, such as the liver (which would result in bleeding). The peritoneal cavity was gently massaged with a finger and thumb to suspend the maximum number of cells. The needle was pulled left toward the user along the left-right axis and up against the peritoneal wall (making sure the bevel was still pointed toward the peritoneal cavity), the lavage solution was slowly drawn back up into the pipette, avoiding the intestines and fat. While drawing the liquid, the intestines were pushed back from the needle point with a finger to create a pocket of lavage fluid, which could be drawn off more efficiently. In the case of abdominal fat accidentally entering the needle, the needle was withdrawn from the entry site, whilst still drawing the syringe to block the entry site with the abdominal fat. A new site was selected to withdraw the remaining fluid. The needle was removed from the cavity when most ( $\approx 4$ -4.5ml assuming no leakage) of the fluid was removed. The needle was then carefully removed from the syringe and disposed of. The fluid inside the syringe was ejected slowly into a 15ml centrifuge tube on ice. The freshly lavaged cells were stored on ice up to 5 hours before use if necessary (the smallest incubation time possible was preferable).

#### **2.6.6 – Pleural lavage**

Mice were sacrificed in accordance with schedule one procedure (rising CO<sup>2</sup> concentration, followed by careful cervical dislocation to confirm death). The cadaver was turned upon its back, the loose skin of the abdomen was pinched together, and a sharp pair of scissors was used to cut a small incision in the skin at an upward 45° angle along the dorsoventral axis (care was taken not to pierce the abdominal wall). The loose skin was torn toward the hips (at a  $\approx 45^\circ$  angle along the left-right axis) on both sides to expose the abdominal wall, then upward toward the thorax to expose the entire ribcage. A 2ml syringe containing 2ml of lavage solution (PBS + 5mM EDTA) was loaded with a 21G hypodermic needle. The needle was inserted into the pleural cavity at a low ( $\approx 20^\circ$ ) angle along the dorsoventral axis (the bevelled tip pointing up) between the lower two ribs, care was taken to avoid piercing the lungs and blood vessels in the pleural wall. The needle was then rotated around 180° so that the bevelled tip pointed down. The syringe was depressed quickly to mix the pleural contents with lavage

solution (the needle-syringe joint was held while depressing the syringe to avoid separation and care was taken to keep the tip of the needle in the cavity). The pleural cavity was tapped roughly with an index finger to suspend the maximum number of cells. The lavage solution was then slowly drawn back up into the pipette, with a slight movement of the needle if no liquid came out. The needle was removed from the cavity when most ( $\approx 1.5$  ml assuming no leakage) of the fluid was removed. The needle was then carefully removed from the syringe and disposed of. The fluid inside the syringe was ejected slowly into a 15ml centrifuge tube on ice. The freshly lavaged cells were stored on ice up to 5 hours before use if necessary (the smallest incubation time possible was preferable).

### **2.6.7 – Adoptive transfer**

Cells were lavaged (see 2.6.5, but using 1ml of lavage fluid) from CD45.1 129S6/SvEv congenic mice, counted (see 2.4) and injected intra-peritoneally (see 2.6.2) into CD45.2 129S6/SvEv congenic mice. Typically, 200-400  $\mu$ l of lavage fluid was transferred (between  $2 \cdot 10^5$  to  $10^6$  cells).

For adoptive transfer of BMM $\emptyset$ : BMM $\emptyset$ s were cultured from femur bone marrow, and transduced with lentivirus (see 2.5.3 and 2.9.4). The media was aspirated from the cells, and the cells washed three times with PBS (aspirating after each wash). PBS (1 ml) was added to each well and the transduced cells removed from the plate with a cell scraper. The cells were gently mixed by pipetting, and counted (see 2.4). Typically,  $1 \cdot 10^5$  to  $2 \cdot 10^5$  cells were transferred in a volume of 200-400  $\mu$ l. An aliquot of cells was kept for flow cytometric analysis and calculation of transfection efficiency (see 2.7).

### **2.6.8 – Femur extraction**

Mice were sacrificed in accordance with schedule one procedure (rising CO<sub>2</sub> concentration, followed by careful cervical dislocation to confirm death). The cadaver was turned upon its back, the loose skin of the abdomen was pinched together, and a sharp pair of scissors was used to cut a small incision in the skin at an upward 45° angle along the dorsoventral axis (care was taken not to pierce the abdominal wall). The loose skin was torn toward the hips (at a  $\approx 45^\circ$  angle along the left-right axis) on both

sides to expose the abdominal wall, then toward both legs to expose the thigh muscles. A pair of sharp scissors was inserted between the femur and muscle (the scissor tip can be used to locate the bone) on the dorsal side of the upper leg and pushed through to the table. The scissors were slowly but forcibly opened (downward pressure toward the table) using the right hand; with the left hand index finger holding the mouse's knee and the thumb holding the left flank of the mouse. This process either removed the bone from the knee or hip joint. If the femur was removed from the hip: the femur was dislocated from the knee joint by bending in the opposite way from the normal range of movement. If the femur was removed from the knee: the femur was held between finger and thumb and pulled away from the hip joint, using a sharp scissors to remove excess ligaments and tissue. In both cases, excess muscle was removed with a scissors, and the bone dried with tissue. The femur was finally placed in ice cold PBS for further processing (see 2.5.3).

## 2.7 – Flow Cytometry

### 2.7.1 – Total cell staining

Lavaged murine peritoneal cells were counted with a bright line haemocytometer (2.4.1), and the cells were aliquoted into a fresh 15 ml centrifuge tube. An equal volume of 2 % (v/v) formaldehyde solution in PBS was added to give a final concentration of 1 % (v/v) formaldehyde. This solution was stored for 20 minutes on ice to fix the cells. The tubes containing the cell suspension were centrifuged in a swivel rotor desktop centrifuge at  $350 \times g$  for 5 minutes at room temperature to pellet the cells (all subsequent centrifugations are performed at the same speed and time). The supernatant was removed by inverting the tube and blotting excess liquid with tissue. The pellet was resuspended in wash solution (PBS with 0.5 % (w/v) bovine serum albumin (BSA), 0.5 % (w/v) saponin, 5 mM EDTA and 2 mM sodium azide) to give a concentration of  $2 \times 10^7$  cells/ml, and 100  $\mu$ l of this was aliquoted to a well of a v-bottom 96-well plate. This plate was centrifuged to pellet the cells. The supernatant was aspirated with a multi-channel pipette. The pellet was resuspended in 30  $\mu$ l of block solution (wash supplemented with 5 % (v/v) rabbit serum and 4  $\mu$ g/ml rat anti-mouse Fc $\gamma$ RII/III (2.4G2)). The cells were incubated for 15 minutes on ice, in the dark. Antibody mixes were formulated (*see table 2.1*) and 20  $\mu$ l was added to the 30  $\mu$ l block/cell solution to achieve a 1  $\times$  working concentration in 50  $\mu$ l total staining volume. If no secondary (e.g. biotin-streptavidin) step was required, then dyes such as DAPI were added to the antibody mix at this stage. This mixture was incubated on ice for 1 hour in the dark. The plate was centrifuged and the supernatant removed. The cells were washed: the plate was centrifuged, the supernatant removed and pellet was resuspended in 150  $\mu$ l wash solution, the plate was centrifuged again and the supernatant aspirated (this was repeated twice). If a biotin-conjugated antibody was used, then the cells were resuspended in 50  $\mu$ l wash containing 2  $\mu$ g/ml of streptavidin-linked fluorochrome. If a DNA dye (e.g. DAPI) was required, it was added to this mixture. This solution was incubated on ice for 30 minutes in the dark. The cells were washed three times as described above, and the pellets resuspended in 150  $\mu$ l wash. The cell solution (150  $\mu$ l) was transferred by pipette into a labelled microtitre tube. To dilute the sample: 150  $\mu$ l of wash solution or 25  $\mu$ g/ml of Draq5 (if required) in wash was added (Draq5 was incubated for 20 minutes at room temperature). The

microtitre tube was inserted into a 5 ml polypropylene tube and the sample was analysed using the Beckman-Coulter Cyan-ADP (9 colour) flow cytometer.

### **2.7.2 – Use of nuclear isolation media (NIM)-DAPI for flow cytometry**

NIM-DAPI (Beckman-Coulter) was used to lyse the adherent cells, and release the nuclei (whilst staining with DAPI). NIM DAPI (400  $\mu$ l) was added to the wells and scraped with a cell scraper to aid in cell lysis and recovery of nuclei. Cells were suspended and mixed by pipetting before incubation for 30 minutes at 4 °C in the dark. After incubation and mixing, only 350  $\mu$ l of lysate was removed, which allowed for accurate nuclei numbers to be assessed (1.1429 times more than counted). The 350  $\mu$ l lysate was transferred to a microtitre tube containing 5  $\mu$ l cell counting beads (Beckman-Coulter) (approximately 5000 beads). This was mixed thoroughly with a pipette before analysing on a Cyan-ADP (9 colour) flow cytometer. The nuclei (DAPI<sup>+</sup>) were counted alongside beads (fluorescent in all channels, however red channels were used), and an equation was used to calculate total DAPI<sup>+</sup> nuclei: (bead count/ bead total)  $\times$  nuclei count = nuclei in 350  $\mu$ l, nuclei in 350  $\mu$ l  $\times$  1.1429 = total nuclei in well. Due to the analysis of individual nuclei, the complicating effects of non cell cycle-associated DNA content were avoided (see chapter 3 of this thesis).

### **2.7.3 – Flow cytometric cell sorting**

Cells were resuspended at  $2 \times 10^7$  cells/ ml in ice cold wash solution without NaN<sub>3</sub> (PBS with 0.5 % (w/v) BSA and 5 mM EDTA) supplemented with 5 % (v/v) rabbit serum and 4  $\mu$ g/ ml rat anti-mouse Fc $\gamma$ RII/III (2.4G2). The cells were incubated on ice for 20 minutes. Fluorescent antibodies (see table 2.1) were added directly to the cell block solution, which was gently pipetted to mix. This was incubated for 30 minutes on ice in the dark. The cells were centrifuged at  $350 \times g$  for 5 minutes at 4 °C, the supernatant removed by inversion and blotting with tissue, and the cells resuspended to  $20 \times 10^6$  cells/ ml in ice cold wash solution to wash. This step was repeated to wash the cells a second time. The cells were then transferred to either a 15 ml centrifuge tube (FACSAria III) or 10 ml polypropylene tube (MoFlo legacy), both were pre-blocked with FCS to limit unwanted cell adherence. The cells were sorted using the MoFlo legacy,

and FACS Aria III as per instruments instruction. An example of cell sort gating is shown in figure 2.1. Cells were collected from the MoFlo legend in a 10 ml polypropylene tube stored on ice. The cells were kept cold in the FACS Aria III by using the inbuilt refrigeration system, and collected in a 15 ml centrifuge tube. Purities were typically 90-98 %.

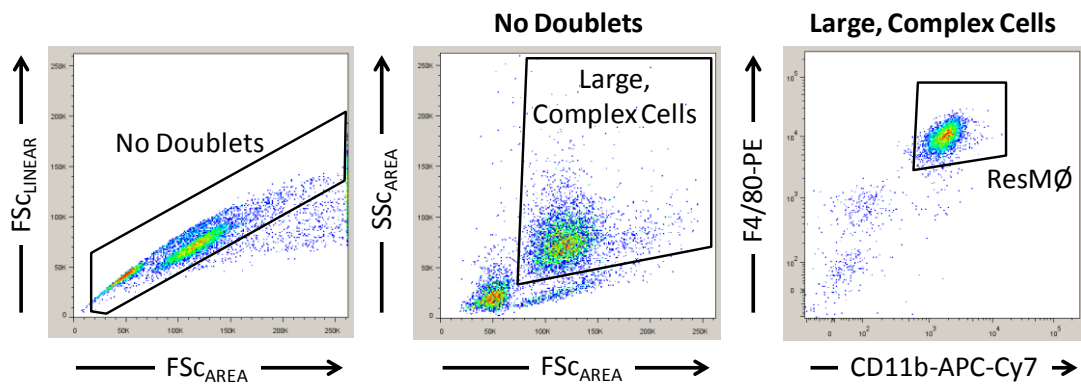


**Figure 2.1. Example of gating in flow cytometric cell sorting**

Example density plots showing pooled cells stained with F4/80 and CD11b from the peritoneal cavities of 5 male 129S6/SvEv mice. The plots show sequential gating from the left to right, and this was used to charge droplets containing ResMØs for sorting on the MoFlo legacy.

## **2.8 – Lentiviral vector cloning**

The pHR'SIN-cPPT-**SEW** (Demaison *et al.*, 2002) plasmid and an eGFP deficient version (pHR'SIN-cPPT-**SXW**) were kindly provided by Dr. Paul Brennan.

### **2.8.1 – Primer design**

In-fusion cloning primers (ordered from Sigma) (table 2.2) were designed to include a 15 base pair (bp) region which overlapped with the regions flanking the restriction endonuclease digestion site in the vector sequence. These primers were used to amplify target genes for expression vectors by PCR, or dimerised (forward and reverse) for short hairpin (sh) ribonucleic acid (RNA) constructs by heating to 98 °C for 5 minutes and then slowly cooling to RT. The new templates formed were gel purified (see 2.8.3), and used in in-fusion cloning in conjunction with restricted starting vectors, to produce new vectors (see 2.8.6).

Starting Plasmid	Restriction	New Plasmid	Primer Pairs / Synthetic templates
SXW	<i>Xho</i> I	GATA6	PCR F: GGATCCCGGGCTCGAGCCACCATGTACCAGACCCTCGCC PCR R: TACCAGGCCTCTCGAGTCAGGCCAGGGCCAGAGCA
		GATA6-Myc	PCR F: GGATCCCGGGCTCGAGCCACCATGTACCAGACCCTCGCC PCR R: TACCAGGCCTCTCGAGTTACAGATCTTCTTCAGAAATAAG TTTTGTTCGGCCAGGGCCAGAGC
		Cre-Myc	PCR F: GGATCCCGGGCTCGAGCCACCATGTCCAATTTACTGACC PCR R: TACCAGGCCTCTCGAGTCACAAGTCTTCTTC
	<i>Mlu</i> I	T2A-rCD2 Intermediate	PCR F: : GCCTGGTACCACGCGTCTCGAGAGCGGCAGCGG PCR R: TCGCGGCCGCACGCGTTTACCGTTTTTCTCTTGCA
		T2A-rCD2 Intermediate	F: GGATCCCGGGCTCGACCACCATGCTCGAGAGCGGCAGC R: GCTGCCGCTCTCGAGCATGGTGGTTCGAGCCGGGATCC
	T2A-rCD2	<i>Xho</i> I	Gata6-T2A-rCD2
Cre-rCD2			PCR F: GCTTGATATCGAATTCGATCCGACGCCCATCTCT PCR R: GGGGCTGCAGGAATTCGTTTAAACAAGGCTTTTCTCAA GGG
SEW or T2A-rCD2	<i>Eco</i> RI	U6 (eGFP or T2A-rCD2)	PCR F: GCTTGATATCGAATTCGATCCGACGCCCATCTCT PCR R: GGGGCTGCAGGAATTCGTTTAAACAAGGCTTTTCTCAA GGG
U6 (eGFP or T2A-rCD2)	<i>Pme</i> I	ICAM-1 shRNA (eGFP)	F: AGAAAAGCCTTGTTTGACGCTGACTTCATTCTCTATTCTCG AGAATAGAGAATGAAGTCAGCGTCTTTTTCGTTTAAACGA ATTCCTGCA R: TGCAGGAATTCGTTTAAACGAAAAAGACGCTGACTTCATT CTCTATTCTCGAGAATAGAGAATGAAGTCAGCGTCAAAC AAGGCTTTTCT
		Non-Silencing shRNA (eGFP or T2A-rCD2)	F: AGAAAAGCCTTGTTTGTCTCGCTTGGGCGAGAGTAAGTA GTGAAGCCACAGATGTACTTACTCTCGCCCAAGCGAGAC TTTTTCGTTTAAACGAATTCCTGCA R: TGCAGGAATTCGTTTAAACGAAAAAGTCTCGCTTGGGCG AGAGTAAGTACATCTGTGGCTTCACTACTTACTCTCGCCC



			AAGCGAGACAAACAAGGCTTTTCT
		Gata6 shRNA (T2A-rCD2)	F: AGAAAAGCCTTGTTTGCCACTACCTTATGGCGTAGAACTC GAGTTCTACGCCATAAGGTAGTGGCTTTTTGTTAAACGA ATTCCTGCA
			R: TGCAGGAATTCGTTTAAACAAAAGCCACTACCTTATGGC GTAGAACTCGAGTTCTACGCCATAAGGTAGTGGCAAACA AGGCTTTTCT

**Table 2.2. In-fusion cloning primers**

Table showing in-fusion cloning primers and the vectors/ restriction endonucleases used to produce new vectors. (Cre = Cre, F = forward oligonucleotide, R = reverse oligonucleotide, PCR = polymerase chain reaction primer).

### 2.8.2 – Restriction endonuclease digestions

Plasmids were cut by restriction endonucleases (NEB) using the appropriate buffer at 37°C for 1 hour. Reactions were terminated by heating to 65°C for 20 minutes. Enzymes used were: *Xho* I, *Mlu* I, *Eco* RI and *Pme* I. Cut vectors were brought out of aqueous solution by adding 0.7 volumes of isopropanol and purified using columns from the QIAquick gel extraction kit (Qiagen) (see 2.8.4).

### 2.8.3 – Agarose gel electrophoresis (AGE)

Agarose powder (Sigma) was added to 0.5 × Tris-Borate EDTA (TBE) solution (Life Technologies) in an autoclave flask (1-2 % (w/v) agarose). The powder was dissolved by heating the solution in a microwave until boiling. This hot gel was left until cool enough to hold without scalding, but not to set. Ethidium bromide (100ng/ml) (Life Technologies) was added before the gel was poured into a gel caster with well moulds. Larger wells were created by placing tape over and between the wells. The gel was left to cool until set. This gel could be stored at 4°C for up to 48 hours. Additional agarose (without ethidium bromide) can be stored at room temperature and re-melted when required. The agarose gel was submerged in a gel tank filled with 0.5 × TBE. DNA loading dye (6 ×) (Promega) was added to the samples to achieve a final concentration of 1 × DNA loading dye. Up to 150 µl of sample was loaded into the wells via gentle pipetting. DNA ladders were loaded into an adjacent well to measure the size of the

DNA bands: 5-10  $\mu$ l of 1kB (kilo base pair) (Invitrogen) or 100bp (base pair) (Promega) ladder was used. The gel was run at 100 volts for 30 minutes to separate DNA bands from contaminants and non-specific products. The gel was viewed under UV (ultraviolet) light where photographs were taken with the Auto-Chemi Darkroom Imaging System (UVP).

#### **2.8.4 – Gel extraction and DNA purification**

Gels were viewed on a UV transilluminator and targeted bands were dissected using a scalpel blade (this was carried out on separate sheets of saran wrap (VWR) to minimise contamination). The gel bands were deposited in pre-weighed 2ml microcentrifuge tubes, and weighed again; the new weight was used to calculate the mass of the gel. This mass was needed to perform DNA purification using the QIAquick gel extraction kit (Qiagen). This was used as per manufacturer's instructions: The gel was dissolved and bound to a column membrane, this membrane was washed with ethanol to remove impurities and then the DNA was eluted with water. DNA concentration was measured using the Nanodrop spectrophotometer (this equipment calculates DNA concentration based on the equation: optical density at 260nm  $\times$  50 ng/  $\mu$ l (constant) = ng/  $\mu$ l of DNA). The kit was also used to purify DNA from a solution, by adding 0.7 volumes of isopropanol (Thermo-Fisher) to the solution, and followed by binding the sample to the column membrane. DNA was stored at -20°C.

#### **2.8.5 – Polymerase chain reaction (PCR)**

PCRs were performed using a Peltier Thermal Cycler (PCT-200); the programme is shown in table 2.3 and was used unless otherwise stated. DNA was stored at -20°C.

Step	Process	Temperature (°C)	Time	Cycle
1	Initial denaturisation/ Hot-start	98	5 minutes	
2	Denaturisation	98	30 seconds	
3	Annealing	60	30 seconds	
4	Extension	72	30 seconds per Kb	to step 2, × 30
5	Final extension	72	10 minutes	
6	Resting	4	∞	

**Table 2.3. The PCR programme**

A table showing the times and temperatures of a PCR reaction, the programme cycled from step 2-4 thirty times. The extension step was 30 seconds per Kb of the PCR product.

GoTaq green polymerase (Promega) was used for conventional PCR reaction mixes, and the reaction mix was as follows: 1× Buffer (MgCl<sub>2</sub> final made up to 2.5 mM), 250-500nM primers, 200nM of each dNTP, 0.05 Units/μl GoTaq DNA polymerase. The final volume was 20 μl per reaction.

The Advantage High Fidelity or High Fidelity-2 kit (Clontech) was used for higher quality proofreading PCR. The reaction mix is as follows: 1 x Buffer, 250-500 nM primers, 1 × dNTP, 1 × Advantage High Fidelity or High Fidelity-2 DNA polymerase mix. The final volume was 50 μl per reaction. Three reactions were pooled after the PCR to obtain the necessary mass of product needed for efficient purification (150 μl). The DNA polymerase mix contained Titanium Taq, which works over a broad range of MgCl<sub>2</sub> concentrations, the kit did not disclose MgCl<sub>2</sub> concentration; it was however optimised for high fidelity.

### 2.8.6 – In-fusion cloning

Cut vector (100 ng) was mixed with insert (50 ng) in 0.2 ml 8-strip tubes (STAR laboratories), and the total volume was made up to 4 μl with water. The In-fusion cloning reaction component (1 μl) (Clontech) was mixed into the solution by pipetting. The tubes were placed in a PTC-200 thermal cycler, and incubated at 50°C for 15 minutes for the recombination reaction. The solutions were diluted by adding 20 μl of water and could be stored at -20°C.

### **2.8.7 – *Escherichia coli* (*E. coli*) transformation via heat shock**

Lysogeny broth (LB) Agar (Sigma) was formulated according to manufacturer's instructions; this involved adding agar tablets to water inside an autoclave flask, and autoclaving to sterilise and dissolve the tablets. The agar could be stored at room temperature for up to a year.

A 50 µl vial of one-shot Top10 competent *E. coli* cells (Life Technologies) was defrosted on ice for 15 minutes, and a vial of sterile super optimal broth with catabolite repression (SOC) (Life Technologies) was placed in a 37°C water bath. During this time, 1 µl of the diluted In-fusion reaction solution (from 2.8.6) was aliquoted into 0.2 ml 8-strip tubes (STAR laboratories). An aliquot (10-50 µl) of defrosted *E. coli* was mixed with the 1 µl solution and was incubated on ice for 30 minutes. The tubes were placed into a ready PTC-200 thermal cycler set at 42°C and held for exactly 30 seconds before transferring them directly back to the ice. The pre-warmed SOC media (100-200 µl) was added to the transformed cells before incubating in a shaking incubator (200 rpm) at 37°C for 1 hour. The tubes were adhered to a rack which was subsequently adhered to the floor of the shaker to promote maximal motion.

During this incubation, the previously made agar solution was re-melted in a microwave and left until cool enough to hold without scalding, but not left to re-set. Ampicillin (100 µg/ ml) was added to the warm agar, and mixed well. The agar (≈20 ml) was poured into 85 mm Petri dishes (Thermo-Fisher) and left to set at RT.

A range (10-100 µl) of transformed cells in SOC media was aliquoted onto separate agar plates and the liquid culture spread out on the agar using a plate spreader (Thermo-Fisher). The plates were then inverted (to prevent condensation) and incubated at 37°C for 12-18 hours. Plates were selected which had separate colonies and these could be stored at 4 °C for up to 1 month.

### **2.8.8 – *E. coli* culture**

LB broth was formulated according to manufacturer's instructions; this involved adding LB tablets to water inside an autoclave flask, and autoclaving to sterilise and dissolve the tablets. The LB broth could be stored at room temperature for up to a year.

A selected *E. coli* colony was touched gently with the end of a pipette tip (10/200 µl), and this tip was ejected into LB broth with ampicillin (100 µg/ ml). Larger volumes were used for plasmid Maxi kits (200 ml) and Midi kits (100ml) in autoclaved 1 L conical flasks, and smaller volumes were used for Mini kits (10ml) in 50 ml centrifuge tubes. These cultures were secured and incubated at 37°C for 18 hours in a shaking incubator (225 rpm). The lids of the centrifuge tubes were left loose, i.e. not screwed down, but loosely taped on, to allow air to enter the tubes. A loose fitting foil was placed over the top of the conical flasks.

The large cultures were poured into 500 ml centrifuge flasks and the small cultures kept in their 50 ml centrifuge tubes. These were centrifuged at 3800 × g for 15 minutes at 4°C, to pellet the cells. The supernatant was poured off and disposed of; the pellet could be stored at -80°C if not used immediately (see below, 2.8.9).

### **2.8.9 – Plasmid DNA extraction**

Qiagen Maxi, Midi and Mini plasmid prep kits were used to extract plasmid DNA from *E. coli*. The kits were used as per manufacturer's instructions: The cell pellets were resuspended and lysed to release plasmid DNA, this was halted after 5 minutes to minimise contamination from bacterial DNA. The solution was centrifuged or sent through a filter to remove the protein-SDS aggregate from the lysate. The supernatant or eluate was placed onto a membrane to bind the DNA, which was then washed with ethanol. The DNA was eluted with water or elution buffer. For the larger kits this eluate was concentrated using isopropanol, then washed with ethanol and the DNA pellet partially dried (the tubes were left inverted over clean tissue for 5-10 minutes) and resuspended in water. DNA concentration was measured using the Nanodrop spectrophotometer (see end of section 2.8.4). DNA was stored at -20°C.

### 2.8.10 – DNA sequencing and validation

DNA sequencing was carried out by Cardiff University Central Biotechnology Services (CBS). A primer (3.2 µl of a 1 µM solution) (see table 2.4) and 300 ng of vector or PCR product was needed per sequence read. The Chromas Lite software (Technelysium) was used to view sequence data and BLAST (basic local alignment search tool) (National Library of Medicine) was used to align and compare sequences. The algorithm parameters were always adjusted to remove the filter for low complexity regions.

Name	Sequence
SXW <i>Eco</i> RI Forward	GGTACAGTGCAGGGGAAAGA
SXW <i>Eco</i> RI Reverse	CAAACCTACAGGTGGGGTCT
SXW <i>Xho</i> I Forward	CTCTATAAAAGAGCTCACAACC
SXW <i>Xho</i> I Reverse	GGGCCACAACCTCCTCATAAA
Pre-trCD2 Reverse	AGACGGTCCCACTGTCTCTG
eGFP Sequencing Forward	AGGACGACGGCAACTACAAG
eGFP Sequencing Reverse	CGATGTTGTGGCGGATCTTG
Gata6 Sequencing Forward	GTGATGTCTGCAGTGGGAGA

**Table 2.4. Sequencing primers**

Table showing the sequences of primers used for DNA sequencing.

## **2.9 – Viral particle production**

### **2.9.1 – Transfection**

Confluent 293-T cells were trypsinised and counted (See 2.5.4). Complete media (10 ml) was aliquoted into T75 tissue culture flasks followed by  $1.8 \times 10^6$  cells. The flasks were rocked gently whilst still vertical, then on the horizontal plane to mix well and ensure maximal seeding efficiency (care was taken not to get any fluid in the lid). The cells were incubated for 24 hours at 37°C. The supernatant was aspirated from the cells, and the cells were washed with 5 ml PBS: the PBS was added and gently rocked over the cells followed by aspiration; and then 12 ml of fresh complete media was added. The flask was briefly placed back into the incubator (37°C).

Cells were transfected using the Effectene transfection kit (Qiagen): The lentiviral plasmid (1µg) was mixed with the pCMVΔ8.91 (750ng) and pMD2G (500ng) plasmid, and this solution was made up to 300 µl with condensation buffer EC. Enhancer (18 µl) was added to the buffer EC-DNA mix, vortexed briefly and left at room temperature for 5 minutes to condense the DNA. Effectene transfection reagent (60 µl) was added and the solution vortexed for 10 seconds; this was left to incubate at room temperature for 10 minutes to form micelle complexes around the condensed DNA. This solution was gently transferred to a 15 ml centrifuge tube containing 2.622 ml of complete media (to make 3 ml total volume), mixed gently with a 5 ml pipette and then added carefully to the flask containing 12 ml media on the cells to bring the total to 15 ml. This flask was rocked gently first vertically then on the horizontal plane to mix and ensure complete coverage of the flask. The flask was incubated at 37°C for 48 hours. The cell supernatant was transferred via pipette into a 50 ml centrifuge tube and centrifuged at  $500 \times g$  for 10 minutes to remove cells and large cell debris. This new supernatant (15 ml) was removed to a fresh 50 ml centrifuge tube and either stored at -80°C or concentrated (see 2.9.2).

### **2.9.2 – Viral particle concentration**

The supernatant (15 ml) from above (2.9.1) was carefully poured into a 50 ml centrifuge tube containing 5 ml of Lenti-X concentrator solution (Clontech), the lid was closed and the tube inverted to mix. This step could have been doubled up within the

same tube (i.e. two flasks: 30 ml supernatant with 10 ml concentrator). This new solution was stored at 4°C for 2-24 hours (until the solution was thoroughly cooled) to enable binding of concentrator particles. The tube was centrifuged at 1500 × g for 45 minutes at 4°C to pellet the virus/ concentrator. The supernatant was poured off carefully and the pellet resuspended gently in 1ml Aim-V media (Life Technologies) or PBS and stored at -80°C. This process resulted in a 15-fold increase in viral concentration. Lentivirus resuspended in Aim-V media could be used on cells in culture without dilution of the media and caused no significant inflammation when injected into mice (quantified by numbers of inflammatory cells, e.g. neutrophils, when compared to injection of PBS).

### **2.9.3 – Multiplicity of infection (MOI) calculations**

The MOI of tagged (usually eGFP) lentiviruses was quantified using Jurkat cells and Poisson distribution (Zhou *et al.*, 2003, Fehse *et al.*, 2004). The number of Jurkat cells (see 2.5.6) seeded with a titrated volume (0-250 µl) of concentrated virus with complete media was kept constant:  $0.3 \times 10^6$  cells in 250 µl total volume were aliquoted into each well of a 24-well plate. The plates were incubated at 37 °C in a humidified incubator. Cells were topped up with an additional 500 µl complete media (see 2.5.6) on day 1. The experiment was terminated on day 2 by pipetting an equal volume of 2 % formaldehyde (Sigma) into the wells and mixing gently. This was left for 20 minutes at RT, to fix cells and virus. Cells were then analysed using flow cytometry and the percentage of infected cells calculated. A standard curve of Poisson distribution (probability of infection distribution) was used to calculate MOI based on the percentage of cells infected. These MOI values were for individual volumes of concentrated virus used; therefore an average MOI per µl of concentrated virus was formulated. The average MOI per µl could be used to calculate the number of viral particles per µl, by dividing the starting number of cells ( $0.3 \times 10^6$ ) by MOI. However, this value does not take into consideration the number of newly generated Jurkat cells during the 2 day incubation (which could have been  $>0.9 \times 10^6$ ) or the infection efficiency. Therefore the MOI per µl was only used to relatively compare viral titres.



#### **2.9.4 – Use of lentiviral particles in culture**

Jurkat cells ( $0.3 \times 10^6$ ) in a volume of 150  $\mu$ l of complete media were aliquoted into wells of a 24-well plate. Dilutions of concentrated virus (in Aim-V media) were added to the wells (100  $\mu$ l total volume), and the plates incubated at 37°C for 72 hours. The viral media was topped up with 500  $\mu$ l every 24 hours. After the 72 hour incubation, cells could then be set up for continued culture (see 2.5.6).

Bone marrow M $\phi$ s (see 2.5.3) were plated into wells of a 6 well plate ( $0.6 \times 10^6$  cells in 1ml complete media supplemented with 20 ng/ $\mu$ l M-CSF), and incubated for 24 hours at 37°C. The media was aspirated, and 750  $\mu$ l complete media supplemented with 20 ng/ $\mu$ l M-CSF was aliquoted onto the cells. Virus (250  $\mu$ l of  $10 \times$  concentrate) was added gently to the wells, and the plate incubated for 5 days at 37°C. Media (500  $\mu$ l) was added to wells every 24 hours.

Lavaged murine peritoneal cells (lavaged with Aim-V instead of lavage solution, see 2.6.5) were centrifuged at  $350 \times g$  for 5 minutes, and the supernatant aspirated with an aspirator pump. The cells were resuspended in 1ml of Aim-V and counted. The cell solution was made up to  $2 \times 10^6$  cells per ml of Aim-V; and 0.25ml ( $0.5 \times 10^6$  cells) was aliquoted into each well of a 48 well Nunc UpCell plate (Thermo-Fisher), containing 0.25ml of concentrated lentiviral particles (see 2.9.2). The cells were topped up with 0.5 ml fresh complete media after 24 hours, and then every 48 hours. The cells were usually analysed 3-5 days after initial culture.

## 2.10 – Real-time PCR

### 2.10.1 – RNA extraction

The RNeasy mini and micro kits with or without optional on-column deoxyribonuclease digestion were used to extract RNA (Qiagen). In brief: Cells were lysed to free nucleic acids, which were brought out of solution with ethanol and bound to a membrane. The nucleic acids were washed to remove chromatin contaminants (with or without an optional deoxyribonuclease digestion), and then contaminating salts were washed away with ethanol. Finally, the ethanol was removed and the RNA eluted with ribonuclease-free dH<sub>2</sub>O (Life Technologies).

RNA concentration was measured using the Nanodrop spectrophotometer (Thermo Scientific) as per manufacturer's instruction. This equipment calculates RNA concentration based on the equation: optical density at 260 nm × 40 ng/ μl (constant) = ng/ μl of RNA.

### 2.10.2 – Reverse transcription

cDNA was synthesised using the reverse transcription kit (Primer Design) or the high capacity cDNA reverse transcription kit (Life technologies). Random hexamers were used to synthesise cDNA from the RNA obtained above using manufacturer's instructions. The cDNA was diluted to 5 ng/ μl with clean dH<sub>2</sub>O, and could be used in real-time PCR (2.10.4).

### 2.10.3 – Primer design

Primers for real-time PCR were usually designed to be intron-spanning (with the exception of genomic real-time PCR) using *Primer3* (Untergasser *et al.*, 2012, Koressaar and Remm, 2007). The intron-spanning aspect ensured that only mRNA and not genomic DNA were amplified. The primer oligos were manufactured by Sigma. The sequences of the real-time PCR primers used in this thesis were:

*Gata6*: F: AAAGCTTGCTCCGGTAACAG, R: TCTCCCACTGCAGACATCAC;

*Ywhaz*: F: TGCAAAAACAGCTTTCGATG, R: CCTGCTTCTGCTTCATCTCC;

Spleen focus forming virus (SFFV) promoter:

F: CCAACCCTCAGCAGTTTCTT, R: AAGCAGGCTGATTGGTTAATTC;

Ywhaz-genomic: F: CCGTCCAGGAAGAGTAGCAG, R: TGAGATGAGAATGAAGGGGG.

#### **2.10.4 – Real-time PCR**

SYBR Green JumpStart Taq ReadyMix (without MgCl<sub>2</sub>) (Sigma) was used for real-time PCR. SYBR Green is a cyanine dye which greatly increases its fluorescence when bound to double stranded (ds) DNA. SYBR Green JumpStart Taq ReadyMix (10 µl) was added to 0.2 µl 6-carboxyl-x-rhodamine (ROX) solution, 2 µl of 25 mM MgCl<sub>2</sub>, 1.8 µl dH<sub>2</sub>O, and 1 µl primer mix (0.5 µg/ ml each primer) to make a gene specific master-mix with a final MgCl<sub>2</sub> concentration of 2.5 mM. A 5 µl volume of cDNA (5 ng/ µl) was aliquoted into a real-time PCR 96-well plate (Applied Biosystems - ABI) containing 15 µl of the gene specific master-mix. The plate was inserted into an ABI-7900HT fast real-time PCR system and the PCR amplification started as per instrument instruction. The amplification procedure started with 10 minutes at 98 °C (to activate the hot-start enzyme) followed by 40 cycles of: 98 °C for 15 seconds then 60 °C for 60 s. The quantity of DNA increases 2-fold every cycle of the reaction during the exponential phase (≈5-35 cycles) of a PCR reaction (assuming 100 % efficiency). The ABI-7900HT recorded this via the increase in SYBR green fluorescence over the time. An arbitrary SYBR fluorescence was chosen at the start of the exponential phase (≈4-5 cycles) for each gene specific PCR group, and the number of cycles taken to reach this arbitrary level was termed the cycle threshold value (Ct) (*figure 2.2*). Ct values were calculated for every gene specific reaction and normalised against the endogenous control *Ywhaz*. These values were expressed as a fold change (using the  $\Delta\Delta$ -Ct method (Livak and Schmittgen, 2001)). The  $\Delta\Delta$ -Ct method includes normalisation against an endogenous control and a chosen control group within the experiment (e.g. 0 hour time point), followed by a transformation ( $2^{\Delta\Delta-Ct}$ ) to account for an assumed doubling in DNA product per cycle. After the last cycle, a dissociation stage (frequently termed a 'melt curve') was performed. This was a gradual rise in temperature from 60 to 98 °C, and recorded the dissociation of SYBR green from dsDNA with 'melting' of the PCR

products. This melt curve was used to decipher whether single or multiple products were formed (example in *figure 2.3*).

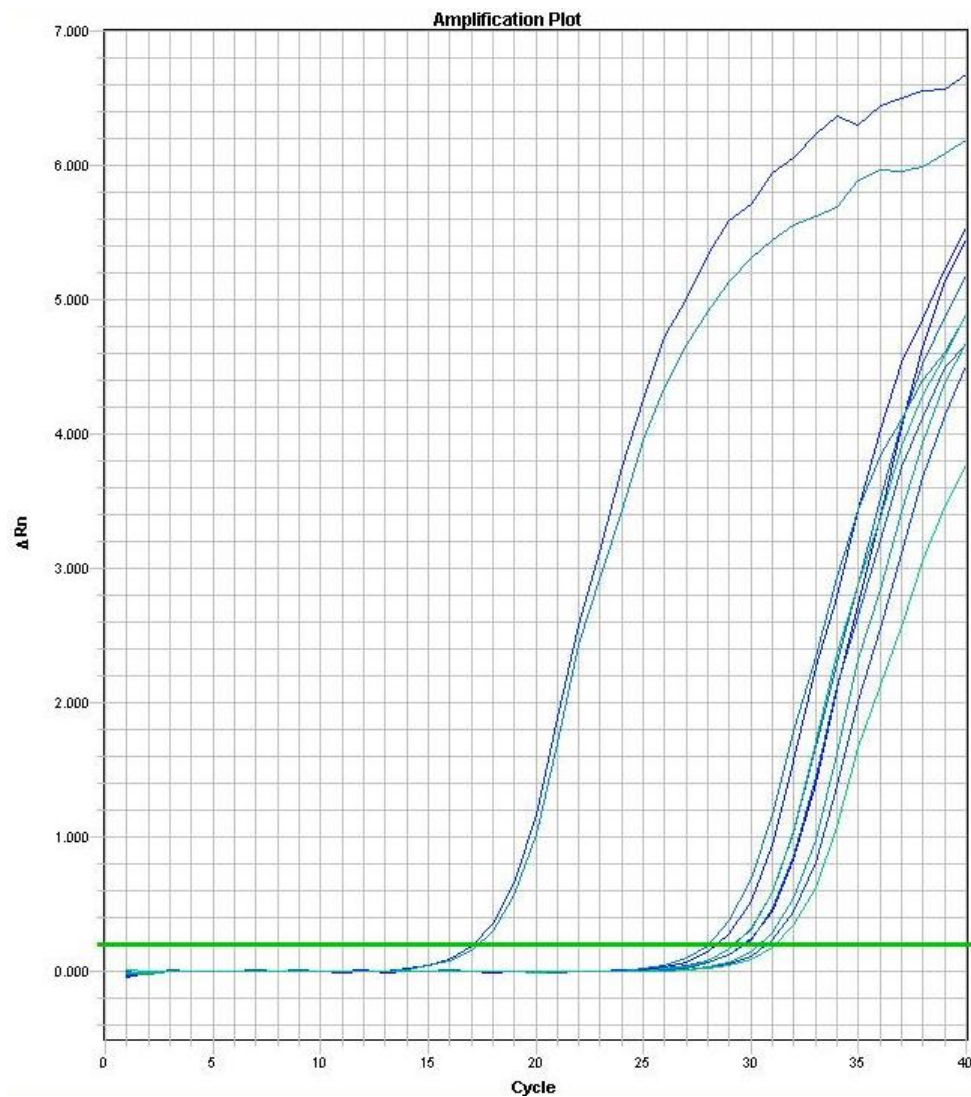


**Figure 2.2. Determination of Ct values**

An example graph showing change in fluorescence (Y) against PCR cycles (X), which can be used to determine Ct values. Reactions are indicated by the escalating thin lines on the graph. The thick horizontal green line denotes an arbitrary number for change in fluorescence. Ct values were generated for each reaction depending on where the green line intersected. This plot shows a *Gata6* specific reaction from cDNA extracted from BMMØs infected with numerous lentiviruses. One of these lentiviruses expressed high levels of Gata6 and the duplicate reactions can be seen on the left side of the graph, exhibiting a lower Ct value. Therefore, fewer cycles were required to reach the arbitrary fluorescence, which translates as a higher level of original template.

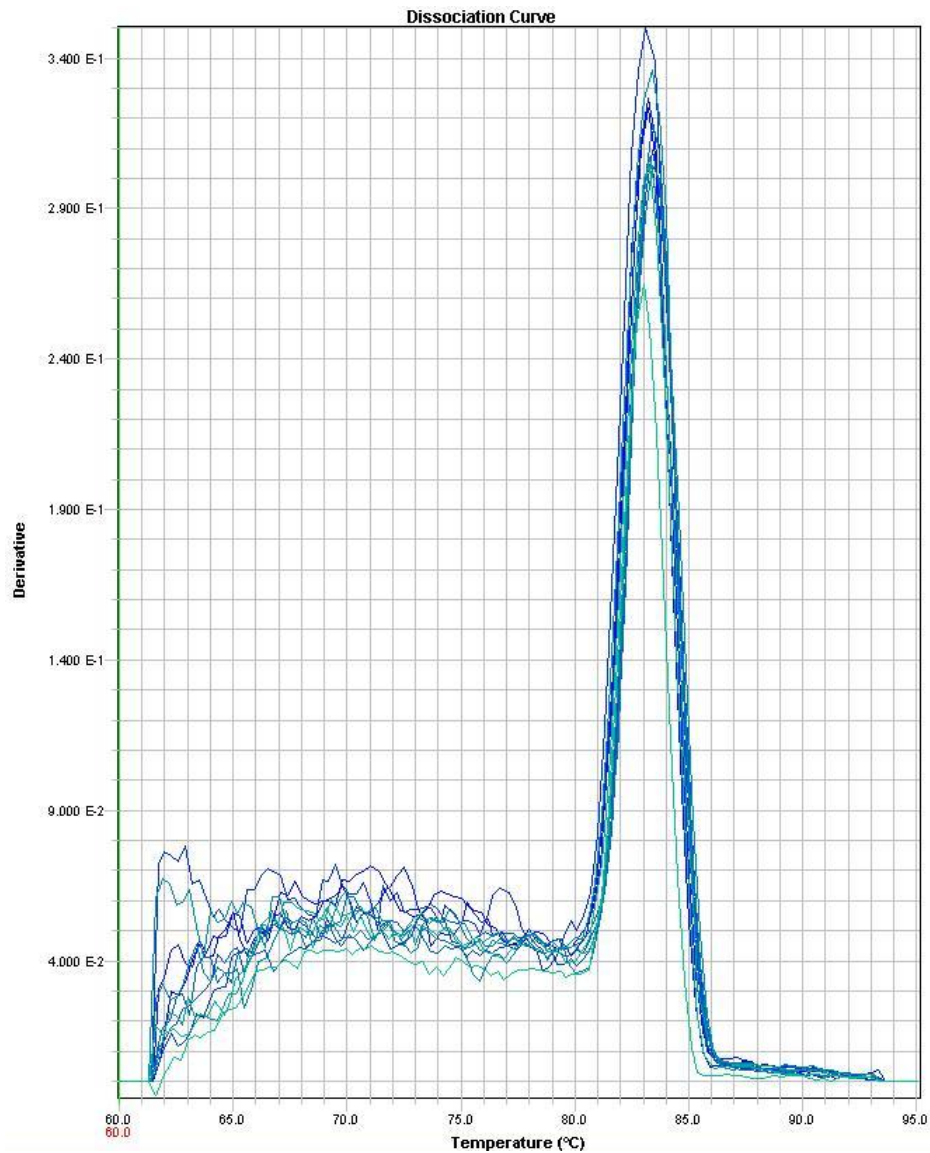


**Figure 2.3. Melt curve example**

Graph showing a derivative of change in fluorescence (Y) against temperature (X). The samples from figure 2.2 were sent though a dissociation stage. The ‘melting’ of the dsDNA products was recorded as a derivative of change in fluorescence (a decrease). The presence of a single peak in this plot suggests that the products were of the same structure/ size. If the plot showed multiple peaks, this would suggest that products with different structures were present.

## **2.11 – Immunocytochemistry**

### **2.11.1 – Cytospins, fixation and permeabilisation**

Cells ( $0.4-1.2 \times 10^5$ ) in 100  $\mu$ l PBS were centrifuged onto polylysine-coated glass slides (Fisher Scientific) using a cytospin 3 (Thermo Scientific). The cells were air-dried for a maximum of 5 minutes, while a circle was drawn tightly around the cells with an ImmEdge (hydrophobic) pen (Fisher Scientific). Three drops of freshly made (or freshly thawed) 4 % (w/v) paraformaldehyde in PBS were added to the cells with a plastic Pasteur pipette to fix the cells. The cells were incubated for 20 minutes at RT. The slides were washed: the slide was inserted into a slide rack filled with fresh PBS (making sure the cells were covered), and left to rest for 1 minute; then the slides were removed and the excess liquid blotted off with tissue. Capillary action with a thin piece of dry tissue was used to remove the excess liquid from the cells, but care was taken not to touch the cells. Next, three drops of 0.1 % TritonX-100 (Sigma) in PBS were added directly to the cells, and left for 15 minutes at RT to permeabilise the cells. The slide was inserted into the same slide rack filled with PBS (making sure the cells were covered), and left to rest for 1 minute. The cells could then be used for staining (2.11.2) or stored at 4 °C in the dark for up to three days before use (still in the PBS-filled slide rack).

### **2.11.2 – Staining**

Cell-containing slides (2.11.1) were removed from the PBS-filled slide rack and the excess liquid blotted off with tissue. Capillary action with a thin piece of dry tissue was used to remove the excess liquid from the cells, but care was taken not to touch the cells. The cells were covered with 30  $\mu$ l of block (PBS with 0.5 % (w/v) BSA, 0.5 % (w/v) saponin, 5 mM EDTA, 2 mM sodium azide, 5 % (v/v) rabbit serum, 4  $\mu$ g/ml rat anti-mouse Fc $\gamma$ RII/III (2.4G2)) and left to incubate at 4°C for 20 minutes. To this block solution, 20  $\mu$ l of 2.5 $\times$  antibody mix was added to give a final concentration of 1 $\times$  antibody (see table 2.1). This solution was incubated at 4 °C in the dark for 1 hour. The cells were washed (as in 2.11.1), before 50  $\mu$ l of streptavidin mix (containing 25 ng/ml DAPI and 2  $\mu$ g/ml streptavidin-fluorochrome) was added. This was incubated for 30

minutes at 4 °C in the dark. Cells were then washed (as in 2.11.1) twice and mounted with a cover slip (2.11.3).

### **2.11.3 – Slide mounting**

The stained slide (2.11.2) was dried with capillary action, taking care not to disturb the cells on the slide. Fluorescence mounting media (Dako) was pipetted onto the cells (3 µl), and a 10 mm diameter thin glass cover slip (Fisher Scientific) carefully lowered on top. The cover slip was carefully flattened with the blunt end of a 200 µl pipette tip so that no air remained between the cover slip and slide. The cells on the slide were viewed by fluorescence microscopy (2.11.4).

### **2.11.4 – Fluorescence microscopy**

The EVOS FL cell imaging system was used to take photographs of cells. This microscope contained bright field capabilities along with 4 light emitting diode (LED) light cubes suitable for imaging eGFP/ AlexaFluor488/ FITC, DAPI/ Pacific Blue, CY5/ APC/ AlexaFluor647, and TexasRed/ DyLight594. Pictures were taken using a 100× oil, 40×, 20× and 10× objective lenses. LED power and exposure time were optimised on an experiment by experiment basis, but were kept constant during an experiment. The microscope was used as per manufacturer's instructions.

### **2.11.5 – Image processing**

Images were processed with GNU image manipulation programme (GIMP) 2.0 to optimise saturation levels, and analysed with image J (National Institutes of Health). Image J was also used to quantify nuclear content of Gata6 in F4/80<sup>+</sup> cells. Images within the same experiment were processed and analysed using the same settings.

## **2.12 – Statistics**

Statistical analyses were conducted using GraphPad Prism. The statistical tests used are indicated as appropriate within the text. *P*-values are summarised as: \* =  $P \leq 0.05$ ; \*\* =  $P \leq 0.01$ ; \*\*\* =  $P \leq 0.001$ . All analyses performed were two-tailed unless stated.



## Chapter 3 - ResMØs self-renew by *in situ* proliferation

## 3.1 – Introduction

### 3.1.1 – Zymosan peritonitis

The peritoneal cavity is a vascular environment which has been widely used experimentally for the study of recruited inflammatory leukocytes, such as monocytes and neutrophils. These inflammatory cells can be recruited to the peritoneal cavity by intra-peritoneal administration of many inflammatory modulators. One such modulator: thioglycollate, has been used previously as a sterile initiator of inflammation, and is characterised by a large influx and retention of monocytes/InfMØs (Hopper, 1986). However, due to the clinical relevance of infection, pathogen derived agents such as zymosan, a cell wall derivative of *Saccharomyces cerevisiae* (Di Carlo and Fiore, 1958), and *Staphylococcus epidermidis* cell free supernatant (SES) (Hurst *et al.*, 2001) have been used to study inflammation in this environment. Zymosan peritonitis has been extensively used in Prof. Phil Taylor's laboratory to study inflammation in the peritoneal cavity (Taylor *et al.*, 2007, Rosas *et al.*, 2010).

The peritoneal cavity contains tissue resident cells which exist under normal homeostatic physiology. These cells include a high proportion of F4/80<sup>high</sup> ResMØs (Austyn and Gordon, 1981), with a lesser presence of F4/80<sup>low</sup> MHCII<sup>high</sup> ResDCs/MØs (Dioszeghy *et al.*, 2008), B and T lymphocytes (Carlow *et al.*, 2009), eosinophils (Ohnmacht *et al.*, 2007) and mast cells (Das *et al.*, 1998). The primary roles of ResMØs in the peritoneal cavity are considered to be immune surveillance, innate defence (Dunn *et al.*, 1985) and the clearance of apoptotic cells (Wong *et al.*, 2010).

Intra-peritoneal injection of zymosan particles triggers an innate immune response, with a characteristic elevation in the number of neutrophils recruited to the peritoneal cavity (Taylor *et al.*, 2007, Rosas *et al.*, 2010). The number of recoverable ResMØs drops after this initial inflammatory stimulus. This fall in ResMØ numbers is termed 'the disappearance reaction,' and is defined as an experiential failure to recover the cells by lavage (Barth *et al.*, 1995). As, mentioned in the general introduction (1.2.2), this could be due to increased adherence to the mesothelial tissues, cell migration to draining lymph nodes, or cell death (Barth *et al.*, 1995). The number of recoverable ResMØs starts to increase during the resolution phase of zymosan induced inflammation, which is characterised by a fall in the number of neutrophils (Rosas *et*

*al.*, 2010). The M $\phi$  element of this resolution phase includes ResM $\phi$ s along with large numbers of recruited monocytes, which differentiate into inflammatory M $\phi$ s (InfM $\phi$ s) (Rosas *et al.*, 2010). This provides circumstantial evidence for the prevalent model (Fogg *et al.*, 2006, Geissmann *et al.*, 2010, Gordon and Taylor, 2005) of ResM $\phi$  renewal: the mononuclear phagocyte system (van Furth *et al.*, 1972). In spite of this, self renewal of M $\phi$ s by proliferation has recently been identified in non-vascular environments; this has been speculated to evolve because leukocyte recruitment is restricted. These proliferating cells are: Langerhans cells of the skin (Chorro and Geissmann, 2010, Chorro *et al.*, 2009) and microglia in the brain (Ajami *et al.*, 2007, Mildner *et al.*, 2007). These cells maintain their population via local proliferation in homeostasis and inflammation. They do not rely on recruited blood monocytes for their renewal and are self sufficient unless there is a catastrophic depletion of the population, such as UV irradiation in the case of Langerhans cells (Merad *et al.*, 2002).

### **3.1.2 –Proliferation**

Proliferation is frequently investigated using DNA content to identify stages of the cell cycle (Brown *et al.*, 2010). Proliferating cells start in G<sub>1</sub> with a 2N DNA content and synthesise new DNA throughout S phase, reaching a 4N DNA content in G<sub>2</sub> before cell division by mitosis (a.k.a. M phase). Studying the proliferation of M $\phi$ s using DNA content alone would be difficult due to the relatively common presence of multinucleated cells, and the potential for phagocytosis of apoptotic bodies (which includes the degrading nuclei). These factors will skew the normal DNA content of cells, giving false positives for S, G<sub>2</sub> and M phases. However, there are many molecular markers which can be used to identify cells in the active phases of the cell cycle (G<sub>1</sub>, S, G<sub>2</sub> and M), which include: Ki67, phospho-histone H3 (pHH3), aurora A kinase and the various cyclins (A, D E, B); the specific expression of these markers is described below.

Ki67 is expressed only by cells in the active cell cycle phases (G<sub>1</sub>, S, G<sub>2</sub> and M) (Scholzen and Gerdes, 2000). Histone H3 is selectively phosphorylated from prophase to early anaphase during cell division (Hans and Dimitrov, 2001, Hendzel *et al.*, 1997), therefore pHH3 can be used (in conjunction with 4N DNA content) as a marker of active mitosis. Aurora A kinase is required for mitotic spindle formation during cell division (Crane *et al.*, 2004). The cyclins are required for progression through the cell

cycle and their expressions and activities increase at specific checkpoints, cyclins D and E are required for G<sub>1</sub>-S transition, A for S-G<sub>2</sub> and B for progression into M (Sanchez and Dynlacht, 2005). However, using these cyclins as markers would be difficult, as they maintain low levels of expression even when not required.

Microarray analysis of monocyte and M $\phi$  populations during inflammation was performed by Dr. Marcela Rosas (see general introduction, 1.3.1) and revealed that transcription factors and soluble mediators linked to proliferation or associated with stem cells were expressed by ResM $\phi$ s; which suggested that ResM $\phi$ s may not be terminally differentiated and could share a capacity for self renewal with M $\phi$ s in non vascular environments, such as Langerhans cells. This generated the hypothesis examined in this chapter.

### **3.1.3 – Hypothesis**

The hypothesis tested in this chapter is that peritoneal ResM $\phi$ s have the capacity for proliferation in homeostatic growth and are capable of self-renewal after inflammatory depletion.

### **3.1.4 – Aims**

- To establish a model for the investigation of the cell cycle in peritoneal ResM $\phi$ s
- To investigate the level of homeostatic ResM $\phi$  proliferation in the post-natal period and in the adult peritoneal cavity
- To investigate peritoneal ResM $\phi$  renewal during acute inflammation

## 3.2 – Results

### 3.2.1 – Doublet discrimination in complex polychromatic flow cytometry

In order to study proliferation on an individual cell basis, it was first necessary to establish a robust flow cytometric assay. Doublets are adhered cell clumps and coincidental events and are generally characterised as events which have an abnormally high signal area to linear ratio, or pulse width to signal ratio. Doublets are frequent artefacts of flow cytometry and contribute to false positives, especially in cell cycle analysis. Doublets were excluded during flow cytometric analysis of cell populations by three methods, which are shown as consecutive gating on forward scatter ( $FSC_{Linear}$  vs  $FSC_{Area}$ ,  $DNA_{Linear}$  vs  $DNA_{Area}$ , and Pulse Width vs  $DNA_{Area}$  (*figure 3.1*).

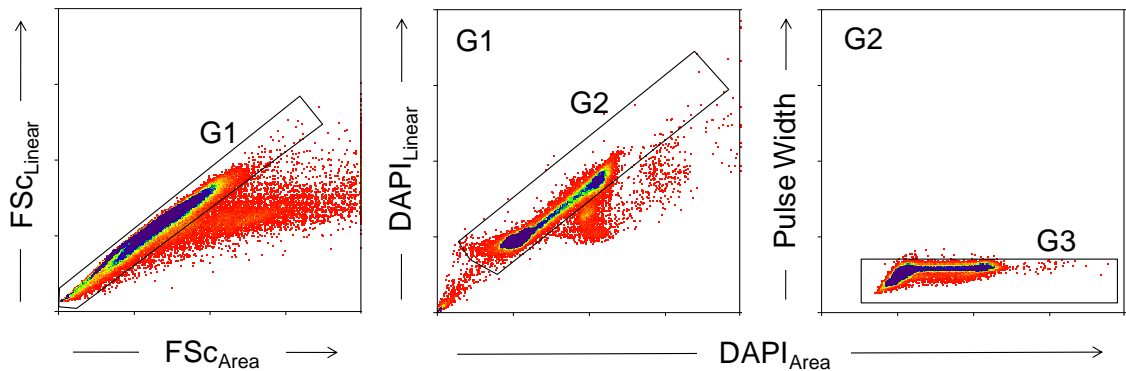


**Figure 3.1. Doublet discrimination in complex multi-parameter flow cytometry**

Representative density plots showing doublet discrimination achieved by consecutive gating on  $FSC_{Linear}$  vs  $FSC_{Area}$  (G1),  $DNA_{Linear}$  vs  $DNA_{Area}$  (G2), and pulse-width (G3). Data shown is from peritoneal lavaged cells and is representative of 6 individual 2 week old female 129S6/SvEv naïve mice from two independent experiments; however this strategy of using the  $FSC_{Linear}$  vs  $FSC_{Area}$  ratio and pulse-width to exclude doublet events was applied to all cells analysed by flow cytometry in this thesis.  $DNA_{Linear}$  and  $DNA_{Area}$  parameters were only used when a DNA stain was present. In the absence of a DNA dye pulse-width vs  $FSC_{Area}$  was used, with the same gating strategy as pulse-width vs  $DNA_{Area}$ .

### 3.2.2 – Definition of ResMØs in complex inflammatory environments

ResMØs are defined by their F4/80<sup>high</sup> phenotype in the peritoneal cavity (Austyn and Gordon, 1981), however they were indistinguishable from eosinophils using F4/80 alone when the cells were fixed and permeabilized (*figure 3.2a: left panel*). The ResMØ marker Tim4 helped to discriminate between ResMØs and eosinophils (*figure 3.2a: left panel*). Tim4 is a phosphatidylserine receptor expressed by CD11b<sup>+</sup> cells in various tissues (Miyanishi *et al.*, 2007). It was identified as a marker primarily restricted to ResMØs by Dr. Marcela Rosas who validated its expression by ≥95 % of ResMØs in the peritoneal cavity of C57BL/6 and 129S6/SvEv mice. Tim4<sup>-</sup> eosinophils have a distinct FSc/ side scatter (SSc) profile after fixation/permeabilization (Taylor *et al.*, 2003), which facilitated their separation from ResMØs and other cells (*figure 3.2a: right panels*). F4/80<sup>low</sup> MHCII<sup>high</sup> Res DCs/MØs and InfMØs arriving during inflammation also complicated the classification of ResMØs (utilising F4/80 and CD11b) (*figure 3.2a: left panels*). However, after eosinophil removal via their FSc/SSc profile, the F4/80<sup>high</sup> phenotype was sufficient for discrimination between these populations, which was confirmed by expression of the restricted ResMØ marker Tim4 (*figure 3.2b: right panels*).

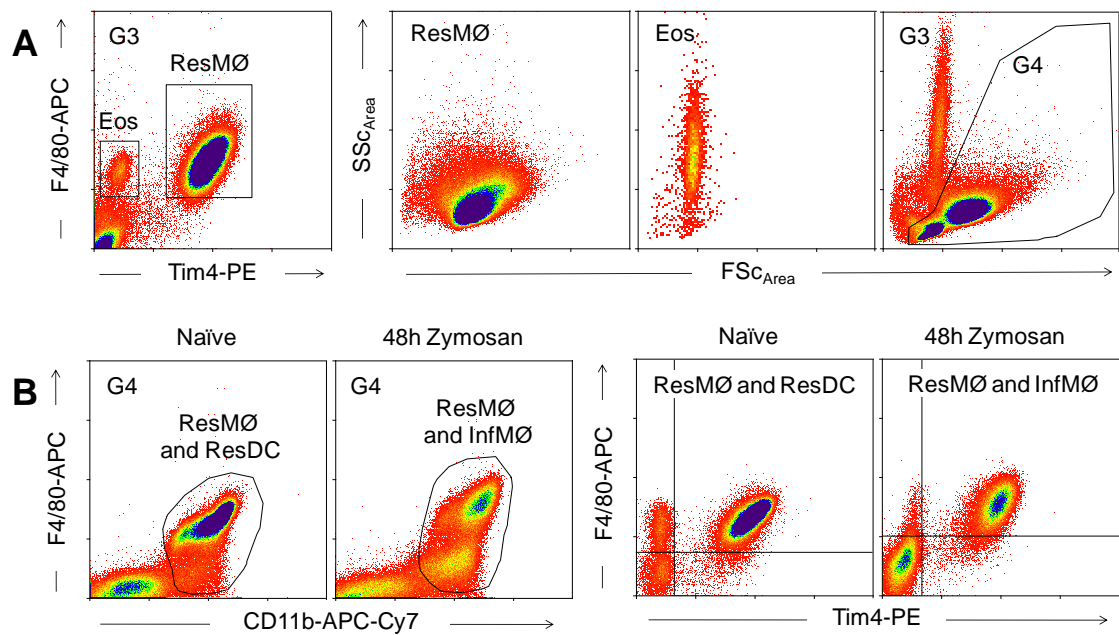


**Figure 3.2. Definition of ResMØs in complex inflammatory environments**

**A)** Representative density plots showing Tim4 expression, which was found to be associated with the F4/80<sup>high</sup> ResMØ profile, separating them from F4/80<sup>+</sup> eosinophils (left panel). The distinctive FSc/ SSc profile of eosinophils after fixation/permeabilization (right panels) was used to exclude them from further analysis (G4).

**B)** Density plots showing gating of F4/80<sup>+</sup> CD11b<sup>+</sup> MØ populations in naïve mice, and mice 48 hours after intra-peritoneal injection of  $2 \times 10^6$  zymosan particles (left panels). The ResMØ and ResDC gate includes both F4/80<sup>high</sup> ResMØs and F4/80<sup>low</sup> MHCII<sup>high</sup> ResDCs/MØs, while the ResMØ and InfMØ gate includes both F4/80<sup>high</sup> ResMØs and F4/80<sup>low</sup> InfMØs. The MØ populations were further examined using Tim4 expression; the majority of F4/80<sup>high</sup> ResMØs showed positive staining (right panels), whereas F4/80<sup>low</sup> MHCII<sup>high</sup> DCs/MØs (ResDCs) and InfMØs were negative. All plots were gated for single events as shown in figure 1 and eosinophils were excluded as shown in (A) (G4). Data shown is representative of 6-7 week old female C57BL/6 mice from one of three similar experiments (n= 5 per group).

### 3.2.3 – Identification of non cell cycle-associated DNA content and ResMØs in cell cycle

Cell cycle analysis was complicated in ResMØs due to the presence of non cell cycle-associated DNA content and irregular nuclear morphology, which included: multinucleate MØs, multi-lobed nuclei, and the presence of phagocytic bodies, the latter more evident during inflammation (*figure 3.3*).

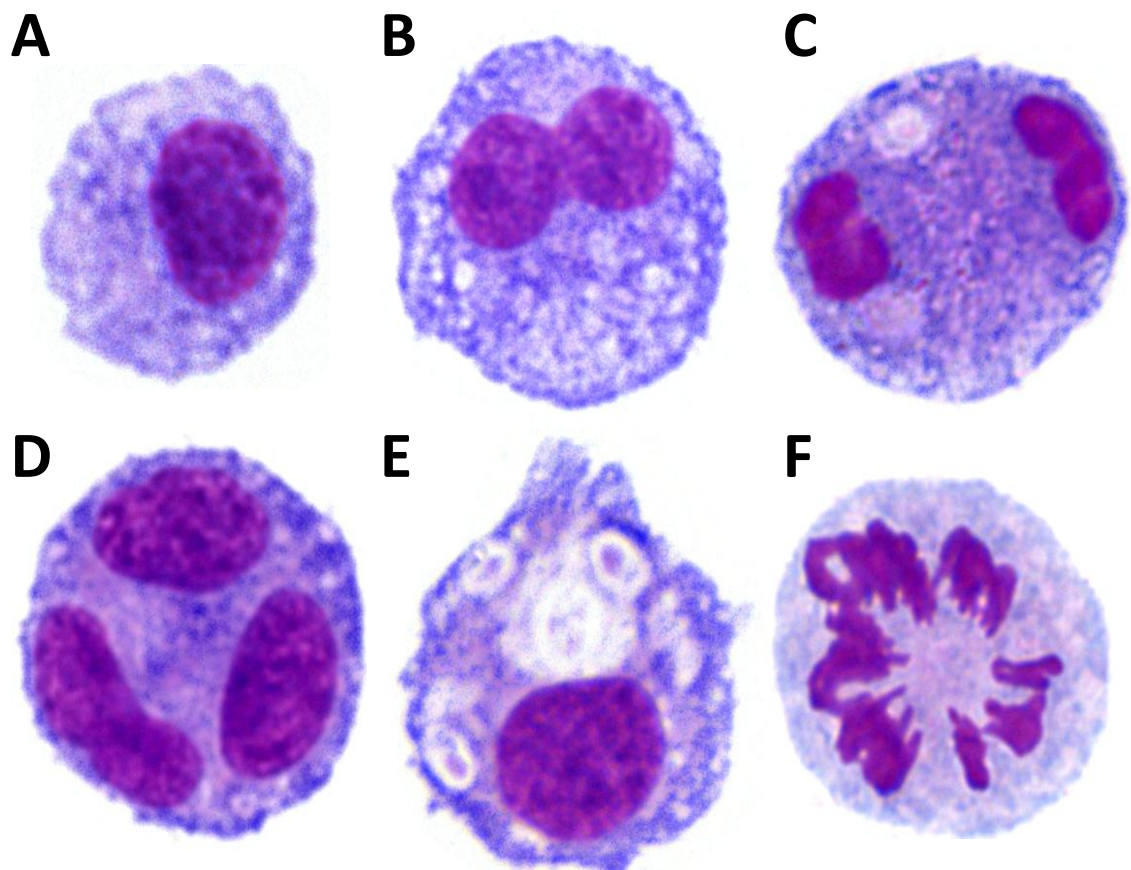


**Figure 3.3. Description of non cell cycle-associated DNA content in ResMØs**

Photographs showing a representation of ResMØs that are: **A)** mononucleate ‘fried egg’, **B)** bilobed **C)**, binucleate, **D)** multinucleate, **E)** phagocytic (containing zymosan particles in this picture, but this could theoretically be apoptotic cell debris) and **F)** mitotic. Cells were purified by flow cytometric cell sorting (Moflo, Beckman Coulter) of F4/80<sup>high</sup> CD11b<sup>high</sup> peritoneal cells from lavages pooled from five 7 week old C57BL/6 female mice, 48 hours after intra-peritoneal injection of  $2 \times 10^6$  zymosan particles. The cells were centrifuged onto slides in a cytospin-3 and fixed, then stained with hematoxylin and eosin. Pictures were taken using a Leica light microscope at 100 × objective magnification under oil.



Flow cytometric analysis of DNA content using nuclear stains was not affected by irregular nuclear shape, but was unable to discriminate between non cell cycle-associated DNA content and those cells in active cell cycle. Therefore, markers for the active stages of the cell cycle were pursued for use in flow cytometry. DNA content staining was used in conjunction with pHH3 in Hoxb8 immortalised MØ precursors (a fast growing cell line) (Rosas *et al.*, 2011) to confirm its selectivity in cells with a 4N DNA content (*figure 3.4*). This confirmation enabled the use of pHH3 expression to detect a small window of cell mitosis (prophase to early anaphase). The  $1.64 \pm 0.17 \%$  (mean  $\pm$  SEM,  $n = 5$ ) of cells with 4N DNA content that expressed pHH3 in this fast growing cell line gave an ‘unnaturally high’ level of pHH3 (only 1.64 %), which provided a basis to evaluate the results from MØ proliferation *in vivo* (see below).

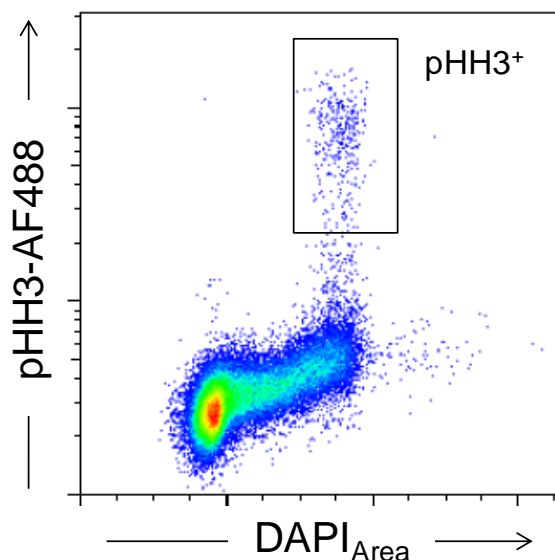


**Figure 3.4. Identification of definitive mitotic events by phosphorylation of histone H3 in cells with 4N DNA content**

Representative density plot showing phospho-histone H3 (pHH3) and DNA (DAPI) staining of a Hoxb8 immortalised MØ precursor cell line made from the bone marrow of 129S6/SvEv mice (Rosas *et al.*, 2011). Data shown is from three independent experiments ( $n = 5$ ).

ResMØs were stained with anti-pHH3 following successful staining of mitosis in the precursor cell line. Positive staining in the 4N DNA population showed that a small number of ResMØs in the adult were mitotic (*figure 3.5: left panel*). The proliferative

marker Ki67 (Kubbutat *et al.*, 1994) was also used to highlight ResMØs in the active cell cycle phases (G<sub>1</sub>, S, G<sub>2</sub> and M), and was able to distinguish them from the Ki67<sup>-</sup> cells in G<sub>0</sub>, ‘binucleate’ cells with 4N DNA content and those cells with >2N, but less than 4N DNA content, which could represent phagocytic events (*figure 3.5: right panel*). Positive staining of pHH3 coincided with a high level of Ki67 staining (*figure 3.5: middle panel*), which provided conclusive evidence for a low level of active proliferation in resting peritoneal ResMØs. This data supported the method for quantification of mitotic events with Ki67<sup>high</sup> staining in addition to pHH3 expression; when bearing in mind that pHH3 is only expressed in a small window in mitosis. The combination of both markers was used to accurately quantify the cell cycle of ResMØs from the resting peritoneal cavity of adult mice (*figure 3.6*).

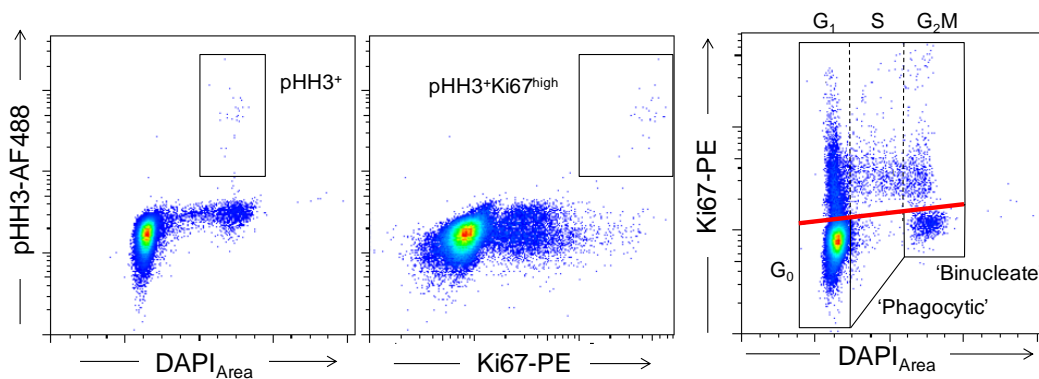


**Figure 3.5. Use of Ki67 and phospho-histone H3 to discriminate between MØs with non cell cycle-associated DNA content and those in cell cycle**

Representative density plots showing ResMØs from the peritoneal cavity. Cells were gated to remove doublets (3.1), eosinophils (3.2) and gated on ResMØs as shown in 3.2b. The cells were stained for DNA content (DAPI), phospho-histone H3 (pHH3) and Ki67. pHH3 labels mitotic cells with 4N DNA content (left panel) and coincides with Ki67<sup>high</sup> staining (middle panel). Ki67 staining of ResMØs (right panel) shows cells within specific stages of the cell cycle. The red line marks the maximal staining from a matched isotype control; cells above this line are positive for Ki67 and are in the active phases of the cell cycle (S, G<sub>2</sub> and M), while the cells below this are negative and therefore not in active cell cycle phases (G<sub>0</sub>, ‘phagocytic’ and ‘binucleate’). Data is representative of one of three similar experiments with 6-7 week old female C57BL/6 mice (n= 5 per group).

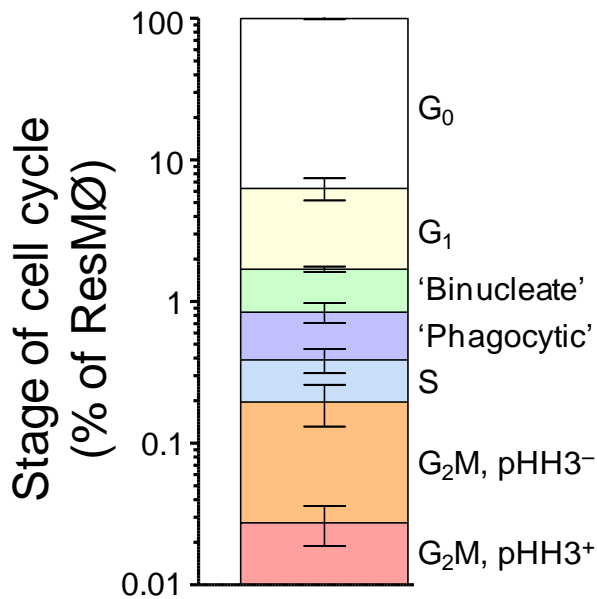


**Figure 3.6. Quantification of cell cycle in adult mice**

Bar graph depicting the percentage of ResMØs in different stages of the cell cycle determined as shown above (*figure 3.5*). The data is from one experiment with 14 week old 129S6/SvEv (n= 5) and similar results were obtained with 7 week old C57BL/6 (n= 3) female mice in an independent experiment; error bars denote the mean  $\pm$  SEM.

### 3.2.4 – ResMØs expand by proliferation during the neonatal period

During the neonatal period a mouse will grow rapidly and dramatically increase in size until growth slows toward adulthood. The peritoneal cavity in these mice also increases in size and volume, therefore the number of cells it can support will increase. Cell quantification was performed during the neonatal period (2 weeks, P14-15), through young adulthood (5 weeks) and into full adulthood (12-16 weeks). The total number of ResMØs increased with age (*figure 3.7a*). The number started off relatively low in neonate mice ( $0.62 \pm 0.09 \times 10^6$ , mean  $\pm$  SEM, n= 6) when the MØs were the dominant cell in the cavity ( $76.8 \pm 1.4$  % of total cells). However, this number rapidly increased as the mice grew, and by 4-5 weeks of age  $2.17 \pm 0.28 \times 10^6$  ResMØs were present in the peritoneal cavity (mean  $\pm$  SEM, n= 6). This expansion slowed, giving a stable number of ResMØs ( $2.8 \pm 0.18 \times 10^6$ ), with a reduced dominance in the cavity ( $38.9 \pm 5$  %) by 12-16 weeks of age (mean  $\pm$  SEM, n= 5). The proliferation of ResMØs during growth was quantified using DNA content and pHH3. The level of proliferation in ResMØs was high in neonatal mice and fell rapidly with age (*figure 3.7b*). This was

quantified as an over 20-fold increase in pHH3<sup>+</sup> cells in neonatal mice compared with that of older (12-16 week old) mice ( $0.25 \pm 0.07$  % vs  $0.011 \pm 0.003$  %, mean  $\pm$  SEM, n= 5-6). However the percentage with DNA >2N only dropped 5-fold from neonate to older mice ( $5.15 \pm 1.65$  % vs  $1.16 \pm 0.12$  %); this indicated that pHH3 has a greater resolution when quantifying proliferation. When these values were correlated (*figure 3.8*), it was revealed that DNA content >2N correlated well with proliferation (pHH3) in younger mice (2 and 4-5 weeks), but did not in older (12-16 weeks) mice, which emphasised the problem of non cell cycle-associated DNA content in the adult mouse.

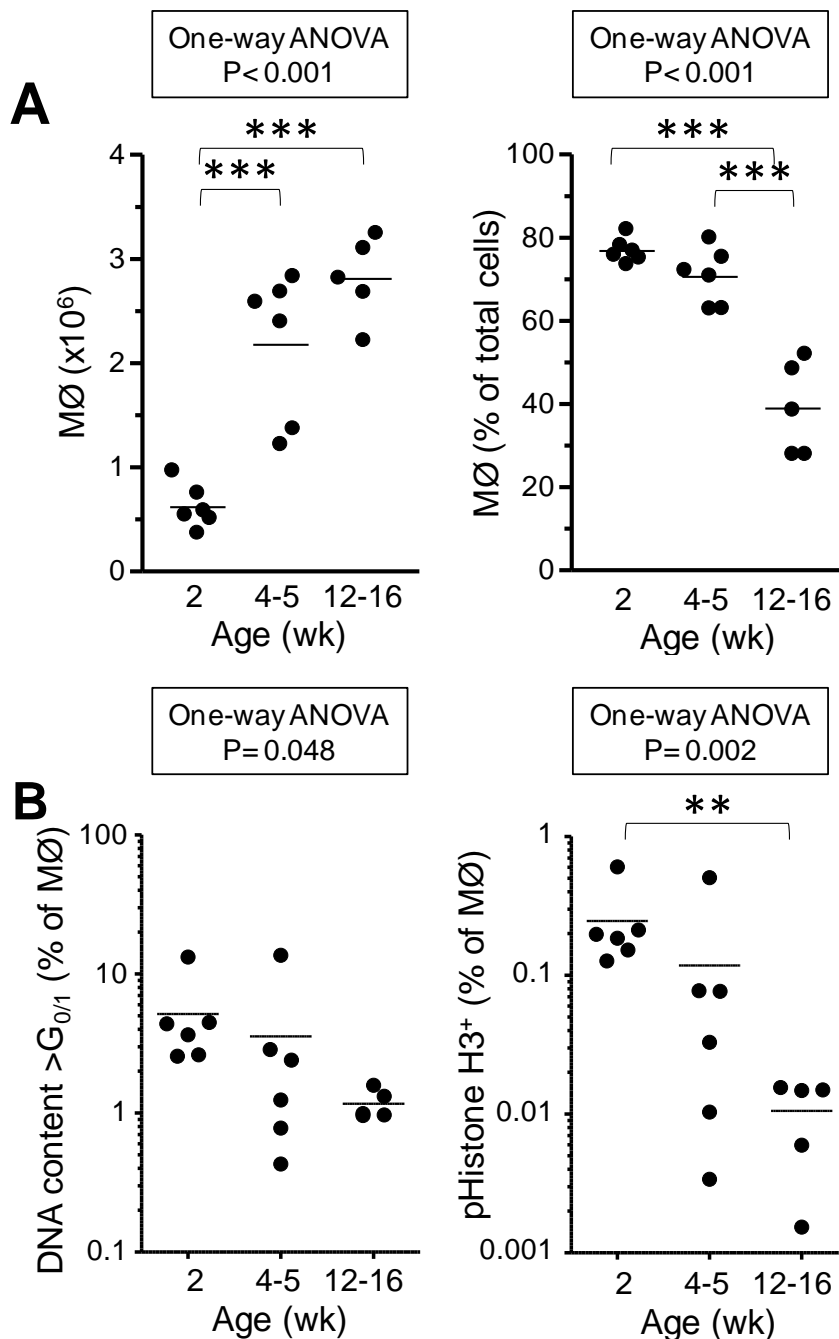


**Figure 3.7. ResMØs proliferate during neonatal growth**

**A)** Graphs showing the total number of ResMØs (left), and ResMØs as a percentage of cells recovered (right) in the peritoneal lavage of mice at different ages. **B)** Graphs showing the proportion of ResMØs of mice at different ages that are either DNA content  $>2N$  (left), or pHH3<sup>+</sup> (right). Horizontal bars denote means. Data were analyzed by one-way ANOVA, with Bonferroni post tests to determine the significance of differences between groups, significance values for the effect of age are indicated, and Bonferroni post tests are shown: \*\* =  $P \leq 0.01$ , \*\*\* =  $P \leq 0.001$ . Each symbol represents an individual 2-16 week old 129S6/SvEv female mouse, and data were pooled from two similar experiments.

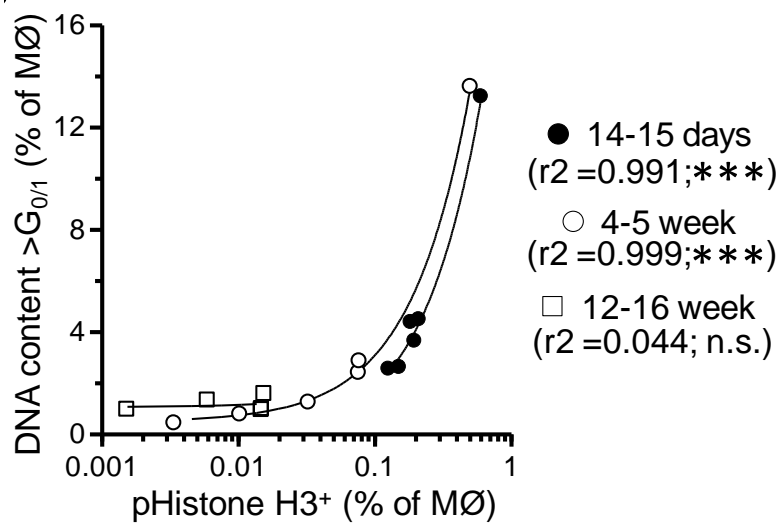


**Figure 3.8. DNA content does not readily correlate with proliferation in older mice**

Graph showing the correlation between percentages of ResMØs with DNA content >2N and those that are pHH3<sup>+</sup>. Data were analyzed by linear regression, and  $r^2$  values are indicated alongside significance testing for a non-zero slope (\*\*\*=  $P \leq 0.001$ ). Each symbol represents an individual 2-16 week old 129S6/SvEv female mouse, and data were pooled from two similar experiments.

### 3.2.5 – ResMØs recover from acute inflammation by proliferation

The numbers of recoverable ResMØs drop in the first few hours after the initiation of inflammation by  $2 \times 10^6$  zymosan particles; this number starts to recover during the resolution phase seen at 48 hours and 72 hours after initiation. InfMØs are also present in the cavity at these time points, and make up a large component of the total MØ population in this model (*figure 3.9*).

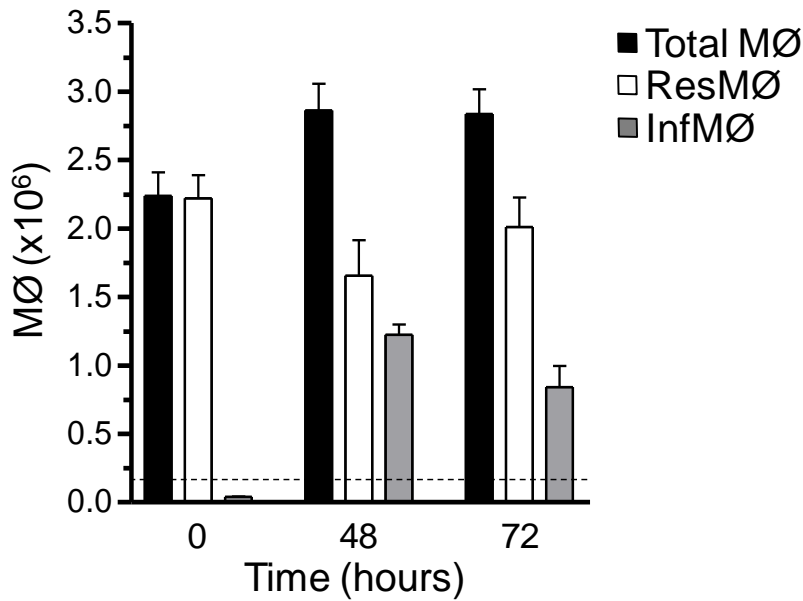


**Figure 3.9. Recovery of ResMØ population during acute inflammation**

Graph showing the number of recoverable ResMØs and InfMØs in the peritoneal lavage of mice at different time points after intra-peritoneal injection of  $2 \times 10^6$  zymosan particles. Error bars denote the mean  $\pm$  SEM of data obtained from one of three similar experiments with 6-7 week old female C57BL/6 mice ( $n = 5$  per group). The dotted line represents a  $\approx 93\%$  reduction in recoverable ResMØs observed 4 hours after zymosan.

The proliferative marker pHH3 was utilised along with MØ gating strategies to investigate proliferation during inflammation. The gating strategies shown in figure 3.10 are the definitions of  $F4/80^{\text{high}}$  ResMØs and  $F4/80^{\text{low}}$  InfMØs in mild acute inflammation, which was previously shown to be based on Tim4 expression on ResMØs (figure 3.2). These strategies are used throughout this thesis, and are frequently referred to within figure legends. ResMØs experienced a burst in proliferation at a specific time point during inflammation (48 hours after  $2 \times 10^6$  particles of zymosan), which coincided with the recovery of their numbers during the resolution (figure 3.10). InfMØ populations (including a small number of  $F4/80^{\text{low}}$  MHCII<sup>high</sup> Res DCs/MØs) did not follow this same proliferative pattern, and showed lower levels of proliferation. This data (pHH3<sup>+</sup> %) was quantified (figure 3.11a) and showed that the burst in ResMØ proliferation at 48 hours was over 12-fold higher than the proliferation at baseline ( $0.64 \pm 0.07\%$  vs  $0.05 \pm 0.01\%$ , mean  $\pm$  SEM respectively,  $n = 5$ ), and the level of proliferation was reduced again at 72 hours ( $0.13 \pm 0.09\%$ ,  $n = 5$ ). Proliferation was

also quantified using DNA content (*figure 3.11a*), which was shown to correlate well with proliferation in younger mice (*figure 3.8*); it also correlated well during inflammation in these 6-7 week old mice (*figure 3.11b*).

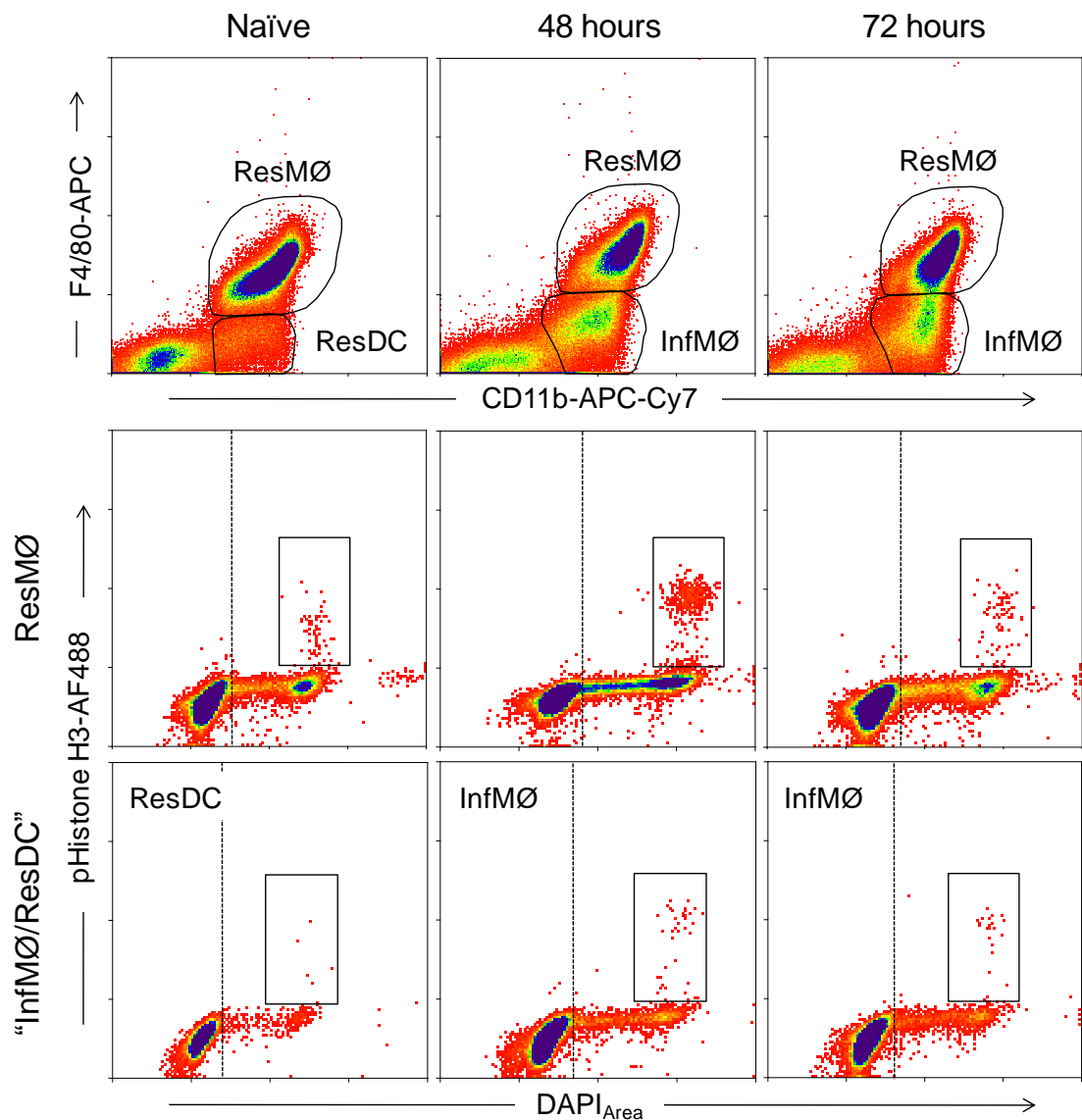


**Figure 3.10. Identification of a proliferative burst in ResMØs during acute inflammation**

Density plots depicting cells stained with F4/80, CD11b, DNA (DAPI) and pHH3 in naïve mice and mice after intra-peritoneal injection of  $2 \times 10^6$  zymosan particles. Cells were pre-gated to remove doublets and eosinophils (as shown in figures 3.1 and 3.2). Representative gating of ResMØ and InfMØ populations is shown in the top panels and their respective pHH3<sup>+</sup> gates (boxes) are shown in the bottom and middle panels. Cells to the right of the dotted vertical lines were described as having >2N DNA content. Note: the InfMØ gate also contains F4/80<sup>low</sup> MHCII<sup>high</sup> Res DCs/MØs (ResDC) in animals after zymosan. Data is representative of the mice used in figure 3.9. The gating



strategies used (ResM $\emptyset$ , ResDC and InfM $\emptyset$ ) are reminiscent of all experiments carried out in this thesis.

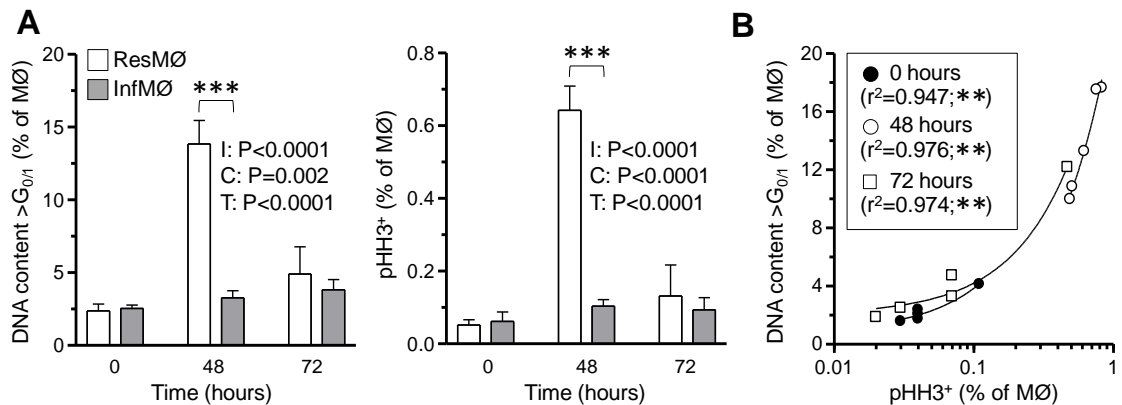


**Figure 3.11. Quantification of phospho-histone H3 expression and increased DNA content of MØs during acute inflammation**

**A)** Graphs showing percentage of cells with DNA content >2N (left), or those that are pHH3<sup>+</sup> with 4N DNA content (right) in naïve mice and mice after intra-peritoneal injection of  $2 \times 10^6$  zymosan particles. Data were analyzed by two-way ANOVA with Bonferroni post tests to determine the influence of cell type and zymosan treatment on MØ proliferation, and significance values are indicated: I= interaction between cell type and zymosan effects, C= cell type, T= effect of zymosan treatment over time, and Bonferroni post tests: \*\*\* =  $P \leq 0.001$ . **B)** Graph showing the correlation between percentage of ResMØs with DNA content >2N and those which were pHH3<sup>+</sup> after zymosan injection. Data were analyzed by linear regression and the  $r^2$  values and the significance of tests for a non-zero slope are indicated (\*\* =  $P \leq 0.01$ ). In both cases (A and B), error bars denote the mean  $\pm$  SEM of data obtained from one of three similar experiments with 6-7 week old female C57BL/6 mice (n= 5 per group).

The cell cycle could be further investigated using DNA content due to the excellent correlation with proliferation during inflammation. The Dean-Jett-Fox algorithm in Flowjo was used to quantify cell cycle stages 48 hours after inflammation (*figure 3.12*). This algorithm uses mathematical modelling to calculate the number of cells in phases of the cell cycle on the assumption that cells in the G<sub>2</sub>M peak have twice the DNA fluorescence compared with G<sub>0</sub>/1, and assumes equal coefficients of variance. However this algorithm had a restricted ability to only detect higher levels of proliferation; so could not be used to quantify low levels of proliferation, such as that seen basally. Therefore, proliferation was characterised in inflammation using the

proliferation marker Ki67. A clear increase in the percentage of total Ki67<sup>+</sup> ResMØs was identified during the proliferative burst at 48 hours vs baseline ( $41.4 \pm 7.0\%$  vs  $3.8 \pm 0.9\%$ , mean  $\pm$  SEM,  $n = 5$ ), and this level was still relatively high 72 hours after inflammation ( $27.3 \pm 2.4\%$ ,  $n = 5$ ) (figure 3.13a). The percentage of Ki67<sup>+</sup> InfMØs did not change significantly throughout inflammation, but started off higher than ResMØs at baseline ( $13.7 \pm 0.6\%$  vs  $3.8 \pm 0.9\%$ , mean  $\pm$  SEM respectively,  $n = 5$ ) (figure 3.13a). The cell cycle stages were characterised with the use of Ki67 along with DNA content as in figure 3.5 to additionally highlight this burst in proliferation (figure 3.13b).

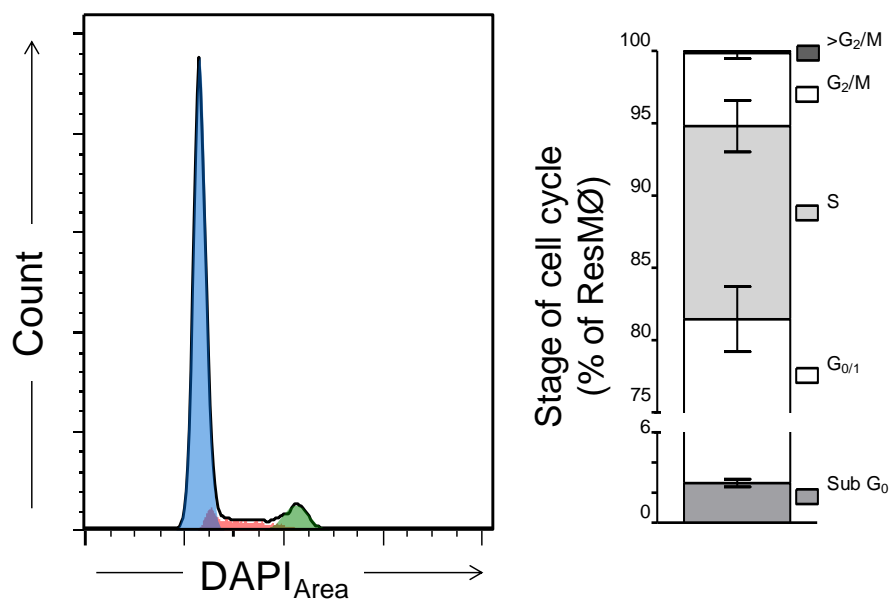


**Figure 3.12. Quantification of cell cycle stages using DNA content during acute inflammation**

Histogram (left) showing the DNA content of ResMØs, this was quantified into stages using the Dean-Jett-Fox cell cycle algorithm in Flowjo, and presented as a bar graph (right). The blue peak denotes G<sub>0/1</sub>, the red area is S phase and the green peak shows G<sub>2/ M</sub>. Error bars denote the mean  $\pm$  SEM of data obtained from one of three similar experiments with 6-7 week old female C57BL/6 mice, 48 hours after intra-peritoneal injection of  $2 \times 10^6$  zymosan particles ( $n = 5$  per group).

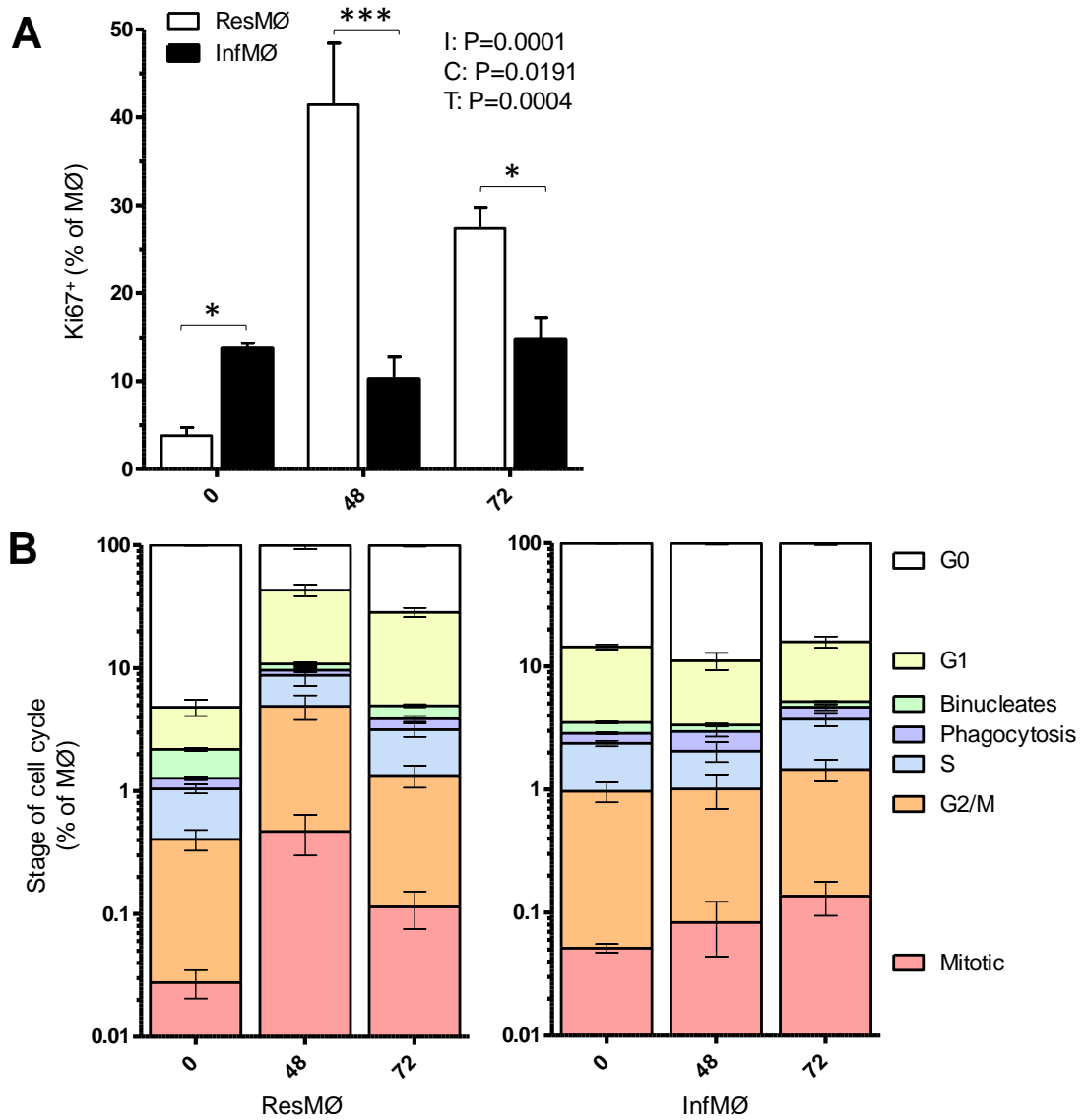


**Figure 3.13. Quantification of cells in cell cycle using Ki67 during acute inflammation**

**A)** Bar graph showing the percentage of total Ki67<sup>+</sup> ResMØs and InfMØs in naïve mice or mice after intra-peritoneal injection of 2×10<sup>6</sup> zymosan particles. Data were analyzed by two-way ANOVA, with Bonferroni post tests to determine influence of cell type and zymosan treatment on Ki67 expression, significance values are indicated: I= interaction between the effects of cell type and zymosan treatment, C= cell type, T= effect of zymosan treatment over time, and Bonferroni post tests: \* = P ≤ 0.05, \*\*\* = P ≤ 0.001.

**B)** Bar graphs showing the percentage ResMØs and InfMØs in different cell cycle phases using Ki67 and DNA staining in naïve mice or mice after intra-peritoneal injection of 2×10<sup>6</sup> zymosan particles. Data was quantified using gating described in figure 3.5. Error bars denote the mean ± SEM of data obtained from one of three similar experiments with 6-7 week old female C57BL/6 mice (n= 5 per group).

### 3.2.6 – ResMØs in the naïve tissue survive inflammation and proliferate

Previous unpublished experiments by Prof. Phil Taylor, showed that during a model for adoptively transferring peritoneal cells using congenic CD45.1 and CD45.2 mice (Komuro *et al.*, 1975) (129S6/SvEv), the ResMØs survived relatively well, with 50 % of the transferred ResMØs still present in the cavity five days after transfer. An adapted model for adoptive transfer was established (*figure 3.15*) to investigate the origins of proliferating ResMØs. Donor CD45.1<sup>+</sup> cells were retrieved via lavage from the naïve peritoneal cavity. These cells were injected into the peritoneal cavity of host CD45.2<sup>+</sup> mice and left for 24 hours. Following this, inflammation was initiated with intra-peritoneal injection of  $2 \times 10^6$  zymosan particles, and left to proceed for 4 hours or 48 hours before cell recovery via lavage. Mice which did not receive zymosan were used as a baseline control to monitor both the transfer and the disappearance reaction seen at 4 hours. This model allowed for comparison between the responses of both donor (CD45.1) and host (CD45.2) cells.

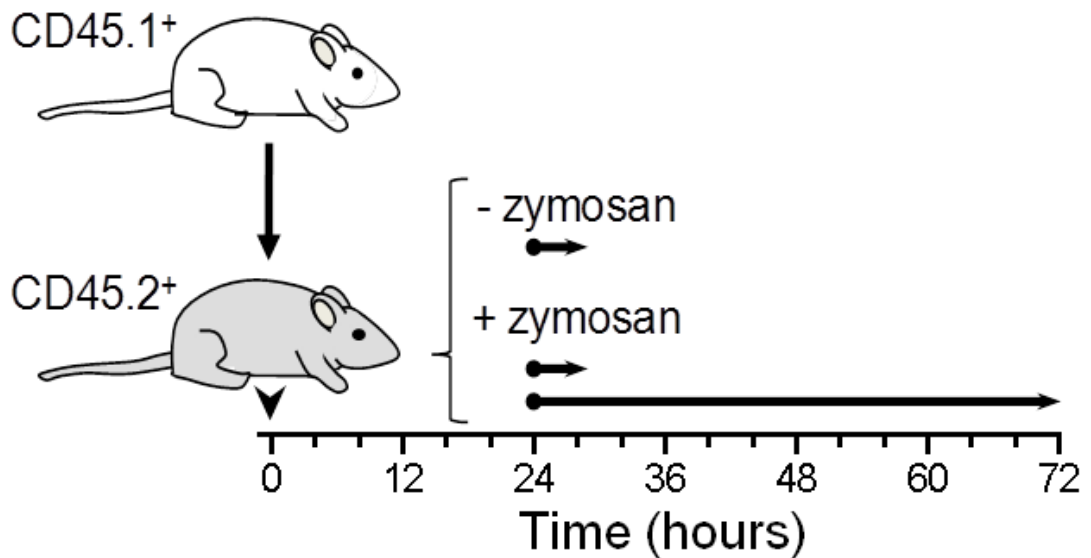


**Figure 3.14. Establishing a model for adoptive transfer of ResMØs prior to acute inflammation**

Summary of the adoptive transfer strategy used to study the cellular responses during acute inflammation ( $2 \times 10^6$  zymosan particles). Donor CD45.1<sup>+</sup> cells (retrieved via lavage, see 2.6.7) were injected into the peritoneal cavity of host CD45.2<sup>+</sup> mice. Zymosan induced inflammation was initiated (or not) 24 hours later, and peritoneal cells were recovered at 28 or 72 hours.

The recovery of donor cells was examined during acute inflammation using specific antibodies against CD45.1 and CD45.2, to separate the donor and host populations during flow cytometric analysis (*figure 3.15*). The number of MØs retrieved was quantified and showed a good survival rate 28 hours after transfer (baseline) ( $76.67 \pm 14.71$  %, mean  $\pm$  SEM,  $n = 5$ ). The majority of InfMØs retrieved 48 hours after inflammation ( $2 \times 10^6$  zymosan particles) were host derived ( $92.96 \pm 1.77$  %, mean  $\pm$  SEM,  $n = 7$ ) (*figure 3.16*). The remaining cells in this InfMØ gate were most likely F4/80<sup>low</sup> MHCII<sup>high</sup> Res DCs/MØs ( $45375 \pm 535$  injected vs  $21803 \pm 2543$  seen in the InfMØ gate at 48 hours, mean  $\pm$  SEM). Donor ResMØs mimicked host ResMØs during inflammation (*figure 3.17: left graph*), with a substantial disappearance reaction 4 hours after inflammation ( $73.28 \pm 3.21$  % vs  $74.72 \pm 5.68$  %, mean  $\pm$  SEM,  $n = 7$ ), followed by recovery of ResMØ numbers at 48 hours. This correlation in cell behaviour was also supported by a stable donor to host ratio over the inflammatory time course (*figure 3.17: right graph*). This data indicated that donor ResMØs were recovering their

lost numbers during the resolution of inflammation, and this was independent from bone marrow-derived monocyte recruitment.

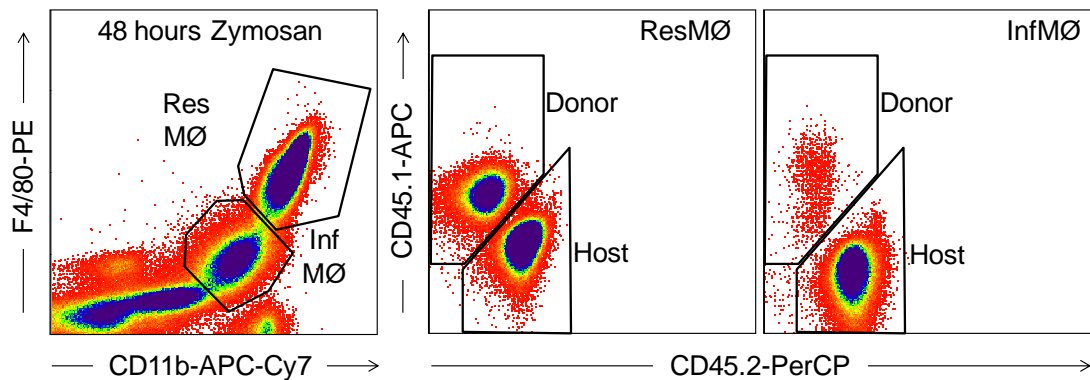


**Figure 3.15. Determination of the persistence of adoptively transferred ResMØs during acute inflammation**

Representative density plots showing CD45.1<sup>+</sup> donor vs CD45.2<sup>+</sup> host cells within the gates for ResMØs and InfMØs from 129S6/SvEv mice (from fig 3.17) 48 hours after intra-peritoneal injection of  $2 \times 10^6$  zymosan particles. F4/80 and CD11b expression were used to discriminate MØs obtained via peritoneal lavage. Cells were gated as in figures 3.1 and 3.2 to remove doublets and eosinophils. Data is representative of 7 mice at the indicated time point.

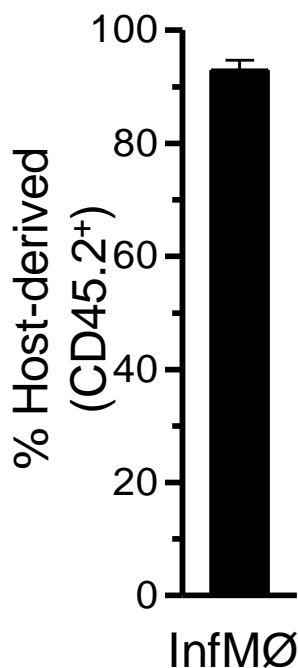


**Figure 3.16. InfMØs are host derived**

Graph showing the CD45.2<sup>+</sup> host InfMØs as a proportion of total InfMØs in the peritoneal lavage of mice, 48 hours after intra-peritoneal injection of  $2 \times 10^6$  zymosan particles. Error bars denote the mean  $\pm$  SEM of data obtained from 5-7 week old donor 129S6/SvEv CD45.1<sup>+</sup> cells and 10-12 week old host 129S6/SvEv (CD45.2<sup>+</sup>) mice (n= 7) pooled from two independent experiments.

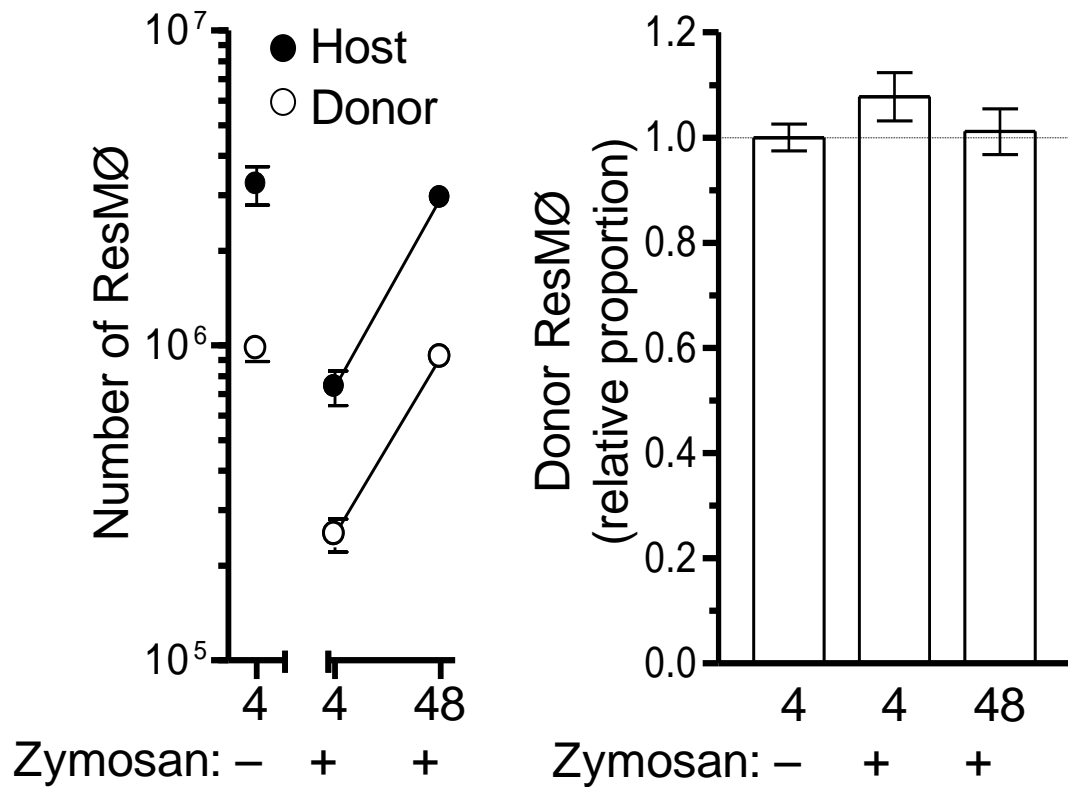


**Figure 3.17. Comparable restoration of host and donor ResMØs after acute inflammation**

Graph (left) showing the number of recoverable donor and host ResMØs in the peritoneal lavage of mice at different time points during zymosan induced inflammation ( $2 \times 10^6$  zymosan particles). White symbols depict CD45.1<sup>+</sup> donor, and black depicts CD45.2<sup>+</sup> host cells. Graph (right) showing the survival of donor ResMØs as a proportion of total ResMØs, this number was additionally made relative to the proportion of donor ResMØs observed in mice that did not receive zymosan. Error bars denote the mean  $\pm$  SEM of data obtained from 5-7 week old donor 129S6/SvEv CD45.1<sup>+</sup> cells and 10-12 week old host 129S6/SvEv (CD45.2<sup>+</sup>) mice in the peritoneal lavage of mice at different time points after zymosan. Data was pooled from two independent experiments (n= 5-7 per group).

Proliferation of ResMØs was investigated using pHH3 and DNA content analysis. Both donor and host cells were proliferating, and there was no significant difference between the proliferation of donor and host ResMØs (*figure 3.18*). The proliferation of donor and host ResMØs at baseline was relatively high (e.g. donor =  $0.16 \pm 0.03$  % pHH3<sup>+</sup>, mean  $\pm$  SEM, n= 5), which was most likely due to the inflammation caused by the injection of the cells 28 hours previously.

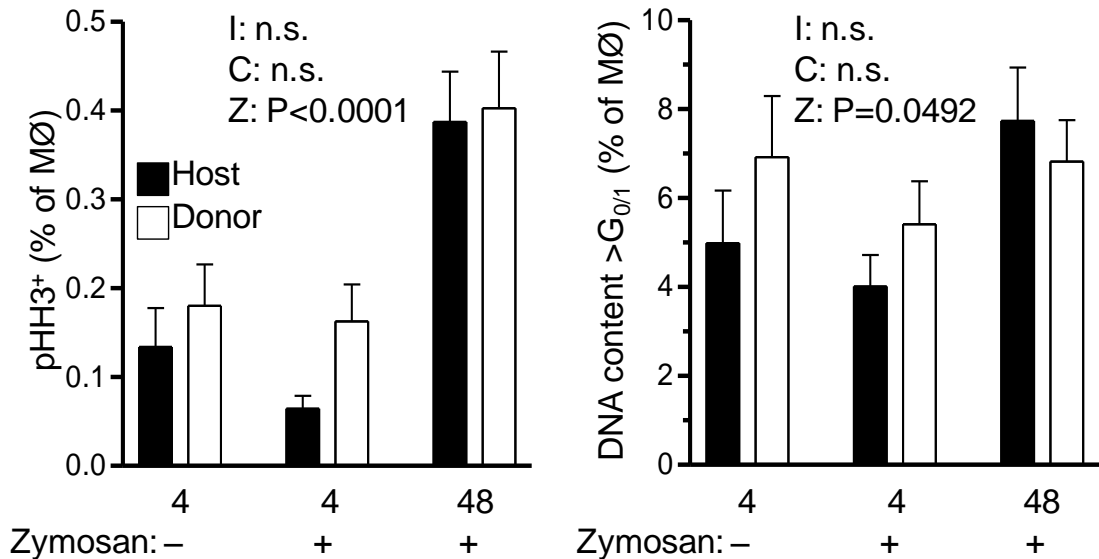


**Figure 3.18. Comparable proliferative response of host and donor ResMØs after acute inflammation**

Graphs showing the percentage of ResMØs that are pHH3<sup>+</sup> (left) or have DNA content >2N (right) in mice at different time points after receiving 2×10<sup>6</sup> zymosan particles. Data were analyzed by two-way ANOVA with Bonferroni post tests to determine differences between groups, and significance values are indicated: I= interaction between the effects of cell type and zymosan treatment, C= cell type, Z= effect of zymosan treatment over time. Error bars denote the mean ± SEM. The data is pooled from two independent experiments with 5-7 week old donor 129S6/SvEv CD45.1<sup>+</sup> cells and 10-12 week old host 129S6/SvEv (CD45.2<sup>+</sup>) mice (n= 5-7 per group).

### 3.2.7 – A significant proportion of ResMØs are generated by proliferation during inflammation

The methods used for looking at active proliferation *in situ* using Ki67 and pHH3 staining give a good indication of active proliferation, but do little to quantify how much proliferation has occurred and how many new daughter cells are generated by this process. The level of ResMØ proliferation observed during inflammation (as measured by % pHH3<sup>+</sup>) was approximately a third of that seen in a fast growing MØ precursor cell line (0.64 ± 0.07 % vs 1.64 ± 0.17 %, mean ± SEM, n= 6), as shown in figure 3.4. This indicated that a significant number of cells would be generated *in situ*. To quantify the level of ResMØ proliferation in the peritoneal cavity Bromodeoxyuridine (BrdU) was used. BrdU is a synthetic compound which can be



incorporated into DNA during DNA replication instead of thymidine; and an antibody against BrdU can be used to label cells that have been through S phase of the cell cycle (Gratzner *et al.*, 1975). BrdU was introduced to the drinking water of the mice at the initiation of inflammation ( $2 \times 10^6$  zymosan particles). ResMØs reported a significant uptake of BrdU (mean of  $\approx 50\%$ ), showing that roughly half of the recovering ResMØs are generated via proliferation, 72 hours after intra-peritoneal injection of  $2 \times 10^6$  zymosan particles. InfMØs had a lower level of BrdU uptake (mean of less than 20 %) (*figure 3.19*), which could have occurred in the bone marrow. This experiment was carried out and analysed by Dr. Marcela Rosas, and is included here because of its relevance.

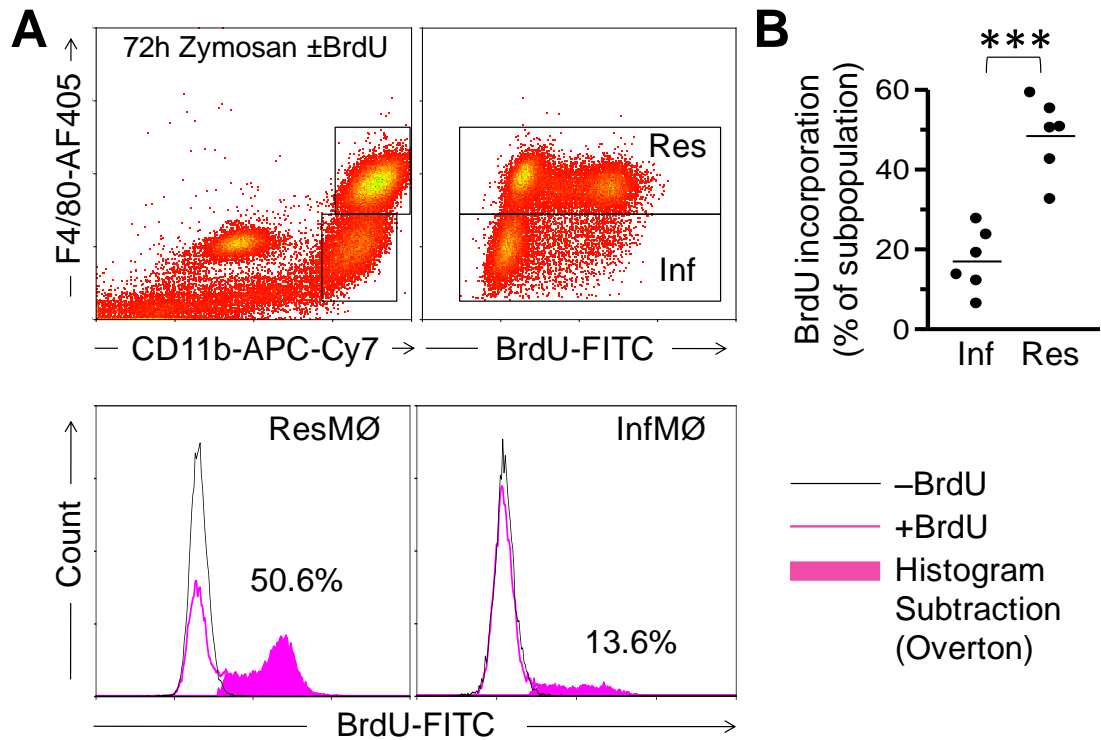


**Figure 3.19. Determination of the number of newly generated ResMØs after acute inflammation by *in vivo* BrdU incorporation**

**A)** Mice were fed BrdU in drinking water (+BrdU) immediately after intra-peritoneal injection of  $2 \times 10^6$  zymosan particles. Density plots (top) show representative BrdU incorporation in gated MØ populations 72 hours after zymosan, and histograms (bottom) showing the proportion of MØs that are BrdU<sup>+</sup> in these mice. Cells were gated as in 3.1 to remove doublets and 3.2 to remove eosinophils. F4/80 and CD11b expression were used to distinguish MØ populations. The data is representative of 6-7 week old C57BL/6 mice from one of two independent experiments. **B)** Graphical representation of the data from (A) above showing BrdU incorporation in ResMØs and InfMØs. Each symbol represents an individual 6-7 week old C57BL/6 mouse from two independent experiments and horizontal bars denote means. Data were analyzed by a paired *t*-test. As stated in the text, this experiment was conducted by Dr. Marcela Rosas.

### 3.3 – Discussion

The aim of this chapter was to investigate the potential for ResMØs to self renew via proliferation during homeostasis and inflammation. Firstly, a model was established to investigate cell cycle in peritoneal MØs. Then proliferation was examined during homeostasis and neonatal growth through to adulthood when ResMØ numbers were expanding. Finally, proliferation was investigated during acute inflammation, when the number of recoverable ResMØs drops after initial stimulus and is eventually restored during the resolution of inflammation.

#### 3.3.1 – Flow cytometric analysis of MØ populations

A model to investigate ResMØ proliferation was established through the use of polychromatic flow cytometry. Specific markers and precise gating strategies were employed to accurately dissect MØ populations during homeostatic and complex inflammatory conditions. Doublets were frequent artefacts of flow cytometry, but great care was taken to exclude these from analysis via gating around their abnormal signal area to linear ratio and pulse width to signal ratio. These ratios were subtly different depending on cell type, for example: lymphocytes are small spherical cells so will have a different ratio from large globular MØs with irregular shapes. Therefore, the order of flow cytometric gating (i.e. whether doublets were removed first then MØs were gated) was decided on a case by case basis, to avoid the removal of large, complex, and potentially proliferating cells.

ResMØs have been extensively studied in Prof. Phil Taylor's group, and are typically classified by their F4/80<sup>high</sup> CD11b<sup>high</sup> phenotype (Rosas *et al.*, 2010), which can be used to distinguish them from all other cell types in the peritoneal cavity. However, the fixation and permeabilization procedure (required for analysis of the cell cycle) slightly altered the flow cytometric profile of the cells. The implications of this were that other cell types now complicated flow cytometric analysis of MØ populations. Eosinophils are highly auto-fluorescent and also express the F4/80 antigen, which was used to gate for MØ populations. Fortunately eosinophils have a distinct FSc/SSc profile after fixation/permeabilization, which was used to exclude them from analysis. This was confirmed by staining of peritoneal cells with Siglec-F (supplemental *figure S1*), which

is selective for eosinophils in the peritoneal cavity (Ohnmacht *et al.*, 2007), and also negative staining for Tim4 in naïve mice; Tim4 is largely restricted to ResMØs in the peritoneal cavity (confirmed by Dr. Marcela Rosas). The Tim4<sup>-</sup> FSc/SSc profile of eosinophils is also shared by mast cells. However, mast cells were CD11b<sup>low/-</sup> (supplemental *figure S2*), while eosinophils had a higher expression of CD11b in the peritoneal cavity; this facilitated their separation during differential counts. This was confirmed with CD117 expression by Dr. Marcela Rosas, which is primarily expressed by mast cells in the peritoneal cavity (Hsu *et al.*, 2010, Miettinen and Lasota, 2005). More eosinophils are recruited to the peritoneal cavity during acute inflammation, along with neutrophils and InfMØs. After fixation and permeabilization, neutrophils become smaller and less granular (supplemental *figure S2*), this was used in conjunction with their F4/80<sup>-</sup> and CD11b<sup>high</sup> phenotype to distinguish them from MØs. F4/80<sup>low</sup> MHCII<sup>high</sup> Res DCs/MØs in the naïve peritoneal cavity and the InfMØs that arrive during the first few days of inflammation (induced by 2×10<sup>6</sup> zymosan particles) have a different F4/80-CD11b profile to ResMØs, even when fixed/ permeabilized. The ResMØ restricted Tim4<sup>+</sup> staining confirmed the F4/80<sup>high</sup> phenotype of ResMØs and the F4/80<sup>low</sup> phenotype of F4/80<sup>low</sup> MHCII<sup>high</sup> Res DCs/MØs and InfMØs, as a consequence the F4/80 antigen was used to distinguish between these MØ subsets.

### 3.3.2 – Nuclear profile of ResMØs

The nuclear profile of ResMØs was found to be complicated by the presence of multi-nucleate MØs, and the potential for phagocytic events. This non cell cycle-associated DNA content concealed the accurate measure of cell cycle. To definitively identify active phases of the cell cycle *in situ*, select markers of proliferation were employed in complex polychromatic flow cytometry. Ki67 and pHH3 were chosen over other markers of proliferation (eg. the cyclins) due to the availability of directly conjugated antibodies for use in flow cytometry, and the specificity of the markers themselves. Ki67 is expressed in all active cell cycle phases, while pHH3 is selective for certain phases of mitosis. Mitotic events were identified in ResMØs from the resting peritoneal cavity using pHH3<sup>+</sup> staining; and this was found to coincide with high Ki67 staining. The specific association of pHH3 with high Ki67 staining may be a sign of Ki67 relocation during mitosis (Scholzen and Gerdes, 2000) or greater antigen availability

due to the breakdown of the nuclear envelope during mitosis. The absence of Ki67<sup>+</sup> expression was also able to distinguish cells with non cell cycle-associated >2N DNA content, such as that found in multinucleate cells. The high levels of non cell cycle-associated DNA content further demonstrates the limitations of cell cycle analysis of ResMØs using DNA content alone. However, Ki67 enabled quantification of the cell cycle stages in adult mice, and confirmed a low-level of homeostatic ResMØ proliferation.

### **3.3.3 – ResMØs proliferate in homeostasis and neonatal growth**

Langerhans cells of the skin are a MØ population that is seeded prenatally. Langerhans cells increase their numbers by a high level of local proliferation in the neonate; and they maintain their numbers through a low level of proliferation in the adult (Chorro *et al.*, 2009). However, this was suggested to be restricted to tissues with limited vasculature. Microarray data of MØ populations during inflammation from Prof. Phil Taylor's group revealed transcripts linked to proliferation or associated with stem cells that were expressed by ResMØs (see 1.3.1). Therefore, the proliferation of ResMØs was examined in the neonate and adulthood to test the hypothesis: that peritoneal ResMØs are akin to Langerhans cells, in that their population is established by a high level of proliferation in the neonate and maintained throughout adulthood. Younger mice have significantly less cells and ResMØs in the peritoneal cavity than older mice. However, younger mice have substantially higher levels of proliferation than the older mice, measured by the definitive mitotic marker pHH3<sup>+</sup>. This proliferation coincides with the expansion of ResMØ numbers; which indicates that peritoneal ResMØ numbers are established in the adult via local proliferation of cells present at, or soon after birth. This has recently been confirmed by fate mapping studies, which show that peritoneal ResMØs are seeded during development (Yona *et al.*, 2012). The level of mitosis correlated with >2N DNA content in the younger mice; but did not correlate in the older mice. This highlights that analysing DNA content alone in ResMØs is insufficient, and explains the need for these specific markers of proliferation (pHH3 and Ki67), especially in older mice.

### **3.3.4 – ResMØs proliferate during acute inflammation to restore depleted numbers**

ResMØ numbers are depleted during zymosan peritonitis and cells with the same phenotype recover approximately 72 hours later (in this mild model of  $2 \times 10^6$  zymosan particles (Rosas *et al.*, 2010)). This 'disappearance' has been attributed to increased adherence, migration to draining lymph nodes, or cell death (Barth *et al.*, 1995). Experiments utilising aliphatic dyes have been interpreted to claim that the cells present before inflammation are the same as those present after (Melnicoff *et al.*, 1989); however this does not acknowledge the transfer of dyes via phagocytosis, or other inflammatory kinetics such as inflammation induced by dye injection. For more definitive understanding, the level of ResMØ proliferation was examined during the recovery phase of inflammation with specific markers of proliferation (pHH3 and Ki67). This identified a burst in proliferative activity in ResMØs 48 hours after zymosan insult. The proportion of ResMØs in this stage of mitosis was approximately a third of that of a fast growing cell line, however the burst in proliferation seen in ResMØs is likely more synchronous than that of the cell line, because it was only recently initiated, and perhaps under stricter physiological control. The extent of ResMØ proliferation was quantified using BrdU incorporation by Dr. Marcela Rosas. Over half the ResMØs incorporated BrdU which shows that half of the end-point population was produced via proliferation in this mild model. This demonstrated that proliferation is a major mechanism for MØ renewal during the resolution of inflammation, but also indicates that much of the initial disappearance reaction could be attributed to increased tissue retention, leading to reduced recovery during lavage.

### **3.3.5 – ResMØs renew *in situ*, without the need for blood monocyte precursors**

Adoptive transfer experiments were used to test for *in situ* proliferation. These experiments mathematically confirmed that the vast majority of proliferating ResMØs in the resolution phase of zymosan induced inflammation (48 hours), were the same as those present in the naïve tissue before challenge. This, along with data from BrdU incorporation shows that the majority of the recovered ResMØ population consists of cells present before zymosan insult; which must have remained adherent to the tissue or lost from the tissue, with the rest (roughly 50 %) reconstituted via proliferation. The

adoptive transfer also confirmed that the InfMØs in the peritoneal cavity were from the periphery, as the vast majority were host derived.

### **3.3.6 – Conclusion**

In conclusion, the studies in this chapter, which have now been published (Davies *et al.*, 2011), showed that: 1) ResMØs contain non cell cycle-associated DNA content, nevertheless precise markers of proliferation can be used to show that there is a low level of homeostatic proliferation in the peritoneal cavity of adult mice; 2) ResMØ numbers are expanded in the neonate and maintained in the adult mouse via local proliferation; and 3) ResMØs restore their population during the resolution of a mild acute inflammation via a burst in local proliferation, that can be independent from blood monocytes, and contributes to the restoration of MØ numbers after acute inflammation. This redefines our understanding of MØ renewal in a vascular tissue (peritoneal cavity), challenging the dogma of the MPS, and opens up new avenues to investigate MØ function in homeostasis and inflammation.

## Chapter 4 – InfMØs proliferate *in situ* during inflammation



## 4.1 – Introduction

### 4.1.1 – Ly-6B<sup>+</sup> InfMØ persistence

Zymosan peritonitis has been extensively used by our research group to study inflammation in the peritoneal cavity (Taylor *et al.*, 2007, Rosas *et al.*, 2010) (and chapter 3 of this thesis). Monocytes recruited to the peritoneal cavity during acute inflammation differentiate into InfMØs and can persist for weeks after the inflammatory stimulus (*figure 4.01*) (Rosas *et al.*, 2010).

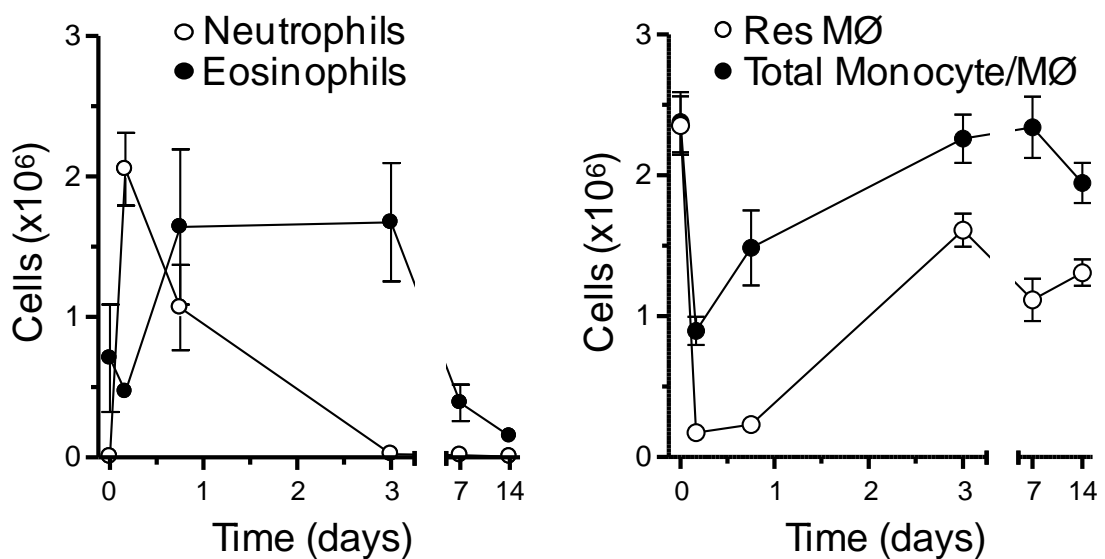


**Figure 4.01. Kinetics of acute zymosan induced peritonitis**

Graphs showing the numbers of neutrophils and eosinophils (left panel), and total monocyte/ MØs and ResMØs (right panel) present at the indicated times after intraperitoneal administration of  $2 \times 10^6$  zymosan particles. The difference in numbers between total monocyte/MØs and ResMØs represents numbers of InfMØs and monocytes. Data represents mean  $\pm$  SEM of 3-5 C57BL/6 female mice (6 weeks old) per time point, taken from one of two similar experiments carried out by Dr. Marcela Rosas (Davies *et al.*, 2013b), and is included because of its relevance.

These InfMØs coexist with a recovering ResMØ population and are heterogeneous. Dr. Marcela Rosas identified differential expression of the antigen 7/4 which is synonymous with Ly-6B on InfMØs. Ly-6B<sup>+</sup> InfMØs also showed differences in the expression of other surface markers, including: CD200R, CD9 and CD11b in comparison

to Ly-6B<sup>-</sup> InfMØ/ResMØs (Rosas *et al.*, 2010). Ly-6B was originally identified on neutrophils (Hirsch and Gordon, 1983), but is also expressed on monocytes and InfMØs that arrive during acute inflammation (Henderson *et al.*, 2003, Taylor *et al.*, 2003). After intra-peritoneal challenge with  $2 \times 10^6$  particles of zymosan, InfMØs are recruited to the peritoneal cavity and maintain their numbers for at least 14 days. This Tim4<sup>-</sup> population of InfMØs contains a proportion of cells that are Ly-6B<sup>+</sup>, which show myeloid cell morphology with an irregular nucleus and large cytoplasm (*figure 4.02*).

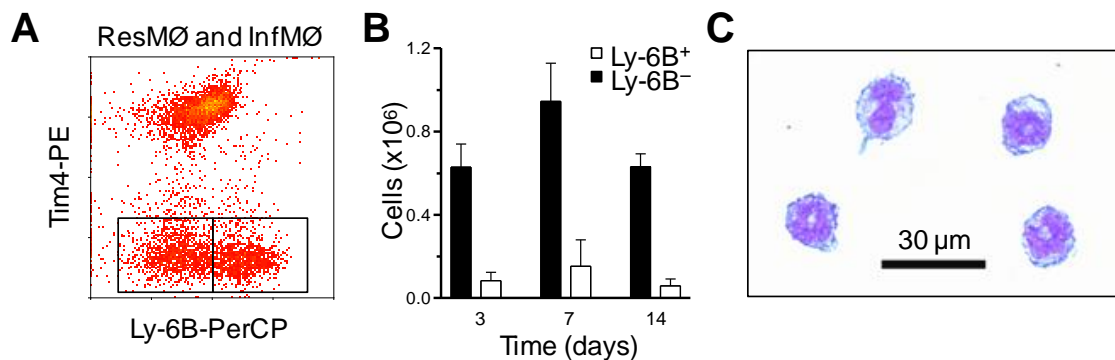


**Figure 4.02. Presence and persistence of Ly-6B<sup>+</sup> InfMØ**

**A)** Representative flow cytometric profiles showing Tim4 and Ly-6B expression on MØs gated using the ResMØ and InfMØ gate (as in *figure 3.10*), and pre-gated to remove doublets (*figure 3.1*) and eosinophils (*figure 3.2a*). It shows that Ly-6B<sup>+</sup> InfMØs are clearly distinct from Tim4<sup>high</sup> ResMØ. The box gates denote Ly-6B<sup>+</sup> and Ly-6B<sup>-</sup> InfMØ populations. **B)** Approximately one fifth of cells classified as InfMØs are Ly-6B<sup>+</sup> and they are detectable for several weeks after induction of a mild inflammatory challenge. Data represents mean  $\pm$  SEM of 3-5 C57BL/6 female mice (6 weeks old) per time point, taken from one of two similar experiments. **C)** The Ly-6B-expressing MØs were gated as indicated (A) and purified (>90 %) by flow cytometric cell-sorting on a Moflo legend (Beckman Coulter). Cells were centrifuged onto slides using a Cytospin 3, then fixed and stained with eosin and methylene blue. Images were acquired on a Leica light microscope at 40 $\times$  objective magnification. Cells were pooled from 10 (6 week old) female C57BL/6 mice 7 days after intra-peritoneal zymosan ( $2 \times 10^6$  particles) (Davies *et al.*, 2013b). This experiment was carried out by Dr. Marcela Rosas, and is included because of its relevance.

#### 4.1.2 – Prospect of Ly-6B<sup>+</sup> InfMØ proliferation

Dr. Marcela Rosas also showed that a large proportion of Ly-6B<sup>+</sup> InfMØs were newly generated by proliferation by utilising BrdU incorporation (Rosas *et al.*, 2010) (also see 3.2.7). This proliferation could have occurred in MØ progenitors in the bone marrow, so only showed that Ly-6B<sup>+</sup> InfMØs were recently generated. However, in the previous chapter of this thesis, it was shown that ResMØs have the capacity to proliferate to establish and maintain their population during homeostatic growth and also to renew their population after inflammatory depletion by a rapid proliferative burst. BrdU was used to quantify this level of proliferation in inflammation (*figure 3.19*). This proliferation was confirmed to occur *in situ* via the use of adoptive transfer experiments (*figures 3.17 and 3.18*) and definitive identification of cells in mitosis (*figure 3.5*). During these and similar experiments the proliferation of InfMØs was measured alongside that of ResMØs. Although, the InfMØs did not show the same pattern of a proliferative burst, they did exhibit a definitive, quantifiable low-level of proliferation (*figure 3.11*); and confirmed the overall low level of BrdU incorporation in total InfMØs as seen in Dr. Rosas' previous study (Rosas *et al.*, 2010).

Microarray analysis of monocyte and MØ populations during inflammation (initiated by  $2 \times 10^6$  particles of zymosan) was performed by Dr. Marcela Rosas as described in the general introduction (1.3.1). Comparison of transcripts differentially expressed between day 7 Ly-6B<sup>+</sup> and Ly-6B<sup>-</sup> MØs identified an enrichment of transcripts that were associated with proliferation in Ly-6B<sup>+</sup> MØ. Notably however, proliferation of ResMØs was substantially attenuated 7 days after  $2 \times 10^6$  particles of zymosan (both in genes associated with proliferation and in cell cycle studies, for an example see the future results chapter 6 - *figure 6.19*). This information was combined with the low level proliferation of InfMØs, and the enrichment of BrdU incorporation in Ly-6B<sup>+</sup> InfMØs seen during inflammation (Rosas *et al.*, 2010). This derived the hypothesis: that Ly-6B<sup>+</sup> InfMØs may not be terminally differentiated and could also have the capacity to proliferate like that of ResMØs, although potentially with distinct control mechanisms. Importantly *in situ* proliferation of monocyte-derived MØs has never been definitively reported.

This cellular proliferation would most-likely be governed by growth factors and other soluble mediators. At the same time that the experiments in chapter 3 of this thesis

were completed (Davies *et al.*, 2011), Jenkins *et al.* reported a high level of ResM $\emptyset$  proliferation in the peritoneal cavity during helminth infection. This proliferation was dependent upon the cytokine IL-4 (Jenkins *et al.*, 2011). IL-4 is produced by a number of cells including: T<sub>H</sub>2 lymphocytes, eosinophils and mast cells (Voehringer *et al.*, 2004). It is known to promote both T<sub>H</sub>2 differentiation through STAT6 (Kaplan *et al.*, 1996) and 'alternative activation' of M $\emptyset$ s: enhancing expression of molecules such as mannose receptor (Stein *et al.*, 1992). There are other cytokines which have also been shown to promote M $\emptyset$  proliferation. M-CSF is frequently used to expand and differentiate M $\emptyset$ s from bone marrow progenitors (Hume and Gordon, 1983). M-CSF is essential for the proliferation of these differentiated progenitors and it's also essential for the formation of osteoclasts from monocytic precursors (Hattersley *et al.*, 1991). A deficiency in M-CSF, such as that seen in the naturally occurring mutation in the osteopetrotic (*op/op*) mouse causes a marked deficiency in many M $\emptyset$  populations, including peritoneal ResM $\emptyset$ s (Wiktor-Jedrzejczak *et al.*, 1990), which could be a result of impaired differentiation or proliferation.

The quantity of zymosan ( $2 \times 10^6$  particles) used in the majority of this thesis promotes a mild, acute model of inflammation that is unlikely to trigger an IL-4 rich T<sub>H</sub>2 environment as seen with helminth infection (Jenkins *et al.*, 2011), although this does not exclude innate sources of IL-4. Whilst it is possible that IL-4 is required for M $\emptyset$  proliferation in the acute zymosan model, it has been suggested that the small proliferative responses of M $\emptyset$ s brought about by IL-4 treatment could be a result of stimulated autocrine signalling from M-CSF (Gordon, 2003). Given the marked impact of the *op* mutation on detectable peritoneal M $\emptyset$  numbers, M-CSF appears a strong target for investigating the control mechanisms for M $\emptyset$  proliferation in homeostasis and acute inflammation.

### 4.1.3 – Hypothesis

The hypothesis tested in this chapter is that peripherally recruited Ly-6B<sup>+</sup> InfMØs have the capacity to proliferate *in situ*, as an alternative mechanism of generation during the resolution of inflammation; and that proliferation of ResMØs and Ly-6B<sup>+</sup> InfMØs is under the control of the growth factor M-CSF in inflammation.

### 4.1.4 – Aims

- To determine whether Ly-6B<sup>+</sup> InfMØs proliferate during acute inflammation
- To investigate the origins of Ly-6B<sup>+</sup> InfMØs in acute inflammation
- To evaluate the roles of IL-4 and M-CSF in MØ proliferation in homeostasis and inflammation

## 4.2 – Results

### 4.2.1 – Definition of Ly-6B<sup>+</sup> InfMØs in complex inflammatory environments

Acute inflammation was initiated by injection of zymosan particles ( $2 \times 10^6$ ) into the peritoneal cavity. During the resolution of this inflammation the cellular kinetics alter drastically, with a short spike in neutrophil numbers followed (and overlapped) by a sustained influx of monocytes, which have the potential to differentiate into InfMØs (see previous *figure 4.01*). Newly arrived monocytes share an F4/80<sup>low</sup> Ly-6B<sup>+</sup> profile with Ly-6B<sup>+</sup> InfMØs (*figure 4.1a*), however, their physical size (measured by FSC<sub>AREA</sub>) and lower CD11b expression could be used to remove them when analysing Ly-6B<sup>+</sup> InfMØs (*figure 4.1b and c*).

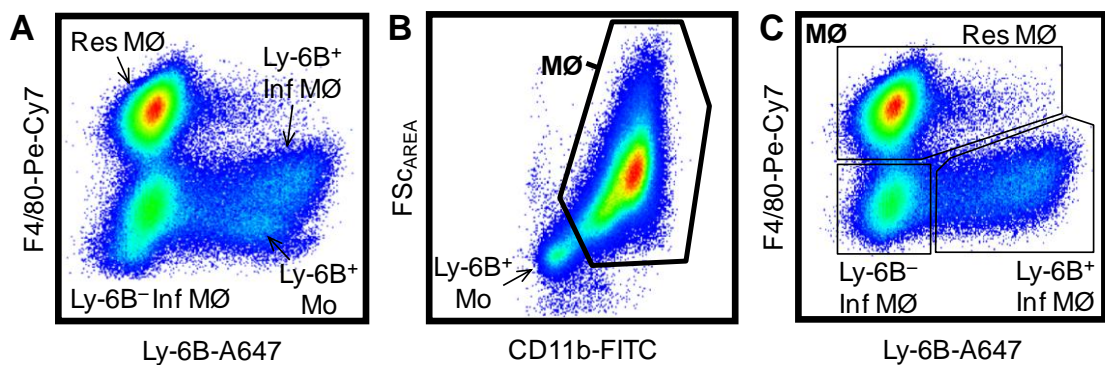


**Figure 4.1. Classification of Ly-6B<sup>+</sup> InfMØs during inflammation**

Representative density plots showing MØs and monocytes from mice 72 hours after the induction of peritonitis with  $2 \times 10^6$  zymosan particles. Plots A and B have been gated using the ResMØ and InfMØ gate (as described in *figure 3.2b*) and pre-gated to remove eosinophils and doublets (*figures 3.1 and 3.2a*). Plot C has been additionally gated with the MØ gate in B, and shows the gating strategy for the identification of ResMØs, Ly-6B<sup>+</sup> and Ly-6B<sup>-</sup> InfMØs after the removal of monocytes. The plots are from a 6-7 week female C57BL/6 mouse, but is representative of all C57BL/6 and 129S6/SvEv mice analyzed in these studies.

#### 4.2.2 – Ly-6B<sup>+</sup> InfMØs proliferate during the resolution of zymosan induced peritonitis

The methods of analysing cell cycle from chapter three were also applied in this chapter; however a high level of Ki67 expression did not always correlate with high levels of mitosis (*figure 4.2a*). This was due to variations in the proportion of cells in the G<sub>1</sub> phase of the cell cycle, indicating that using measures for the ‘active’ phases of the cell cycle were most reliable in identifying MØ proliferation. Therefore, the S, G<sub>2</sub> and M phases of the cell cycle were combined into an ‘SG<sub>2</sub>M’ measure (*figure 4.2b*), which gave an accurate reading of active proliferation that is not restricted to certain phases of mitosis (as seen with pHH3 staining). During zymosan peritonitis (2x10<sup>6</sup> particles) most ResMØs are not recoverable during the first few hours, but recover by a burst in proliferation 48 hours after stimulus. By 72 hours the proportion of ResMØs in the SG<sub>2</sub>M phases of the cell cycle decreases to near basal levels and is comparable to that of InfMØs (*figure 3.11*). At this time point InfMØs have a low level of proliferation classified and quantified as: 1) >G<sub>0/1</sub> DNA content of 4.36 ± 0.52 % (mean ± SEM, n= 5); 2) SG<sub>2</sub>M of 3.06 ± 0.50 %; and 3) 0.08 ± 0.05 % pHH3<sup>+</sup> (quantified from mice in *figure 4.3*). However, Ly-6B<sup>+</sup> MØs have a clearly enriched level of proliferation when compared with Ly-6B<sup>-</sup> MØs in all measures of proliferation: 15.20 ± 1.15 % vs 3.64 ± 0.50 % >G<sub>0/1</sub> DNA content, 10.8 ± 1.48 % vs 2.52 ± 0.45 % SG<sub>2</sub>M and 0.34 ± 0.05 % vs 0.06 ± 0.01 % pHH3<sup>+</sup> respectively (quantified from mice in *figure 4.3*).

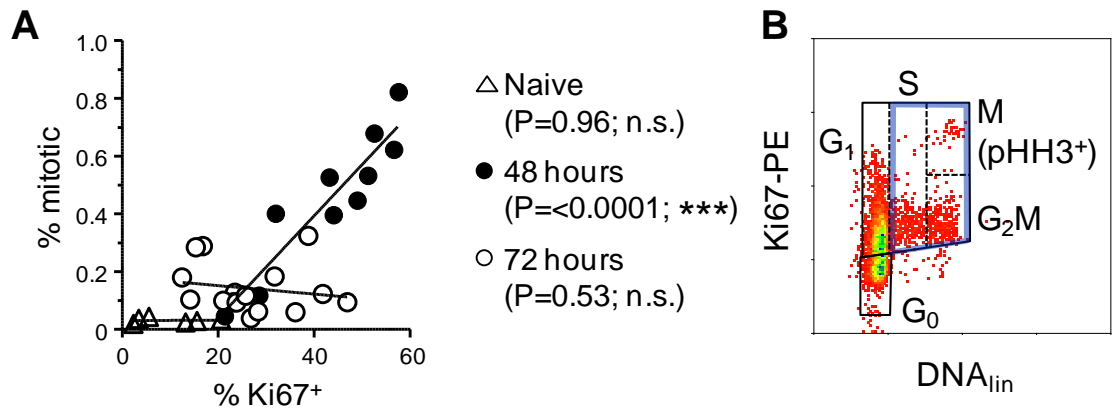


**Figure 4.2. Considerations for the use of Ki67 as a measure of cell division**

**A)** A linear correlation plot showing total Ki67 expression vs indicators of active mitosis (4N DNA content associated with pHH3 or Ki67<sup>high</sup> phenotype) in naïve mice and mice 48 and 72 hours after the induction of peritonitis with  $2 \times 10^6$  zymosan particles. All mice used were 6-7 week female C57BL/6 and each symbol represents an individual mouse pooled from 3 independent experiments. Linear correlation analysis was performed and  $P$ -values showing significance testing for a non-zero slope are indicated (\*\*\*) =  $P \leq 0.001$ ). **B)** Representative density plot showing the stages of the cell cycle after staining with Ki67 and DAPI (DNA). The boxes indicate active cell cycle stages (SG<sub>2</sub>M) which are Ki67<sup>+</sup> with >2N DNA content, the 'inactive' cell cycle stages with 2N DNA G<sub>1</sub> (Ki67<sup>+</sup>) and G<sub>0</sub> (Ki67<sup>-</sup>), but do not include non cell cycle-associated DNA content as shown in *figure 3.5*. Note that high Ki67 staining with 4N DNA content always correlated with pHH3 staining, so could be used as an additional comparative measure of mitosis. SG<sub>2</sub>M gating is highlighted in blue. The data shown is of Ly-6B<sup>+</sup> InfMØs (as shown in *figure 4.1*) 72 hours after the induction of peritonitis with  $2 \times 10^6$  zymosan particles in 6-7 week C57BL/6 female mice, however the gating strategy shown is representative of all proliferating cells in this thesis.



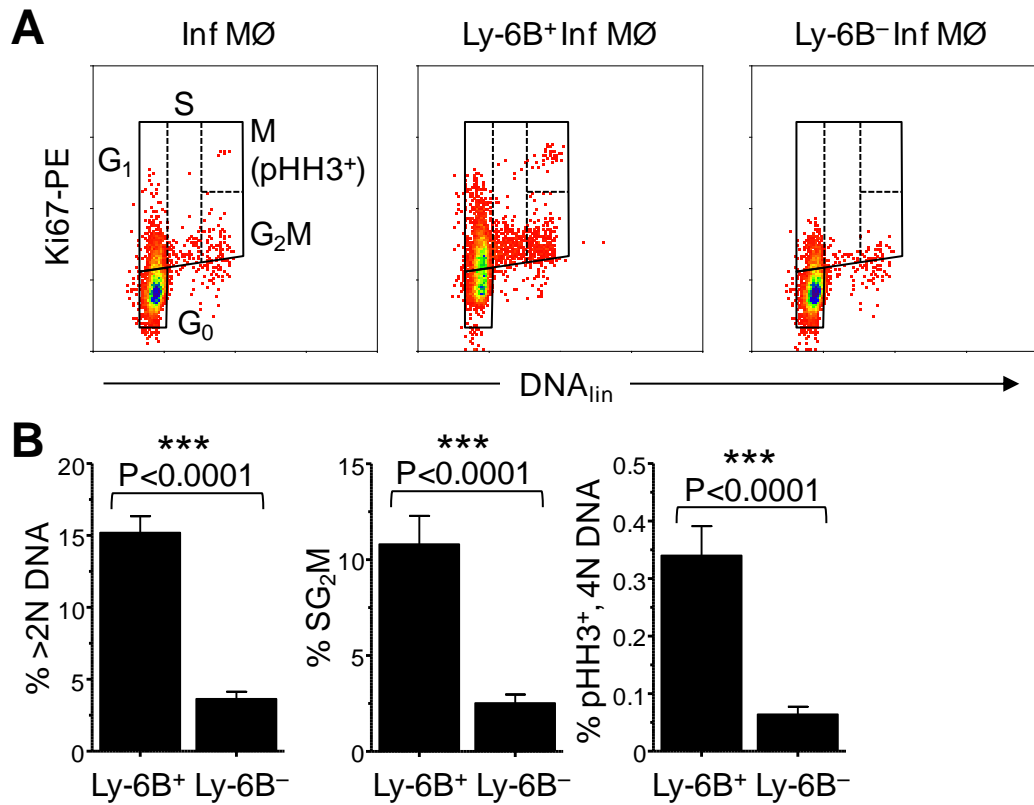


**Figure 4.3. Ly-6B-expressing InfMØs are actively dividing *in situ***

**A)** Representative density plots showing cells stained for Ki67 and DNA (DAPI), cells were gated on MØ populations as shown in figure 4.1 and also pre-gated to remove eosinophils (*figure 3.2a*) and doublets (*figure 3.1*). The plots show total InfMØ populations (left), Ly-6B<sup>+</sup> cells (middle) and their Ly-6B<sup>-</sup> counterparts (right) 72 hours after the induction of peritonitis with  $2 \times 10^6$  zymosan particles. The boxes indicate the cell cycle stages as shown in figure 4.2b. Data was derived from individual mice and are representative of at least 3 experiments with 6-7 week old C57BL/6 female mice (typically 3-5 mice per experiment). **B)** The levels of proliferation within the two populations of InfMØs from one of the experiments shown above (A) was measured by the proportion of cells with >2N DNA content (left), >2N DNA content with Ki67 expression ('SG<sub>2</sub>M', middle), and pHH3<sup>+</sup> (right). Data is expressed as mean  $\pm$  SEM of 5 mice per group. Data were analyzed by a paired *t*-test and significance values are indicated.

#### 4.2.3 – Proliferation of Ly-6B<sup>+</sup> InfMØs is not restricted to zymosan peritonitis

A higher number of zymosan particles ( $2 \times 10^7$ ) or 1 ml of 4 % (w/v) thioglycollate broth were used as alternative initiators of peritoneal inflammation, to determine whether Ly-6B<sup>+</sup> MØ proliferation is restricted to a lower dose of zymosan ( $2 \times 10^6$  particles). The higher dose of zymosan resulted in increased numbers of InfMØs, with a substantial presence of Ly-6B<sup>+</sup> MØs, but it also resulted in a reduced number of recoverable ResMØs when compared to the low dose, as expected (Taylor *et al.*, 2003, Taylor *et al.*, 2005b) (*figure 4.4*). The Ly-6B<sup>+</sup> MØs are also proliferating during inflammation caused by this high dose and at a significantly higher level than the Ly-6B<sup>-</sup> InfMØs (*figure 4.5*). In contrast, the thioglycollate broth resulted in a near complete depletion of ResMØs compared to that of low dose zymosan ( $0.17 \pm 0.03 \times 10^6$  vs  $2.15 \pm 0.42 \times 10^6$  mean  $\pm$  SEM respectively, n= 3) and no evident Ly-6B<sup>+</sup> InfMØ population 72 hours after injection into the peritoneal cavity (*figure 4.4*). However, if cells were lavaged 1 week after thioglycollate injection, small numbers of both Ly-6B<sup>+</sup> InfMØ and ResMØ populations could be identified (*figure 4.6*), with the Ly-6B<sup>+</sup> InfMØs having high (0.67  $\pm$  0.12 % 4N DNA content, Ki67<sup>high</sup>, mean  $\pm$  SEM, n= 5) and comparable levels of proliferation to that of the high dose zymosan model after 72 hours (0.66  $\pm$  0.13 % pHH3<sup>+</sup>) (*figure 4.5*).

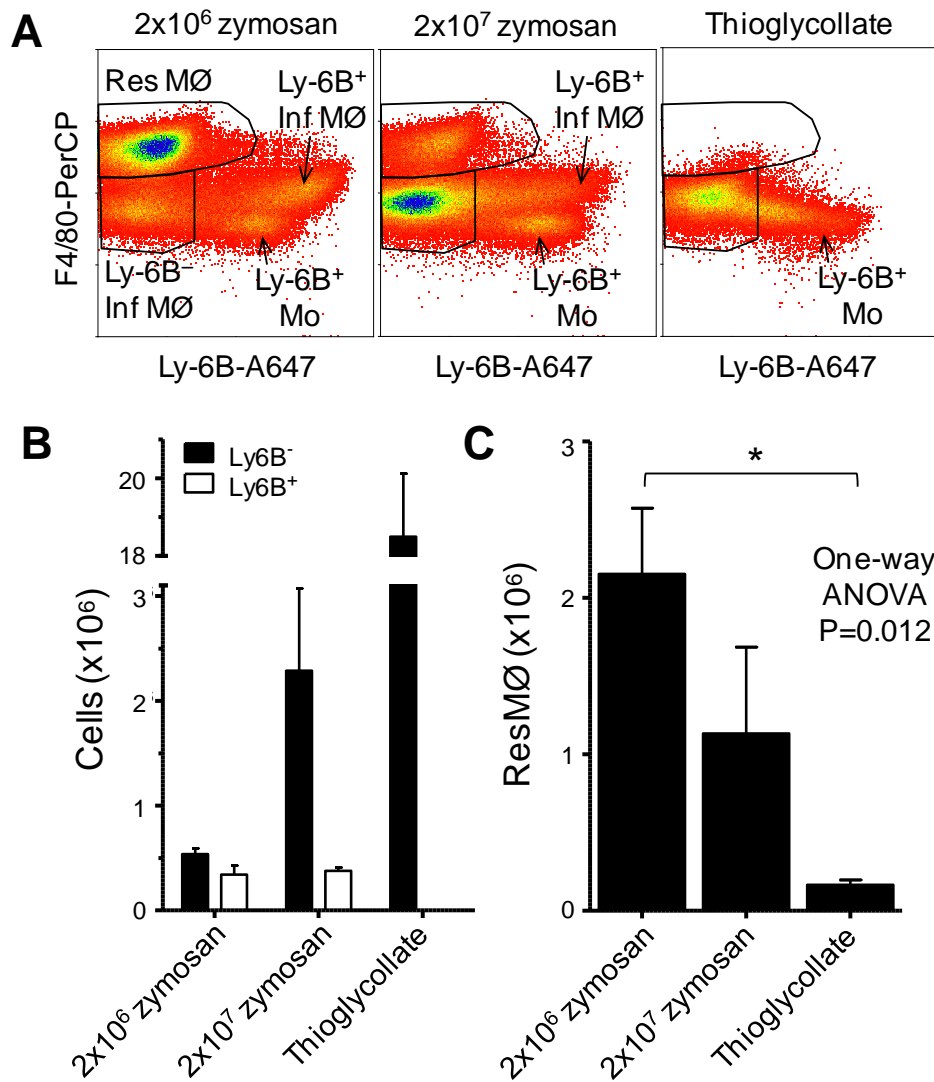


**Figure 4.4. MØ populations during peritonitis**

**A)** Representative flow cytometric profiles showing F4/80 and Ly-6B expression in MØs gated using the ResMØ and InfMØ gate (as described in *figure 3.2b*), and also pre-gated to remove eosinophils (*figure 3.2a*) and doublets (*figure 3.1*). Cells were taken from mice 72 hours after induction of peritonitis with zymosan (both  $2 \times 10^6$  and  $2 \times 10^7$  particles) or 1ml of 4 % (w/v) thioglycollate broth, as indicated. The presence of Ly-6B<sup>+</sup> monocyte and Ly-6B<sup>+</sup> InfMØ populations are shown. Flow cytometric plots are representative of at least 3 C57BL/6 female mice per group from one of two similar experiments. **B)** Bar graph showing a quantification of Ly-6B<sup>+</sup> and Ly-6B<sup>-</sup> MØ numbers. Note that Ly-6B<sup>+</sup> InfMØs were undetectable 72 hours after thioglycollate broth. **C)** Bar graph showing a quantification of ResMØ numbers analysed by one-way ANOVA with Bonferroni post tests (\* =  $P \leq 0.05$ ) to define the significance of differences between the groups, the ANOVA *P*-value is indicated. Data in both B and C are from the experiment described in A.

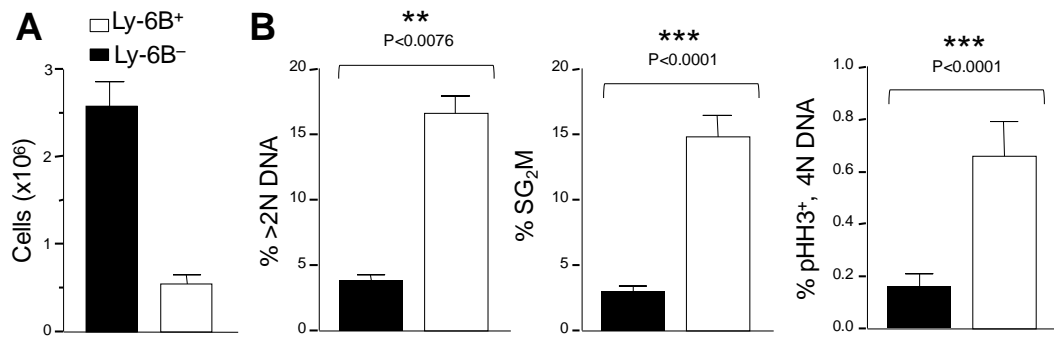


**Figure 4.5. MØ proliferation during high dose zymosan peritonitis**

**A)** Graph showing numbers of Ly-6B<sup>+</sup> and Ly-6B<sup>-</sup> InfMØs recovered from mice 72 hours after intra-peritoneal injection of  $2 \times 10^7$  particles of zymosan. **B)** Graphs showing proliferation of Ly-6B<sup>+</sup> and Ly-6B<sup>-</sup> InfMØs 72 hours after the induction of peritonitis with  $2 \times 10^7$  zymosan particles. The level of proliferation within the two populations of InfMØs was measured by the proportion of cells with >2N DNA content (left), >2N DNA content with Ki67 expression ('SG<sub>2</sub>/M', middle), and pHH3<sup>+</sup> (right). Data were analyzed by a paired *t*-test and significance values are indicated. Data (A and B) are expressed as mean  $\pm$  SEM of 5 mice per group (7-9 week old female 129S6 mice) and is from one of 2 similar experiments.

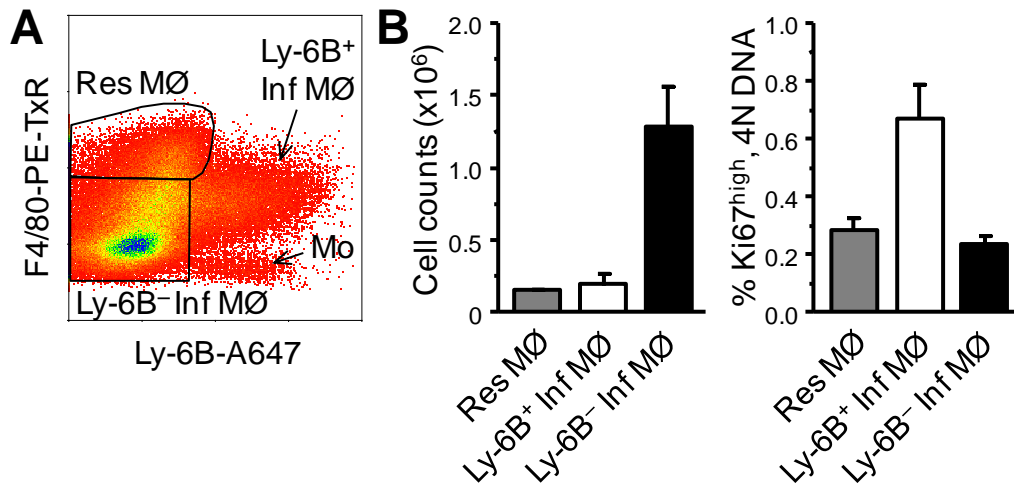


**Figure 4.6. MØ proliferation during thioglycollate peritonitis**

**A)** Representative density plot showing F4/80 and Ly-6B expression in MØs from the peritoneal cavity of mice 7 days after intra-peritoneal injection of 1ml of 4 % (w/v) thioglycollate broth. The plot has been pre-gated using the ResMØ and InfMØ gate (as described in *figure 3.2b*) and to remove eosinophils and doublets (*figures 3.1 and 3.2a*). The cell populations are indicated. **B)** Bar graph showing quantification of the total cell numbers of 3 populations from A, and their levels of proliferation, measured by Ki67<sup>high</sup> and DNA (DAPI) staining. Ki67<sup>high</sup> cells with 4N DNA content were classified as mitotic. Data shown is from five 9 week old 129S6 mice from one of two independent experiments.

#### 4.2.4 – Both Ly-6B<sup>+</sup> and Ly-6B<sup>-</sup> InfMØs are derived from the bone marrow.

The adoptive transfer experiments in chapter three of this thesis (*figures 3.15 and 3.16*) indicated that InfMØs were not derived from the cells present in the naïve peritoneal cavity, so are likely recruited from the periphery. To definitively determine whether InfMØs (specifically those expressing Ly-6B) were peripherally recruited cells, derived from the bone marrow, a collaborative study was performed with Prof. Judith Allen and Dr. Steven Jenkins in Edinburgh. Partial bone marrow chimeric mice were constructed for these studies by Dr. Steven Jenkins who: shielded the abdomen of anaesthetized C57BL/6 CD45.1 mice with a 2-inch lead screen before exposing them to a single dose of 9.5 Gy radiation. This was followed by intra-venous injection of 6x10<sup>6</sup> donor bone marrow cells from congenic C57BL/6 CD45.2 mice. Chimeric mice were left for 6 weeks before analysis of the chimerism in myeloid populations in the blood. After this time, the chimeric mice showed a good level of blood myeloid cell chimerism of

around 15-40 % (*figure 4.7a*), and were subsequently injected intra-peritoneally with  $2 \times 10^6$  particles of zymosan a day after the blood testing to initiate acute inflammation. Peritoneal cells were recovered 72 hours after initiation of the inflammation by lavage. ResMØs showed very low levels of chimerism ( $0.29 \pm 0.09$  %, mean  $\pm$  SEM, n= 6), while Ly-6B<sup>+</sup> and Ly-6B<sup>-</sup> InfMØs showed substantial levels of chimerism (*figure 4.7b*), which correlated well with the chimerism seen in the Ly-6C<sup>high</sup> blood monocytes from the same animals 4 days previously (*figure 4.7c*).

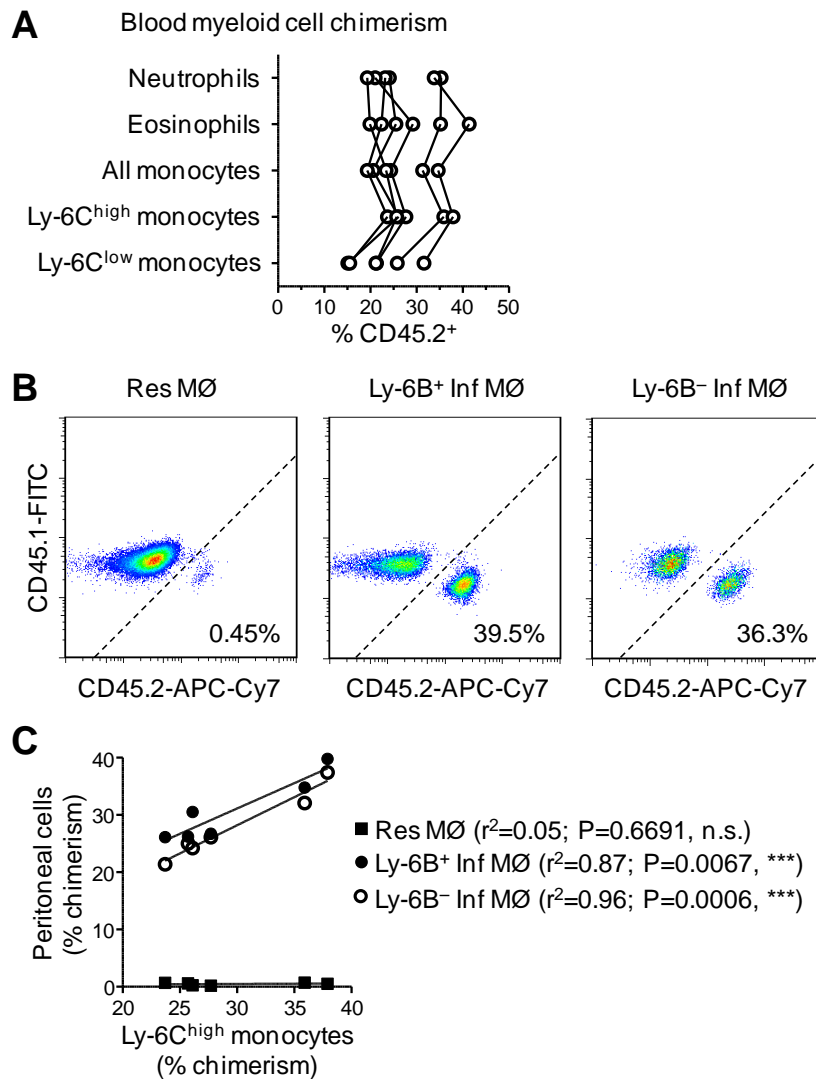


**Figure 4.7. Both Ly-6B<sup>+</sup> and Ly-6B<sup>-</sup> InfMØs are derived from the bone marrow and are quite distinct from ResMØ, which have the potential to self-renew**

**A)** Graph showing analysis of blood myeloid cell chimerism one day before induction of peritonitis (see below), a stable chimerism is seen in all partial chimeras generated by Steve Jenkins (described in 4.2.4). Each line links the data from an individual mouse. **B)** Representative flow cytometric plots gated from the populations as gated in figure 4.1 stained with antibodies against CD45.1 and CD45.2 to determine the level of chimerism between CD45.1 recipient cells and CD45.2 donor cells, 72 hours after the induction of peritonitis by intra-peritoneal administration of  $2 \times 10^6$  zymosan particles. The dashed line represents the divide between donor and recipient cells. **C)** Graphical representation of the chimerism in all of the experimental animals, correlating the chimerism of the 3 peritoneal MØ subsets with that of Ly-6C<sup>high</sup> blood monocytes within the same animal. Data were analyzed by linear regression, and  $r^2$  values are indicated alongside significance testing for a non-zero slope (\*\*\*) =  $P \leq 0.001$ ). Each symbol represents an individual irradiation chimera.

#### 4.2.5 – M-CSF is required but not sufficient for substantial ResMØ proliferation

M-CSF is a cytokine required for growth and differentiation of MØ progenitors in bone marrow (Hume and Gordon, 1983); therefore the role of M-CSF was investigated in peritoneal MØ proliferation. Exogenous recombinant M-CSF was added to cultured ResMØs to determine whether M-CSF could stimulate ResMØ proliferation *ex vivo*. Peritoneal cells were cultured for 7 or 12 days, with or without M-CSF. M-CSF treatment resulted in increased numbers of recovered, intact MØ nuclei (*figure 4.8a*); and an over three fold increase in proliferation measured by >2N DNA content. For example, at 7 days of culture 'media only' had  $3.87 \pm 0.42$  % >2N DNA (mean  $\pm$  SEM, n= 3) while M-CSF addition had  $12.3 \pm 0.24$  %. The higher cell numbers seen in M-CSF treated cells compared with media alone could be accounted for by this higher level of proliferation (*figure 4.8a*) or an increase in cell survival; as typically only 200,000 ResMØs were seeded, and the number recovered in the M-CSF treatment was  $187,345 \pm 35,307$  nuclei (mean  $\pm$  SEM) at 12 days. However, active proliferation with M-CSF treatment *in vitro* was confirmed by 5-ethynyl-2'-deoxyuridine (EdU) uptake into proliferating cells. EdU is an alternative to BrdU, it will be incorporated during DNA synthesis instead of thymidine in S phase (Buck *et al.*, 2008). EdU was added to culture media ( $\pm$  M-CSF) on day 6 of a 7 day adherent peritoneal cell culture to assess the proliferation. In one day  $4.9 \pm 0.92$  % (mean  $\pm$  SEM, n= 4) of cells incorporated EdU (*figure 4.8b*), which provides evidence for proliferation in a small percentage of the cells. When EdU was added every day in a 3 day culture  $21.88 \pm 8.72$  % (mean  $\pm$  SEM, n= 3) of the cells incorporated EdU (*figure 4.8c*). This suggests that only a small number of cells have the potential to proliferate *in vitro*, but that their daughter cells accumulate in the culture. Additionally, this proliferation coupled with cell death could explain the stagnation of cell numbers in M-CSF supplemented culture (200,00 cells cultured vs  $187,345 \pm 35,307$  cells recovered).



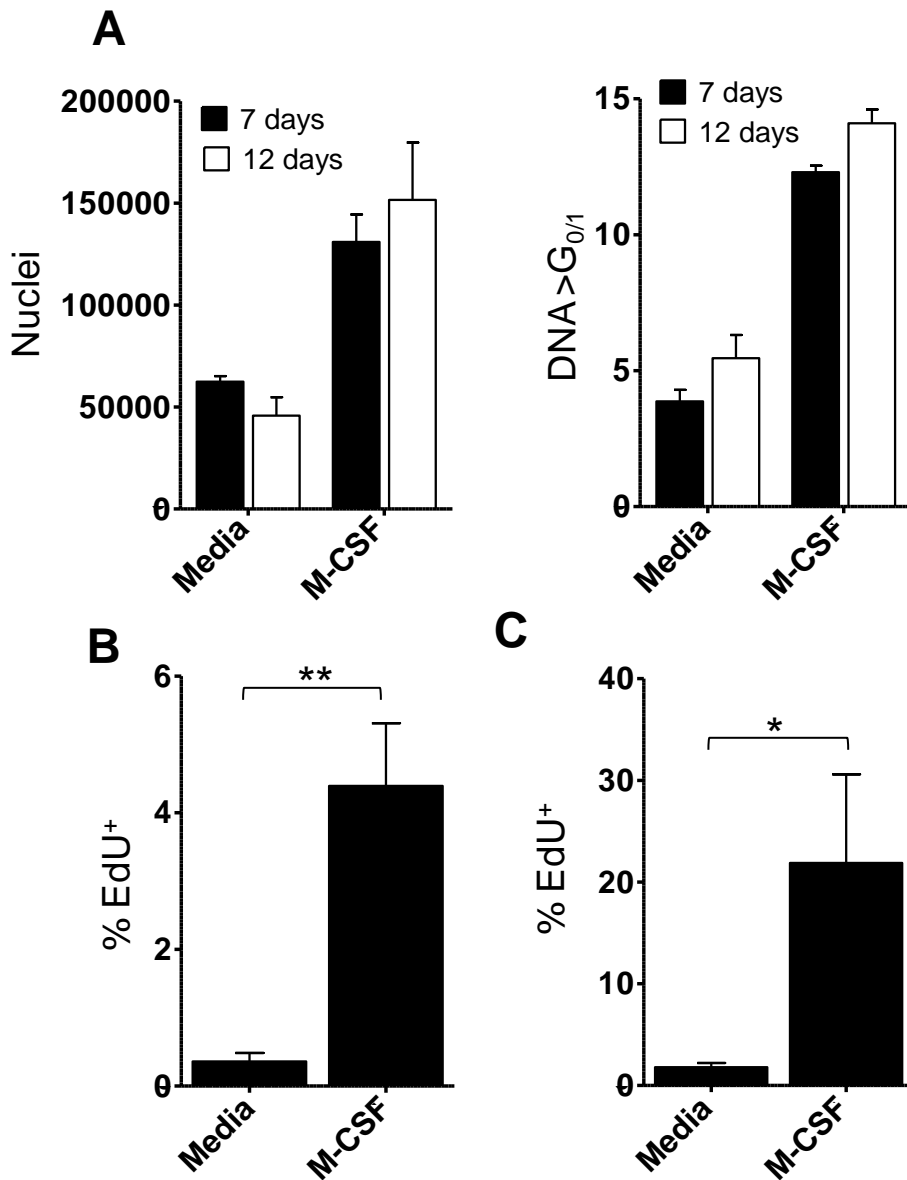


**Figure 4.8. Exogenous M-CSF promotes ResMØ proliferation *ex vivo***

**A)** Bar graphs showing the number of nuclei (left) and % DNA >2N (right) retrieved from adherent peritoneal cells (the vast majority being ResMØs) cultured for 7 or 12 days  $\pm$  20 ng/ml M-CSF. Data were analysed by two-way ANOVA with M-CSF treatment and time as the two groups. The interactions between the effects of M-CSF and time in culture was non-significant, however the effect of M-CSF treatment was statistically significant on both numbers  $P= 0.0007$  (left) and proliferation  $P\leq 0.0001$  (right). There was also a significance in proliferation with the time that cells were cultured (7 or 14 days),  $P= 0.0158$ . Data is from one of two similar experiments using separate wells ( $n= 3$ ) of cultured peritoneal cells from a pool of three 15 week old female 129S6/SvEv Dectin-1<sup>-/-</sup> mice (different strains of mice were used depending on availability – see methods 2.6.1).

**B) (from previous page)** Bar chart showing the level of EdU incorporation in ResMØs after culture for 7 days  $\pm$  20 ng/ml M-CSF. EdU (1.25  $\mu$ g/ml) was added on day 6 of culture to assess the proliferation at this late stage. Data were analysed by a one tailed Student's *t*-test and the significance value is indicated (\*\* =  $P \leq 0.01$ ). Data is from one experiment using separate wells of cultured peritoneal cells from two 10 week old male 129S6/SvEv mice (duplicate wells were used per mouse for  $\pm$  M-CSF treatment,  $n = 4$ ). **C)** Bar chart showing the level of EdU incorporation in ResMØs (gated as in *figure 3.10*) after culture for 3 days  $\pm$  20 ng/ml M-CSF. EdU (1.25  $\mu$ g/ml) was added (media refreshed, including M-CSF) every day of culture to assess the total proliferation. Data were analysed by a one tailed Student's *t*-test and the significance value is indicated (\* =  $P \leq 0.05$ ). Data were pooled from two independent experiments ( $n = 3$  per group) from individual Gata6-WT mice (different strains of mice were used depending on availability – see methods 2.6.1).

To determine whether M-CSF could also promote ResMØ proliferation *in vivo*, 0.4 $\mu$ g of recombinant M-CSF was administered to mice via intra-peritoneal injection. Exogenous M-CSF caused an increase in proliferation compared to the carrier control (0.5 % BSA in PBS (w/v)), as measured by: total Ki67<sup>+</sup>, >2N DNA content, >2N DNA content that were Ki67<sup>+</sup>, and pHH3<sup>+</sup> ResMØs (*figure 4.9*). The trend showed increased proliferation with all measures. The minimum was a 40 % increase in mean total Ki67 expression, and the maximum was a 116 % increase in mean pHH3 expression ( $n = 10$ ). However, only >2N DNA content and pHH3<sup>+</sup> values were significant by Student's *t*-test. Media = media alone

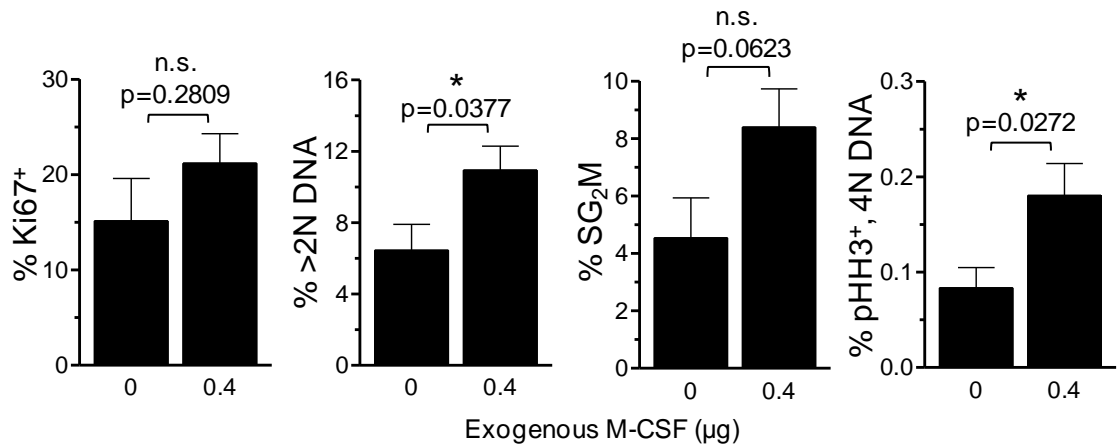


**Figure 4.9. M-CSF is not sufficient for substantial ResMØ proliferation *in vivo***

Bar graphs showing the proliferation (measured by Ki67, pHH3 and DNA) of ResMØs 24 hours after intra-peritoneal administration of 0.4 µg of recombinant M-CSF or carrier control. SG<sub>2</sub>M shows Ki67<sup>+</sup> cells with >2N DNA content. Data shown represents mean ± SEM of 10 mice per group (7 week old female C57BL/6) pooled from 2 identical experiments. Data were analyzed by a Student's *t*-test and significance values are indicated.

A neutralising antibody against M-CSF (clone 5A1) was administered intra-peritoneally to determine whether M-CSF is needed for ResMØ proliferation. The antibody binds to M-CSF *in situ* and blocks its biological activity (Lokeshwar and Lin, 1988). All measures of peritoneal ResMØ proliferation were completely ablated 48 hours after intra-peritoneal administration of 0.5mg anti-M-CSF (*figure 4.10*). For example, the percentage of cells in SG<sub>2</sub>M (Ki67<sup>+</sup> >2N DNA) was 1.23 ± 0.1 % in IgG injected mice and 0.07 ± 0.01 % in M-CSF neutralised mice (mean ± SEM, n= 3 and 4 respectively). The number of ResMØs was also significantly reduced after anti-M-CSF treatment (*figure 4.10*) compared to IgG control, reduced from 4.12 ± 0.64x10<sup>6</sup> to 2.5 ± 0.24x10<sup>6</sup> (mean ± SEM). The antibody against M-CSF was additionally administered at the same time as 2x10<sup>6</sup> zymosan particles, and the proliferation examined after 48 hours. The ResMØ proliferative burst usually seen 48 hours after zymosan was still intact with IgG control, but was entirely blocked by anti-M-CSF treatment (*figure 4.11b, c*). The numbers of recoverable ResMØs 48 hours after zymosan were also reduced by anti-M-CSF, to only 66 % (based upon means, n= 5) of the level seen with the IgG control (*figure 4.11a*).

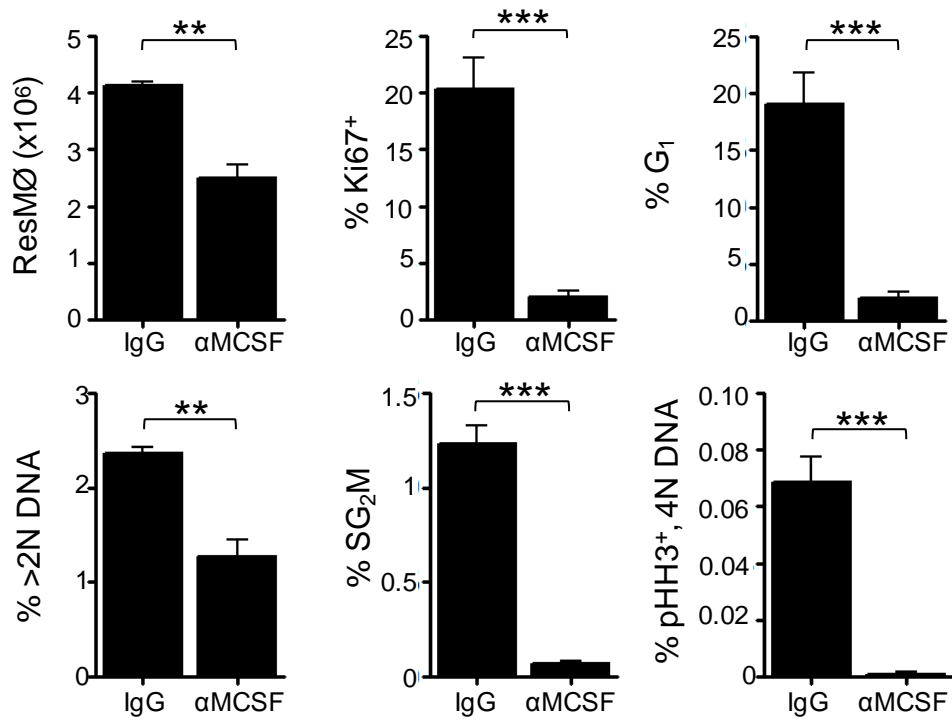


**Figure 4.10. M-CSF is required for homeostatic ResMØ proliferation**

Bar graphs denoting ResMØ numbers (top left) and various measures of proliferation calculated using DNA (DAPI), Ki67 and pHH3 48 hours after 0.5mg anti-M-CSF or IgG isotype control antibody. Data were analyzed by Student's *t*-test and significance values are indicated, \*\* =  $P \leq 0.01$ , \*\*\* =  $P \leq 0.001$ . Data is from one experiment with 9-12 week 129S6/SvEv female mice ( $n = 3-4$  mice per group), but similar results were obtained with Gata6-WT mice (different strains of mice were used depending on availability – see methods 2.6.1).

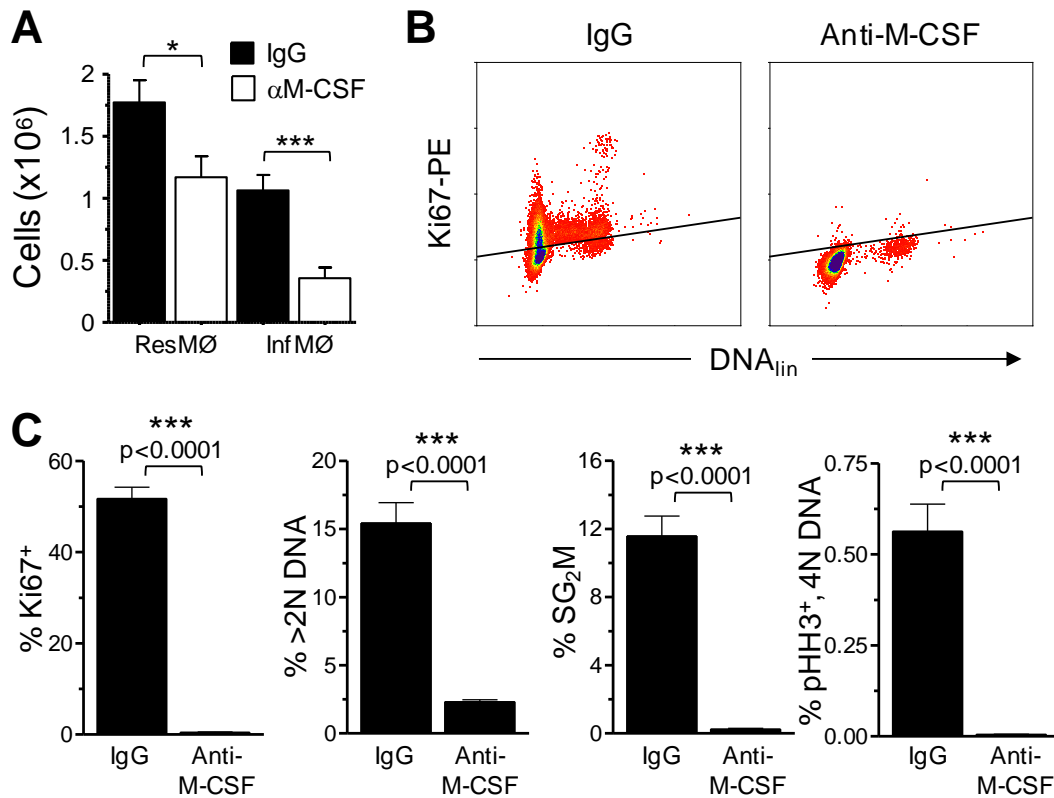


**Figure 4.11. M-CSF is required for ResMØ proliferation during acute inflammation**

**A)** Bar graph showing the numbers of ResMØs and InfMØs 48 hours after the intra-peritoneal injection of  $2 \times 10^6$  zymosan particles in conjunction with 0.5 mg of either anti-M-CSF or rat IgG isotype control (as indicated). **B)** Representative flow cytometric plots showing cells gated for ResMØs as previously described (*figure 3.10* and also *figures 3.1/3.2* for doublet/ eosinophil discrimination), after the same treatment as in (A). Cells were stained for Ki67 and DNA to measure proliferation, the diagonal dashed line represents the maximal staining seen with a matched isotype control for Ki67 **C)** Bar graphs showing quantification of proliferation from (A) measured by Ki67, pHH3 and DNA. SG<sub>2</sub>M shows Ki67<sup>+</sup> cells with >2N DNA content. Data shown represents the mean  $\pm$  SEM of 5 mice per group (7 week old female C57BL/6) from one of 2 similar experiments. Data were analyzed by a Student's *t*-test and significance values are indicated, \* =  $P \leq 0.05$ , \*\*\* =  $P \leq 0.001$ .

The number of InfMØs seen 48 hours after acute peritonitis induced with  $2 \times 10^6$  zymosan particles was examined with anti-MCSF treatment or IgG isotype control. The number of recoverable InfMØs was significantly reduced after M-CSF treatment compared with isotype control, which included both Ly-6B<sup>-</sup> and Ly-6B<sup>+</sup> MØs (*figure4.12*). Due to two strains of inbred mice being used, the data was analysed by a

two-way ANOVA using M-CSF treatment as one group and strain of mice the other group, which showed significant reductions in cell numbers with M-CSF treatment.

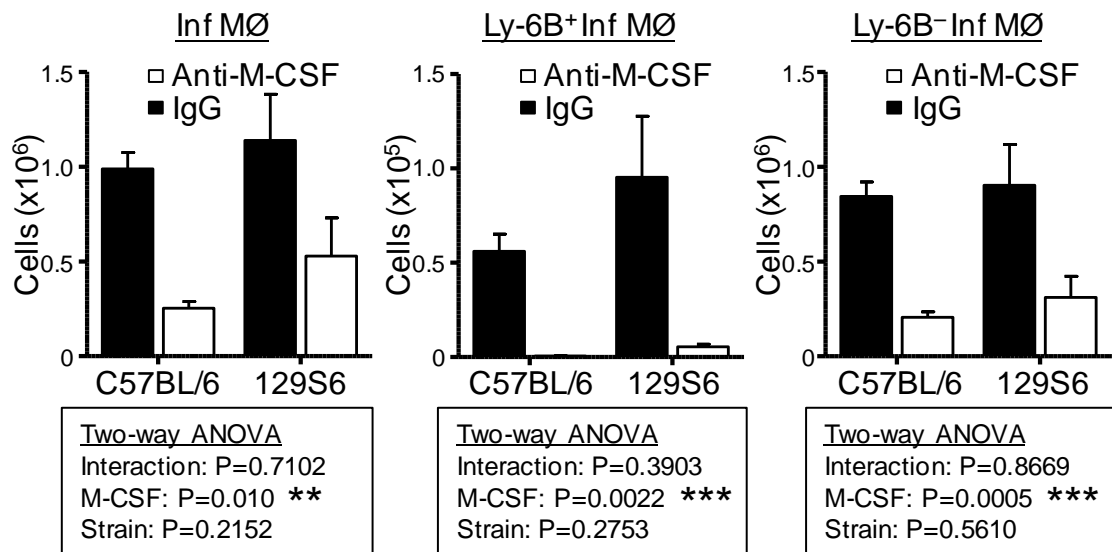


**Figure 4.12. Ly-6B-expressing InfMØs are M-CSF-dependent**

Bar graphs showing quantification of InfMØ numbers 48 hours after acute peritonitis induced with  $2 \times 10^6$  zymosan particles in conjunction with 0.5 mg of either anti-M-CSF or rat IgG isotype control. Data shown represents the mean  $\pm$  SEM of two independent experiments, one conducted with 7-8 week old female C57BL/6 mice (n= 5 per group) and the other with 9-12 week old female 129S6/SvEv (n= 3-6 per group). Data was analyzed by two-way ANOVA with the significance of the effects of both M-CSF blockade and strain of mouse indicated, \*\* =  $P \leq 0.01$ , \*\*\* =  $P \leq 0.001$ .

The M-CSF dependence of ResMØ proliferation could be attributed to availability of M-CSF in the peritoneal cavity. Therefore, the quantity of M-CSF was assessed from lavage fluid. The level of M-CSF quantified in the peritoneal cavity of naïve mice was (in the majority, n= 10) between 1 and 1.5 ng, this number did not significantly change 48 hours after  $2 \times 10^6$  zymosan particles (*figure 4.13*).

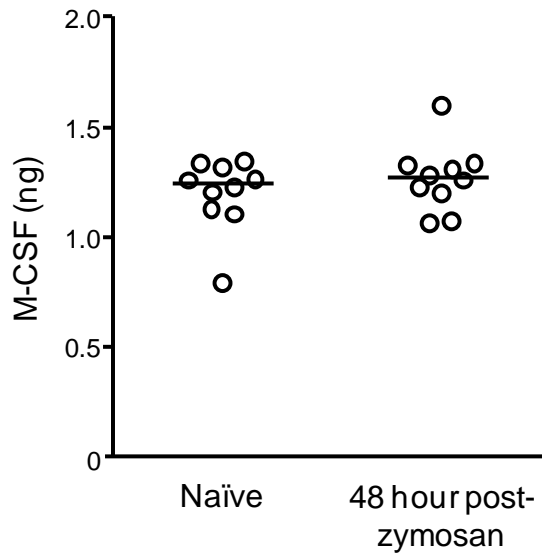


**Figure 4.13. Measurement of M-CSF in homeostasis and inflammation**

Column scatter plot showing M-CSF in the lavage fluid of naïve mice and mice 48 hours after the induction of peritonitis with  $2 \times 10^6$  zymosan particles measured by enzyme-linked immunosorbent assay. Data is adjusted for lavage volume and expressed as total M-CSF in the peritoneal cavity. Each symbol represents an individual 6 week old C57BL/6 female mouse and data was pooled from 2 independent experiments. The horizontal bars denote the means. The enzyme-linked immunosorbent assay was carried out by Dr. Selinda Orr for incorporation into this thesis.

#### 4.2.6 – IL-4 is not essential for M $\phi$ proliferation during acute inflammation

The high level of ResM $\phi$  proliferation in the peritoneal cavity during a helminth infection seen by Jenkins *et al.*, was dependent upon the cytokine IL-4 (Jenkins *et al.*, 2011). Therefore IL-4 was investigated during the proliferative activity of M $\phi$ s after peritonitis induced by  $2 \times 10^6$  zymosan particles. The proliferative burst of ResM $\phi$ s was investigated 48 hours after intra-peritoneal zymosan in conjunction with a neutralising antibody against IL-4 (clone 11B11) or rat IgG isotype control. The 11B11 antibody binds to IL-4 and inhibits its biological activity (Ohara and Paul, 1985). ResM $\phi$  numbers and levels of proliferation measured by Ki67, pHH3 and DNA were not significantly different between anti-IL-4 treatment and control (*figure 4.14*). The populations of both Ly-6B $^+$  and Ly-6B $^-$  InfM $\phi$ s were also investigated 48 hours after zymosan. Note: the numbers of Ly-6B $^+$  InfM $\phi$ s (*figure 4.15a*) seen 48 hours after  $2 \times 10^6$  zymosan particles are much lower than after 72 hours (*figure 4.4*). However, these cells were

still proliferating at a relatively high level, which was around 3-fold higher than the Ly-6B<sup>-</sup> InfM $\phi$ s (figure 4.15b). IL-4 blockade caused a significant but relatively mild reduction in proliferation in both populations of InfM $\phi$ s (figure 4.15b). The number of Ly-6B<sup>+</sup> InfM $\phi$ s was also significantly reduced (figure 4.15a) from  $76 \times 10^3 \pm 17 \times 10^3$  to  $33 \times 10^3 \pm 6 \times 10^3$  (mean  $\pm$  SEM, n= 8 and 11 respectively), although not to the same effect as seen in M-CSF blockade (figure 4.12). The number of Ly-6B<sup>-</sup> InfM $\phi$ s was not significantly altered.

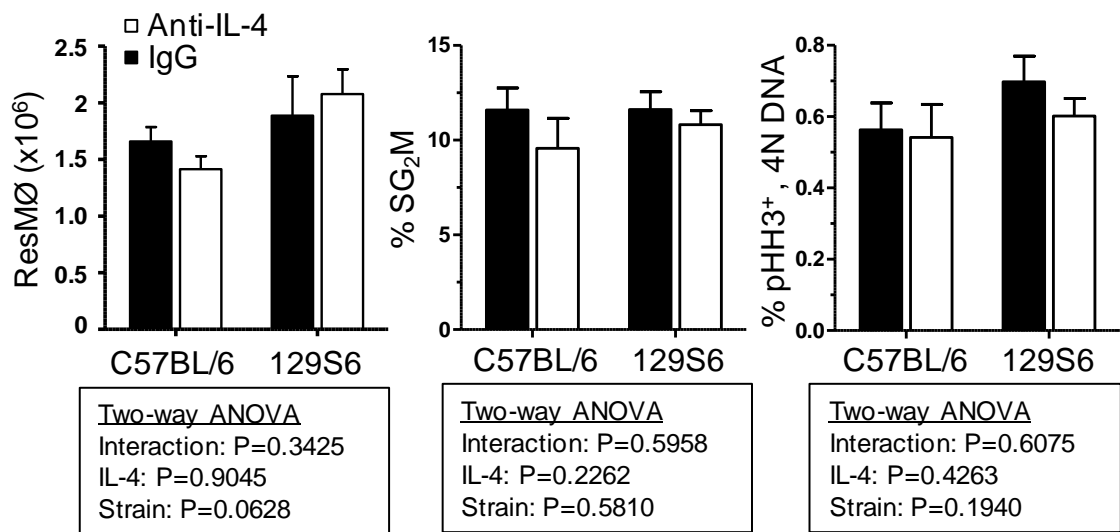


**Figure 4.14. No role for IL-4 on ResM $\phi$  proliferation during acute inflammation**

Bar graphs showing the number of ResM $\phi$ s, and measurements for proliferation, 48 hours after intra-peritoneal injection of  $2 \times 10^6$  zymosan particles in conjunction with 0.5 mg of either anti-IL-4 or rat IgG isotype control. SG<sub>2</sub>M phases of the cell cycle were measured by Ki67<sup>+</sup> cells with >2N DNA content. Data were analysed by two-way ANOVA as indicated. Data shown represents the mean  $\pm$  SEM of 5 mice per group (7 week old female C57BL/6) from one of 2 similar experiments.



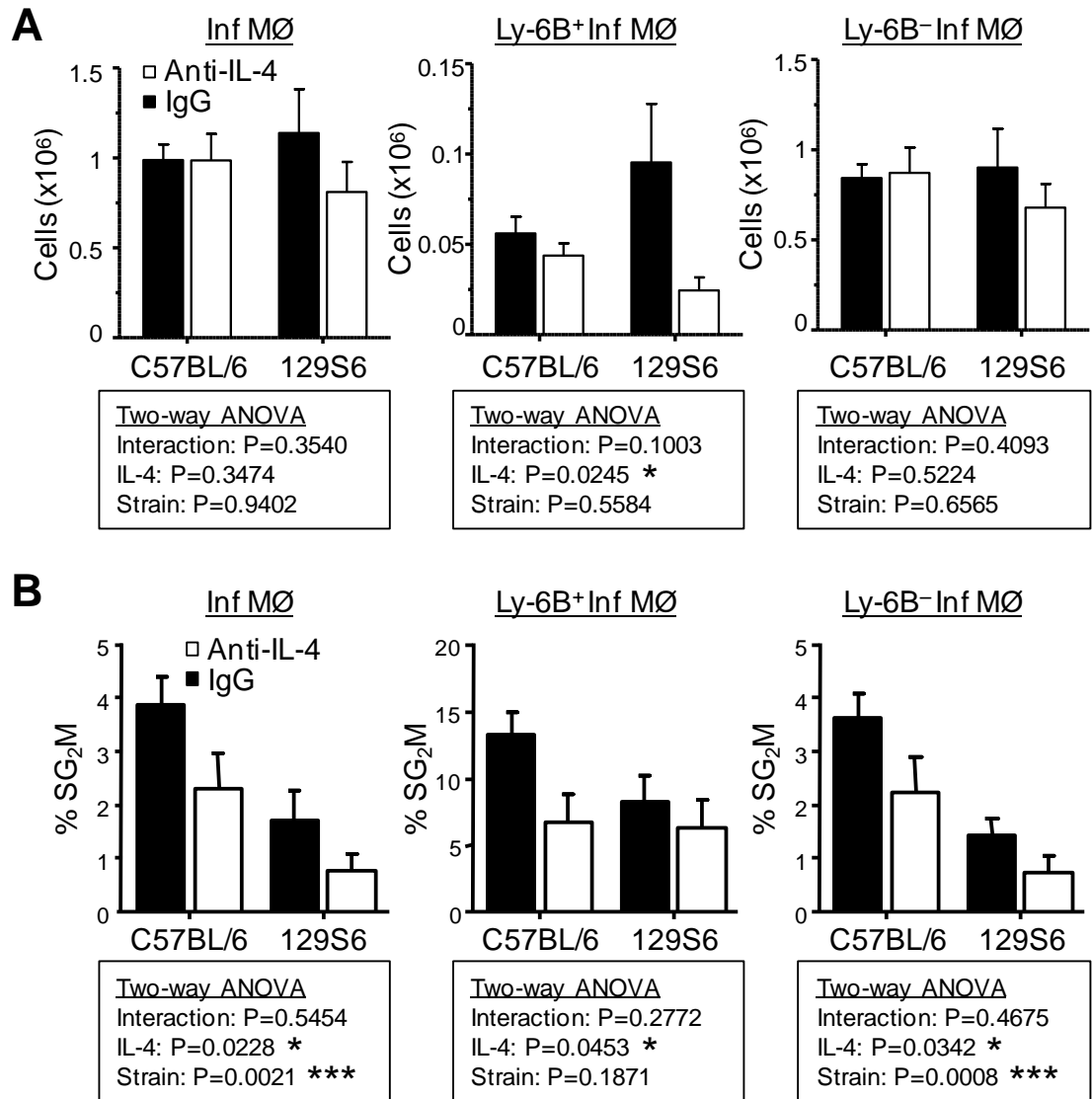


**Figure 4.15. IL-4 blockade has a limited effect on InfMØ proliferation during acute inflammation**

**A)** Bar graphs showing quantification of InfMØ numbers, 48 hours after acute peritonitis induced with  $2 \times 10^6$  zymosan particles in conjunction with 0.5 mg of either anti-IL-4 or rat IgG isotype control. **B)** Bar graphs showing analysis of proliferation in InfMØ subsets in mice after the same treatment as in (A). Proliferation was measured with Ki67 and DNA, SG<sub>2</sub>M shows Ki67<sup>+</sup> cells with >2N DNA content. Data shown for (A) and (B) represents mean  $\pm$  SEM from two-independent experiments with 7-8 week old female C57BL/6 n= 5 mice per group and 9-12 week old female 129S6 mice (n= 3-6 mice per group). Data were analyzed by a Two-way ANOVA with the significance of the effects of IL-4 neutralization and mouse strain indicated, \* =  $P \leq 0.05$  \*\*\* =  $P \leq 0.001$ .

The apparent effects of IL-4 blockade with 11B11 were further investigated using IL-4 receptor  $\alpha$  knockout mice (*Il4ra*<sup>-/-</sup>). *Il4ra*<sup>-/-</sup> mice were originally generated by gene targeting in BALB/c mice (Noben-Trauth *et al.*, 1997), but were backcrossed onto a C57BL/6 background recently by Prof. Frank Brombacher in Cape Town. These C57BL/6·*Il4ra*<sup>-/-</sup> mice were kindly supplied by Prof. Judith Allen, Dr. Steven Jenkins assisted in experimental procedures. No significant differences were seen in ResM $\emptyset$  or InfM $\emptyset$  cell numbers and proliferation between WT C57BL/6 mice and *Il4ra*<sup>-/-</sup> mice, 72 hours after intra-peritoneal administration of 2x10<sup>6</sup> zymosan particles.

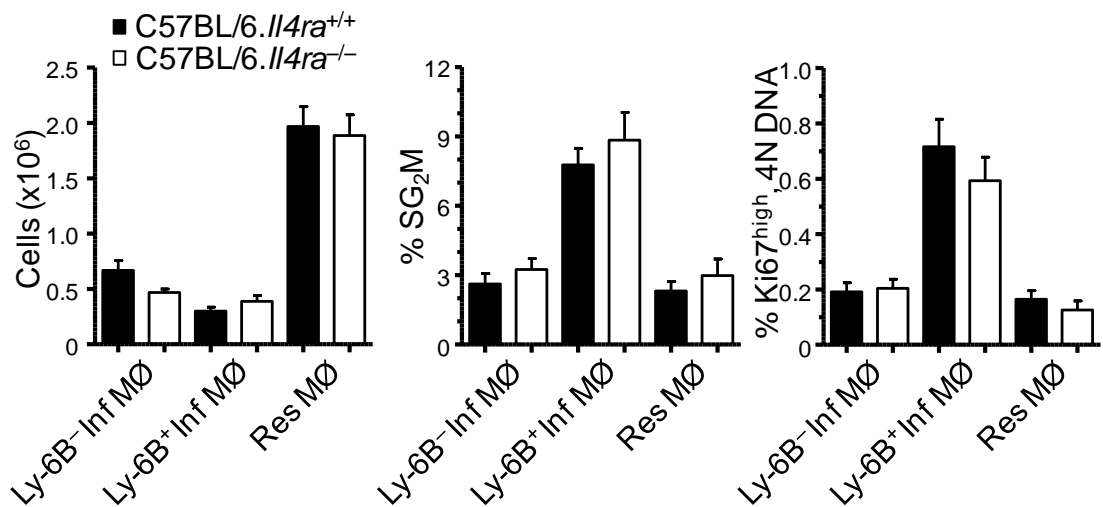


**Figure 4.16. Lack of an essential role for IL-4/ IL-4 receptor  $\alpha$  on M $\emptyset$  proliferation during acute inflammation**

Bar charts showing the number and proliferation of ResM $\emptyset$  and InfM $\emptyset$  subsets, 72 hours after induction of peritonitis with 2x10<sup>6</sup> zymosan particles in wild type and IL-4 receptor  $\alpha$  deficient mice on the C57BL/6 background. Proliferation was measured by Ki67 and DNA. SG<sub>2</sub>M shows Ki67<sup>+</sup> cells with >2N DNA content. Data shown represents mean  $\pm$  SEM of one experiment with 6 week old female mice (n= 9-10 per group). Data were analysed by two-way ANOVA, no significant differences were observed.

## 4.3 – Discussion

The aims of this chapter were to: 1) investigate whether Ly-6B<sup>+</sup> InfMØs have the capacity to proliferate *in situ*; 2) investigate the origins of Ly-6B<sup>+</sup> InfMØs; and 3) investigate the role of M-CSF and IL-4 in the control of ResMØ and InfMØ proliferation.

### 4.3.1 – Ly-6B<sup>+</sup> InfMØs

In 2010, Dr. Marcela Rosas identified the antigen recognised by the 7/4 antibody as Ly-6B (Rosas *et al.*, 2010). Ly-6B is a member of the Ly-6 family of proteins, however this family's functional activities are poorly categorised (Lee *et al.*, 2013). *In vivo* treatment with the 7/4 antibody leads to a reduction in neutrophil and monocyte numbers in the blood (Rosas *et al.*, 2010) similar to the neutropenia seen with Ly-6G blockade, however blockade of Ly-6B does not affect the migration of neutrophils seen with a limited blockade of Ly-6G (Wang *et al.*, 2012a). The function of Ly-6B on monocytes or MØs is not known (Lee *et al.*, 2013) and is purely used here as a marker for MØ subsets. Dr. Rosas found that Ly-6B<sup>+</sup> InfMØs that arrived during inflammation were newly generated, and had incorporated substantially higher levels of BrdU compared with their Ly-6B<sup>-</sup> counterparts in the resolution phase of inflammation (Rosas *et al.*, 2010). This incorporation was assumed to occur in the bone marrow. However the results from chapter 3 of this thesis show that ResMØs can proliferate in the peritoneal cavity; this provides an alternate hypothesis for the origin of BrdU incorporation seen in Ly-6B<sup>+</sup> InfMØs: *in situ* proliferation.

Ly-6B<sup>+</sup> InfMØ populations elicited during inflammation were examined using flow cytometry. The cells needed to be fixed and permeabilized in order to subsequently look at the cell cycle. After removing doublets (*figure 3.1*) and eosinophils (*figure 3.2*) and broadly gating on MØs (shown in *figure 3.2b*), monocytes were frequently seen in the population. These Ly-6B<sup>+</sup> monocytes exhibited less F4/80 expression as shown in F4/80 vs Ly-6B flow cytometric plots (*figures 4.1, 4.4a and 4.6a*), however there was sometimes a slight overlap with the Ly-6B<sup>+</sup> InfMØ population, when shown in this fashion. Fortunately, these monocytes could be excluded from analysis via their lower expression of CD11b and a slightly smaller FSc profile (*figure 4.1*). Excluding the monocytes here allowed for accurate separation of these populations and refined

analysis when viewed as F4/80 vs Ly-6B expression, the monocytes are only included in the representative plots to emphasise their existence in this complex inflammatory environment.

#### **4.3.2 – Ly-6B<sup>+</sup> InfMØs proliferate during inflammation**

Having established an accurate gating strategy for Ly-6B<sup>+</sup> InfMØ, the cell cycle was investigated as in chapter 3 of this thesis. However, the measure of cell cycle using 'SG<sub>2</sub>M' calculations was now frequently chosen over pHH3<sup>+</sup> or Ki67<sup>high</sup> calculations. SG<sub>2</sub>M is calculated by gating on cells that have >2N DNA content and are Ki67<sup>+</sup>. This measure of proliferation includes all active levels of the cell cycle and can be more sensitive than pHH3<sup>+</sup> or Ki67<sup>high</sup> staining when a low level of proliferation is observed. Therefore, the 'all inclusive' SG<sub>2</sub>M calculation was used for a more holistic analysis of MØ proliferation.

Intra-peritoneal injection of 2x10<sup>6</sup> zymosan particles causes inflammation characterised by an early influx of neutrophils followed by an accumulation of InfMØs, including Ly-6B<sup>+</sup> InfMØs (Rosas *et al.*, 2010). The new gating strategies and cell cycle calculations were applied to Ly-6B<sup>+</sup> InfMØs 72 hours after zymosan. This revealed that Ly-6B<sup>+</sup> InfMØs have a significant capacity for proliferation; these levels of proliferation (measured by DNA, Ki67 and pHH3) were in some cases (*figures 4.5 and 4.6*) higher than the proliferative burst of ResMØs seen 48 hours after 2x10<sup>6</sup> zymosan (*figure 3.11*), and notably this occurs at different time points during inflammation. The proliferation was also much higher than the low levels seen in Ly-6B<sup>-</sup> InfMØs. This matches the data from the microarray (1.3.1), which showed an enrichment of genes associated with proliferation in Ly-6B<sup>+</sup> InfMØs.

#### **4.3.3 – Ly-6B<sup>+</sup> InfMØ and ResMØ proliferation is a general phenomenon in inflammation**

A higher dose (2x10<sup>7</sup> particles) of zymosan and thioglycollate broth were used to show that both the existence of Ly-6B<sup>+</sup> InfMØs, and the MØ proliferation seen with the low dose of zymosan (2x10<sup>6</sup> particles) are not restricted to one model. The higher dose of zymosan resulted in a similar number of Ly-6B<sup>+</sup> InfMØs, but less ResMØs than the low

dose, due to the increased zymosan load on the ResMØs, and a higher more sustained influx of neutrophils (Taylor *et al.*, 2003, Taylor *et al.*, 2005b). The thioglycollate broth injection resulted in a more substantial recruitment of monocytes from the blood, but with no detectable Ly-6B<sup>+</sup> InfMØs, and only a small number of ResMØs 72 hours after injection. Injection of 1ml 4 % thioglycollate is the standard practice for eliciting InfMØs (Hopper, 1986); however it causes greater peritoneal inflammation than the doses of zymosan used in this study. It is possible that a smaller dose of thioglycollate would be more akin to the low doses of zymosan used. If thioglycollate inflammation is left to resolve for a longer time (7 days), then ResMØs are recoverable in greater numbers than 72 hours, and Ly-6B<sup>+</sup> InfMØs are detectable. Both of these MØ populations were proliferating, which means that proliferation of ResMØs and Ly-6B<sup>+</sup> InfMØs is a general characteristic of the resolution of peritoneal inflammation and is not just restricted to mild doses of zymosan.

#### **4.3.4 – Ly-6B<sup>+</sup> InfMØs are bone marrow-derived**

The adoptive transfer experiments in chapter three of this thesis (*figures 3.15-19*) showed that InfMØs were primarily host derived, not originating from the naïve peritoneal cavity, and were therefore likely peripherally recruited. To verify this, a collaborative study was established with Prof. Judith Allen and Dr. Steven Jenkins in Edinburgh in order to assess the origins of Ly-6B<sup>+</sup> InfMØs. Partial bone-marrow chimeras were created by Dr. Steven Jenkins (Jenkins *et al.*, 2011). Six weeks later, after confirming chimerism, zymosan peritonitis was initiated in these mice and left to resolve for 72 hours. Both Ly-6B<sup>-</sup> and Ly-6B<sup>+</sup> InfMØs were chimeric (which correlated well with blood chimerism), so were likely bone-marrow derived. ResMØs were not chimeric, which supported conclusions made from the adoptive transfer experiments carried out in chapter 3 of this thesis (*figures 3.14-3.18*), in that ResMØs do not rely on blood monocytes for their renewal, but self-renew via local proliferation.

#### **4.3.5 – M-CSF dependency of MØs**

M-CSF addition is used to expand bone marrow MØ cultures ex-vivo (Hume and Gordon, 1983). Therefore, exogenous M-CSF was added to cultured peritoneal cells.

M-CSF addition caused increased proliferation and/ or survival of the adherent peritoneal cells, the vast majority are likely ResMØs (Davies and Gordon, 2005). The level of >2N DNA content could be used as a good measure for active proliferation due to the nature of the NIM-DAPI used to extract the cell nuclei. Over 10 % of the cells were in active phases of the cell cycle (SG<sub>2</sub>M) 7 and 12 days after culture with M-CSF (*figure 4.8a*); however these could have been adherent cells other than MØs. EdU incorporation *in vitro* could be used in conjunction with expression of the MØ markers F4/80 and CD11b in flow cytometry, to accurately identify MØ proliferation. EdU incorporation showed that only around 5 % of the ResMØs had actively proliferated on the last day of a 7 day culture with M-CSF (*figure 4.8b*). This was supported by a ≈20 % EdU incorporation after 3 days of culture (*figure 4.8c*). Additionally, Jessica Llewellyn (a master's student in our laboratory) showed that roughly 50 % of cells had incorporated BrdU 7 days after culture (unpublished data). This data suggests that only a small proportion of <5 % of peritoneal MØs have the capacity to proliferate in culture in these experiments, and that their daughter cells accumulate in culture, but this needs to be formally addressed. Either a form of contact inhibition could be limiting the proliferation, or perhaps stem cell-like subset of ResMØs was proliferating. A method of testing these hypotheses would be to try different seeding densities, measuring EdU uptake daily, and pulse-chase labelling the cells with both EdU and BrdU. However, the specific processes *in vitro* were not a focus of this thesis, especially when the physiological relevance of these observations was uncertain. This uncertainty is due to the loss of homeostatic controls, such as the transcription factor Gata6 mentioned later in this thesis (chapter 6).

The effect of M-CSF was tested *in vivo* by a single intra-peritoneal injection of recombinant M-CSF. This caused a significant, but small increase in ResMØ proliferation, which was not as high as that seen in the proliferative burst 48 hours after zymosan peritonitis (chapter 3 of this thesis). Daily intra-venous injection of recombinant M-CSF has previously been shown to increase the number of peritoneal MØs, which was attributed to a 10-fold increase in circulating monocytes (Hume *et al.*, 1988). However on reflection, this could also be a result of increased local proliferation. The peritoneal cavity itself contains high levels of constitutive M-CSF in naïve animals and similar levels were present 48 hours after zymosan. This suggests

the proliferative burst is not primarily controlled by the availability of M-CSF, but by other factors, perhaps the levels and/ or the function of the M-CSF receptor, or alternative regulatory mechanisms.

Blockade of M-CSF with the 5A1 antibody caused a complete ablation of all measures of proliferation in naïve mice and on the proliferative burst seen in mice 48 hours after intra-peritoneal zymosan. This shows that M-CSF is essential for proliferation, but its addition is not sufficient to replicate the high levels of ResMØ proliferation seen after peritonitis, again implicating additional proliferative controls. Anti-M-CSF treatment also caused a substantial decrease in ResMØ numbers; which could be a result of the failure of ResMØs to recover via proliferation from the inflammation caused by intra-peritoneal injection of anti-M-CSF (plus carrier). Indeed similar losses of ResMØs were seen in conjunction with anti-M-CSF 48 hours after zymosan. The numbers of InfMØs were also severely reduced after zymosan in conjunction with anti-M-CSF, specifically the numbers of Ly-6B<sup>+</sup> InfMØs; which were reduced by a higher proportion relative to Ly-6B<sup>-</sup> InfMØs. However, this could be due to the presence of F4/80<sup>low</sup> MHCII<sup>high</sup> Res DCs/MØs (which are still present during inflammation) 'contaminating' the Ly-6B<sup>-</sup> InfMØs gate. The general reduction in InfMØs could be attributed to either: i) a reduction in recruitment, ii) *in situ* differentiation (although significant numbers of monocytes were not seen in the peritoneal cavity), iii) proliferation (at least with the Ly-6B<sup>+</sup> InfMØs), or iv) survival. Continuous blockade of M-CSF after birth results in most of the defects seen in the *op* mouse: including reduced levels of tissue MØs and growth defects (Wei *et al.*, 2005). Additionally, M-CSF blockade in the adult has been shown to deplete tissue MØs and 'non classical' Gr1<sup>-</sup> (Ly-6C<sup>/low</sup>) monocytes but increase the numbers of 'classical' Gr1<sup>+</sup> (Ly-6C<sup>+high</sup>) monocytes (MacDonald *et al.*, 2010). These studies have attributed the reduction of tissue MØs to the loss of differentiation from 'non-classical' monocytes (Hume and MacDonald, 2012), which were assumed to be the precursors of ResMØs. However, the loss of tissue MØs could also be attributed to the ablation of homeostatic maintenance by *in situ* proliferation. These previous blockade studies could have also explained the preferential loss of Ly-6B<sup>+</sup> InfMØs seen with anti-M-CSF treatment during zymosan peritonitis; in that the precursors of Ly-6B<sup>+</sup> InfMØs could be 'non classical' monocytes. However, it has recently been shown that 'classical' monocytes are precursors to 'non-classical'

monocytes (Yona *et al.*, 2012), therefore investigating the monocytic origin of these cells would be difficult and impractical in the inflammatory setting. After taking these findings into account, it is more likely that the peripheral recruitment of the whole InfMØ population has been inhibited by M-CSF blockade.

#### **4.3.6 – MØ proliferation is not dependent upon IL-4**

The cytokine IL-4 was implicated in proliferation of peritoneal ResMØs after helminth infection (Jenkins *et al.*, 2011). However, the environment created 48 hours after intra-peritoneal administration of  $2 \times 10^6$  particles of zymosan was considered to be different from the IL-4 rich T<sub>H</sub>2 environment seen in the Jenkins *et al.* study. Hence the role of IL-4 in this model was expected to be minimal. IL-4 was blocked with the antibody 11B11 in the peritoneal cavity of mice 48 hours after zymosan. This blockade did not affect ResMØ proliferation or numbers, but had a small but significant reducing effect on Ly-6B<sup>+</sup> InfMØ numbers and proliferation of InfMØs as a whole.

The effects of using blocking antibodies can be variable due to the way they are produced (i.e. levels of endotoxin and other contaminants) and potential secondary effects in the inflammatory process, so a second collaborative study was established with Prof. Judith Allen and Dr. Steven Jenkins in Edinburgh in order to test the findings when using the blocking antibody 11B11 on Ly-6B<sup>+</sup> InfMØs. Zymosan was injected into WT and *Il4ra*<sup>-/-</sup> mice. There was no significant difference between MØ numbers or any measures of proliferation between the two groups. This clearly demonstrates that IL-4 is not essential for MØ proliferation in the zymosan model. Either way, the effect of IL-4 on Ly-6B<sup>+</sup> InfMØs during an acute inflammatory response is limited at best and not necessary for proliferation. In contrast, M-CSF was an essential growth factor for MØ proliferation. Perhaps there is a homeostatic feedback loop for ResMØs, under the control of the M-CSF receptor; which limits proliferation in homeostasis where there the number of ResMØs are sufficient, but drives proliferation when there is a loss in normal homeostatic numbers as seen in zymosan induced inflammation. IL-4 seemingly has the ability to bypass this mechanism during helminth infection to drive proliferation and expand ResMØ numbers beyond homeostatic levels (Jenkins *et al.*, 2013).



Interestingly, the times at which ResM $\phi$ s and Ly-6B<sup>+</sup> InfM $\phi$ s are actively proliferating is distinct. ResM $\phi$ s undergo a burst in proliferation 48 hours after 2x10<sup>6</sup> zymosan particles, and this returns to near homeostatic levels 72 hours after zymosan. On the other hand Ly-6B<sup>+</sup> InfM $\phi$ s continue to proliferate at high levels 72 hours after zymosan and beyond. This indicates that there are alternative and distinct intrinsic control mechanisms between these two populations. These specific mechanisms have been largely undetermined; however one mechanism for the proliferative control of ResM $\phi$ s is explored in chapter six of this thesis.

#### **4.3.7 – Conclusion**

In conclusion, the studies in this chapter, which have now been published (Davies *et al.*, 2013b), showed that: 1) a subset of InfM $\phi$ s that are Ly-6B<sup>+</sup> proliferate during inflammation; 2) these Ly-6B<sup>+</sup> InfM $\phi$ s are derived from the bone marrow and are recruited to the inflammatory lesion; 3) M-CSF is required but not sufficient for ResM $\phi$  proliferation; 4) M-CSF is required for either recruitment, survival or proliferation of Ly-6B<sup>+</sup> InfM $\phi$ s; 5) IL-4 receptor  $\alpha$  is not necessary for ResM $\phi$  or InfM $\phi$  proliferation; and 6) proliferation of these different M $\phi$  populations is under distinct mechanistic control. This demonstrates that blood monocyte (bone marrow)-derived M $\phi$ s are capable of proliferation and are not terminally-differentiated, which additionally challenges the dogma of the MPS (as with chapter 3 of this thesis). The identification that local M $\phi$  proliferation is ablated by anti-M-CSF treatment should be considered when targeting M-CSF for treatment of diseases like rheumatoid arthritis (Korkosz *et al.*, 2012) and cancer (Hume and MacDonald, 2012); and also when designing novel strategies to combat these chronic diseases.

## **Chapter 5 – Lentiviral modification of MØ gene expression**

## 5.1 – Introduction

### 5.1.1 – Lentiviral vectors

Lentiviruses are a type of retrovirus (RNA containing virus) which can infect non-dividing cells (Naldini, 1998). A well known lentivirus is the human immunodeficiency virus (HIV) which causes acquired immunodeficiency syndrome (AIDS). Lentiviral vectors have been used to deliver target genes to non-dividing cells and are frequently derived from the genome of HIV-1 (Naldini, 1998). Retroviral vectors in general are valued because they do not force translation of any viral proteins, meaning they can be accepted in most cellular systems. The pHR'SIN-cPPT-SEW (SEW) (Demaison *et al.*, 2002) vector and an enhanced green fluorescent protein (eGFP) deficient version (pHR'SIN-cPPT-SXW) (SXW) were kindly provided by Dr. Paul Brennan. These vectors had been modified to lack virulent proteins, which were: the group antigens (*gag*), reverse transcriptase-containing *pol*, regulator of expression of viron proteins (*rev*), envelope protein (*env*), viral infectivity factor (*vif*), viral protein R (*vpr*), viral protein unique (*vpu*), trans-activator of transcription (*tat*), and negative factor (*nef*). This left the viral vector unable to infect or replicate without help. Therefore, helper constructs are required to generate infectious viral particles. The pCMVR8.91 (pCMVΔ8.91) (containing *gag*, *pol*, and *rev*) and pMD2G (containing vesicular stomatitis virus G protein (VSV-G)) expression vectors can be used in combination with the lentiviral vector to produce infectious lentiviral particles (albeit they are still unable to replicate) (Zufferey *et al.*, 1997). The supplemented VSV-G envelope protein is valued for its ability to infect a broad range of cell types in multiple species (Burns *et al.*, 1993). The lack of the *tat* protein in the lentiviral vector also means that the long terminal repeats (LTRs) of the vector were unable to be transcribed into foreign viral RNA. Therefore, a new transcriptional initiation system was introduced; consisting of the SFFV promoter and Woodchuck post-transcriptional regulatory element (WPRE) (an enhancer) to facilitate the transcription of the transgenes (Demaison *et al.*, 2002). The SFFV promoter is from the Friend strain of SFFV virus, which usually infects erythrocytes, however this strong promoter is frequently used in retroviral vectors to enforce transgene expression (Demaison *et al.*, 2002). The WPRE is known to enhance the expression of retroviral transgenes (Zufferey *et al.*, 1999). The formation of this SEW construct (Demaison *et al.*, 2002) resulted in a safe lentiviral delivery system, which

can infect a broad range of cell types (including myeloid cells) and can efficiently express genes of interest in infected cells.

### **5.1.2 – RNA interference**

RNA interference can be delivered through lentiviral vectors, to achieve sustained knockdown of target gene expression (Abbas-Terki *et al.*, 2002). RNA interference describes a wide range of RNA silencing processes in which RNA can be degraded or its action inhibited (Meister and Tuschl, 2004). One such method is via the production of dsRNA, usually through sh (short hairpin) RNA; where complementary RNA folds into a hairpin structure and base-pairs to form ds-shRNA. These shRNAs are processed by the ribonucleases Drosha (Lee *et al.*, 2003) and Dicer (Bernstein *et al.*, 2001) and loaded into RNA silencing complexes (RISC), which target specific RNA structures/ sequences for degradation (Hammond *et al.*, 2000).

### **5.1.3 – Markers used to identify infected cells**

Lentivirally delivered transgenes usually contain a tag or marker, which can be used to identify infected cells. The artificial protein eGFP is frequently chosen as a marker for viral infection, because it can be readily detected using its fluorescent properties. GFP was originally identified in *Aequorea victoria* jellyfish in the 1960s as the protein which absorbed bioluminescent blue light from aequorin and re-emitted this as green light (Shimomura *et al.*, 1962, Morise *et al.*, 1974). An enhanced version of GFP was created 30 years later by introducing the S65T and F64L mutations, which enhanced brightness and thermo-stability of the protein at 37 °C (Heim *et al.*, 1995, Cormack *et al.*, 1996). However, this new eGFP protein was further improved in brightness and thermo-stability (at 37 °C) with introduction of the V164A and S175G mutations (Siemering *et al.*, 1996), to produce what will be referred to in this thesis as eGFP. Numerous, slightly different versions of eGFP exist within the literature, and their nomenclature has been poorly categorised. Apart from eGFP, several hundred diverse GFP derivatives have now been formulated with colours ranging from cyan and yellow to orange and red (Rizzo *et al.*, 2009).

Other markers can also be used to track viral infections, such as Myc-tags, poly-histidine-tags (6 histidine residues) and proteins such as truncated rat CD2 (trCD2). The Myc-tag is a 10 amino acid long sequence based upon the c-Myc protein, which has been used extensively to tag proteins since its first use (Munro and Pelham, 1986). The rat CD2 (rCD2) protein was truncated at the cytoplasmic tail to produce trCD2 (King *et al.*, 1998). This protein is not able to mediate CD2 cytoplasmic signalling in infected cells, and infected cells expressing rat CD2 can be detected with a monoclonal antibody (which will not bind to mouse CD2).

#### **5.1.4 – Hypothesis**

The hypothesis tested in this chapter is that lentiviruses can be used to efficiently modulate gene expression in ResMØs *in vivo*.

#### **5.1.5 – Aims**

- To create an efficient method for quantifying viral titre
- To infect ResMØs with lentivirus *in vitro*
- To infect ResMØs with lentivirus *in vivo*
- To produce lentiviral vectors that express and/ or knockdown genes of interest
- To investigate the efficacy of ResMØ lentiviral infection *in vivo*

## 5.2 – Results

### 5.2.1 – Lentiviral titre calculations *in vitro*

Methods for quantifying viral titre were investigated to allow comparison between different viral preparations. Flow cytometry was used to quantify the level of eGFP expression in Jurkat cells infected with virus produced from the SEW plasmid. Jurkat cells are considered to be an ‘easy target’ for viral infection (Zhou *et al.*, 2003), and were used to efficiently measure viral titre. The level of infection was quantified as total median fluorescent intensity (MFI) and the proportion of eGFP<sup>+</sup> cells (*figure 5.1*). Real-time PCR (with a standard curve) was used to calculate the viral integration in these infections to give copy number per pg of DNA (*figure 5.1*). A relative MOI was also calculated using the proportion of eGFP<sup>+</sup> cells and Poisson distribution (see methods 2.9.3). The MOI calculated from infected Jurkat cells was used when necessary for relative quantification of viral titre in specific lentiviral productions.

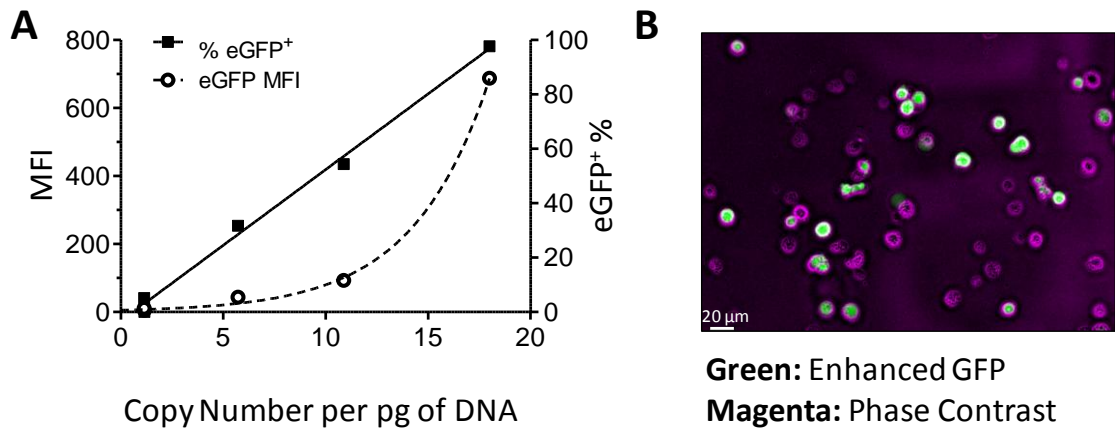


**Figure 5.1. eGFP viral titre using flow cytometry and real-time PCR**

**A)** Scatter plot showing MFI (left Y) and the percentage of cells infected with an eGFP-expressing lentivirus (right Y) vs the copy number of virus detected per pg of DNA (X). Non linear regression analysis was used to create the dotted line (eGFP<sup>+</sup> %) ( $R^2=0.9987$ ), and linear regression was used to create the solid line (MFI) on the graph ( $R^2=0.9949$ ,  $P$ -value for significantly non-zero slope = 0.0002). Copy numbers per pg of DNA were calculated using genomic real-time PCR, using the integrated viral SFFV promoter and making this relative to genomic *Ywhaz*. A known quantity of lentiviral plasmid was used to create a standard curve, from which copy number values were calculated. Data represents a pilot experiment conducted prior to infection of MØs. **B)** Confirmation of eGFP infection of Jurkat cells from (A) using fluorescence microscopy. Image was captured using the 20× objective lens on the EVOS microscope, and is an overlay of phase contrast and eGFP expression.

### 5.2.2 – Lentiviral infection of BMMØs and ResMØs *in vitro*

After confirming that the SEW virus was able to transduce Jurkat cells, mature BMMØs and ResMØs were infected with the SEW lentivirus *in vitro*. Both BMMØ and ResMØ cultures exhibited eGFP<sup>+</sup> cells 3 days after transduction with SEW (*figure 5.2a*). The ResMØs cultures (adherent peritoneal cell cultures) also included lymphocytes (SSc<sup>low</sup>), interestingly these cells had noticeably less eGFP<sup>+</sup> expression compared with that of the ResMØs (SSc<sup>high</sup>) (*figure 5.2b*). The SEW virus was titrated in ResMØ cultures and showed non-linear regression with a maximal infection of 68.8 % eGFP<sup>+</sup> cells (*figure 5.3*), using 250 µl of 10 × concentrated virus containing supernatant (see methods 2.9.2).

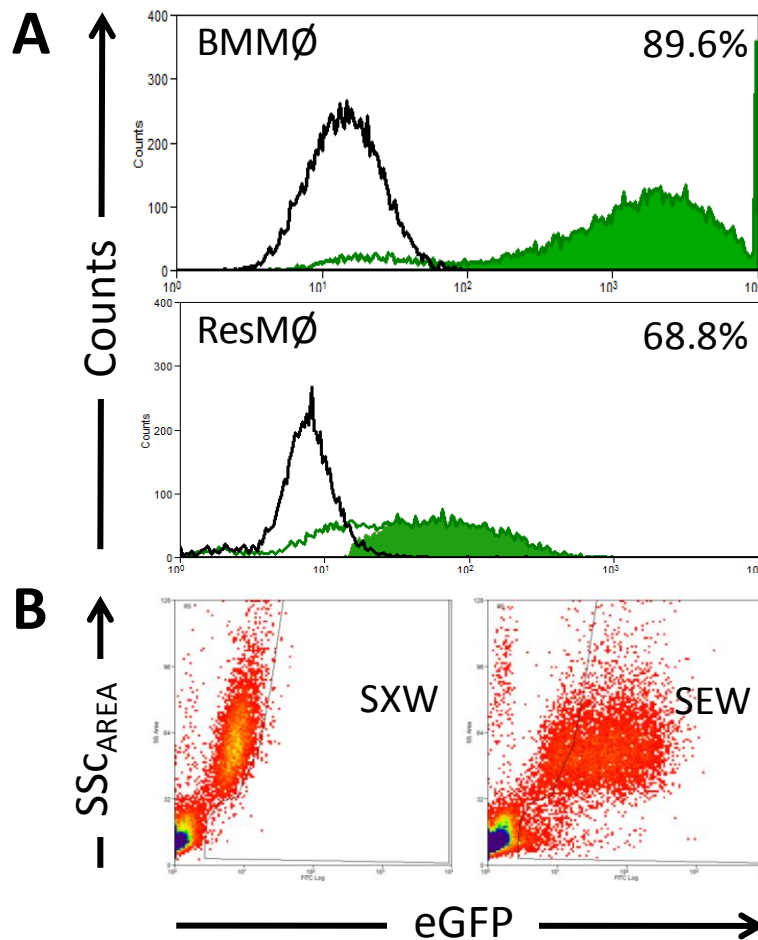


**Figure 5.2. Lentiviral infection of BMMØs and ResMØs**

**A)** Representative histograms showing the percentage of infected BMMØs and ResMØs (calculated using Overton channel by channel subtraction – the filled histogram) 3 days after transduction with an eGFP-expressing virus. The black histogram shows autofluorescence from an empty vector virus, and the green outline histogram shows fluorescence from cells infected with the eGFP-expressing virus. Note: the BMMØ and ResMØ infection levels are not directly comparable, as they were separate experiments with different conditions. **B)** Representative density plots depicting the prevalence of ResMØ infection over lymphocytes 3 days after lentiviral infection *in vitro*. In general, ResMØs have a higher FSc/ SSc profile than other resting peritoneal cells, albeit a small percentage of eosinophils and DCs were included in the ResMØ population and were not distinguished in this initial study. Lymphocytes and cell debris had a lower FSc/ SSc profile (bottom left of plots). BMMØs and peritoneal cells were seeded *in vitro* from 129S6/SvEv mice (see methods 2.5). Data is representative of a single preliminary experiment using 6 titrations of lentivirus, the plots shown used 250  $\mu$ l of 10  $\times$  concentrated virus. SXW = empty vector virus, SEW = eGFP expressing virus.



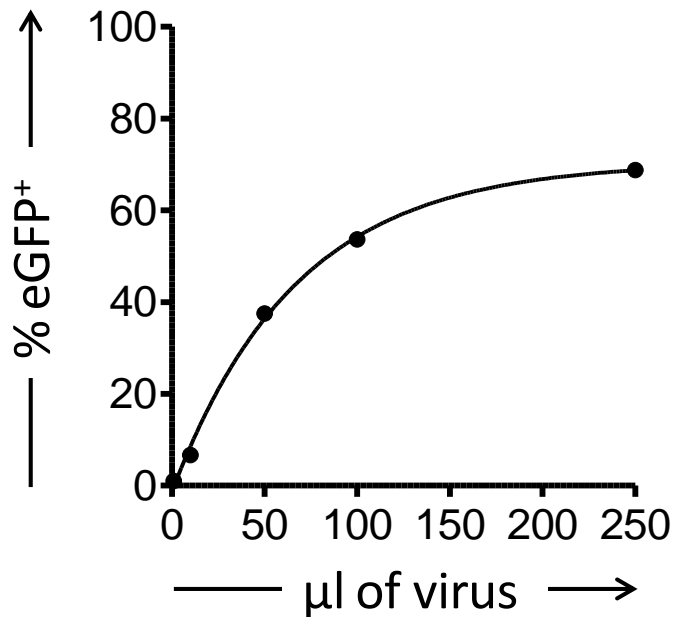


**Figure 5.3. eGFP viral titre in ResMØs *in vitro***

Scatter plot showing the percentage of ResMØs infected with an eGFP-expressing lentivirus vs the µl of virus used. Non linear regression analysis was used to create the line on the graph ( $R^2= 0.9937$ ). Data shown is from the same experiment as figure 5.2.

### 5.2.3 – Specific lentiviral infection of ResMØs *in vivo*

Following the successful infection of *in vitro* cultured peritoneal ResMØs, virus was injected into the peritoneal cavities of mice in order to assess the level of peritoneal cell infection. *In vivo* injection of SEW resulted in a high level of infection selective for ResMØs in the lavage retrieved from the peritoneal cavity (*figure 5.4*). Two additional repeats of the experiment shown in figure 5.4 showed that there was  $50.27 \pm 4.062$ -fold (mean  $\pm$  SEM) enrichment of ResMØ infection *in vivo*, when compared to all other cells in the peritoneal cavity (n= 5 total).

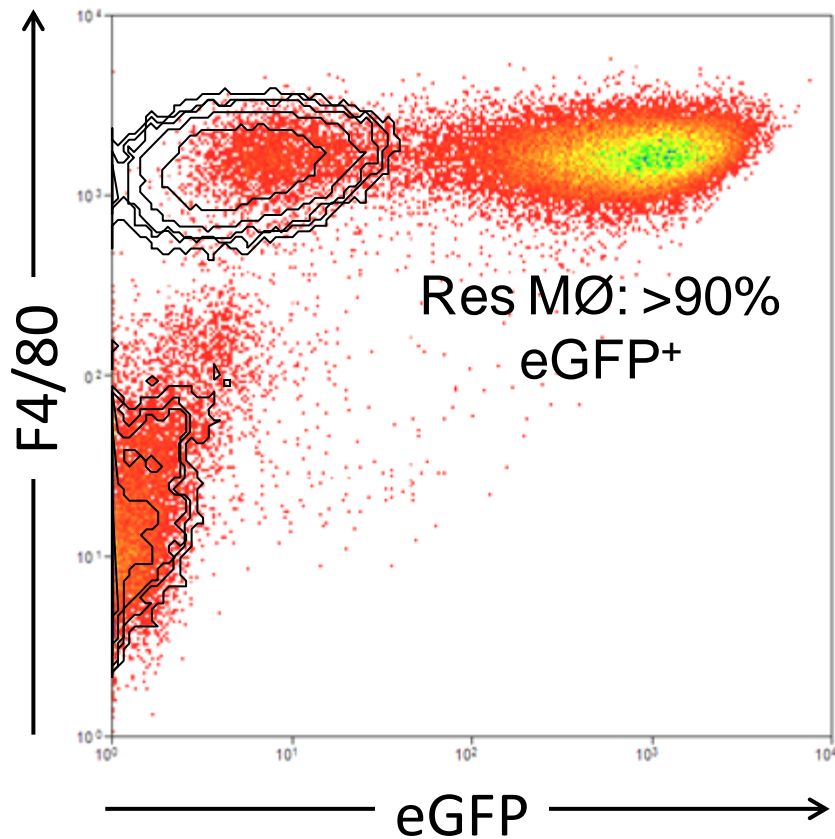


**Figure 5.4. Specific lentiviral infection of ResMØs *in vivo***

**A)** Representative density plot showing peritoneal cells stained with F4/80, 7 days after *in vivo* intra-peritoneal infection with an eGFP-expressing lentivirus. The overlaid contour plot indicates the representative autofluorescence seen in an uninfected mouse. Data shown is from a single preliminary experiment with 129S6/SvEv mice (n= 1 per group), but the selective *in vivo* infection of ResMØs (F4/80<sup>high</sup>) is representative of all experiments carried out in this thesis.

#### 5.2.4 – Lentiviral knockdown of target gene expression in ResMØs *in vivo*

Having achieved efficient *in vivo* infection of ResMØs, lentiviruses were produced to modify gene expression. A murine U6 promoter was inserted into the *Eco* RI site of the SEW lentiviral vector, and shRNA hairpin sequences were inserted into the *Pme* I site immediately following the promoter generated by this cloning. This created a system where RNA polymerase III would produce shRNAs from this sequence after viral integration (Kunkel *et al.*, 1986); and the shRNAs would target mRNA for degradation (Hammond *et al.*, 2000). Lentiviruses containing shRNA against *Icam1* mRNA and non-silencing control were formulated using this method. Transduction of ResMØs *in vivo*

with the *Icam1* shRNA targeting lentivirus resulted in a drastic decrease in ICAM-1 protein expression, when compared to the non-silencing control (*figure 5.5*).

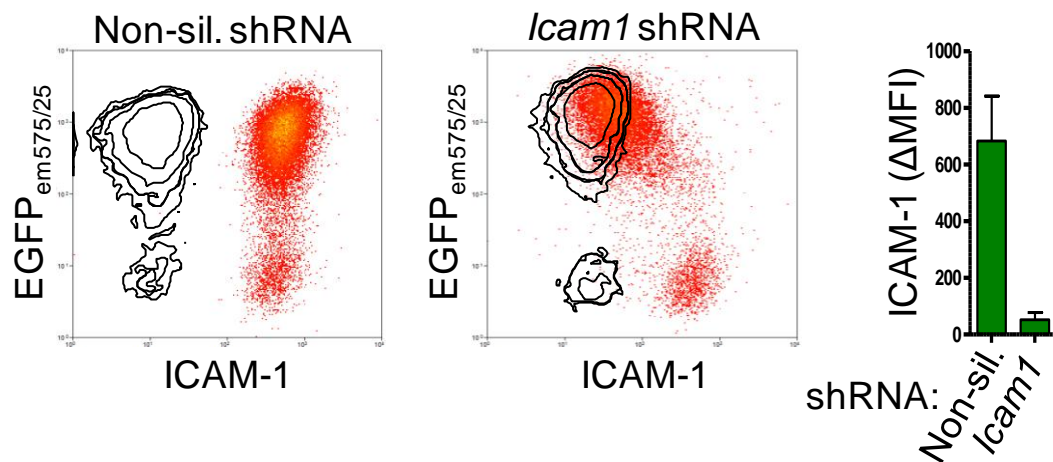


**Figure 5.5. Lentiviral knockdown of ICAM-1 expression in ResMØs *in vivo***

Representative density plots showing knockdown of ICAM-1 protein levels in ResMØs (gated as in figure 3.10), 7 days after intra-peritoneal delivery of a shRNA (eGFP-tagged)-expressing lentivirus. The overlaid contours show the fluorescence of the ICAM-1 IgG isotype control. The bar graph shows quantification of ICAM-1 MFI in cells infected with ICAM-1-targeting and non-silencing shRNA-expressing lentiviruses. Data shown is representative of one of two independent experiments using 14 week old female 129S6 mice (n= 2/group).

### 5.2.5 – Validation of a lentiviral expression vector

As with the knockdown vectors (above), expression vectors were produced as a modulator of gene expression. For this thesis (specifically chapter 6), the short form of the transcription factor Gata6 (Takeda *et al.*, 2004) was inserted into the *Xho* I restriction site of the SXW (eGFP deficient) vector. This new Gata6-expressing virus was used to transfect cultured BMMØs. Upon transfection, the level of Gata6 mRNA (measured by real-time PCR) increased over 10,000-fold when compared to SXW infection (*figure 5.6*).

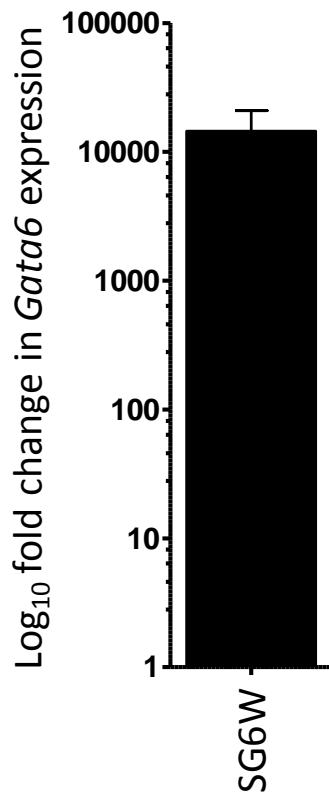


**Figure 5.6. Validation of the Gata6-expressing lentivirus**

Bar graph showing the fold change in Gata6 mRNA expression in BMMØs, 3 days after infection with a Gata6-expressing lentivirus. Data shown was made relative to both the endogenous control *Ywhaz*, and control SXW lentiviral infection. Data (n= 2) is from one of two independent experiments using 129S6/SvEv mice.

### 5.2.6 – Lentiviral vectors constructed for this thesis

Using similar strategies as mentioned above, other expression and knockdown vectors were produced from the SEW and SEW vectors (*figure 5.7*). Some of the expression vectors included a trCD2 tag linked to the expressed gene via a T2A (the template T2A-CD2 was kindly supplied by Dr. James Mathews). The 2A sequence was originally identified in the foot-and-mouth disease virus and was found to be ‘self-cleaving’ (Ryan *et al.*, 1991). This has been used in viral vectors to produce two protein products from one mRNA transcript (Szymczak *et al.*, 2004). Other vectors included a Myc-tag, which can be detected with an antibody. These vectors were used for work carried out in chapter 6 of this thesis.

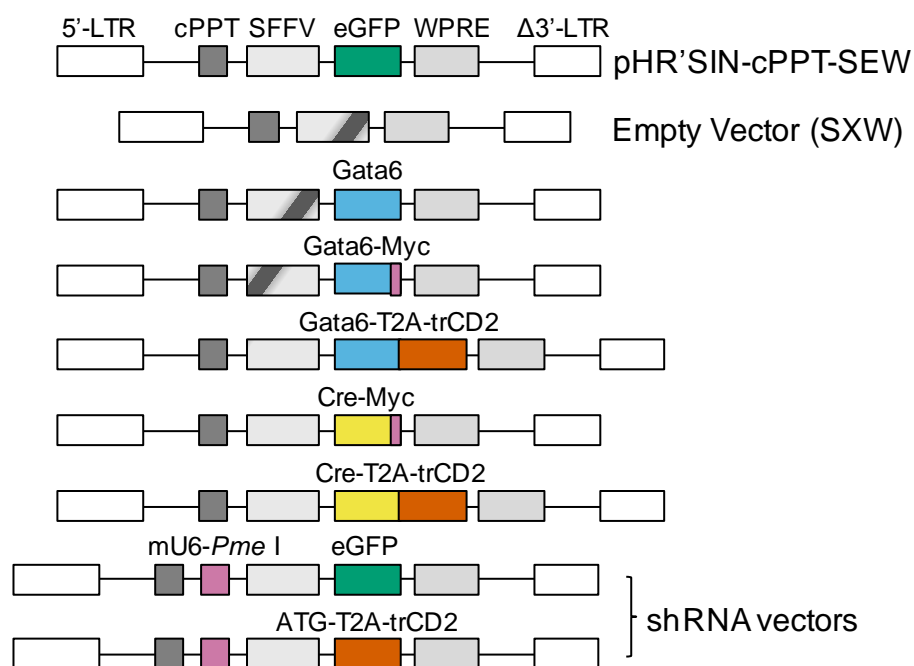


**Figure 5.7. Schematic of lentiviral vectors produced for this thesis**

Schematic showing the content between the long terminal repeats (LTRs) of some of the lentiviral plasmids produced in this thesis. Individual sequence units are labelled: cPPT = central polypurine tract, SFFV = spleen focus forming virus promoter, WPRE = woodchuck post-transcriptional regulatory element, mU6 = mouse U6 promoter, eGFP = enhanced green fluorescent protein, trCD2 = truncated rat CD2.

### 5.2.7 – Preferential inflammatory loss of infected ResMØs *in vivo*

The efficacy of the lentiviral vectors in ResMØs was examined *in vivo* over a longer time course (up to two weeks), to determine whether viral integration and expression of transgenes was stable, or whether infected cells or were lost over time. The level of infection seen two weeks after intra-peritoneal injection of SEW or trCD2-expressing lentiviruses decreased significantly from the level seen 1 week after infection (*figure 5.8a*). This was accompanied by a sharp increase in the number of recruited InfMØs (*figure 5.8b*), which is indicative of a post inflammatory environment (chapters 3 and 4 of this thesis).

This loss in expression levels was attributed to immune rejection of the trCD2 or eGFP tags, which are not native proteins to the mouse. Therefore, mice which had been genetically modified to contain an eGFP gene were acquired. Foxp3-eGFP mice were bred in-house by the JBIOS facility and were a kind gift from Prof. Alexander Rodensky

(Memorial Sloan-Kettering Cancer Center, New York). These mice express low levels of eGFP in regulatory T-cells (Kim *et al.*, 2007), and therefore would have gained immune tolerance to eGFP. These Foxp3-eGFP mice were used in combination with eGFP-expressing lentiviral vectors. Unlike WT 129S6/SvEv mice, Foxp3-eGFP mice maintain a constant level of infected peritoneal ResMØs for up to 3 weeks, with no signs of inflammation (*figure 5.9*). However, the infected cells were again lost when the mice were left for 6 weeks (42 days) after lentiviral infection (*figure 6.10*).

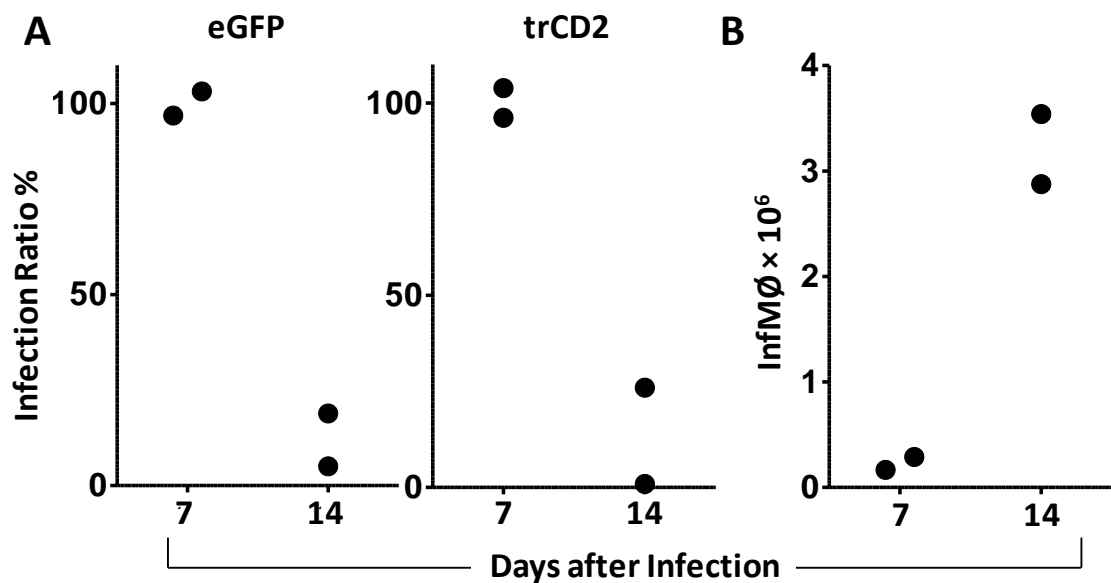


**Figure 5.8. Preferential inflammatory loss of infected ResMØs *in vivo***

**A)** Bar graphs showing the ratio of infection 7 and 14 days after intra-peritoneal delivery of trCD2 and eGFP-expressing lentiviruses. Data was made relative to the infection levels seen in mice 7 days after lentiviral delivery. Data shown for trCD2 and eGFP are from two separate experiments in 129S6/SvEv mice (n= 2 per group). **B)** Bar graph showing the number of InfMØs quantified from the eGFP infected mice in (A). Data shown is from a single experiment in 129S6/SvEv mice (n= 2 per group), but similar results were obtained (for both A and B) 14 days after intra-peritoneal delivery of ICAM-1 and non-silencing shRNA (eGFP-tagged)-expressing lentiviruses (n= 4).

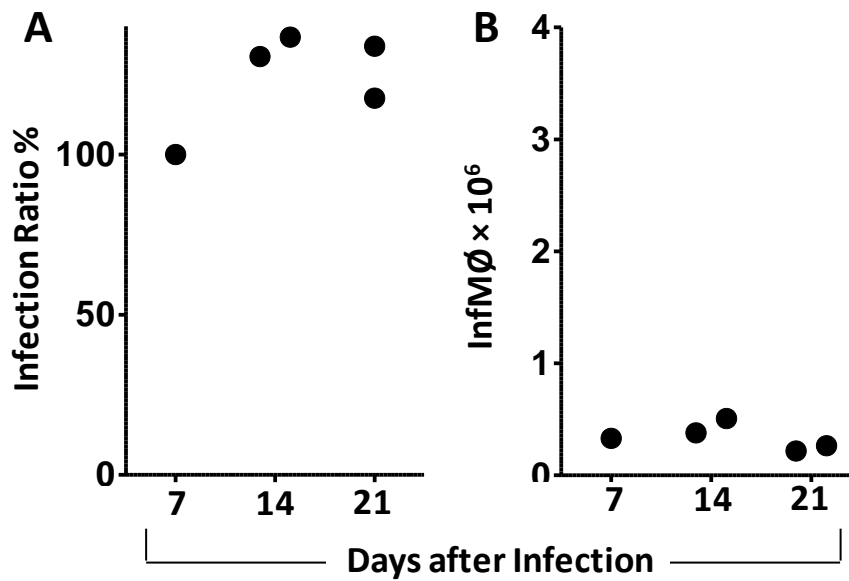


**Figure 5.9. Preferential inflammatory loss of infected ResMΦs is prevented in Foxp3-eGFP mice**

**A)** Bar graph showing the ratio of infection 7, 14 and 21 days after intra-peritoneal delivery of eGFP-expressing lentivirus. Data was made relative to the infection levels seen in mice 7 days after lentiviral delivery. **B)** Bar graph showing the number of InfMΦs quantified from (A), which includes MHCII<sup>high</sup> MΦ/ DCs (Dioszeghy *et al.*, 2008). Data shown is from one preliminary experiment in Foxp3-eGFP mice (n= 1-2 per group).

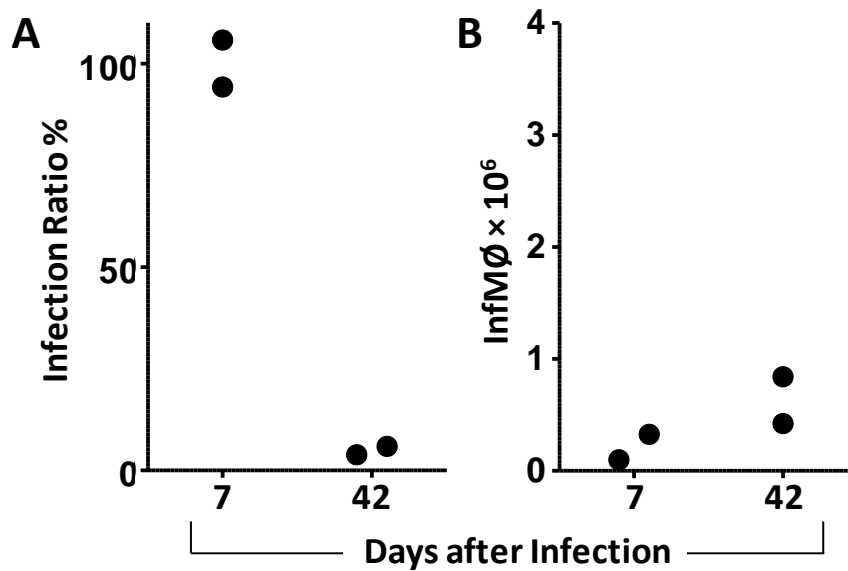


**Figure 5.10. Foxp3-eGFP mice only offer limited protection from the loss of infected ResMφs *in vivo***

**A)** Bar graph showing the ratio of infection 7 and 42 days after intra-peritoneal delivery of eGFP-expressing lentivirus. Data was made relative to the infection levels seen in mice 7 days after lentiviral delivery. **B)** Bar graph showing the number of InfMφs quantified from (A) which includes MHCII<sup>high</sup> Mφ/ DCs (Dioszeghy *et al.*, 2008). Data shown is from one preliminary experiment in Foxp3-eGFP mice (n= 2 per group).



## 5.3 – Discussion

The aims of this chapter were to: 1) create an efficient method for quantifying viral titre; 2) infect ResMØs with lentivirus *in vitro*; 3) infect ResMØs with lentivirus *in vivo*; 4) produce lentiviral vectors that express and/ or knockdown genes of interest; and 5) investigate the efficacy of ResMØ lentiviral infection *in vivo*.

### 5.3.1 – Viral titre

Viral titre could be quantified a number of ways: the MOI could be calculated using infection of Jurkat cells and Poisson distribution, viral RNA could be extracted and quantified with real-time PCR, or viral integration into the genomic DNA could be investigated with real-time PCR. Viral integration was quantified against a standard curve using lentiviral plasmid to produce a value for viral copy number (*figure 5.1*). However, this value was not considered to be accurate, due to the difference in PCR efficiency using a plasmid or extracted DNA. Therefore, the value was considered relative, so could only be used to relatively compare viral titre. This however, was not considered the most efficient method for viral titre measurement. Due to the relative ease of infection of Jurkat cells: Poisson distribution could be applied to calculate viral titre (see methods 2.9.3). Tagged (eGFP/ trCD2/ Myc) virus could be detected in cells using flow cytometry; this gave a value for the percentage of cells infected. This percentage could be extrapolated from a Poisson distribution curve to give a relative number for MOI. Multiple titres were extrapolated this way to give an average MOI per  $\mu\text{l}$  of virus, which could be used to compare different viral productions.

Viral titre used *in vivo* was not usually quantified or kept consistent due to the natural variability of injections and individual mice. An infection percentage of 5-95 % was considered acceptable, as both infected and non-infected cells could be analysed reliably by flow cytometry. However, this did not take into account any secondary effects, such as a change in secreted factors or other juxtacrine effects. For example, if a secreted factor such as adenosine was reduced with lentiviral knockdown of an important enzyme (e.g. CD73), then the level of infection would have an impact on the total availability of adenosine in the system. Therefore, in some circumstances it would be important to keep infection levels consistent. In this chapter infection percentages

were typically between 40-60 % when using 200-400 µl of concentrated virus per intra-peritoneal injection.

The lentiviruses used in this thesis frequently showed non-linear regression between viral titre used and measures of infection (MFI, %<sup>+</sup> cells) when infecting different cell types with lentivirus *in vitro*. The non linear regression leading to a maximal infection level (68.8 % seen in the ResMØ cultures (*figure 5.3*)) *in vitro* could be attributed to toxic effects of the virus, lentiviral concentrator or 293T proteins and/ or debris that may have inevitably been concentrated with the virus; which could lead to cell death. However, this was not further investigated in this thesis, as *in vivo* delivery of virus could infect a larger proportion of cells (*figure 5.4*). This could be attributed to the presence of a 'clearance system' in an *in vivo* environment, which was not present *in vitro*.

### **5.3.2 – Selective infection of ResMØs**

Interestingly, even though the SEW lentivirus has been shown to infect myeloid cells and B cells alike with similar efficiencies (Demaison *et al.*, 2002), the SEW lentivirus used in this thesis selectively infected MØs over other peritoneal cells (including B cells), both *in* and *ex vivo*. This could be attributed to the Lenti-X Concentrator (Clontech) used to concentrate the virus. This concentrator contains polyethylene glycol (PEG), which is known to be recognised by MØ scavenger receptors (Shibuya-Fujiwara *et al.*, 2001). This scavenger receptor mediated phagocytosis of what could potentially be PEGylated clusters of viral particles, could explain the selectivity for infection of professional phagocytes (MØs). However, investigation into the mechanism of the selective viral uptake was not an objective of this thesis.

### **5.3.3 – Immune rejection of infected ResMØs**

The number of eGFP/ trCD2-tagged lentivirally infected cells *in vivo* dropped dramatically 2 weeks after infection. This was associated with inflammation, suggesting host rejection of foreign proteins (eGFP/ trCD2). The rat CD2 protein was truncated to prevent downstream signalling (King *et al.*, 1998), however this was only in the cytoplasmic region. Truncated rat CD2 has the additional disadvantage that it is

homologous to mouse CD2 (76 % identity (Yagita *et al.*, 1988)). Therefore, it could still have bound to receptors, activated juxtacrine signalling and altered cell adhesion. The 76 % identity also meant that foreign peptides (24 %) would have been presented to cells of the adaptive immune system, which could trigger an immune response against trCD2-expressing cells. The eGFP used is a synthetic protein, originally found in jellyfish (Shimomura *et al.*, 1962). This would have also produced foreign peptides and triggered an immune response. The use of transgenic eGFP mice (Foxp3-eGFP) overcame this rejection at 2 weeks, and no loss in eGFP-expressing cells was observed up to 3 weeks after infection (*figure 5.9*). This supports the theory for immune rejection of ResMØs expressing foreign proteins. It has also been reported that VSV-G coated lentiviruses cannot efficiently infect myeloid cells, due to the SAM domain and HD domain-containing protein 1 (Bobadilla *et al.*, 2012, Hrecka *et al.*, 2011, Laguette *et al.*, 2011). However, the data presented herein suggests that this cannot fully restrict lentiviral integration, even *in vivo* (*figure 5.9*). The lack of InfMØs seen 6 weeks after SEW infection (*figure 5.10*) could be attributed to a non-inflammatory loss of cells, or that the cells were lost between 3 and 6 weeks after infection when InfMØs could be cleared. The loss of eGFP expression could also be explained by gene silencing mechanisms, such as epigenetic modification (He *et al.*, 2005). However, the *in vivo* model of infecting peritoneal ResMØs of transgenic eGFP mice with eGFP-expressing lentiviruses could be used efficiently for up to 3 weeks.

#### **5.3.4 – Conclusion**

In conclusion, the methodology produced in this chapter shows that ResMØs can be efficiently infected with lentiviruses both *in* and *ex vivo* to modulate gene expression. Gene expression was modulated through the use of expression cassettes for transgene expression, and shRNA to induce RNA silencing of target mRNA. These lentiviral vectors provide a powerful tool to dissect specific MØ functions *in vivo*, and can be applied to investigate the role of MØs in homeostasis and inflammation.

## **Chapter 6 – Gata6 controls ResMØ renewal**

## 6.1 – Introduction

Previously, this thesis has examined ResMØ phenotype (chapter 3), and the renewal of MØs during inflammation (chapters 3-4). Additionally, an efficient, specific system for the *in vivo* lentiviral manipulation of ResMØs was established (chapter 5). This work creates a platform from which specific gene function can be probed *in vivo* in a physiological context. During this chapter, this knowledge is applied to the functional analysis of Gata6.

As previously mentioned (general introduction, 1.3.1), microarray analysis of monocyte and MØ populations during peritoneal inflammation was performed by Dr. Marcela Rosas in Prof. Phil Taylor's group. This identified a list of ~800 ResMØ restricted genes, which included Tim4 (Miyanishi *et al.*, 2007), SignR1 (Taylor *et al.*, 2004) and CRig (He *et al.*, 2008); but also revealed atypical transcription factors with unknown functions in MØs. One such transcription factor was Gata6. This zinc finger transcription factor is described in more detail in the general introduction (1.3.2), but has been implicated in proliferation and differentiation in a different cellular context (Beuling *et al.*, 2011).

### 6.1.1 – Pleural ResMØs

In this chapter pleural ResMØs were also investigated. Pleural ResMØs exist in the serous membrane of the pleural cavity, which is similar to the peritoneal membrane (Negrini *et al.*, 1993). Both the pleural and peritoneal ResMØs from these membranes share an F4/80<sup>high</sup> CD11b<sup>high</sup> phenotype, and have the ability to proliferate in T<sub>H</sub>2 mediated inflammation (Jenkins *et al.*, 2011). These comparable phenotypes, responses and environments could suggest that both serosal MØ populations are likely regulated by similar mechanisms.

### **6.1.2 – Hypothesis**

The hypothesis tested in this chapter is that both the proliferation and phenotype of peritoneal and pleural ResMØs is mediated by the transcription factor Gata6.

### **6.1.3 – Aims**

- To determine whether Gata6 is selectively expressed by peritoneal and pleural ResMØs
- To investigate the effect of Gata6 on peritoneal ResMØ proliferation and phenotype
- To investigate the effect of Gata6 on pleural ResMØ proliferation and phenotype
- To determine the effect of Gata6 deficiency on the inflammatory response

## 6.2 – Results

### 6.2.1 – Gata6 is expressed selectively by peritoneal ResMØ

Previous microarray experiments carried out by Dr. Marcela Rosas in Prof. Phil Taylor's laboratory showed that ResMØs selectively express the transcription factor Gata6, when compared to multiple populations of MØs and monocytes during inflammation. This result was supported by quantitative real-time PCR analysis of *Gata6* mRNA expression in ResMØs. *Gata6* expression was  $6210 \pm 1462$ -fold higher in ResMØs (mean  $\pm$  SEM; n= 3) than cultured BMMØs (see methods 2.5.3) (*figure 6.1a*). However to confirm it's selectivity to ResMØs specifically in the peritoneal cavity, inflammation was initiated by  $2 \times 10^6$  particles of zymosan which resulted in mixed populations of MØs including InfMØs. The expression of Gata6 was  $10.44 \pm 0.76$ -fold higher in naïve ResMØs than InfMØs retrieved from the peritoneal cavity 48 hours after this inflammation. The ResMØs from the same inflammatory environment had a comparable level of *Gata6* expression with naïve ResMØs (*figure 6.1b*). Immunostaining of peritoneal cells confirmed selective Gata6 expression at the protein level, with a visible, nuclear rich content of Gata6 in F4/80<sup>high</sup> ResMØs (*figure 6.1c*).

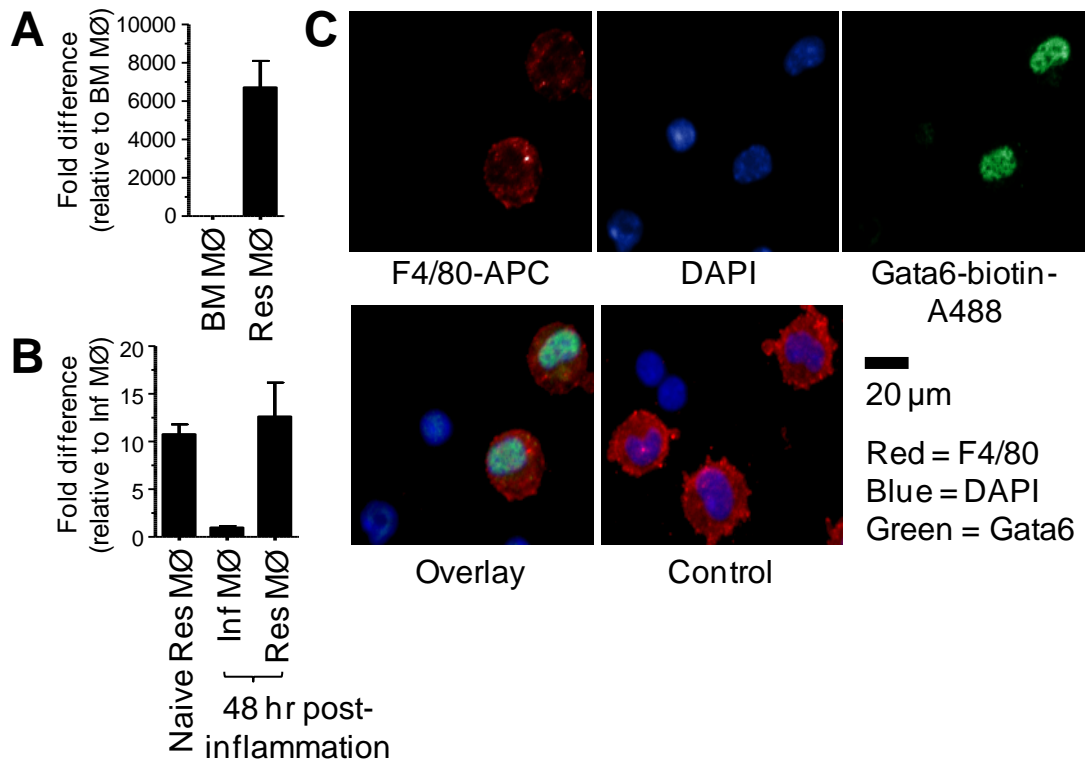


**Figure 6.1. Gata6 is selectively expressed by ResMφ**

**A)** Bar graph showing relative mRNA expression of *Gata6* in purified (by flow cytometry) ResMφs and cultured BMMφs (see 2.5.3). Expression data for *Gata6* was made relative to BMMφs and the endogenous control *Ywhaz*, and represents the mean  $\pm$  SEM of 3 independent samples per group. **B)** Graph showing relative mRNA expression of *Gata6* in flow cytometrically purified InfMφs and ResMφs isolated 48 hours after acute inflammation induced with zymosan ( $2 \times 10^6$  particles) and compared with ResMφs from naïve animals. Expression data for *Gata6* was made relative to InfMφs and the endogenous control *Ywhaz*, and represents the mean  $\pm$  SEM of 2 independent samples per group. **C.** Pictures showing cytospun peritoneal cells stained with Gata6 (green), F4/80 (red) and DAPI (blue), shown as three separate images and a merge (overlay). The control picture represents residual binding from streptavidin-AlexaFluor488 in the absence of the *Gata6* biotin antibody. Data is representative of 8 ‘Gata6-WT’ mixed sex mice (4 slides per mouse and 4 pictures per slide) from 2 independent experiments. The scale bar is indicated. APC = Allophycocyanin, A488 = AlexaFluor488.



### 6.2.2 – Knockdown of *Gata6* expression results in a reduction in F4/80 protein

To determine the impact of a reduction in *Gata6* expression: lentiviruses were constructed (see chapter 5, 5.2.6) to introduce stable production of shRNA molecules against *Gata6* mRNA into ResMØs. Stable transduction of peritoneal ResMØs with *Gata6* targeting shRNA was performed via intra-peritoneal injection. This infection significantly reduced F4/80 levels in ResMØs compared with non-silencing control (*figure 6.2*) after 7 days. Due to the alteration in the normal F4/80<sup>high</sup> phenotype of ResMØ, the ResMØ specific marker Tim4 (Miyanishi *et al.*, 2007) was used to identify ResMØ populations, and this applies to all the experiments conducted in this chapter.

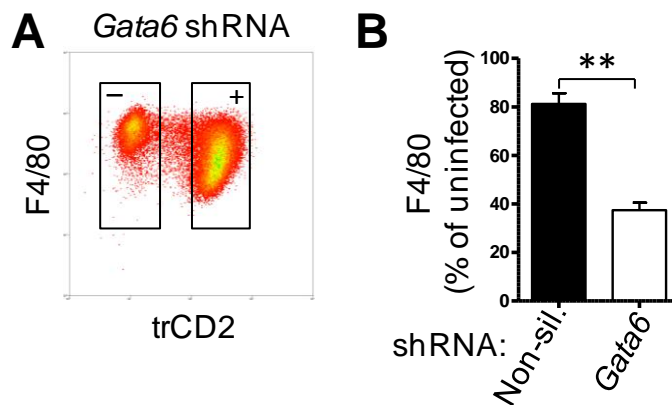


**Figure 6.2. Knockdown of *Gata6* causes a reduction in F4/80 protein expression**

**A)** Representative flow cytometry plot comparing F4/80 expression in 12-16 week male 129S6/SvEv ResMØ, 7 days after intra-peritoneal infection with a *Gata6*-specific shRNA or non-silencing (Non-sil) control (indicated by expression of the trCD2 tag). The boxes show trCD2<sup>-</sup> and trCD2<sup>+</sup> cell populations. The plot was gated on Tim4<sup>+</sup> CD11b<sup>high</sup> cells and pre-gated to remove eosinophils and doublets as previously shown (*figures 3.1 and 3.2*). **B)** Quantification of the impact of *Gata6* shRNA on F4/80 expression compared to non-silencing shRNA. Data was made relative to uninfected cells in the same environment and represents mean ± SEM of n= 3 mice per group from one of two independent experiments. Statistical analysis was performed using a Student's *t*-test, the *P*-value is indicated on the graph ( $P \leq 0.01 = **$ ).

### 6.2.3 – Knockout of the *Gata6* gene causes a marked reduction in the F4/80 phenotype of adult ResMØ

Mice which contained a floxed *Gata6* allele (*Gata6*<sup>tm2.1Sad</sup>) have been generated previously (Sodhi *et al.*, 2006). Cre could be employed to recombine the flanking loxP sites (floxed) and delete exon 2 of the *Gata6* gene, this resulted in more than half of the protein length being lost which translates to a loss of function (Sodhi *et al.*, 2006). These mice (*Gata6*<sup>tm2.1Sad</sup>) were used in conjunction with a Cre-expressing lentiviral vector to stably knock out normal *Gata6* expression in adult peritoneal MØ *in vivo*. *Gata6* knockout resulted in a marked reduction in the canonical F4/80<sup>high</sup> profile of ResMØs (figure 6.3), which could be rescued by reconstitution with *Gata6*-expressing lentiviruses (figure 6.4). Infection of WT 129S6/SvEv mice with Cre-expressing lentivirus did not alter F4/80 expression (figure 6.3).

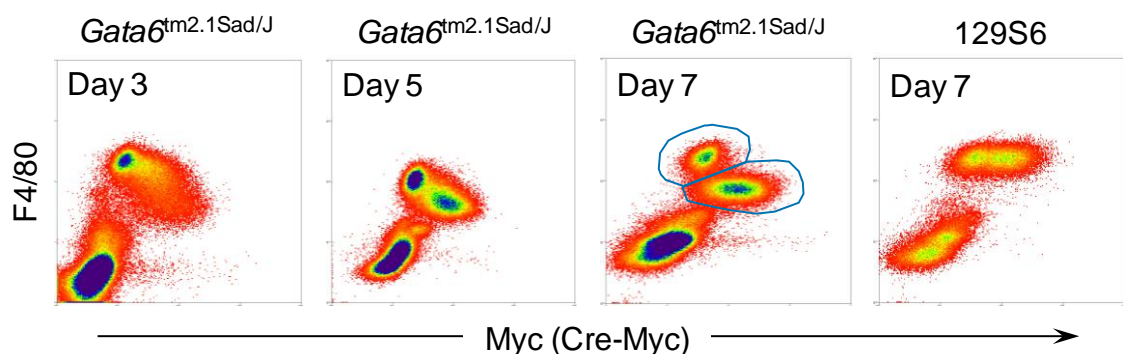


**Figure 6.3. Selective knockout of *Gata6* in ResMØs results in a reduction of F4/80 expression**

Representative density plots showing infection of *Gata6*<sup>tm2.1Sad</sup> mice with a lentiviral vector encoding a Myc-tagged Cre (Cre-Myc) over a week time course (left panels), compared with 129S6 mice at day 7 (far right panel). The plots show F4/80 and Cre-Myc expression, the blue gates indicate two separate populations of Cre<sup>-</sup> F4/80<sup>high</sup> and Cre<sup>+</sup> F4/80<sup>low</sup> ResMØs. Plots were pre-gated to remove eosinophils and doublets as previously described (figures 3.1 and 3.2a). Data was compiled from preliminary experiments with at least 2 mice per time point.

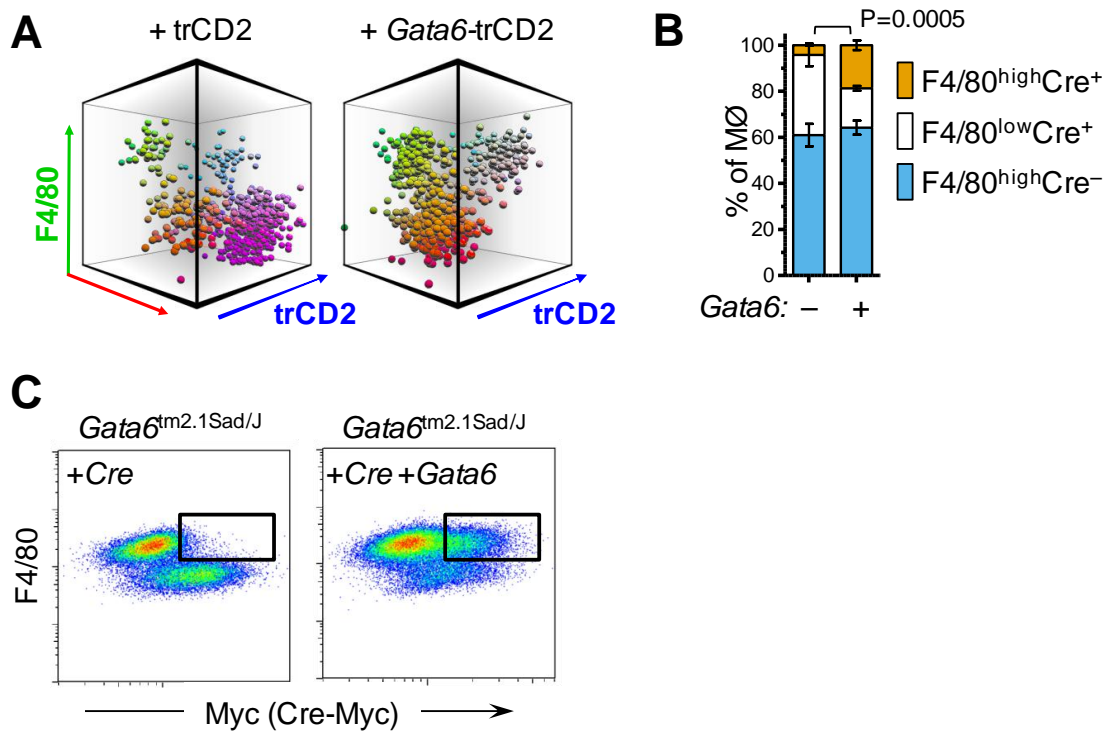


**Figure 6.4. *Gata6* reconstitution in *Gata6*-KO<sup>mye</sup> ResMØs restores F4/80 expression**

**A)** Representative 3D bubble plots showing F4/80 expression in *Gata6*<sup>tm2.1Sad</sup> mice co-infected with a Myc-tagged Cre (Cre-Myc), and either control or *Gata6*-expressing virus (indicated by expression of the trCD2 tag) for 7 days. The persistence of the F4/80<sup>high</sup> phenotype in Cre-Myc<sup>+</sup> trCD2<sup>+</sup> cells can be seen with the *Gata6*-expressing virus (white/grey dots, right panel) in comparison to the F4/80<sup>low</sup> Cre-Myc<sup>+</sup> trCD2<sup>+</sup> population seen when control virus was used (magenta dots, left panel). Data represents 3-4 mice per group from one of three similar experiments. **B)** A bar graph showing quantification of the phenotype conversion shown in (A). The prevalence of F4/80<sup>high</sup> Cre<sup>+</sup> cells was compared between *Gata6* reconstitution (+) and control virus (-) by Student's *t*-test with the *P*-value indicated. **C.** Representative density plots showing F4/80 expression on cells co-infected with the Cre-Myc lentivirus and a non-tagged *Gata6*-expressing lentivirus (right panel) or empty vector control (left panel) for 7 days. Data shown is from *Gata6*<sup>tm2.1Sad</sup> 8-14 week old male mice (n= 4/group). Plots (A, C) were gated on F4/80<sup>+</sup> CD11b<sup>high</sup> cells and pre-gated to remove eosinophils and doublets as previously described (figures 3.1 and 3.2a).

#### 6.2.4 – Gata6 knockout in the myeloid lineage gives viable ResMØs with an altered F4/80 phenotype

Gata6 is essential for the formation of major organs during development, thus the loss of Gata6 in all cells is lethal during embryogenesis (Morrisey *et al.*, 1996). Therefore, Lysozyme M (*Lyz2*) Cre ‘knock-in’ congenic mice (*Lyz2<sup>Cre</sup>*, B6.129P2-*Lyz2<sup>tm1(cre)lfo</sup>*) (Clausen *et al.*, 1999) were crossed with conditional KO *Gata6<sup>tm2.1Sad</sup>* mice (Sodhi *et al.*, 2006) to generate a mouse strain with a select myeloid deficiency of Gata6 (*Gata6-KO<sup>mye</sup>*) (*figure 6.5*). The peritoneal cells of *Gata6-KO<sup>mye</sup>* mice were analysed by flow cytometry. This revealed a marked change in the canonical F4/80 phenotype of ResMØs (*figure 6.6*); creating F4/80<sup>low</sup> ResMØs synonymous with data retrieved from the lentiviral-shRNA knockdown (*figure 6.2*) and lentiviral Cre-mediated knockout of Gata6 (*figure 6.3*). Interestingly, there was a small ( $\approx 5\%$ ) population of residual F4/80<sup>high</sup> ResMØs in *Gata6-KO<sup>mye</sup>* mice.

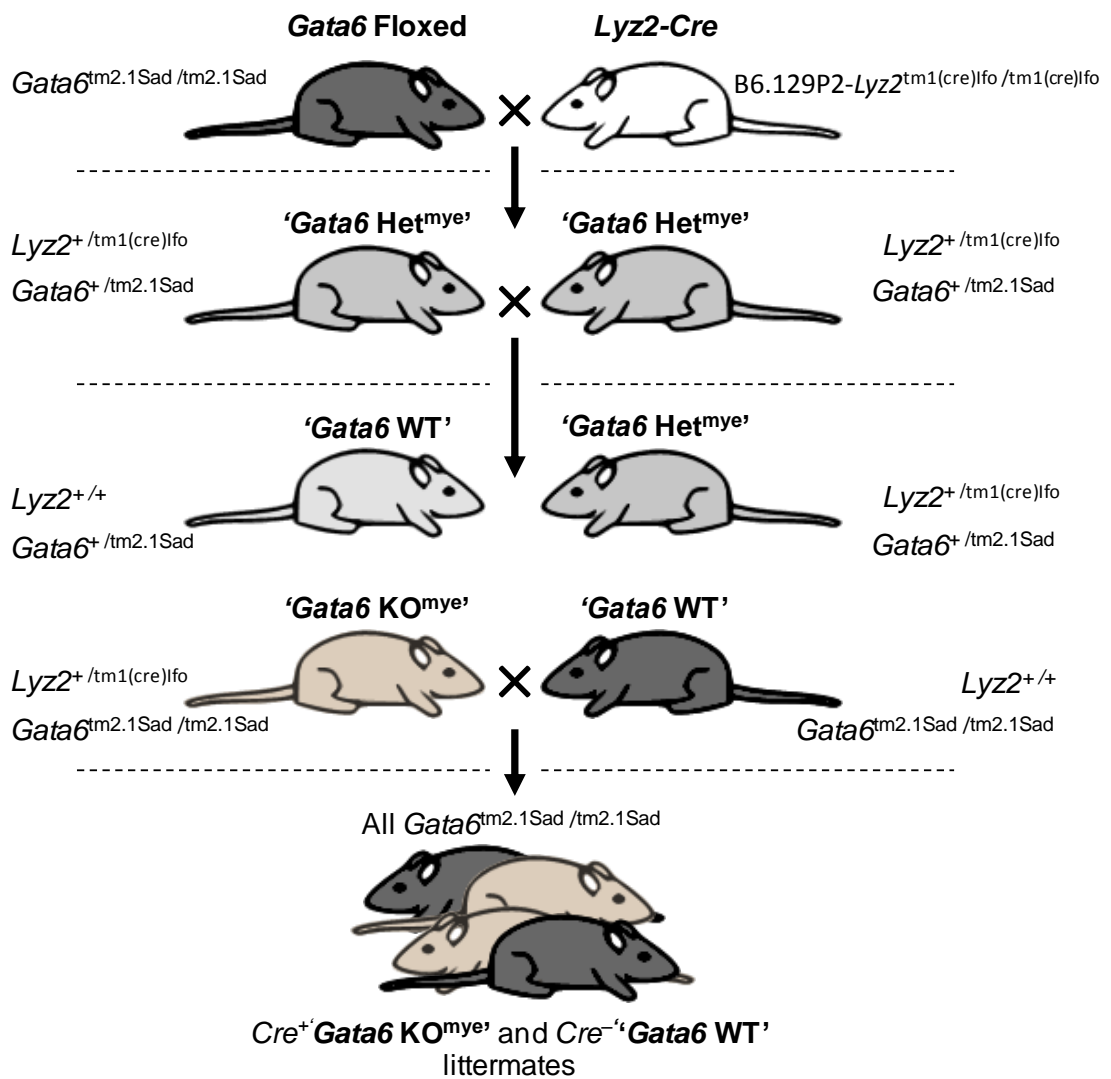


**Figure 6.5. Breeding strategy to generate  $Gata6$ -KO<sup>mye</sup> mice**

A diagram showing the breeding strategy used to yield  $Gata6$ -KO<sup>mye</sup> and WT littermates. X symbols indicate breeding and arrows indicate offspring. The dotted lines partition separate generations.

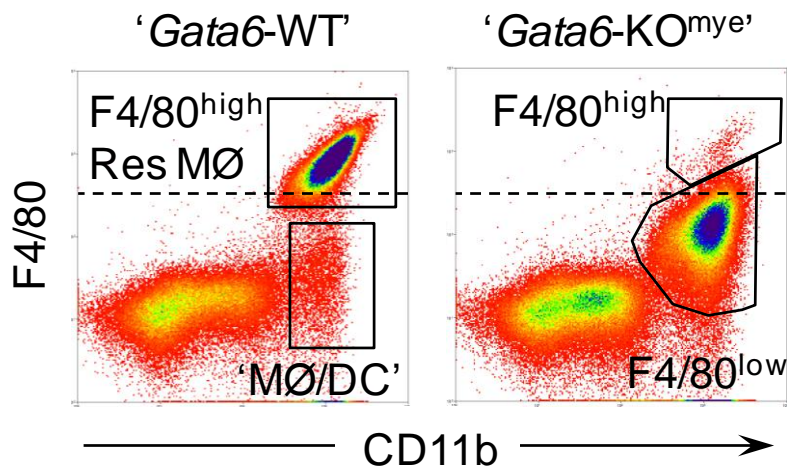


**Figure 6.6. ResMØs of *Gata6-KO<sup>mye</sup>* mice have a reduced F4/80 phenotype**

Representative density plots showing F4/80 and CD11b expression on MØ populations after excluding doublets and eosinophils as previously described (*figures 3.1 and 3.2a*). Gated populations are annotated and show F4/80<sup>low</sup> and F4/80<sup>high</sup> MØs. Note: the F4/80<sup>low</sup> MØ population contains DC and ‘DC-like’ cells (MHCII<sup>+</sup> MØs). These plots are from naïve 8 week old female mice, but are representative of all *Gata6-WT* and *Gata6-KO<sup>mye</sup>* mice used in this study.

To determine whether the F4/80<sup>high</sup> ResMØs from *Gata6-KO<sup>mye</sup>* mice have ‘normal’ levels of Gata6, a polyclonal antibody was used to examine Gata6 protein expression in peritoneal cells (*figure 6.7a*). Nuclear Gata6 content was quantified (see methods 2.11) and revealed that F4/80<sup>high</sup> ResMØs have significantly higher levels of Gata6 than F4/80<sup>low</sup> MØs in *Gata6-KO<sup>mye</sup>* mice (*figure 6.7b*). However, this population likely also contained DCs and ‘DC-like’ cells, although ResMØs were still the majority cell type. When averaged per mouse, the F4/80<sup>high</sup> ResMØs from *Gata6-KO<sup>mye</sup>* contained a comparable level of Gata6 with that of WT mice (*figure 6.7c*). A similar experiment to *figure 6.4* was used to reconstitute the Gata6 of *Gata6-KO<sup>mye</sup>* mice via intra-peritoneal injection of a Gata6-expressing lentivirus. This supported previous data (*figure 6.4*), in that the F4/80 phenotype was ‘rescued’ toward that of WT ResMØs in transduced cells (*figure 6.8*). Dr. Marcela Rosas additionally phenotyped and genotyped the F4/80<sup>high</sup> ResMØs from *Gata6-KO<sup>mye</sup>* mice, and showed that there was no Cre activity (i.e. exon 2 of *Gata6* was present). Therefore, the cells were considered effectively ‘WT’ for this chapter (see discussion).

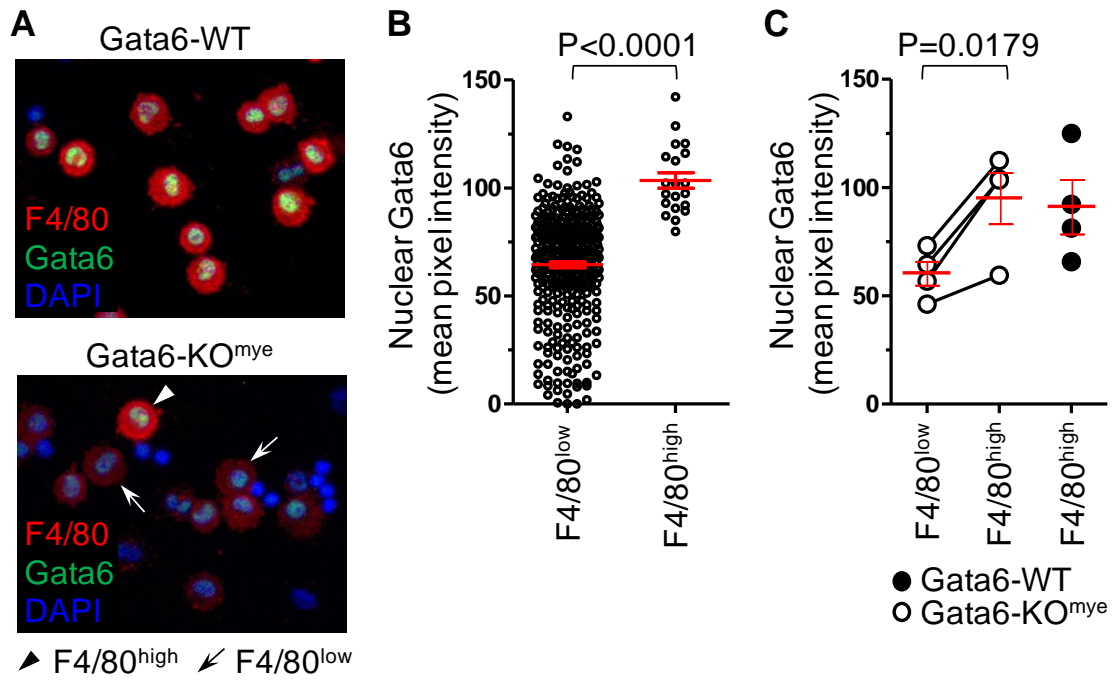


**Figure 6.7. F4/80<sup>high</sup> resident MØs in *Gata6*-KO<sup>mye</sup> express normal Gata6 levels**

**A)** Representative immunofluorescent images of Gata6 expression (green) in the nuclei (blue) of MØs from WT and *Gata6*-KO<sup>mye</sup> mice, identified by F4/80 expression (red). Examples of F4/80<sup>high</sup> and F4/80<sup>low</sup> MØs are indicated in the lower panel by arrowheads and arrows respectively. **B)** Nuclear Gata6 was quantified using Image J and expressed as mean pixel intensity after selecting the nuclear DAPI staining. Symbols denote individual MØs from a representative *Gata6*-KO<sup>mye</sup> mouse. Red lines indicate the mean ± SEM of the group. Data were analyzed by Student's *t*-test. **C)** Symbols represent individual mice and the F4/80<sup>high</sup> and F4/80<sup>low</sup> MØs from the same *Gata6*-KO<sup>mye</sup> mice are linked by lines. Red lines indicate the mean ± SEM of the groups. Data were analyzed by paired *t*-test. A mean of 188 ± 61 MØs (mean ± SEM) were quantified for each mouse. Data is representative of 4 mice (12-16 weeks old) from one of two similar experiments. The data analysis using Image J was performed by Prof. Phil Taylor.

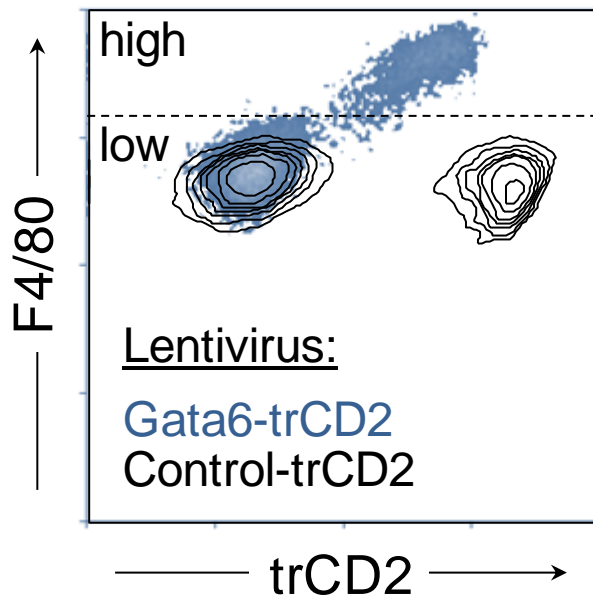


**Figure 6.8. Reconstitution of *Gata6* restores F4/80 expression in *Gata6-KO*<sup>mye</sup> ResMØ**

Density plot showing F4/80 expression 7 days after intra-peritoneal infection of *Gata6-KO*<sup>mye</sup> mice with a *Gata6*-expressing lentivirus (detected via a self-cleaving truncated rat CD2 (trCD2)). This results in the acquisition of an F4/80<sup>high</sup> phenotype in the transduced cells. The control rCD2 virus infected cells (overlaid contour plot) do not have altered F4/80 expression. Plots are pre-gated on F4/80<sup>+</sup> CD11b<sup>+</sup> MHCII<sup>low/-</sup> MØs (after removing eosinophils and doublets (*figures 3.1 and 3.2a*)). Data is from 12-14 week old male mice and is representative of two experiments with 2-3 mice per group.

### 6.2.5 – Knockout of *Gata6* has a cell-intrinsic effect on peritoneal ResMØ proliferation and polyploidy

*Gata6* has been implicated in control of cell differentiation and proliferation (Beuling *et al.*, 2011). Therefore, levels of proliferation were calculated for *Gata6-KO*<sup>mye</sup> and WT mice using the SG<sub>2</sub>M strategy discussed in chapter 4 of this thesis (*figure 6.9a*). The quantified basal proliferation of *Gata6-KO*<sup>mye</sup> ResMØs (specifically gating the ‘true-KO’ F4/80<sup>low</sup> ResMØs) was significantly higher than ResMØs from both WT and heterozygous (‘Het’) mice. The percentage of cells in SG<sub>2</sub>M was 3.16 ± 0.63 % vs 0.66 ± 0.12 % (mean ± SEM, n= 5 and 3 respectively) in the *Gata6-KO*<sup>mye</sup> vs WT mice, a near 5-fold increase (*figure 6.9b*). Interestingly, the level of polyploidy (% >2N DNA content, Ki67<sup>-</sup>) was also dramatically higher in *Gata6-KO*<sup>mye</sup> ResMØs, at 13.34 ± 1.41 % (mean ± SEM, n= 5), which is over 8-fold greater than the level seen in WT mice (1.65 ± 0.35 %,



mean  $\pm$  SEM,  $n = 3$ ) (figure 6.9b). This results in an increased number of large multi-nucleated M $\phi$ s as shown in figure 6.9c.

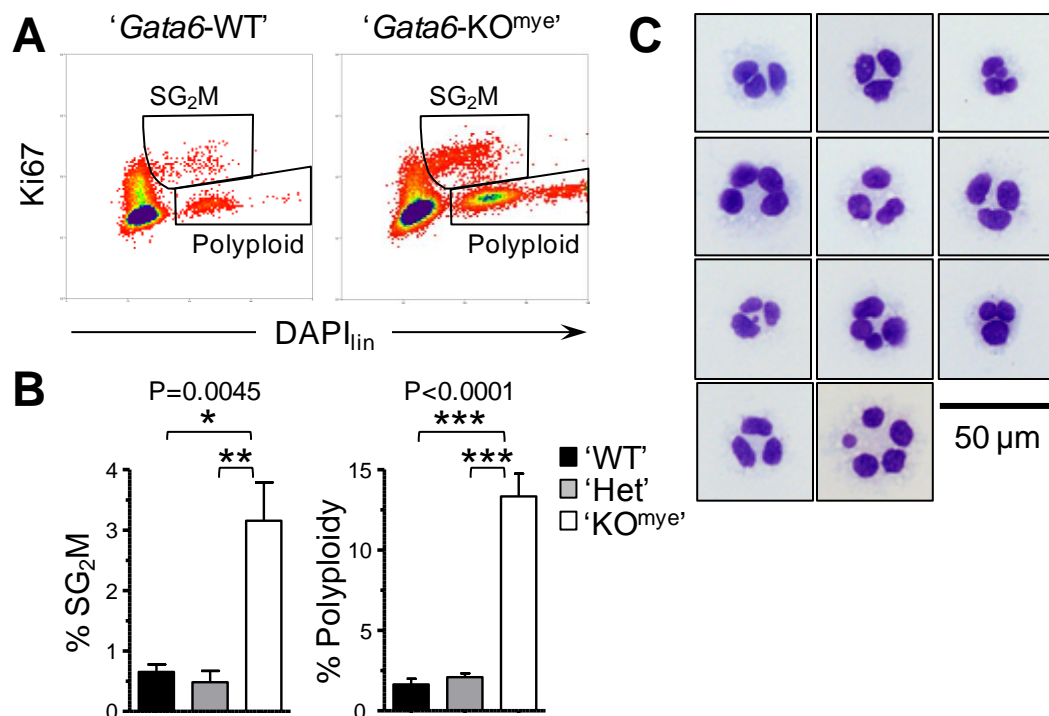


**Figure 6.9. *Gata6-KO<sup>mye</sup>* ResM $\phi$ s exhibit increased levels of proliferation and polyploidy**

**A)** Representative density plots showing SG<sub>2</sub>M and polyploidy for the F4/80<sup>high</sup> ResM $\phi$ s of WT mice and F4/80<sup>low</sup> ResM $\phi$ s of *Gata6-KO<sup>mye</sup>* mice, as indicated in figure 6.6 (above). SG<sub>2</sub>M calculations were based on the gating strategy from figure 4.2b. Cells with >2N DNA content, but negative for Ki67 expression were considered to be polyplloid. **B)** Graphs showing the quantification of SG<sub>2</sub>M and polyploidy in ResM $\phi$ s from both groups. Data is represented as mean  $\pm$  SEM and was analysed by one-way ANOVA ( $P$ -value as indicated) with Bonferonni post tests (\*,  $P \leq 0.05$ ; \*\*,  $P \leq 0.01$ ; \*\*\*,  $P \leq 0.001$ ). **C.** Photographs of larger polyplloid cells within *Gata6-KO<sup>mye</sup>* mice as observed on eosin and methylene blue stained cytopsin preparations, under oil immersion. The scale bar is as indicated and pictures were taken at 100 $\times$  objective magnification. Data (A-C) is derived from one of two independent experiments with 6-7 week old mice (KO<sup>mye</sup>,  $n = 5$ ; 'Het',  $n = 4$ ; WT,  $n = 3$ ).

The residual F4/80<sup>high</sup> ResMØs seen in *Gata6*-KO<sup>mye</sup> mice (figure 6.6 and 6.7) were used as internal controls for subsequent experiments. Proliferation was examined between F4/80<sup>high</sup> and F4/80<sup>low</sup> ResMØs in *Gata6*-KO<sup>mye</sup> mice. This revealed that the F4/80<sup>low</sup> ResMØs had higher levels of proliferation and polyploidy than the F4/80<sup>high</sup> ResMØs within the same environment (figure 6.10). This data was supported by alternative experiments using *Gata6*<sup>tm2.1Sad</sup> mice. These alternate experiments compared the level of proliferation in lentiviral Cre-mediated *Gata6* knockout ResMØs to that seen in non-infected WT ResMØs (as in figure 6.3, comparing the blue ringed populations). This revealed that the level of proliferation increased when *Gata6* expression was removed in adult mice (figure 6.11). Control viruses lacking Cre, e.g. rCD2 or eGFP-expressing lentiviruses caused a slight consistent decrease in SG<sub>2</sub>M, but an increase in polyploidy upon infection (examples in supplemental figure S3 and figure 6.20).

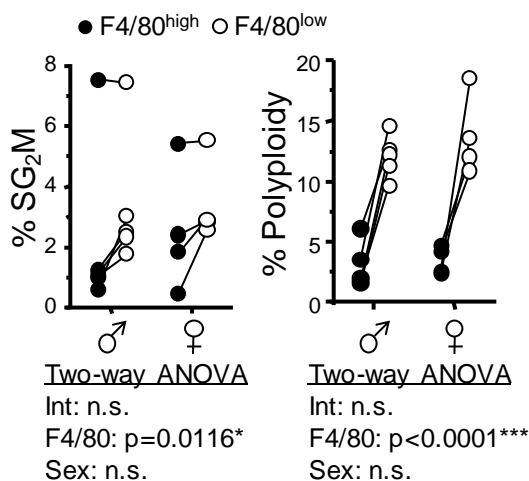


**Figure 6.10. F4/80<sup>low</sup> ResMØs show increased proliferation and polyploidy in comparison to the rare F4/80<sup>high</sup> ResMØs in the same *Gata6*-KO<sup>mye</sup> mice**

Graphs showing quantification of proliferative differences within the same *Gata6*-KO<sup>mye</sup> mice, between the bulk F4/80<sup>low</sup> ResMØ population and the rare residual F4/80<sup>high</sup> ResMØ, gated as shown in figure 6.9 (above). Data symbols represent individual mice (6-7 week old) with readings from the same mice connected by lines (n= 5♂ and 4♀). Data were pooled from two similar experiments and analysed by a paired two-way ANOVA. Int = interaction between groups, Exp = effect of experiment.

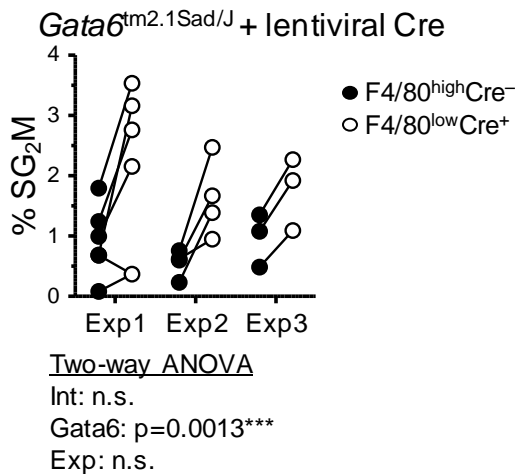


**Figure 6.11. Selective knockout of *Gata6* in ResMØs in adulthood causes an increase in proliferation**

Graph showing ResMØs, 7 days after intra-peritoneal delivery of a Cre-expressing lentivirus to *Gata6*<sup>tm2.1Sad</sup> mice. The proportion of cells in the SG<sub>2</sub>M phases of cell cycle (calculated as in figure 6.9) were compared between F4/80<sup>low</sup> Cre<sup>+</sup> ResMØs and F4/80<sup>high</sup> Cre<sup>-</sup> ResMØs. The data shows 3 independent experiments with individual mice indicated by paired (line connected) data points (n= 3-6/experiment) (8-14 weeks old). Data was analysed by a paired two-way ANOVA, *P*-values are indicated. Int = interaction between groups, Exp = effect of experiment.

### 6.2.6 – Knockout of *Gata6* has a cell-intrinsic effect on pleural ResMØ proliferation, polyploidy and phenotype

Pleural ResMØs are serosal tissue MØs that share a similar phenotype (F4/80<sup>high</sup>, CD11b<sup>high</sup>, majority Tim4<sup>+</sup>) with peritoneal ResMØs (figure 6.12). Therefore the level of *Gata6* expression was relatively quantified in pleural ResMØ, using BMMØs as a ‘negative’ control and ResMØs as a ‘positive’ control. The level of *Gata6* expression was comparable in pleural and peritoneal cells (figure 6.12a). Interestingly, the *Gata6*-KO<sup>mye</sup> F4/80<sup>low</sup> peritoneal phenotype (figure 6.6) is reflected in pleural ResMØs (figure 6.12b). When quantified, proliferation of the F4/80<sup>low</sup> pleural ResMØs was higher than the F4/80<sup>high</sup> population within the same *Gata6*-KO<sup>mye</sup> mice (figure 6.13). Additionally, the level of polyploidy seen in *Gata6*-KO<sup>mye</sup> mice was substantially increased compared to WT, with 9.28 ± 1.33 % vs 1.62 ± 0.20 % (mean ± SEM, n= 8 and 12 respectively) polyploidy respectively (figure 6.14a); and a visible increase in the number of multinucleate cells viewed under the microscope (figure 6.14b).

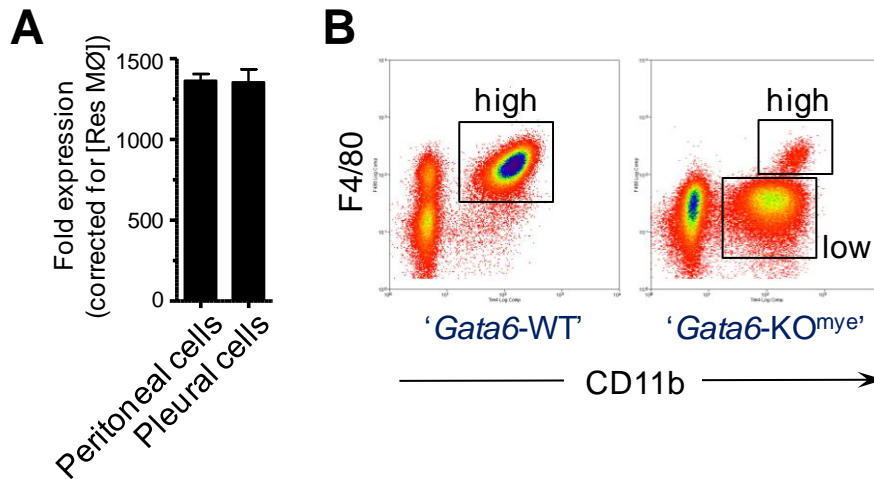


**Figure 6.12. Pleural ResMØs also express *Gata6* mRNA and are phenotypically altered in *Gata6-KO*<sup>mye</sup> mice**

**A)** A bar graph showing *Gata6* expression in mRNA extracted from total peritoneal and pleural leukocytes, the majority of which are Tim4<sup>+</sup> ResMØs (see B). The data was made relative to the endogenously expressed gene *Ywhaz* and expression of *Gata6* in BMMØs, and was corrected for numbers of ResMØs in peritoneal and pleural lavages. Data shows mean  $\pm$  SEM from one of two independent experiments in 12-16 week 129S6 mice (n = 3 per group). **B)** Density plots showing F4/80 and CD11b expression on ResMØs from the pleural cavity of *Gata6-KO*<sup>mye</sup> and WT mice. Plots were gated on F4/80<sup>+</sup> CD11b<sup>high</sup> cells after gating to remove eosinophils and doublets as previously described (figures 3.1 and 3.2a). Boxes indicate F4/80<sup>high</sup> and F4/80<sup>low</sup> populations. Data is representative of 6-8 week old female mice from one of two independent experiments (n= 4 per group).

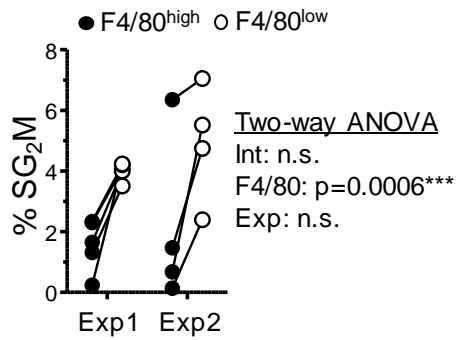


**Figure 6.13. Pleural F4/80<sup>low</sup> ResMØs show increased proliferation compared with contemporary F4/80<sup>high</sup> ResMØs in *Gata6-KO<sup>mye</sup>* mice**

A graph showing the proliferative differences within the same *Gata6-KO<sup>mye</sup>* mice between the bulk F4/80<sup>low</sup> pleural ResMØ population and the minority F4/80<sup>high</sup> pleural ResMØ, gated as shown in figure 6.6 (above). Data symbols represent individual 6-8 week old female mice with readings from the same mice connected by lines. Data shows two similar experiments and was analysed by a paired two-way ANOVA, *P*-values are indicated. Int = interaction between groups, Exp = effect of experiment.

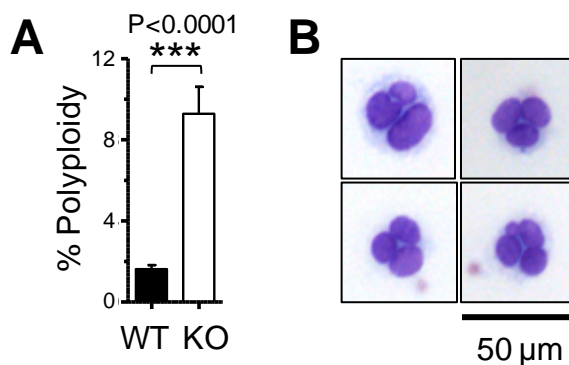


**Figure 6.14. Pleural ResMØs show increased polyploidy in *Gata6-KO<sup>mye</sup>* mice**

**A)** Graph showing quantification of polyploidy in F4/80<sup>low</sup> pleural MØs from the *Gata6-KO<sup>mye</sup>* compared to the F4/80<sup>high</sup> pleural MØs in WT mice. Data represents mean ± SEM of 6-8 week old female mice pooled from two independent experiments (WT, n= 12; KO<sup>mye</sup>, n= 8). Data were analysed by Student's *t*-test, and the *P*-value is indicated. **B)** Photographs of multinucleate cells in the pleural lavage of *Gata6-KO<sup>mye</sup>* mice from A. Images of cytospun cell preparations were acquired on a Leica PMLB light microscope at 100× objective magnification after staining for eosin and methylene blue. The scale bar is indicated.

### 6.2.7 – Absence of *Gata6* results in a reduced ability of ResMØs to recover after inflammation by proliferation

ResMØs are lost during the early hours of inflammation ( $2 \times 10^6$  zymosan particles), but recover 48 hours after stimulus (see chapter 3). The cellular content of the peritoneal cavity was investigated in *Gata6*-KO<sup>mye</sup> and WT mice during inflammation (naïve, 4 and 48 hours after stimulus) using flow cytometry. Neutrophils were quantified using their CD11b<sup>high</sup> F4/80<sup>-</sup> profile (confirmed with Ly-6G and Ly-6B expression). Mast cells were indistinguishable from eosinophils purely by their FSc/ SSc profile. However, although both of these cells were F4/80<sup>+</sup>, they could be separated by the expression of CD11b, as mast cells, unlike eosinophils, lack this surface marker (see 3.3.1). MØs were quantified by their CD11b<sup>+</sup> F4/80<sup>+</sup> phenotype after removal of neutrophils, eosinophils and mast cells; and further subdivided by their expression of Tim4. Finally, DC-like cells (a mixture of MHCII<sup>+</sup> MØs and DCs) were quantified using their MHCII<sup>+</sup> CD11c<sup>+</sup> CD226<sup>+</sup> profile (defining characteristics established by Dr. Chia-Te Liao in Prof. Phil Taylor's laboratory).

When quantified, the number of neutrophils and mast cells were not significantly different between *Gata6*-KO<sup>mye</sup> and WT mice throughout this inflammation (*figure 6.15a*). However, the number of eosinophils was significantly higher in naïve *Gata6*-KO<sup>mye</sup> than WT mice, and throughout inflammation (*figure 6.15a*). In naïve mice, this was quantified as  $252,296 \pm 107,733$  vs  $57,574 \pm 21,831$  (mean  $\pm$  SEM,  $n = 8$  per group) in *Gata6*-KO<sup>mye</sup> and WT mice respectively (a  $\approx 5$ -fold increase). The number of Tim4<sup>+</sup> MØs was significantly lower in *Gata6*-KO<sup>mye</sup> in comparison to WT mice throughout inflammation, but notably during the resolution phase (48 hours after zymosan). Where there were only  $61,485 \pm 18,960$  (mean  $\pm$  SEM,  $n = 5$ ) Tim4<sup>+</sup> MØs in *Gata6*-KO<sup>mye</sup> mice compared to  $1,308,000 \pm 171,672$  in WT mice ( $n = 11$ ) (*figure 6.15a*). The numbers of Tim4<sup>+</sup> MØs in *Gata6*-KO<sup>mye</sup> mice 48 hours after inflammation were also significantly reduced compared to naïve *Gata6*-KO<sup>mye</sup> mice, suggesting a failure to recover from inflammation. It was not possible to calculate the number of Tim4<sup>-</sup> MØs/ DCs 4 hours after inflammation, due to the complexity of flow cytometric staining and the limitations of the markers used (Tim4 staining was unaffected). However, the total number of Tim4<sup>-</sup> MØs/ DCs was calculated for naïve mice and mice 48 hours after inflammation. This revealed that *Gata6*-KO<sup>mye</sup> mice had significantly lower numbers of

total MØs/ DCs than WT mice (*figure 6.15b*) throughout inflammation. Albeit, when DC-like cells were specifically quantified, *Gata6*-KO<sup>mye</sup> mice had higher numbers than their WT counterparts throughout inflammation (*figure 6.15b*). This was pronounced in naïve animals, with *Gata6*-KO<sup>mye</sup> mice having >3 times the number of DC-like cells than WT mice (as measured by means, n= 8).

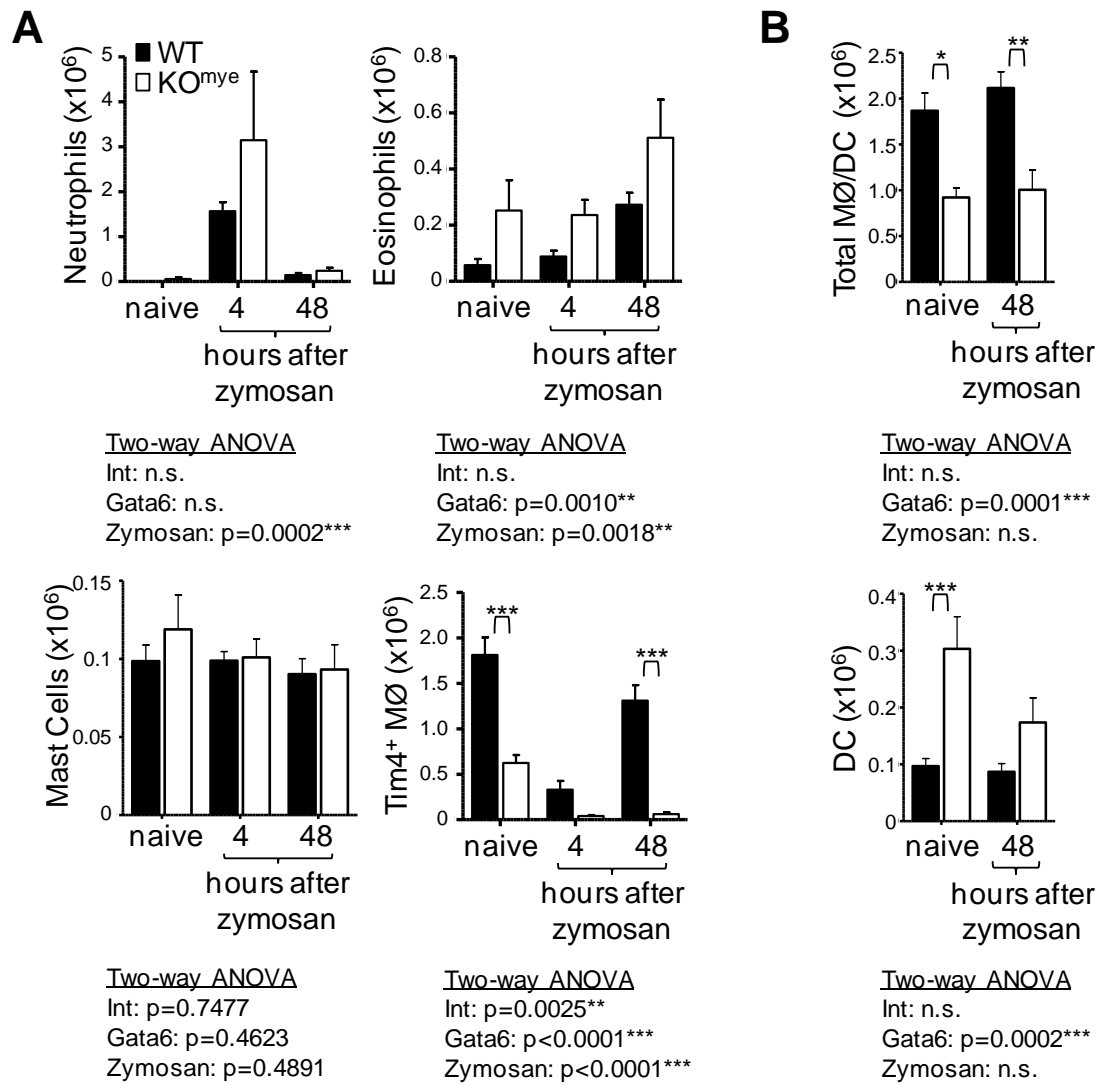


**Figure 6.15. *Gata6*-KO<sup>mye</sup> Tim4<sup>+</sup> MØs are poorly recoverable 48 hours after zymosan induced inflammation**

Graphs showing the quantification of cell types present in the peritoneal cavity of naïve mice and mice 4 and 48 hours after an intra-peritoneal injection of zymosan ( $2 \times 10^6$  particles). Data in (B) does not contain cell counts from 4 hours after inflammation due to analytical complexity. Data was analysed by two-way ANOVA (*P*-values are indicated) with Bonferroni post tests (\*,  $P \leq 0.05$ ; \*\*,  $P \leq 0.01$ ; \*\*\*,  $P \leq 0.001$ ). Int = interaction. Data shown is pooled from two independent experiments in 7-9 week old female *Gata6*-KO<sup>mye</sup> and WT mice ( $n=5-11$ /group). DCs were quantified by using a gating strategy formulated by Dr. Chia Te Liao, which is described at the end of section 6.2.7.



The low number of recoverable Tim4<sup>+</sup> MØs seen in *Gata6*-KO<sup>mye</sup> mice during inflammation was further investigated using delivery of a Cre-expressing lentivirus into *Gata6*<sup>tm2.1Sad</sup> mice (Sodhi *et al.*, 2006), as in figure 6.3. Peritonitis was initiated by 2x10<sup>6</sup> zymosan particles in mice 7 days after an *in vivo* lentiviral transduction with Cre-expressing and control viruses (tagged with trCD2). Both transduced (*Gata6*-KO) and non-transduced (WT) cells were analysed in naïve mice and mice 4 hours after zymosan. The recovery of cells transduced with Cre (*Gata6*-KO) was reduced by approximately 50 % in comparison to non-transduced cells and the transduced cells from the trCD2 control virus (figure 6.16).

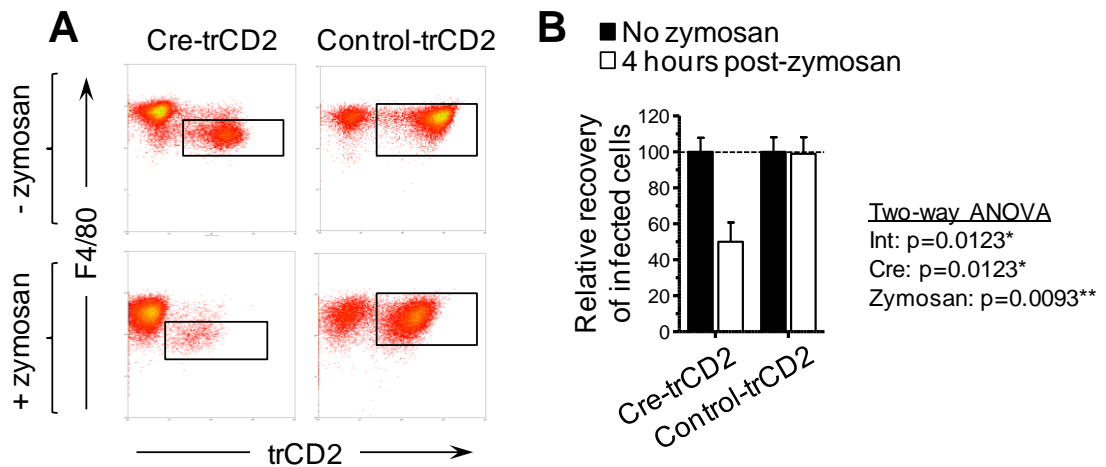


**Figure 6.16. Selective knockout of *Gata6* promotes a loss of ResMØs during inflammation**

**A)** Representative flow cytometric plots showing expression of F4/80 and trCD2 by peritoneal cells from *Gata6*<sup>tm2.1Sad/J</sup> mice, 7 days after intra-peritoneal administration of Cre-trCD2 or control trCD2 lentivirus. These mice were either injected or not ('naïve') with 2x10<sup>6</sup> zymosan particles 4 hours before experimental end-point. Data was derived from one of two independent experiments (n= 4/group). **B)** Graph depicting quantification of the relative proportion of virally infected cells in the mice challenged with zymosan; this was normalised to the proportion of infected cells in the 'naïve' mice that have not received zymosan. The data were analysed by two-way ANOVA (*P*-values are indicated). Data represents the mean ± SEM of 7-8 mixed sex mice (8-12 weeks old) per group, pooled from two independent experiments.

In WT mice, ResMØs undergo a burst in proliferation to restore the numbers lost during inflammation (chapter 3 of this thesis). The failure of Tim4<sup>+</sup> MØs to recover after inflammation in *Gata6*-KO<sup>mye</sup> mice could therefore be a consequence, at least in part, of defective proliferation. Thus markers of proliferation were investigated during the inflammatory response to 2×10<sup>6</sup> zymosan particles. WT ResMØs went through the normal proliferative burst 48 hours after zymosan (measured using SG<sub>2</sub>M, as in *figure 6.9a*), while *Gata6*-KO<sup>mye</sup> MØs maintained an unaltered low level of proliferation (*figure 6.17*). This (although higher than naïve WT mice) was only 3.20 ± 0.76 % SG<sub>2</sub>M (mean ± SEM, n= 5) in *Gata6*-KO<sup>mye</sup> mice compared to 16.20 ± 1.30 % SG<sub>2</sub>M in WT mice (n= 11). Interestingly, F4/80<sup>high</sup> cells have significantly higher levels of proliferation than F4/80<sup>low</sup> MØs within the same environment in *Gata6*-KO<sup>mye</sup> mice; as measured by SG<sub>2</sub>M, G<sub>1</sub> and *in vivo* EdU incorporation during a late stage of inflammation (*figure 6.18*).

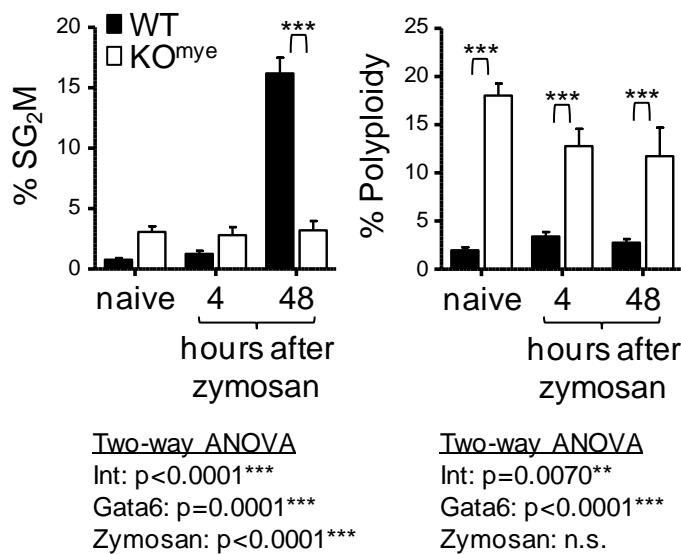


**Figure 6.17. *Gata6*-KO<sup>mye</sup> Tim4<sup>+</sup> MØs do not undergo a proliferative burst 48 hours after initiation of inflammation**

Quantification of SG<sub>2</sub>M and polyploidy in Tim4<sup>+</sup> MØs from naïve mice, and mice 4 and 48 hours after an intra-peritoneal injection of zymosan (2×10<sup>6</sup> particles) (as in *figure 6.15*). Data was analysed by two-way ANOVA (*P*-values are indicated) with Bonferroni post tests (\*\*\*, *P* ≤ 0.001). Int = interaction. Data shown is pooled from two independent experiments in 7-9 week old female *Gata6*-KO<sup>mye</sup> and WT mice (n= 5-11 per group).

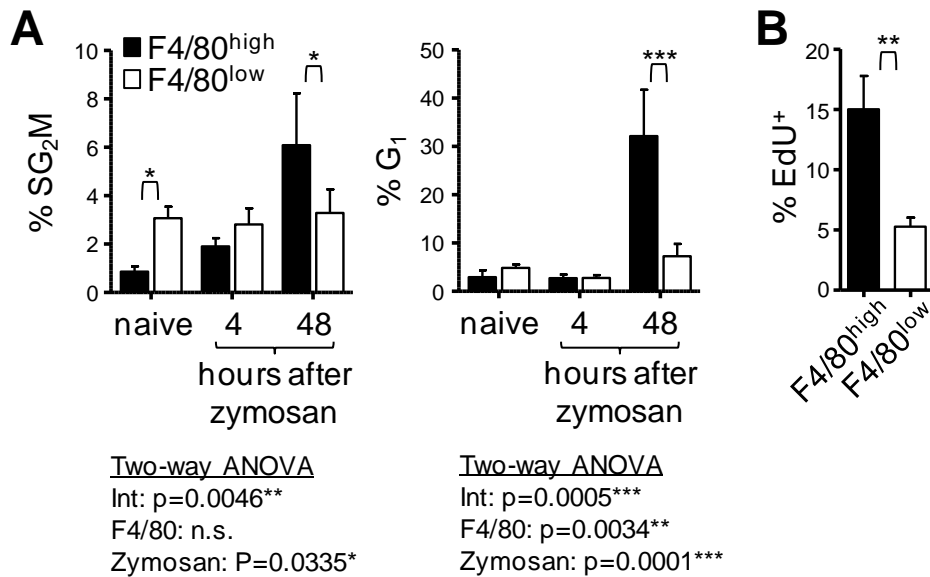


**Figure 6.18. F4/80<sup>high</sup> but not F4/80<sup>low</sup> Tim4<sup>+</sup> MØs undergo a proliferative burst 48 hours after initiation of inflammation in *Gata6*-KO<sup>mye</sup> mice**

**A)** Graphs showing differences between SG<sub>2</sub>M and G<sub>1</sub> in Tim4<sup>+</sup> F4/80<sup>low</sup> MØs and rare Tim4<sup>+</sup> F4/80<sup>high</sup> MØs within the same *Gata6*-KO<sup>mye</sup> naïve mice, and mice 4 and 48 hours after an intra-peritoneal injection of zymosan (2×10<sup>6</sup> particles) (as in *figure 6.15*). Data was analysed by two-way ANOVA (*P*-values are indicated) with Bonferroni post tests (\*, *P* ≤ 0.05;\*\*\*, *P* ≤ 0.001). Int = interaction. Data shown is pooled from two independent experiments in 7-9 week old female *Gata6*-KO<sup>mye</sup> and WT mice (n= 5-11 per group). **B)** Bar graph showing EdU incorporation by Tim4<sup>+</sup> MØs from the *Gata6*-KO<sup>mye</sup> mice 48 hours after induction of peritonitis with 2x10<sup>6</sup> zymosan particles, and 16 hours after subsequent intra-peritoneal administration of a 1mg pulse of EdU. Data represents the mean ± SEM of 8 mice pooled from 2 independent experiments and is analysed by a paired *t*-test (\*\*= *P* ≤ 0.01).

Tim4<sup>+</sup> MØs do not recover normal numbers 48 hours after zymosan (2×10<sup>6</sup> particles) in *Gata6*-KO<sup>mye</sup> mice. However, when the time course after zymosan is extended to 7 days, a higher number of Tim4<sup>+</sup> MØs can be recovered by lavage in *Gata6*-KO<sup>mye</sup> mice (*figure 6.19a*). Although this number (290,203 ± 62,332, mean ± SEM – 7 days after zymosan, n= 4) is significantly lower than that seen in WT mice (2,087,000 ± 261,873, n= 4), and lower than *Gata6*-KO<sup>mye</sup> naïve mice (440,609 ± 10,706, n= 3); it suggests that the cells have recovered slightly when compared to the 4 and 48 hours time points from the previous experiment (41,090 ± 10,581 and 61,485 ± 18,960 respectively, n= 7 and 4) (*figure 6.15*). When the proliferation was measured by SG<sub>2</sub>M,

it was found to be higher in the F4/80<sup>low</sup> Tim4<sup>+</sup> MØs of *Gata6*-KO<sup>mye</sup> mice when compared to both the F4/80<sup>high</sup> MØs of WT mice (figure 6.19b) and F4/80<sup>high</sup> ResMØs within the same *Gata6*-KO<sup>mye</sup> mouse (figure 6.19c), 7 days after zymosan. This level was also much higher than that seen in naïve *Gata6*-KO<sup>mye</sup> mice (figure 6.17) and comparable to that seen in the F4/80<sup>high</sup> MØs of *Gata6*-KO<sup>mye</sup> mice 48 hours after zymosan (figure 6.18).

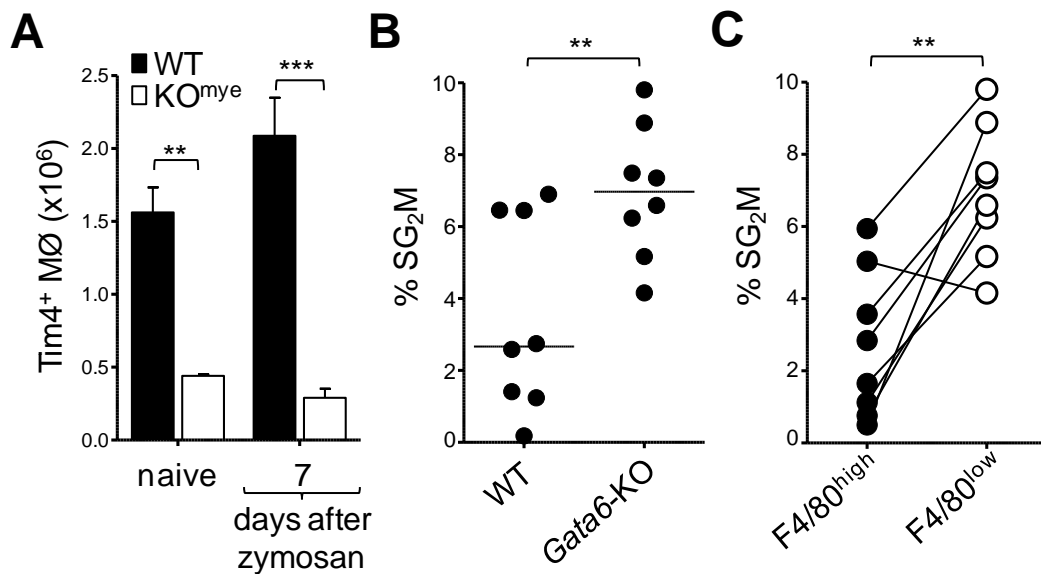


**Figure 6.19. Tim4<sup>+</sup> MØs start to recover 7 days after zymosan inflammation**

**A)** Graph depicting the number of recoverable Tim4<sup>+</sup> MØs in naïve mice and mice 7 days after intra-peritoneal administration of 2x10<sup>6</sup> particles of zymosan. Data was analysed by two-way ANOVA with Bonferroni post tests (\*\*,  $P \leq 0.01$ ;\*\*\*,  $P \leq 0.001$ ). The  $P$ -value was not significant for interaction and zymosan, but was <0.0001 for effect of *Gata6*. Data shows mean  $\pm$  SEM of one experiment with 10 week old female mice (n= 3 naïve and n= 4 for 7-day zymosan), but is representative of two independent experiments with *Gata6*-KO<sup>mye</sup> and WT mice. **B)** Graph showing the difference in SG<sub>2</sub>M in Tim4<sup>+</sup> MØs from *Gata6*-KO<sup>mye</sup> and WT mice. Data was analysed by  $t$ -test, with significance indicated (\*\*,  $P \leq 0.01$ ). The bar shows the median. **C.** Graph showing the difference in SG<sub>2</sub>M in Tim4<sup>+</sup> F4/80<sup>low</sup> MØs and rare Tim4<sup>+</sup> F4/80<sup>high</sup> MØs (linked by lines) within the same *Gata6*-KO<sup>mye</sup> mice. Data was analysed by paired  $t$ -test, with significance indicated (\*\*,  $P \leq 0.01$ ). Data shown (B-C) is a pool of two independent experiments with 10-12 week female mice. Each dot represents a single mouse.

A microarray study by Dr. Marcela Rosas identified *Map3k8* (Rosas *et al.*, 2014) as a potential regulator of the increased homeostatic proliferation seen in *Gata6*-KO<sup>mye</sup> mice, since it was significantly >2.5-fold increased in ResMØs in the absence of *Gata6*. To test the role of *Map3k8* in ResMØ proliferation, WT (FoxP3-eGFP, see chapter 5, 5.27) ResMØs were lentivirally transduced with *Map3k8*-targeting shRNA or non-silencing shRNA *in vivo*, and left for 7 days before inflammation was initiated with  $2 \times 10^6$  particles of zymosan (to trigger a proliferative response). Addition of *Map3k8*-targeting shRNA resulted in decreased proliferation compared to control, 48 hours after zymosan (measured by SG<sub>2</sub>M and Ki67<sup>high</sup> mitotic cells) (figure 6.20).

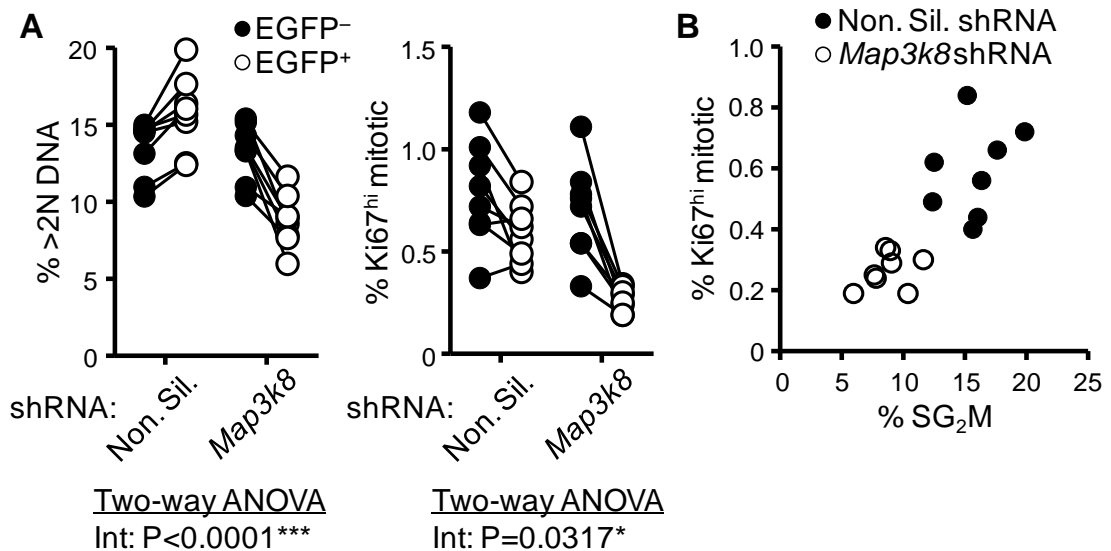


**Figure 6.20. *Map3k8* controls ResMØ proliferation**

**A)** Graphs showing the proportion of ResMØs with >2N DNA content and Ki67<sup>high</sup> expression (mitotic, see 3.23), which were transduced (eGFP<sup>+</sup>) or non-transduced (eGFP<sup>-</sup>) (linked by lines) with lentivirus, within the same FoxP3-eGFP mice. **B)** Graphical representation of the transduced (eGFP<sup>+</sup>) ResMØs in (A), showing the difference in the % SG<sub>2</sub>M vs % Ki67<sup>high</sup> (mitotic) cells between *Map3k8* and non-silencing (Non. Sil.) shRNA. Data was a pool of two independent experiments with 13-21 week old mixed sex mice 9 days after intra-peritoneal transduction with lentiviruses, and 2 days after  $2 \times 10^6$  particles of zymosan. Data was analysed by two-way ANOVA and interaction (Int) significance values are indicated.

### 6.2.8 – Myeloid Gata6 deficiency is associated with delayed clearance of neutrophils from the peritoneal cavity during inflammation

The number of neutrophils seen 4 hours after intra-peritoneal delivery of  $2 \times 10^6$  particles of zymosan is comparable between *Gata6*-KO<sup>mye</sup> and WT mice. However, this is a mild model of inflammation (see *figure 6.15*), and a higher dose of zymosan ( $2 \times 10^7$  particles) is known to exhibit less M $\phi$  dependency on the initiation of inflammation, invoking alternative mechanisms (Taylor *et al.*, 2007, McDonald *et al.*, 2012, Rosas *et al.*, 2008, Mullaly and Kubes, 2007). Zymosan peritonitis was initiated using this higher dose in *Gata6*-KO<sup>mye</sup> and WT mice, and the cellular content of the peritoneal cavity was analysed 20 and 40 hours later. This highlighted again, the lower number of Tim4<sup>+</sup> M $\phi$ , but also revealed an increased retention of neutrophils in *Gata6*-KO<sup>mye</sup> mice 40 hours after stimulus, in spite of the comparable level of neutrophil recruitment seen at 20 hours (*figure 6.21*). Interestingly, there was no significant difference in the numbers of eosinophils, but slightly higher Tim4<sup>-</sup> M $\phi$ s in *Gata6*-KO<sup>mye</sup> than WT mice.

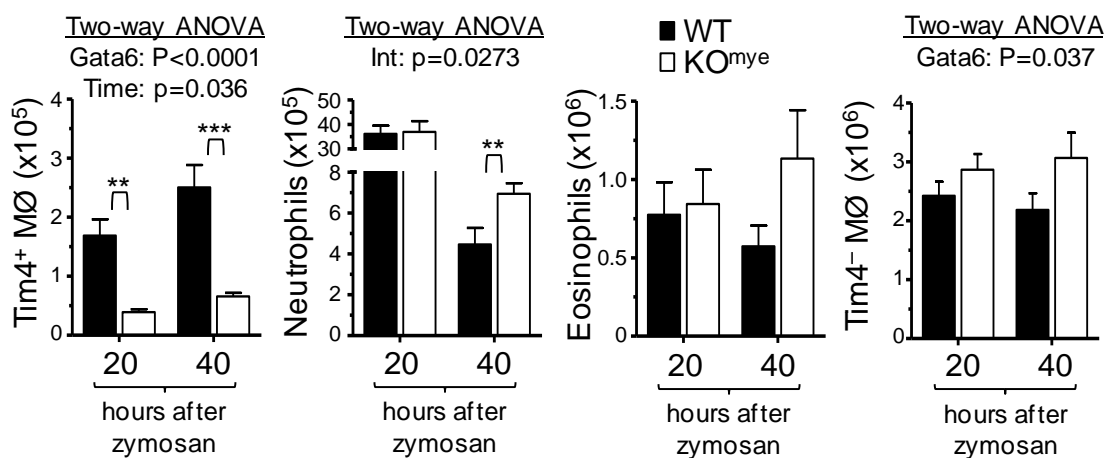


**Figure 6.21. Absence of Gata6 results in alterations in the resolution from inflammation**

Bar graphs showing the quantification of cell types 20 and 40 hours after an intra-peritoneal injection of a higher dose of zymosan ( $2 \times 10^7$  zymosan particles). Data was analysed by two-way ANOVA (significant *P*-values are indicated) with Bonferroni post tests (\*\*, *P* ≤ 0.01; \*\*\*, *P* ≤ 0.001). Data represents the mean ± SEM of individual mice pooled from 3 independent experiments (n= 11-13 per group/time).

### 6.2.9 – Enforced expression of *Gata6* in adoptively transferred BMM $\phi$ s alters their phenotype and peritoneal retention

Previous experiments in this chapter have highlighted the transcription factor *Gata6* as a controller of cell phenotype and proliferative renewal. The data from figures 6.15 and 6.16, suggest that the loss of *Gata6* can have a negative influence on the retention of ResM $\phi$ s in the peritoneal cavity. InfM $\phi$ s recruited during inflammation can last for weeks after inflammatory stimulus, but are eventually lost (Bellingan *et al.*, 1996, Bellingan *et al.*, 2002, Gautier *et al.*, 2013). Therefore, an experiment was designed in order to examine the effect of *Gata6* on cell phenotype and retention specifically in the peritoneal environment. The bone marrow is the source of InfM $\phi$ s (*figure 4.7*), so BMM $\phi$ s were chosen to represent a non-ResM $\phi$  population. Cultured BMM $\phi$ s from 129S6.CD45.1 congenic mice were transduced *in vitro* with lentiviral vectors encoding a self-cleaving *Gata6*-truncated rat CD2 (trCD2) fusion protein, or control-trCD2. An equal number of transduced cells (between 35-60 % virally infected in independent experiments) were transferred intra-peritoneally into naïve 129S6 mice (CD45.2). Peritoneal cells were harvested after three days. Approximately 10-fold more *Gata6*-transduced BMM $\phi$ s were present in the peritoneal cavity compared to control-transduced and non-transduced BMM $\phi$ s (*figure 6.22*). Due to the complexity of the experiment, only a small number of infected cells were injected (35,000-120,000). However, the raw numbers of infected cells retrieved from the peritoneal cavity for both experiments were:  $2618 \pm 146$  vs  $460 \pm 132$  (experiment 1, n=3 per group) and  $14630 \pm 3670$  vs  $539 \pm 282$  (experiment 2, n=3 per group), for *Gata6*-expressing lentivirus vs control respectively (mean  $\pm$  SEM). However this raw data does not take infection frequency into account (see *figure 6.22* for relative numbers). These *Gata6*-transduced BMM $\phi$ s also had a significantly higher level of F4/80 expression (*figure 6.12d*), approaching that of host ResM $\phi$ .

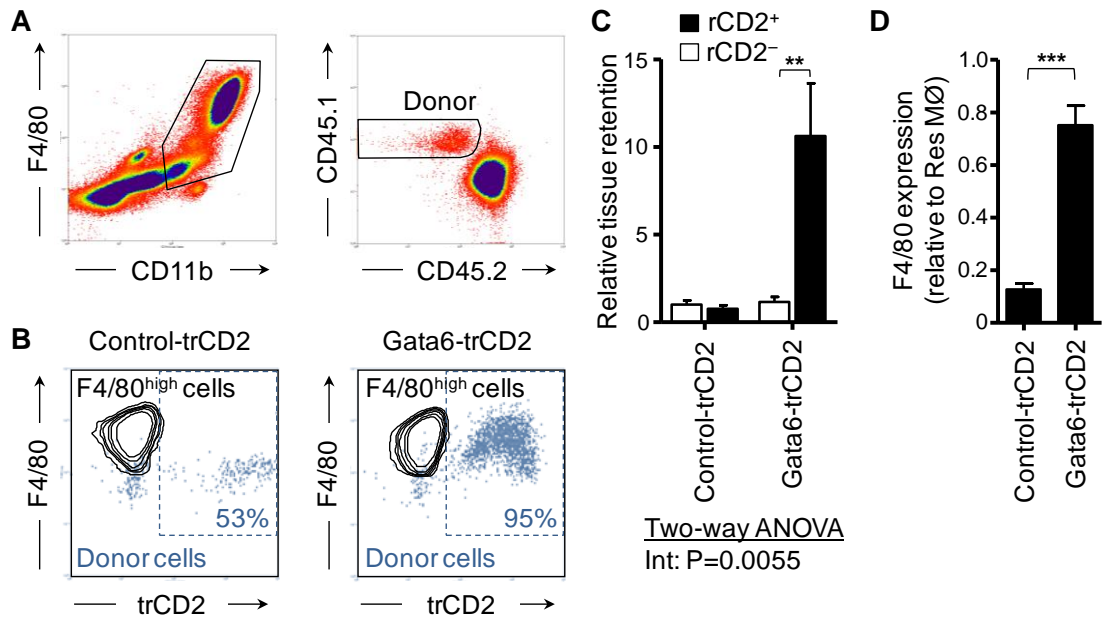


**Figure 6.22. Enforced Gata6 expression promotes retention of bone marrow-derived MØs in the peritoneum with an F4/80<sup>high</sup> phenotype**

**A)** Representative density plots showing gating of F4/80<sup>+</sup> CD11b<sup>+</sup> MØs (left panel) from the peritoneal cavity of recipient CD45.2<sup>+</sup> mice, 3 days after adoptive transfer of donor CD45.1<sup>+</sup> BMMØs; which had been previously infected *in vitro* with *Gata6*-trCD2 or trCD2 (control) lentivirus (see methods 2.6.7). Donor cells (gate in the right panel) could be separated from recipient cells by expression of the CD45.1 and CD45.2 alloantigens. **B)** Representative density plots showing the F4/80 expression of lentivirally modified donor cells (trCD2<sup>+</sup>) and their unmodified counterparts (trCD2<sup>-</sup>), when transduced with control-trCD2 (left) or *Gata6*-trCD2 (right). Overlaid contour plots show the F4/80<sup>high</sup> phenotype of the endogenous recipient ResMØs. Percentages denote the proportion of transferred cells that were transduced at the time of analysis (trCD2<sup>+</sup>). **C.** Graphical representation of the data shown in A and B. Data is expressed as ‘relative tissue retention’, where 1 denotes the mean number of non-transduced (trCD2<sup>-</sup>) cells retained in control-trCD2-transduced BMMØ receiving mice. **D.** Graph showing quantified F4/80 expression in transduced BMMØs, made relative to recipient ResMØs (=1 on the scale). Data (A-D) represents the mean ± SEM of 8-12 week old recipient CD45.2 129S6/SvEv mice pooled from two similar experiments (3 male, 3 female). Donor bone marrow was cultured from 12-16 week old sex-matched mice. Data were analyzed by Two-way ANOVA (C) (*P*-value indicated for interaction (Int)) with Bonferroni post tests, and Student’s *t*-test (D) (\*\*, *P* ≤ 0.01; \*\*\*, *P* ≤ 0.001).



## 6.3 – Discussion

The aims of this chapter were to: 1) determine whether Gata6 is selectively expressed by peritoneal and pleural ResMØs; 2) investigate the effect of Gata6 on peritoneal ResMØ proliferation and phenotype; 3) investigate the effect of Gata6 on pleural ResMØ proliferation and phenotype; and 4) determine the effect of Gata6 on the inflammatory response.

### 6.3.1 – Selective expression of Gata6 in peritoneal and pleural ResMØ

Microarray analysis of monocyte and MØ populations during peritoneal inflammation was performed by Dr. Marcela Rosas, and revealed Gata6 as a selectively expressed transcription factor in peritoneal ResMØs (general introduction, 1.3.1). Pleural ResMØs are similar to peritoneal ResMØs. Therefore quantitative PCR analysis was performed to analyse the level of Gata6 expression in these tissues. Both the ResMØs from the pleural and peritoneal cavities expressed Gata6 (*figures 6.1 and 6.12*). Though absolute quantification was not carried out, ResMØs expressed over a thousand-fold more transcript than BMMØs, and over ten times more than InfMØs from the same inflammatory environment. These InfMØs were purified alongside ResMØs using flow cytometric sorting, and the level of purity seen was 90-95 %. Therefore the higher level of Gata6 seen in InfMØs (only a tenth of the level seen in ResMØs, compared with a thousandth of the level of ResMØs, in BMMØs) is likely, at least in part, attributed to contamination by 5-10 % ResMØs.

### 6.3.2 – Phenotypic changes in ResMØ after Gata6-depletion

*In vivo* delivery of a lentivirus expressing *Gata6*-targeting shRNA molecules resulted in a significant reduction in protein expression of the canonical MØ marker F4/80 (*figure 6.2*). The decreased Gata6 expression itself was not quantified because this was a preliminary study. However, shRNA knockdown is known to not completely ablate mRNA. The shRNA sequences used in this study were obtained from Sigma Aldrich and have been previously validated to provide  $\geq 70$  % knockdown, an unofficial industry

standard. Therefore, a more efficient strategy was formulated to further investigate the effect of a total loss of Gata6.

Mice which contained a floxed *Gata6* allele (*Gata6*<sup>tm2.1Sad</sup>) were generated by Sodhi and colleagues in 2006. The addition of a Cre enzyme can be used in these mice to recombine loxP sites and excise the floxed region; therefore inactivating the gene. In *Gata6*<sup>tm2.1Sad</sup> mice, only exon 2 of *Gata6* was floxed, meaning that only exon 2 would be deleted. This resulted in a short (177 amino acid) Gata6 protein still being translated in these mice (Sodhi *et al.*, 2006). The mutant Gata6 was 268 amino acids shorter than short Gata6 isoform, and 416 amino acids shorter than long Gata6 isoform and this translates to a loss of function (Sodhi *et al.*, 2006). In this study, Gata6 was deleted in *Gata6*<sup>tm2.1Sad</sup> mice using intra-peritoneal delivery of a Cre-expressing lentivirus. This resulted in the slow formation (over time) of a new population of F4/80<sup>low</sup> ResMØs (*figure 6.3*), confirming the result seen with delivery of Gata6 targeting shRNA (*figure 6.2*). Cre delivery to WT 129S6/SvEv mice did not alter F4/80 expression in ResMØs. This shows that the reduction in F4/80 levels is accredited to Gata6 deletion and not reported Cre toxicity (Schmidt-Supprian and Rajewsky, 2007) or viral infection. The reduction of F4/80 protein levels seen in Cre transduced *Gata6*<sup>tm2.1Sad</sup> ResMØs could be rescued by co-transduction with Gata6-expressing lentiviruses (*figures 6.4*). Showing again that the reduction in F4/80 is a result of Gata6 deletion and not Cre mediated toxicity.

The results from the lentiviral experiments above (*figures 6.3-6.4*) were also investigated using a *Gata6*-KO<sup>mye</sup> mouse strain. This strain was generated using Lysozyme M (*Lyz2*) Cre 'knock-in' congenic mice (*Lyz2*<sup>Cre</sup>, B6.129P2-*Lyz2*<sup>tm1(cre)lfo</sup>) (Clausen *et al.*, 1999) crossed with conditional KO *Gata6*<sup>tm2.1Sad</sup> mice (Sodhi *et al.*, 2006), as in *figure 6.5*. These mice exhibited a gross F4/80<sup>low</sup> ResMØ phenotype in both the pleural (*figure 6.12*) and peritoneal cavities (*figure 6.6*), which was comparable to the result seen in lentiviral Cre delivery to the peritoneum of *Gata6*<sup>tm2.1Sad</sup> mice. This phenotype could be reversed toward that seen in WT mice, by using intra-peritoneal delivery of a Gata6-expressing lentivirus (*figure 6.8*). This additionally supports that this is a Gata6-mediated phenotype, not attributed to Cre toxicity (Schmidt-Supprian and Rajewsky, 2007), and that addition of the short form of Gata6 alone is sufficient for phenotype restoration.

### 6.3.3 – Identification of ‘WT’ F4/80<sup>high</sup> ResMØs in *Gata6*-KO<sup>mye</sup> mice

Interestingly, ≈5 % of the ResMØs in *Gata6*-KO<sup>mye</sup> mice were F4/80<sup>high</sup> in the peritoneal cavity, a result not seen with Cre delivery. This could be attributed to the incomplete penetrance of *Lyz2*<sup>Cre</sup> recombination, which is known to be only ≈95 % in peritoneal ResMØs (Clausen *et al.*, 1999). Therefore, the level of Gata6 expression was investigated in *Gata6*-KO<sup>mye</sup> mice using a polyclonal antibody against full length Gata6. This antibody also bound to the small 177 amino acid Gata6 after exon 2 deletion. However, significantly reduced levels of Gata6 were seen in F4/80<sup>low</sup> ResMØs compared to F4/80<sup>high</sup> ResMØs (when quantified – *figure 6.7*). Dr. Marcela Rosas has additionally shown that these F4/80<sup>high</sup> cells are phenotypically normal (confirmed by a panel of markers) and express Gata6 mRNA containing exon 2 (which Cre deletes) (Rosas *et al.*, 2014). Therefore, they can be considered effectively ‘WT’ cells, and were seen in both the peritoneal (*figure 6.6*) and pleural (*figure 6.12*) cavities of *Gata6*-KO<sup>mye</sup> mice.

### 6.3.4 – Gata6 effects cell proliferation and euploidy in a cell-intrinsic manner

Gata6 is a known regulator of cell proliferation (Beuling *et al.*, 2011) and promotes G<sub>1</sub> cell cycle arrest (Perlman *et al.*, 1998). Loss of Gata6 caused an increase in homeostatic ResMØ proliferation (*figure 6.9*). Comparison of both: F4/80<sup>high</sup> and F4/80<sup>low</sup> ResMØs in *Gata6*-KO<sup>mye</sup> mice (*figure 6.10*), and Cre transduced and non-transduced *Gata6*<sup>tm2.1Sad</sup> mice (*figure 6.11*), show that this increase in proliferation was a cell-intrinsic effect of Gata6, and not secondary to environmental alterations. Similar results were also seen in the pleural cavity (*figure 6.13*). Additionally, Gata6 has been reported to control nuclear envelope stability. In transformed cells loss of Gata6 caused an increase in polyploidy via failed cytokinesis, due to the loss of emerin in the nuclear envelope (Capo-chichi *et al.*, 2009). The loss of Gata6 in ResMØs increased the level of polyploidy, resulting in a dramatic increase in the number of multi-nuclear ResMØs in the pleural (*figure 6.14*) and peritoneal (*figure 6.9*) cavities. This was also an intrinsic effect seen with the absence of Gata6 (*figure 6.10*). However, MØs are known to fuse under certain conditions, such as that seen with IL-4 stimulation (Helming and Gordon, 2007). Therefore the increased level of polyploidy could also be explained by cell

fusion, but this was not specifically investigated, as it was considered beyond the scope of this thesis.

### **6.3.5 – Conditional myeloid knockout of Gata6 results in altered homeostatic cell numbers**

When the cellular content of the peritoneal cavity was quantified, *Gata6*-KO<sup>mye</sup> mice exhibited a much lower level of Tim4<sup>+</sup> ResMØs compared to WT mice (*figure 6.15*). This is likely to affect the tissue physiology, especially in inflammation where ResMØs are known to be important modulators (see chapter 1). This reduction could be linked to failed cytokinesis (Capo-chichi *et al.*, 2009), decreased tissue retention (mirroring an increased tissue retention of Gata6 transduced BMMØs), cell death, or a change in environmental factors, such as the availability of growth factors. However, the number of eosinophils and F4/80<sup>low</sup> MHCII<sup>high</sup> Res DCs/MØs is increased in *Gata6*-KO<sup>mye</sup> mice (*figure 6.15*). The mechanisms for this are currently being investigated by Drs. Marcela Rosas and Chia-Te Liao in Prof. Phil Taylor's laboratory, and are not included in this thesis.

### **6.3.6 – Absence of Gata6 results in a reduced ability of ResMØs to recover after inflammation by proliferation**

The response of ResMØs in the peritoneal cavity of *Gata6*-KO<sup>mye</sup> mice was investigated during acute inflammation ( $2 \times 10^6$  particles of zymosan). The number of recoverable ResMØs (by lavage) is reduced 4 hours after inflammation, but this number returns to normal levels by 48 hours in WT mice. ResMØs of *Gata6*-KO<sup>mye</sup> mice were substantially reduced 4 hours after inflammation, but did not recover greatly by 48 hours after stimulus (*figure 6.15*). However, the number of Tim4<sup>+</sup> ResMØs seen 7 days after stimulus was approaching 'normal' levels in *Gata6*-KO<sup>mye</sup> mice (*figure 6.19a*). Thus, it looked as though these cells could recover, but this interpretation is complicated by the potential for InfMØs to acquire Tim4 expression during the late resolution phase of inflammation, and hence a reduction in clarity over cell identification (see below). Consequently, this would require further experimentation using models such as bone marrow chimeras. The preferential loss of *Gata6*-KO ResMØs 4 hours after

inflammatory stimulus was confirmed as being intrinsically controlled in the absence of *Gata6*, by using Cre transduction of *Gata6*<sup>tm2.1Sad</sup> mice (*figure 6.16*). The mechanism for this preferential loss is not known, but could be attributed to an altered activation state in *Gata6*-KO<sup>mye</sup> ResMØs (currently being studied by Dr. Marcela Rosas), which could lead to altered cell adhesion and/ or cell death. The failure of ResMØs to recover 48 hours after inflammation could also, at least in part, be a result of the dysregulated proliferation seen in *Gata6*-KO<sup>mye</sup> mice. Therefore, proliferation was investigated during zymosan induced inflammation.

ResMØs undergo a burst in proliferation to recover their numbers after inflammation (Chapter 3 of this thesis). *Gata6*-KO<sup>mye</sup> peritoneal ResMØs however do not go through this key stage, and therefore cannot recover the numbers lost during inflammation (*figure 6.17*). The absence of *Gata6* is intrinsically responsible for the failure of *Gata6*-KO<sup>mye</sup> ResMØs to increase their basal proliferation rate. This was confirmed by comparing the proliferation of F4/80<sup>low</sup> and F4/80<sup>high</sup> ResMØs within the same peritoneal environment of *Gata6*-KO<sup>mye</sup> mice. F4/80<sup>high</sup> ResMØs increased their basal proliferation rate 48 hours after zymosan, whilst F4/80<sup>low</sup> ResMØs maintained their higher homeostatic level (*figure 6.18*). However, when the Tim4<sup>+</sup> F4/80<sup>low</sup> ResMØs of *Gata6*-KO<sup>mye</sup> mice were examined 7 days after zymosan, their numbers were approaching that seen in naïve *Gata6*-KO<sup>mye</sup> mice. These cells themselves exhibited increased proliferation when compared to both WT cells (*figure 6.19b*), and F4/80<sup>high</sup> ResMØs within the same peritoneal environment of *Gata6*-KO<sup>mye</sup> mice (*figure 6.19c*). This suggests that the MØs from *Gata6*-KO<sup>mye</sup> mice can increase their abnormal basal proliferation to recover from inflammation, albeit at a later stage. Although, the origins of these MØs comes into question at this late stage, as a significant proportion of these Tim4<sup>+</sup> MØs express Ly-6B; which is usually a marker for recruited MØs (Rosas *et al.*, 2010) that proliferate during inflammation (see chapter 4). So this could represent a phenotype conversion, or convergence of InfMØs toward the ResMØ phenotype as seen in complex immune scenarios (Rosas *et al.*, 2010). However, this data demonstrates that the mechanisms for MØ renewal during inflammation are distinct and markedly altered in *Gata6*-KO<sup>mye</sup> mice.

### 6.3.7 – Potential mechanism for altered ResMØ proliferation

M-CSF was found to be required for the proliferation of ResMØs during inflammation (chapter 4 of this thesis), and IL-4 is known to drive MØs beyond homeostatic levels of proliferation (Jenkins *et al.*, 2013). However, the absence of IL-4 signalling had no effect on the burst of proliferation seen in acute inflammation, and addition of M-CSF could not emulate the massive increase in proliferation (chapter 4 of this thesis). The precise mechanism for the switch to increased homeostatic proliferation in acute inflammation, and how this is dysregulated in the absence of Gata6 is not yet known, and requires further investigation. However, a single preliminary experiment revealed that M-CSF antibody blockade completely abrogated ResMØ proliferation in naïve *Gata6-KO<sup>mye</sup>* mice, mirroring the result seen in figure 4.11. Additionally, knockdown of *Map3k8* with shRNA resulted in decreased ResMØ proliferation during acute inflammation (figure 6.20). *Map3k8* or tumour progression locus 2 (*Tpl2*) is a protein kinase which promotes increased cell proliferation in a different cellular context (Patriotis *et al.*, 1993). Considering that *Gata6-KO<sup>mye</sup>* ResMØs have increased levels of *Map3k8* mRNA (Rosas *et al.*, 2014), this could, in part, explain the increased homeostatic proliferation seen in these mice. However, the mechanisms controlling ResMØ proliferation during homeostasis and inflammation are likely distinct. Consequently, the precise mechanism of *Map3k8* control of ResMØ proliferation requires further investigation.

### 6.3.8 – The absence of Gata6 is associated with alterations in inflammatory resolution

The number of neutrophils seen 4 hours after  $2 \times 10^6$  particles of zymosan is not significantly different between *Gata6-KO<sup>mye</sup>* and WT mice (figure 6.15). However, a higher dose of zymosan ( $2 \times 10^7$  particles) is known to exhibit less MØ dependency on the initiation of inflammation, by invoking alternative mechanisms (Taylor *et al.*, 2007, McDonald *et al.*, 2012, Rosas *et al.*, 2008, Mullaly and Kubes, 2007). When the higher dose of zymosan was used in *Gata6-KO<sup>mye</sup>* mice, the number of neutrophils seen was significantly higher than WT mice 40 hours after zymosan – during the resolution phase, with the same numbers being recruited at 20 hours (figure 6.21). This shows that the clearance of neutrophils from the peritoneal cavity is impaired in *Gata6-KO<sup>mye</sup>*

mice. Additionally, slightly more Tim4<sup>-</sup> MØs (InfMØ) were recruited (*figure 6.21*). These defects are associated with the MØ abnormalities and the lower number of Tim4<sup>+</sup> ResMØs seen in these mice (*figure 6.21*). A continued presence of neutrophils could be detrimental to the tissue environment and could impair wound healing (Dovi *et al.*, 2004). Therefore, normal ResMØ phenotype, which controls normal ResMØ numbers both promote the normal resolution of the inflammatory response after 2x10<sup>7</sup> particles of zymosan.

### **6.3.9 – Gata6 imparts a peritoneal-like phenotype and increases the tissue retention of BMMØs**

An experiment was formulated to determine whether Gata6 controls the retention of MØs in the peritoneal cavity. BMMØs (which are effectively deficient in Gata6 expression – *figure 6.1*) were transduced with a Gata6-expressing or control lentivirus and adoptively transferred into the peritoneal cavity of congenic mice. The expression of Gata6 on these cells increased their retention 10-fold, and gave them an F4/80<sup>high</sup> phenotype comparable to the host's ResMØs (*figure 6.22*). This suggests that Gata6 confers a peritoneal (and by analogy also pleural) specific phenotype to these cells, which increases their retention and/ or survival in the cavity. These cells had a very low level of proliferation, which was not quantifiable due to experimental constraints (a low number of cells were injected and recovered). However, the level was low enough (<0.05 % SG<sub>2</sub>M, almost non-existent) to suggest an increased proliferation was not responsible for increased cell numbers in the Gata6 transduced BMMØs.

### **6.3.10 –Microarray analysis of Gata6-deficient ResMØs**

As part of the Immunological Genome Project, Gautier and colleagues carried out a global microarray analysis on diverse ResMØ populations between tissues, which included peritoneal ResMØ, microglia and numerous DC populations. This array identified Gata6 as a peritoneal MØ specific transcription factor (Gautier *et al.*, 2012b). This array was combined with Dr. Marcela Rosas' previous array on MØs in peritoneal inflammation to formulate a gene list for peritoneal specific genes both between and within the tissue; which included Gata6 (Rosas *et al.*, 2014). Dr. Marcela Rosas carried

out an additional microarray study (validated with protein expression studies) on *Gata6*-KO<sup>mye</sup> vs WT ResMØs (Rosas *et al.*, 2014). This identified 690 genes which were regulated by >2-fold in the absence of Gata6 (294 up and 396 down). This list preferentially included genes (215 probe sets) that were considered important for the peritoneal ResMØ specific phenotype (microarray study outlined in 1.3.1). These genes include membrane proteins (e.g. CD73) and regulators of proliferation (e.g. Map3k8), which implicate Gata6 as a master controller of peritoneal ResMØ phenotype. However, pleural MØs also express Gata6 (*figure 6.12*), so this could be expanded to include other serosal ResMØ.

### 6.3.11 –Conclusion

In conclusion, the main studies in this chapter, which are in a manuscript currently in submission (Rosas *et al.*, 2014), show that: 1) Gata6 is selectively expressed by peritoneal and pleural ResMØs; 2) both peritoneal and pleural ResMØs require Gata6 for maintenance of their F4/80<sup>high</sup> phenotype 3) the absence of Gata6 causes a dysregulation of both peritoneal and pleural ResMØ proliferation and polyploidy; 4) the absence of ResMØ Gata6 is associated with delayed neutrophil clearance in inflammation; 5) Gata6 expression imparts a ResMØ-like phenotype upon BMMØs and increases their peritoneal retention and/ or survival; and 6) proliferative recovery of ResMØs during inflammation is driven in part by Map3k8. This chapter, along with Dr. Rosas' microarray studies, shows that serosal ResMØ phenotype is intrinsically linked to their ability to self renew by proliferation via the master transcription factor Gata6. The development of viable *Gata6*-deficient ResMØs in the *Gata6*-KO<sup>mye</sup> mouse provides a unique opportunity to further investigate the functional interactions between tissue-resident cells and their tissue. This will aid in the identification of novel approaches to promote tissue homeostasis, the resolution of inflammation and host defence.



## **Chapter 7 – General Discussion**

## 7.1 – MØ origins and self-renewal

### 7.1.1 – Past reflection

ResMØs were originally classified as part of the reticuloendothelial system, where the origin of new cells was considered to be local expansion in the tissue (Aschoff, 1924). At the same time, blood monocytes were identified as the source of some phagocytic cells (Sabin, 1925), however the remaining ResMØs were still considered to be tissue derived. In 1968 this changed; Ralph van Furth and Zanvil Cohn showed that major populations of MØs were derived from blood monocytes, and this concept was applied to all MØs including ResMØs (van Furth and Cohn, 1968). During later years however, this claim was disputed by a number of research groups due to evidence of proliferation (Parwaresch and Wacker, 1984, Sawyer *et al.*, 1982, Czernielewski and Demarchez, 1987), the apparent longevity of ResMØs (Melnicoff *et al.*, 1988), and the fact that MØ populations were present in the yolk sac before primitive haematopoiesis (Naito *et al.*, 1996). These studies were not conclusive enough to change the dogma of the MPS. However, the work carried out during this time supplied researchers with fundamental evidence, which slowly formed a well founded hypothesis. Unfortunately for the field, the key questions on ResMØ origins could not be answered for years to come. However, the evidence supporting the tissue origin of ResMØs gradually accumulated (Takahashi, 2000, Naito *et al.*, 1996), and in 2000 Ovchinnikov and colleagues concluded that embryonic phagocytes were of a separate lineage and this raised the possibility of their persistence into adulthood (Ovchinnikov, 2008, Lichanska and Hume, 2000). This theory was cemented with the breakthrough work on Langerhans cells and microglia, which are self-renewing populations (Merad *et al.*, 2002, Ajami *et al.*, 2007, Mildner *et al.*, 2007, Chorro *et al.*, 2009). These seminal works in themselves contradict the basic principles of the MPS, but the authors (Chorro *et al.*, 2009) suggested that this may be restricted to tissues with limited vasculature.

### 7.1.2 – Current paradigms

Langerhans cells (Chorro *et al.*, 2009) and microglia (Ajami *et al.*, 2007) self-renew by *in situ* proliferation. Supporting these pioneering studies: the origin of Langerhans cells was found to be foetal liver and yolk sac MØs (Hoeffel *et al.*, 2012), whilst microglial cells were found to derived primarily from the yolk sac (Ginhoux *et al.*, 2010). The development of both Langerhans cells and microglia are under the control of IL-34, an alternative ligand for the M-CSF receptor (Greter *et al.*, 2012, Wang *et al.*, 2012b).

The data presented within this thesis has contributed to the growing knowledge on MØ origins and renewal (Davies *et al.*, 2013b, Davies *et al.*, 2011). ResMØs from the peritoneal cavity, a vascular environment, proliferate: at low levels to maintain their numbers during homeostasis (chapter 3), at higher levels during neonatal growth, and undergo a burst in proliferation after acute inflammation to restore their depleted population (chapter 3). This was independent from the bone marrow (chapter 3 and 4), and by analogy the MPS, like that of Langerhans cells and microglia, but in a vascularised tissue. These studies (Davies *et al.*, 2011) were supported by a later publication, which confirmed the self-renewing capacity of peritoneal ResMØs (Hashimoto *et al.*, 2013). Pleural ResMØs also show a low level of homeostatic proliferation (chapter 6.2.6 and (Jenkins *et al.*, 2011)), and may share other renewal characteristics with peritoneal ResMØs.

In 2012, Yona *et al.* showed that these ResMØs were seeded into the peritoneal cavity before birth, and do not require blood monocytes for homeostatic renewal (Yona *et al.*, 2012). Additionally, Schulz *et al.* discovered that the transcription factor Myb was responsible for the development of haematopoietic stem cells; but that another population of primitive MØs that are F4/80<sup>high</sup> was Myb independent and gave rise to a number of ResMØs populations in multiple tissues (Schulz *et al.*, 2012). These articles, released at similar times, changed the field by showing that that many ResMØs have pre-natal origins and do not rely on blood monocytes for their renewal under steady state conditions (Schulz *et al.*, 2012, Yona *et al.*, 2012). A list of these self renewing populations is shown in table 7.1; figure 7.1 shows these self-renewing populations amongst other MØ populations in multiple tissues. Current paradigms state that MØs can be of 3 main origins: haematopoiesis in the adult bone marrow, or derived from the yolk sac and/ or foetal liver during development (Davies *et al.*, 2013a).

## Tissue Macrophages

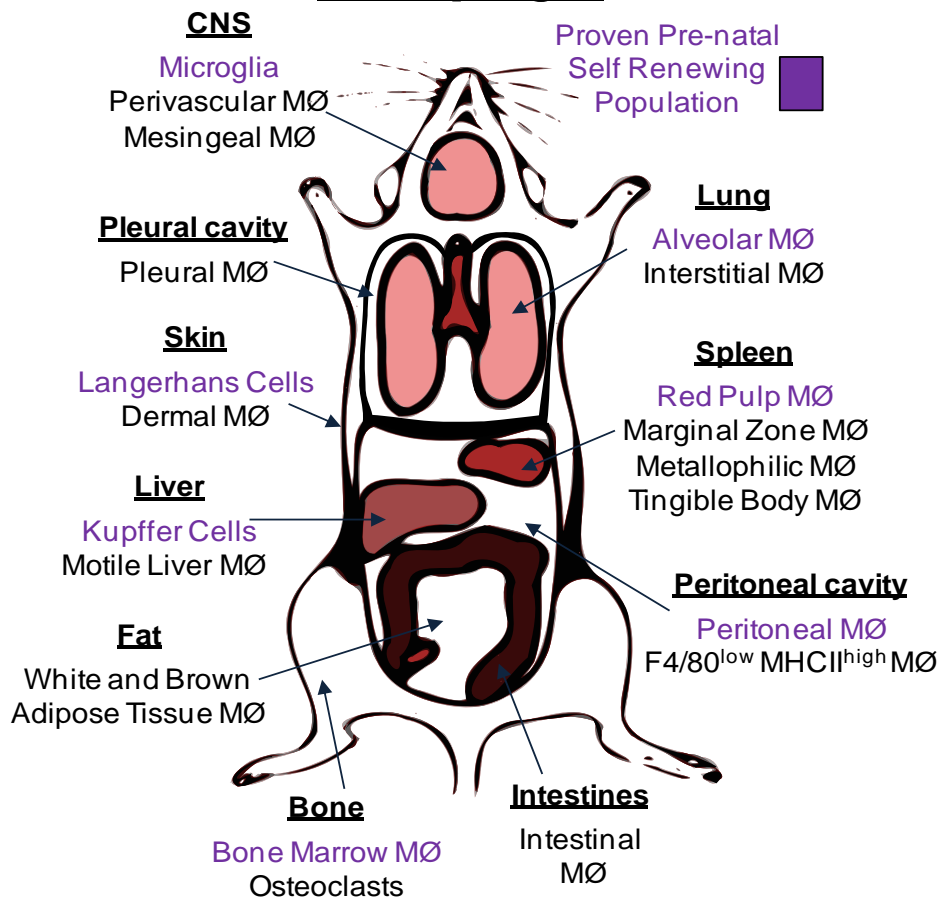


**Figure 7.1. MØ heterogeneity within different tissues**

Diagram showing the extensity of MØ heterogeneity between tissues, purple text indicates self-renewing populations. These self-renewing populations are expanded on in table 7.1.

Self renewing MØ	Notes
Bone Marrow MØ	Self renewing population (Hashimoto <i>et al.</i> , 2013).
CNS Microglia	Derived from yolk sac and maintained during inflammation independently of the bone marrow (Ajami <i>et al.</i> , 2007, Ginhoux <i>et al.</i> , 2010, Ajami <i>et al.</i> , 2011).
Liver Kupffer cells	Pre-natal origins (Yona <i>et al.</i> , 2012). Maintained in the adult independently of the bone marrow (Schulz <i>et al.</i> , 2012).
Alveolar MØ	Maintained in the adult in homeostasis and inflammation independently of the bone marrow (Murphy <i>et al.</i> , 2008, Hashimoto <i>et al.</i> , 2013, Guilliams <i>et al.</i> , 2013).
Peritoneal MØ	Pre-natal origins (Yona <i>et al.</i> , 2012). Maintained in adult in homeostasis and inflammation independently of the bone marrow (Davies <i>et al.</i> , 2011).
Pleural MØ	Maintained in adult during homeostasis and can expand during T <sub>h</sub> 2 inflammation, independently of the bone marrow (Jenkins <i>et al.</i> , 2011)
Langerhans cells	Derived from yolk sac/ foetal liver and maintained independently of the bone marrow (Chorro <i>et al.</i> , 2009, Hoeffel <i>et al.</i> , 2012).
Spleen red pulp MØ	Pre-natal origins (Yona <i>et al.</i> , 2012, Schulz <i>et al.</i> , 2012). Maintained in adult independently of the bone marrow (Hashimoto <i>et al.</i> , 2013).

**Table 7.1. Self-renewing MØ populations**

Table showing self renewing MØ populations in different tissues, some with known pre-natal origins (seeded into the tissue before birth). The locations of these populations are better represented in figure 7.1. CNS = central nervous system. This table was adapted from (Davies *et al.*, 2013b).

The proliferation of peritoneal ResMØs is dependent upon the growth factor M-CSF (chapter 4). InfMØs also require M-CSF for recruitment/ retention and/or proliferation in the peritoneal cavity (chapter 4). Both peritoneal and pleural ResMØs can also proliferate in T<sub>h</sub>2 inflammation, which is dependent on the cytokine IL-4 (Jenkins *et al.*, 2011). However, IL-4 is not required for proliferation of both ResMØs and InfMØs during acute inflammation ( $2 \times 10^6$  particles of zymosan) (chapter 4). Although, both peritoneal and pleural ResMØs can proliferate beyond homeostatic levels controlled by M-CSF, with IL-4 during T<sub>h</sub>2 inflammation (Jenkins *et al.*, 2013).

Additionally, InfMØs can also proliferate within an inflammatory lesion (chapter 4). This suggests that InfMØs can expand their numbers during inflammation, perhaps

limiting the need for additional monocyte recruitment. A reduction in monocyte recruitment has been associated with improved wound healing (Kaikita *et al.*, 2004), but this is likely more complicated as the monocyte/ MØ milieu is poorly categorised during this process (Gurtner *et al.*, 2008).

All of these studies shed new light onto the origins of MØs and opens new avenues for studies on molecular control of the specific phenotypes of resident cells. One such study by the Immunological genome project shows a broad separation of MØs and DCs, but also tissue-specific gene regulation (Gautier *et al.*, 2012b, Miller *et al.*, 2012). The significance of this study is that MØs in different tissues have distinct gene profiles.

## 7.2 – MØ tissue specific phenotype and function

### 7.2.1 – Gata6 as a transcriptional regulator of ResMØ phenotype and renewal

Chapter 6 of this thesis investigated the effects of Gata6-depletion upon peritoneal and pleural ResMØs. In summary, Gata6 is selectively expressed by peritoneal and pleural ResMØs, which require Gata6 for: 1) the maintenance of their F4/80<sup>high</sup> phenotype, 2) regulation of normal proliferation, and 3) maintenance of euploidy. Gata6 expression also imparts a ResMØ-like phenotype upon BMMØs and increases their peritoneal retention and/ or survival.

In addition to these studies, Dr. Marcela Rosas carried out a microarray analysis of *Gata6*-KO<sup>mye</sup> vs WT ResMØs (Rosas *et al.*, 2014), and combined this with her previous microarray on the ResMØ specific gene profile (mentioned in the general introduction of this thesis 1.3.1). This revealed that the majority of genes considered to be ResMØ specific were altered (the vast majority down-regulated) in the absence of Gata6. This implies that Gata6 is a master controller of the ResMØ specific phenotype.

The results from chapter 6 of this thesis, along with Dr. Rosas microarray studies, show that serosal ResMØ phenotype is intrinsically linked to their ability to self renew by proliferation via the master transcription factor Gata6. The studies on Gata6 in chapter 6 of this thesis have been incorporated into a manuscript currently in submission (Rosas *et al.*, 2014), a summary of which is depicted in figure 7.2.

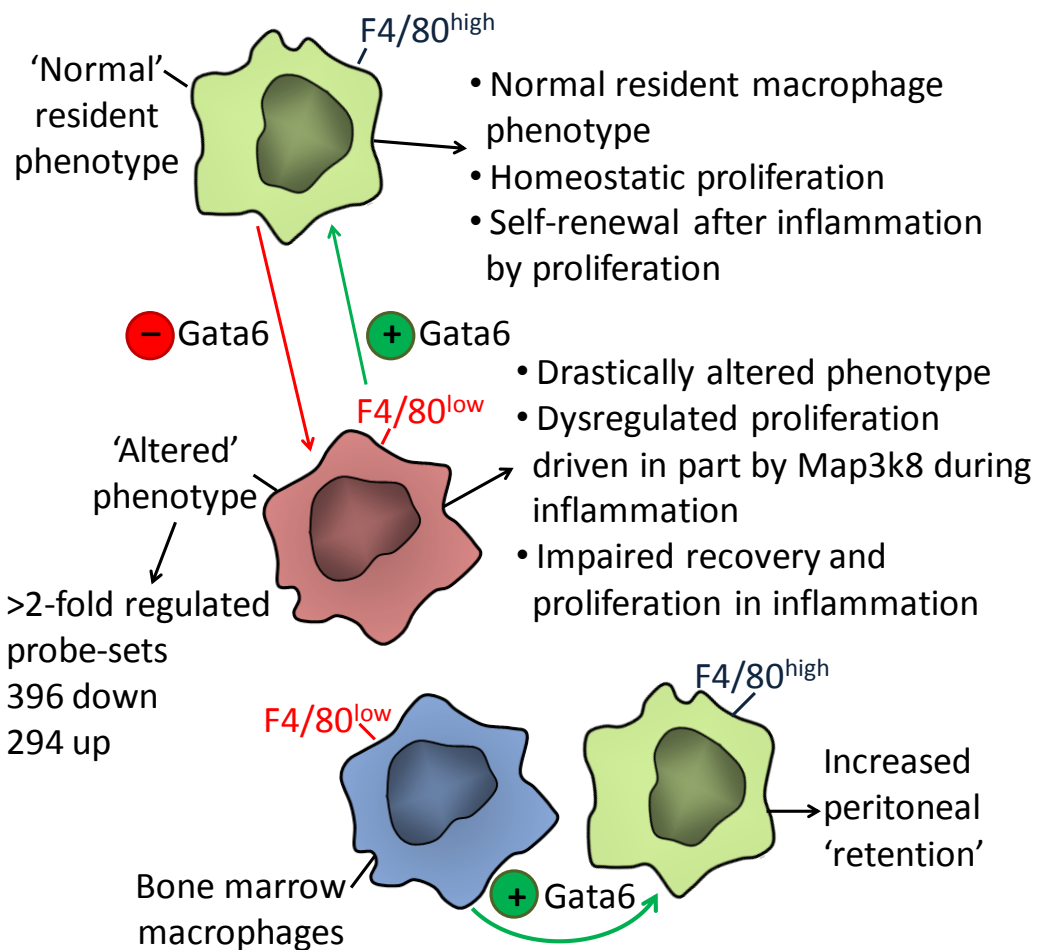


**Figure 7.2. Summary of the role of Gata6 in ResMØs**

Diagram showing the effects of Gata6 on MØs, including its removal from ResMØs and addition to BMMØs. The >2-fold regulated probe-sets in the *Gata6*-deficient ResMØs (red cell) were from a microarray study between *Gata6*-KO<sup>mye</sup> and WT ResMØs (Rosas *et al.*, 2014).

### 7.2.2 – Other examples of MØ transcriptional regulation

Generally, when discussing transcriptional control of MØ populations, the chief transcription factor considered is SFFV proviral integration oncogene (Spi) 1 (or PU.1). PU.1 deficient mice lack monocytes and MØs (including most ResMØ populations) (Scott *et al.*, 1994), but also show deficiencies in other haematopoietic cells, such as neutrophils (Anderson *et al.*, 1998). The loss of MØs in these mice could be explained by the loss of PU.1 enhanced expression of the M-CSF receptor (Zhang *et al.*, 1994). The spontaneous osteopetrotic (*op/op*) mutation has significant defects in many MØ populations, which were attributed to a point mutation in the gene for M-CSF (Yoshida



*et al.*, 1990). The defects of the *op* mouse were also evident in the mice deficient in its receptor (Dai *et al.*, 2002). These defects include increased bone mass (osteopetrosis), which is attributed to loss of osteoclasts that resorb bone, a lack of teeth, due to a failure for the tooth buds to erupt (Van Wesenbeeck *et al.*, 2002), and decreased fat storage, attributed to defects in adipose tissue MØs (Wiktor-Jedrzejczak *et al.*, 1991). Many of the defects in PU.1 deficient mice are shared in M-CSF and M-CSF receptor deficient mice. Consequently, PU.1 is important for the formation of most ResMØ populations, however it does not discriminate between cells of different origin or tissue niche. The functions of which require fine-tuning by tissue-specific transcription factors, as demonstrated by these studies of Gata6 in the peritoneal cavity.

Specific transcriptional control of the development of specific MØ populations has been identified in other tissues. Examples of which are listed below.

Langerhans cells of the epidermis are controlled by the transcriptional regulators: inhibitor of DNA binding 2 (Id2) (Hacker *et al.*, 2003) and Runt-related transcription factor 3 (Runx3) (Fainaru *et al.*, 2004). Deletion of Id2 resulted in a complete loss of Langerhans cells, but also some DC populations; whilst loss of Runx3 impaired only Langerhans cell development. In the spleen, only red pulp MØs were ablated in the absence of the transcriptional regulator Spi-C (Kohyama *et al.*, 2009); whilst metallophilic and marginal zone MØs were specifically lost in liver X receptor  $\alpha$  (LXR $\alpha$ ) deficient mice (A-Gonzalez *et al.*, 2013).

Genetic deletion of these transcriptional controllers usually results in the disappearance of a specific MØ subset, and consequently, a loss of tissue-specific function. In the Gata6-KO<sup>mye</sup> mouse however, the ResMØs are viable, albeit with an altered phenotype and function. Therefore unlike previous studies, the Gata6-KO<sup>mye</sup> mouse provides a unique opportunity to further investigate the functional interactions between ResMØs and their host tissue; which has been poorly categorised in the peritoneal cavity.

## 7.3 – Conclusion

### 7.3.1 – Conclusions

In conclusion, the studies in this thesis contribute to the field of M $\phi$  biology in several ways; the main findings are listed below, with associated manuscripts, published or in submission.

- Peritoneal cavity (a vascular tissue) ResM $\phi$ s proliferate *in situ* to maintain their population during homeostasis and neonatal growth (Davies *et al.*, 2011)
- Peritoneal ResM $\phi$ s proliferate independently of the bone marrow during inflammation, to restore their depleted population (Davies *et al.*, 2011). This is M-CSF dependent, but IL-4 is not required (Davies *et al.*, 2013b)
- A subset of bone marrow monocyte-derived M $\phi$ s can also proliferate *in situ* during inflammation (Davies *et al.*, 2013b)
- The transcription factor Gata6 has a cell-intrinsic effect on pleural and peritoneal M $\phi$  proliferation and phenotype (Rosas *et al.*, 2014)
- Proliferative recovery of ResM $\phi$ s during inflammation is driven in part by Map3k8 (Rosas *et al.*, 2014)

### 7.3.2 – Future perspectives and experimentation

This thesis, along with other work, has answered definitive questions on M $\phi$  origins, renewal and transcriptional control. The precise mechanisms for ResM $\phi$  renewal by proliferation are not fully understood. This thesis shows critical roles for the growth factor M-CSF, and the secondary regulator Map3k8. However the mechanistic fine-tuning needed for distinct M $\phi$  subsets proliferating at different times in the same environment during inflammation is not known. Additionally, the potential for phenotype conversion of monocyte-derived M $\phi$ s to ResM $\phi$ s is not clear. Understanding of these mechanisms may lead to novel paradigms in the approach to disease treatment. Especially when considering M-CSF blockade trials in diseases such as cancer, in which the milieu of M $\phi$  subsets, and their specific functions have not been categorised.

Additionally, specific to this thesis the individual mechanisms controlled by the transcription factor Gata6 need to be investigated. Such mechanistic studies are already underway in Prof. Phil Taylor's laboratory. The advantages of viable Gata6-deficient ResM $\phi$  will help drive this research, as will the method for specific lentiviral infection of ResM $\phi$ s *in vivo*. Another interesting prospect is the control of extreme M $\phi$  heterogeneity. Prof. Phil Taylor's group identified at least 16 separate populations in the F4/80<sup>high</sup> ResM $\phi$ s using only 4 markers (Tim4, SignR1, CRlg, CD73). These cell subsets probably represent the 'tip of the iceberg,' and they would be expected to be functionally distinct. Tissue niche or epigenetic phenomena are likely to play a role in this: chromatin remodelling plays a large part in M $\phi$  gene regulation (Bowdridge and Gause, 2010), however the mechanisms for this in the control of ResM $\phi$  heterogeneity and tissue specificity are not currently known.

Eventually, the tissue-specific controllers of M $\phi$  phenotype may be identified in other tissues. This could reveal novel functions of specific M $\phi$  subsets, which could pave the way for tissue-specific treatments aimed at M $\phi$ s. An example is tumour-associated M $\phi$ s, which have been poorly categorised. It is likely that the new tumour tissue contains its own ResM $\phi$  population, which may be specialised for the tumour environment. As cancer is considered by many as an inflammatory disease, the tumour environment also likely hosts monocyte-derived InfM $\phi$ s. A full categorisation of M $\phi$ s within the tumour environment and their specific functions will perhaps lead to M $\phi$ -specific therapies to improve disease outcome.

## Supplemental appendix figures

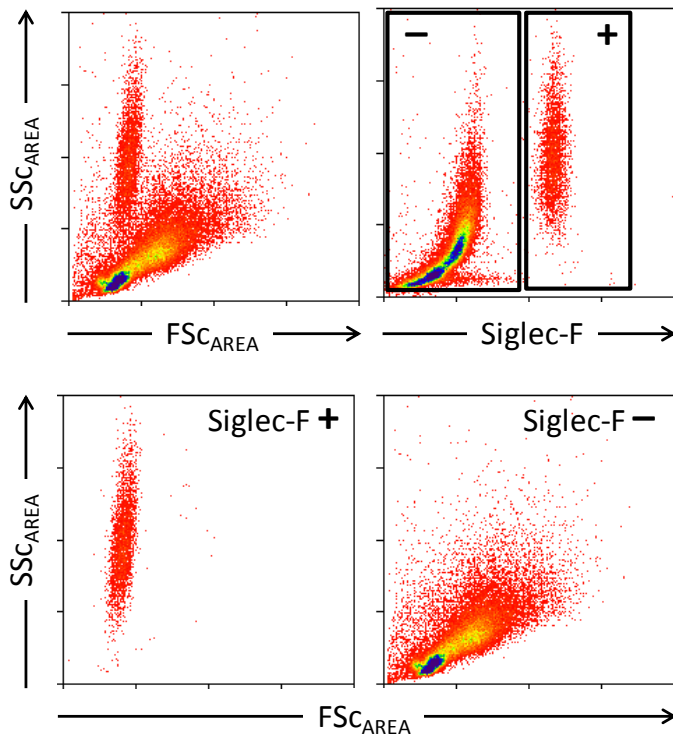


**Figure S1. Eosinophil Siglec-F expression**

Density plots showing the light scatter profile of eosinophils and non eosinophils. Expression of Siglec-F is shown on eosinophils with a high side scatter profile as described in figure 3.2a. Cells were from the pleural cavity of mice from figure 4.11. Plots were pre-gated to remove doublets as previously described (*figure 3.1*). Boxes indicate Siglec-F<sup>+</sup> and <sup>-</sup> populations and are used to gate the density plots in the lower two panels.

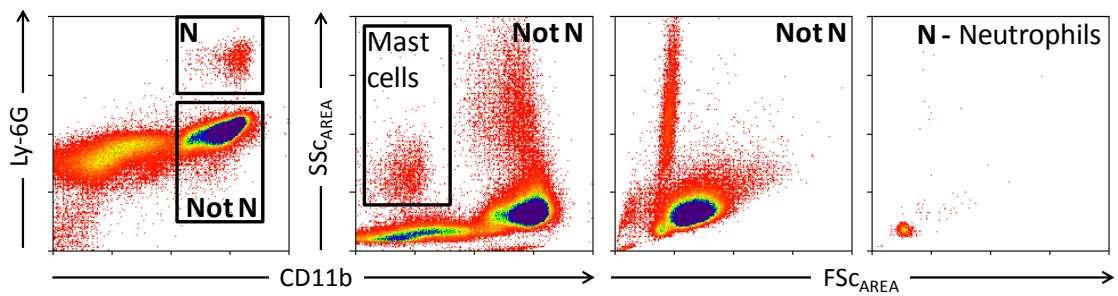


**Figure S2. Description of mast cells and neutrophils in flow cytometry**

Representative density plots showing the small light scatter profile of CD11b<sup>+</sup> Ly-6G<sup>+</sup> fixed/ permeabilized neutrophils, and the CD11b<sup>low/-</sup> profile of mast cells, 2 days after intra-peritoneal injection of  $2 \times 10^6$  zymosan particles. Plots were pre-gated to remove doublets as previously described (*figure 3.1*), the three right panels are gated as shown in the far left panel. N = neutrophils, Not N = not neutrophils. Cells shown were from mice in *figure 3.9*.

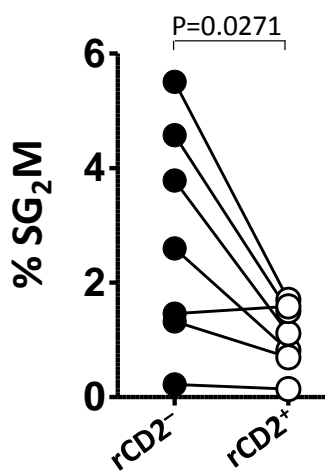


**Figure S3. Decrease in proliferation upon viral infection**

Scatter plot showing a decrease in proliferation in ResM $\phi$ s, 7 days after intra-peritoneal injection of a trCD2-expressing non-silencing lentivirus (measured by SG2M as shown in *figure 4.2*). Data shown compares transduced and non-transduced cells from mice used in *figure 6.2*. Data was analysed by paired Student's *t*-test, and the *P*-value is indicated.

## Bibliography

- A-GONZALEZ, N., GUILLEN, J. A., GALLARDO, G., DIAZ, M., DE LA ROSA, J. V., HERNANDEZ, I. H., CASANOVA-ACEBES, M., LOPEZ, F., TABRAUE, C., BECEIRO, S., HONG, C., LARA, P. C., ANDUJAR, M., ARAI, S., MIYAZAKI, T., LI, S., CORBI, A. L., TONTONOZ, P., HIDALGO, A. & CASTRILLO, A. (2013) The nuclear receptor LXRalpha controls the functional specialization of splenic macrophages. *Nat Immunol*, 14, 831-9.
- ABBAS-TERKI, T., BLANCO-BOSE, W., DEGLON, N., PRALONG, W. & AEBISCHER, P. (2002) Lentiviral-mediated RNA interference. *Hum Gene Ther*, 13, 2197-201.
- AJAMI, B., BENNETT, J. L., KRIEGER, C., MCNAGNY, K. M. & ROSSI, F. M. (2011) Infiltrating monocytes trigger EAE progression, but do not contribute to the resident microglia pool. *Nat Neurosci*, 14, 1142-9.
- AJAMI, B., BENNETT, J. L., KRIEGER, C., TETZLAFF, W. & ROSSI, F. M. (2007) Local self-renewal can sustain CNS microglia maintenance and function throughout adult life. *Nat Neurosci*, 10, 1538-43.
- ANDERSON, K. L., SMITH, K. A., PIO, F., TORBETT, B. E. & MAKI, R. A. (1998) Neutrophils deficient in PU.1 do not terminally differentiate or become functionally competent. *Blood*, 92, 1576-85.
- ASCHOFF, L. (1924) Das reticuloendotheliale System. *Erg. Inn. Med. Kinderheilk*, 26.
- AUSTYN, J. M. & GORDON, S. (1981) F4/80, a monoclonal antibody directed specifically against the mouse macrophage. *Eur J Immunol*, 11, 805-15.
- BARTH, M. W., HENDRZAK, J. A., MELNICOFF, M. J. & MORAHAN, P. S. (1995) Review of the macrophage disappearance reaction. *J Leukoc Biol*, 57, 361-7.
- BEANES, S. R., DANG, C., SOO, C. & TING, K. (2003) Skin repair and scar formation: the central role of TGF-beta. *Expert Rev Mol Med*, 5, 1-22.
- BELLINGAN, G. J., CALDWELL, H., HOWIE, S. E., DRANSFIELD, I. & HASLETT, C. (1996) In vivo fate of the inflammatory macrophage during the resolution of inflammation: inflammatory macrophages do not die locally, but emigrate to the draining lymph nodes. *J Immunol*, 157, 2577-85.
- BELLINGAN, G. J., XU, P., COOKSLEY, H., CAULDWELL, H., SHOCK, A., BOTTOMS, S., HASLETT, C., MUTSAERS, S. E. & LAURENT, G. J. (2002) Adhesion molecule-dependent mechanisms regulate the rate of macrophage clearance during the resolution of peritoneal inflammation. *J Exp Med*, 196, 1515-21.
- BERNSTEIN, E., CAUDY, A. A., HAMMOND, S. M. & HANNON, G. J. (2001) Role for a bidentate ribonuclease in the initiation step of RNA interference. *Nature*, 409, 363-6.
- BEULING, E., BAFFOUR-AWUAH, N. Y., STAPLETON, K. A., ARONSON, B. E., NOAH, T. K., SHROYER, N. F., DUNCAN, S. A., FLEET, J. C. & KRASINSKI, S. D. (2011) GATA factors regulate proliferation, differentiation, and gene expression in small intestine of mature mice. *Gastroenterology*, 140, 1219-1229 e1-2.
- BOBADILLA, S., SUNSERI, N. & LANDAU, N. R. (2012) Efficient transduction of myeloid cells by an HIV-1-derived lentiviral vector that packages the Vpx accessory protein. *Gene Ther*, 20, 514-20.
- BORREGAARD, N., SORENSEN, O. E. & THEILGAARD-MONCH, K. (2007) Neutrophil granules: a library of innate immunity proteins. *Trends Immunol*, 28, 340-5.
- BOS, N. A., KIMURA, H., MEEUWSEN, C. G., DE VISSER, H., HAZENBERG, M. P., WOSTMANN, B. S., PLEASANTS, J. R., BENNER, R. & MARCUS, D. M. (1989) Serum immunoglobulin levels and naturally occurring antibodies against carbohydrate antigens in germ-free BALB/c mice fed chemically defined ultrafiltered diet. *Eur J Immunol*, 19, 2335-9.
- BOWDRIDGE, S. & GAUSE, W. C. (2010) Regulation of alternative macrophage activation by chromatin remodeling. *Nat Immunol*, 11, 879-81.
- BRANCATO, S. K. & ALBINA, J. E. (2011) Wound macrophages as key regulators of repair: origin, phenotype, and function. *Am J Pathol*, 178, 19-25.

- BRINKMANN, V., REICHARD, U., GOOSMANN, C., FAULER, B., UHLEMANN, Y., WEISS, D. S., WEINRAUCH, Y. & ZYCHLINSKY, A. (2004) Neutrophil extracellular traps kill bacteria. *Science*, 303, 1532-5.
- BROWN, G. D. & GORDON, S. (2001) Immune recognition. A new receptor for beta-glucans. *Nature*, 413, 36-7.
- BROWN, M. R., SUMMERS, H. D., REES, P., SMITH, P. J., CHAPPELL, S. C. & ERRINGTON, R. J. (2010) Flow-based cytometric analysis of cell cycle via simulated cell populations. *PLoS Comput Biol*, 6, e1000741.
- BUCK, S. B., BRADFORD, J., GEE, K. R., AGNEW, B. J., CLARKE, S. T. & SALIC, A. (2008) Detection of S-phase cell cycle progression using 5-ethynyl-2'-deoxyuridine incorporation with click chemistry, an alternative to using 5-bromo-2'-deoxyuridine antibodies. *Biotechniques*, 44, 927-9.
- BURNS, J. C., FRIEDMANN, T., DRIEVER, W., BURRASCANO, M. & YEE, J. K. (1993) Vesicular stomatitis virus G glycoprotein pseudotyped retroviral vectors: concentration to very high titer and efficient gene transfer into mammalian and nonmammalian cells. *Proc Natl Acad Sci U S A*, 90, 8033-7.
- CAILHIER, J. F., PARTOLINA, M., VUTHOORI, S., WU, S., KO, K., WATSON, S., SAVILL, J., HUGHES, J. & LANG, R. A. (2005) Conditional macrophage ablation demonstrates that resident macrophages initiate acute peritoneal inflammation. *J Immunol*, 174, 2336-42.
- CAPO-CHICHI, C. D., CAI, K. Q., TESTA, J. R., GODWIN, A. K. & XU, X. X. (2009) Loss of GATA6 leads to nuclear deformation and aneuploidy in ovarian cancer. *Mol Cell Biol*, 29, 4766-77.
- CARLOW, D. A., GOLD, M. R. & ZILTENER, H. J. (2009) Lymphocytes in the peritoneum home to the omentum and are activated by resident dendritic cells. *J Immunol*, 183, 1155-65.
- CHENG, S. S., LUKACS, N. W. & KUNKEL, S. L. (2002) Eotaxin/CCL11 is a negative regulator of neutrophil recruitment in a murine model of endotoxemia. *Exp Mol Pathol*, 73, 1-8.
- CHORRO, L. & GEISSMANN, F. (2010) Development and homeostasis of 'resident' myeloid cells: the case of the Langerhans cell. *Trends Immunol*, 31, 438-45.
- CHORRO, L., SARDE, A., LI, M., WOOLLARD, K. J., CHAMBON, P., MALISSEN, B., KISSENPFFENNIG, A., BARBAROUX, J. B., GROVES, R. & GEISSMANN, F. (2009) Langerhans cell (LC) proliferation mediates neonatal development, homeostasis, and inflammation-associated expansion of the epidermal LC network. *J Exp Med*, 206, 3089-100.
- CLAUSEN, B. E., BURKHARDT, C., REITH, W., RENKAWITZ, R. & FORSTER, I. (1999) Conditional gene targeting in macrophages and granulocytes using LysMcre mice. *Transgenic Res*, 8, 265-77.
- COHEN, H. B., BRIGGS, K. T., MARINO, J. P., RAVID, K., ROBSON, S. C. & MOSSER, D. M. (2013) TLR stimulation initiates a CD39-based autoregulatory mechanism that limits macrophage inflammatory responses. *Blood*, 122, 1935-45.
- CORMACK, B. P., VALDIVIA, R. H. & FALKOW, S. (1996) FACS-optimized mutants of the green fluorescent protein (GFP). *Gene*, 173, 33-8.
- CRANE, R., GADEA, B., LITTLEPAGE, L., WU, H. & RUDERMAN, J. V. (2004) Aurora A, meiosis and mitosis. *Biol Cell*, 96, 215-29.
- CZERNIELEWSKI, J. M. & DEMARCHEZ, M. (1987) Further evidence for the self-reproducing capacity of Langerhans cells in human skin. *J Invest Dermatol*, 88, 17-20.
- DAEMS, W. T., BREDEROO, P. (1971) The Fine Structure and Peroxidase Activity of Resident and Exudate Peritoneal Macrophages in the Guinea Pig. *The Reticuloendothelial System and Immune Phenomena: Advances in Experimental Medicine and Biology* 15, 19-31.
- DAI, X. M., RYAN, G. R., HAPPEL, A. J., DOMINGUEZ, M. G., RUSSELL, R. G., KAPP, S., SYLVESTRE, V. & STANLEY, E. R. (2002) Targeted disruption of the mouse colony-stimulating factor 1 receptor gene results in osteopetrosis, mononuclear phagocyte deficiency, increased primitive progenitor cell frequencies, and reproductive defects. *Blood*, 99, 111-20.

- DAS, A. M., FLOWER, R. J. & PERRETTI, M. (1998) Resident mast cells are important for eotaxin-induced eosinophil accumulation in vivo. *J Leukoc Biol*, 64, 156-62.
- DAVIES, J. Q. & GORDON, S. (2005) Isolation and culture of murine macrophages. *Methods Mol Biol*, 290, 91-103.
- DAVIES, L. C., JENKINS, S. J., ALLEN, J. E. & TAYLOR, P. R. (2013a) Tissue Resident Macrophages. *Nature Immunology*, 14, 986 - 995.
- DAVIES, L. C., ROSAS, M., JENKINS, S. J., LIAO, C. T., SCURR, M. J., BROMBACHER, F., FRASER, D. J., ALLEN, J. E., JONES, S. A. & TAYLOR, P. R. (2013b) Distinct bone marrow-derived and tissue-resident macrophage lineages proliferate at key stages during inflammation. *Nat Commun*, 4, 1886.
- DAVIES, L. C., ROSAS, M., SMITH, P. J., FRASER, D. J., JONES, S. A. & TAYLOR, P. R. (2011) A quantifiable proliferative burst of tissue macrophages restores homeostatic macrophage populations after acute inflammation. *Eur J Immunol*, 41, 2155-2164.
- DAVIS, A. E., 3RD, CAI, S. & LIU, D. (2004) The biological role of the C1 inhibitor in regulation of vascular permeability and modulation of inflammation. *Adv Immunol*, 82, 331-63.
- DE LA HARPE, J. & NATHAN, C. F. (1989) Adenosine regulates the respiratory burst of cytokine-triggered human neutrophils adherent to biologic surfaces. *J Immunol*, 143, 596-602.
- DEMAISON, C., PARSLEY, K., BROUNS, G., SCHERR, M., BATTMER, K., KINNON, C., GREZ, M. & THRASHER, A. J. (2002) High-level transduction and gene expression in hematopoietic repopulating cells using a human immunodeficiency [correction of immunodeficiency] virus type 1-based lentiviral vector containing an internal spleen focus forming virus promoter. *Hum Gene Ther*, 13, 803-13.
- DENNIS, G., JR., SHERMAN, B. T., HOSACK, D. A., YANG, J., GAO, W., LANE, H. C. & LEMPICKI, R. A. (2003) DAVID: Database for Annotation, Visualization, and Integrated Discovery. *Genome Biol*, 4, P3.
- DI CARLO, F. J. & FIORE, J. V. (1958) On the composition of zymosan. *Science*, 127, 756-7.
- DIOSZEGHY, V., ROSAS, M., MASKREY, B. H., COLMONT, C., TOPLEY, N., CHAITIDIS, P., KUHN, H., JONES, S. A., TAYLOR, P. R. & O'DONNELL, V. B. (2008) 12/15-Lipoxygenase regulates the inflammatory response to bacterial products in vivo. *J Immunol*, 181, 6514-24.
- DOVI, J. V., SZPADERSKA, A. M. & DIPIETRO, L. A. (2004) Neutrophil function in the healing wound: adding insult to injury? *Thromb Haemost*, 92, 275-80.
- DUNN, D. L., BARKE, R. A., KNIGHT, N. B., HUMPHREY, E. W. & SIMMONS, R. L. (1985) Role of resident macrophages, peripheral neutrophils, and translymphatic absorption in bacterial clearance from the peritoneal cavity. *Infect Immun*, 49, 257-64.
- FAINARU, O., WOOLF, E., LOTEM, J., YARMUS, M., BRENNER, O., GOLDENBERG, D., NEGREANU, V., BERNSTEIN, Y., LEVANON, D., JUNG, S. & GRONER, Y. (2004) Runx3 regulates mouse TGF-beta-mediated dendritic cell function and its absence results in airway inflammation. *EMBO J*, 23, 969-79.
- FEHSE, B., KUSTIKOVA, O. S., BUBENHEIM, M. & BAUM, C. (2004) Poisson--it's a question of dose. *Gene Ther*, 11, 879-81.
- FIELDING, C. A., JONES, G. W., MCLOUGHLIN, R. M., MCLEOD, L., HAMMOND, V. J., UCEDA, J., WILLIAMS, A. S., LAMBIE, M., FOSTER, T. L., LIAO, C. T., RICE, C. M., GREENHILL, C. J., COLMONT, C. S., HAMS, E., COLES, B., KIFT-MORGAN, A., NEWTON, Z., CRAIG, K. J., WILLIAMS, J. D., WILLIAMS, G. T., DAVIES, S. J., HUMPHREYS, I. R., O'DONNELL, V. B., TAYLOR, P. R., JENKINS, B. J., TOPLEY, N. & JONES, S. A. (2014) Interleukin-6 signaling drives fibrosis in unresolved inflammation. *Immunity*, 40, 40-50.
- FOGG, D. K., SIBON, C., MILED, C., JUNG, S., AUCOUTURIER, P., LITTMAN, D. R., CUMANO, A. & GEISSMANN, F. (2006) A clonogenic bone marrow progenitor specific for macrophages and dendritic cells. *Science*, 311, 83-7.
- GANZALO, J. A., JIA, G. Q., AGUIRRE, V., FRIEND, D., COYLE, A. J., JENKINS, N. A., LIN, G. S., KATZ, H., LICHTMAN, A., COPELAND, N., KOPF, M. & GUTIERREZ-RAMOS, J. C. (1996)



- Mouse Eotaxin expression parallels eosinophil accumulation during lung allergic inflammation but it is not restricted to a Th2-type response. *Immunity*, 4, 1-14.
- GAUTIER, E. L., CHOW, A., SPANBROEK, R., MARCELIN, G., GRETER, M., JAKUBZICK, C., BOGUNOVIC, M., LEBOEUF, M., VAN ROOIJEN, N., HABENICHT, A. J., MERAD, M. & RANDOLPH, G. J. (2012a) Systemic analysis of PPAR $\gamma$  in mouse macrophage populations reveals marked diversity in expression with critical roles in resolution of inflammation and airway immunity. *J Immunol*, 189, 2614-24.
- GAUTIER, E. L., IVANOV, S., LESNIK, P. & RANDOLPH, G. J. (2013) Local apoptosis mediates clearance of macrophages from resolving inflammation in mice. *Blood*, 122, 2714-22.
- GAUTIER, E. L., SHAY, T., MILLER, J., GRETER, M., JAKUBZICK, C., IVANOV, S., HELFT, J., CHOW, A., ELPEK, K. G., GORDONOV, S., MAZLOOM, A. R., MA'AYAN, A., CHUA, W. J., HANSEN, T. H., TURLEY, S. J., MERAD, M., RANDOLPH, G. J., BEST, A. J., KNELL, J., GOLDRATH, A., BROWN, B., JOJIC, V., KOLLER, D., COHEN, N., BRENNAN, P., BRENNER, M., REGEV, A., FLETCHER, A., ELPEK, K., BELLEMARE-PELLETIER, A., MALHOTRA, D., TURLEY, S., JIANU, R., LAIDLAW, D., COLLINS, J., NARAYAN, K., SYLVIA, K., KANG, J., GAZIT, R., GARRISON, B. S., ROSSI, D. J., KIM, F., RAO, T. N., WAGERS, A., SHINTON, S. A., HARDY, R. R., MONACH, P., BEZMAN, N. A., SUN, J. C., KIM, C. C., LANIER, L. L., HENG, T., KRESLAVSKY, T., PAINTER, M., ERICSON, J., DAVIS, S., MATHIS, D. & BENOIST, C. (2012b) Gene-expression profiles and transcriptional regulatory pathways that underlie the identity and diversity of mouse tissue macrophages. *Nat Immunol*.
- GEISSMANN, F., JUNG, S. & LITTMAN, D. R. (2003) Blood monocytes consist of two principal subsets with distinct migratory properties. *Immunity*, 19, 71-82.
- GEISSMANN, F., MANZ, M. G., JUNG, S., SIEWEKE, M. H., MERAD, M. & LEY, K. (2010) Development of monocytes, macrophages, and dendritic cells. *Science*, 327, 656-61.
- GINHOUX, F., GRETER, M., LEBOEUF, M., NANDI, S., SEE, P., GOKHAN, S., MEHLER, M. F., CONWAY, S. J., NG, L. G., STANLEY, E. R., SAMOKHVALOV, I. M. & MERAD, M. (2010) Fate mapping analysis reveals that adult microglia derive from primitive macrophages. *Science*, 330, 841-5.
- GORDON, S. (2003) Alternative activation of macrophages. *Nat Rev Immunol*, 3, 23-35.
- GORDON, S. (2007) The macrophage: past, present and future. *Eur J Immunol*, 37 Suppl 1, S9-17.
- GORDON, S. (2008) Elie Metchnikoff: father of natural immunity. *Eur J Immunol*, 38, 3257-64.
- GORDON, S. & TAYLOR, P. R. (2005) Monocyte and macrophage heterogeneity. *Nat Rev Immunol*, 5, 953-964.
- GORGANI, N. N., HE, J. Q., KATSCHKE, K. J., JR., HELMY, K. Y., XI, H., STEFFEK, M., HASS, P. E. & VAN LOOKEREN CAMPAGNE, M. (2008) Complement receptor of the Ig superfamily enhances complement-mediated phagocytosis in a subpopulation of tissue resident macrophages. *J Immunol*, 181, 7902-8.
- GRATZNER, H. G., LEIF, R. C., INGRAM, D. J. & CASTRO, A. (1975) The use of antibody specific for bromodeoxyuridine for the immunofluorescent determination of DNA replication in single cells and chromosomes. *Exp Cell Res*, 95, 88-94.
- GRETER, M., LELIOS, I., PELCZAR, P., HOEFFEL, G., PRICE, J., LEBOEUF, M., KUNDIG, T. M., FREI, K., GINHOUX, F., MERAD, M. & BECHER, B. (2012) Stroma-derived interleukin-34 controls the development and maintenance of langerhans cells and the maintenance of microglia. *Immunity*, 37, 1050-60.
- GUILLIAMS, M., DE KLEER, I., HENRI, S., POST, S., VANHOUTTE, L., DE PRIJCK, S., DESWARTE, K., MALISSEN, B., HAMMAD, H. & LAMBRECHT, B. N. (2013) Alveolar macrophages develop from fetal monocytes that differentiate into long-lived cells in the first week of life via GM-CSF. *J Exp Med*.
- GURTNER, G. C., WERNER, S., BARRANDON, Y. & LONGAKER, M. T. (2008) Wound repair and regeneration. *Nature*, 453, 314-21.

- HACKER, C., KIRSCH, R. D., JU, X. S., HIERONYMUS, T., GUST, T. C., KUHL, C., JORGAS, T., KURZ, S. M., ROSE-JOHN, S., YOKOTA, Y. & ZENKE, M. (2003) Transcriptional profiling identifies Id2 function in dendritic cell development. *Nat Immunol*, 4, 380-6.
- HAMMOND, S. M., BERNSTEIN, E., BEACH, D. & HANNON, G. J. (2000) An RNA-directed nuclease mediates post-transcriptional gene silencing in *Drosophila* cells. *Nature*, 404, 293-6.
- HANS, F. & DIMITROV, S. (2001) Histone H3 phosphorylation and cell division. *Oncogene*, 20, 3021-7.
- HARVEY, B. P., QUAN, T. E., RUDENGA, B. J., ROMAN, R. M., CRAFT, J. & MAMULA, M. J. (2008) Editing antigen presentation: antigen transfer between human B lymphocytes and macrophages mediated by class A scavenger receptors. *J Immunol*, 181, 4043-51.
- HASHIMOTO, D., CHOW, A., NOIZAT, C., TEO, P., BEASLEY, MARYÂ B., LEBOEUF, M., BECKER, CHRISTIANÂ D., SEE, P., PRICE, J., LUCAS, D., GRETER, M., MORTHA, A., BOYER, SCOTTÂ W., FORSBERG, E. Â C., TANAKA, M., VANÂ ROOIJEN, N., GARCÃA-SASTRE, A., STANLEY, E. Â R., GINHOUX, F., FRENETTE, PAULÂ S. & MERAD, M. (2013) Tissue-Resident Macrophages Self-Maintain Locally throughout Adult Life with Minimal Contribution from Circulating Monocytes. *Immunity*, 38, 792-804.
- HATTERSLEY, G., OWENS, J., FLANAGAN, A. M. & CHAMBERS, T. J. (1991) Macrophage colony stimulating factor (M-CSF) is essential for osteoclast formation in vitro. *Biochem Biophys Res Commun*, 177, 526-31.
- HE, J., YANG, Q. & CHANG, L. J. (2005) Dynamic DNA methylation and histone modifications contribute to lentiviral transgene silencing in murine embryonic carcinoma cells. *J Virol*, 79, 13497-508.
- HE, J. Q., WIESMANN, C. & VAN LOOKEREN CAMPAGNE, M. (2008) A role of macrophage complement receptor CR1g in immune clearance and inflammation. *Mol Immunol*, 45, 4041-7.
- HEIM, R., CUBITT, A. B. & TSIEN, R. Y. (1995) Improved green fluorescence. *Nature*, 373, 663-4.
- HELMING, L. & GORDON, S. (2007) Macrophage fusion induced by IL-4 alternative activation is a multistage process involving multiple target molecules. *Eur J Immunol*, 37, 33-42.
- HENDERSON, R. B., HOBBS, J. A., MATHIES, M. & HOGG, N. (2003) Rapid recruitment of inflammatory monocytes is independent of neutrophil migration. *Blood*, 102, 328-35.
- HENDZEL, M. J., WEI, Y., MANCINI, M. A., VAN HOOSER, A., RANALLI, T., BRINKLEY, B. R., BAZETT-JONES, D. P. & ALLIS, C. D. (1997) Mitosis-specific phosphorylation of histone H3 initiates primarily within pericentromeric heterochromatin during G2 and spreads in an ordered fashion coincident with mitotic chromosome condensation. *Chromosoma*, 106, 348-60.
- HICKSTEIN, D. D., OZOLS, J., WILLIAMS, S. A., BAENZIGER, J. U., LOCKSLEY, R. M. & ROTH, G. J. (1987) Isolation and characterization of the receptor on human neutrophils that mediates cellular adherence. *J Biol Chem*, 262, 5576-80.
- HIRSCH, S. & GORDON, S. (1983) Polymorphic expression of a neutrophil differentiation antigen revealed by monoclonal antibody 7/4. *Immunogenetics*, 18, 229-39.
- HOEFFEL, G., WANG, Y., GRETER, M., SEE, P., TEO, P., MALLERET, B., LEBOEUF, M., LOW, D., OLLER, G., ALMEIDA, F., CHOY, S. H., GRISOTTO, M., RENIA, L., CONWAY, S. J., STANLEY, E. R., CHAN, J. K., NG, L. G., SAMOKHVALOV, I. M., MERAD, M. & GINHOUX, F. (2012) Adult Langerhans cells derive predominantly from embryonic fetal liver monocytes with a minor contribution of yolk sac-derived macrophages. *J Exp Med*, 209, 1167-81.
- HOPPER, K. E. (1986) Kinetics of macrophage recruitment and turnover in peritoneal inflammatory exudates induced by *Salmonella* or thioglycollate broth. *J LeukOc Biol*, 39, 435-46.
- HRECKA, K., HAO, C., GIERSZEWSKA, M., SWANSON, S. K., KESIK-BRODACKA, M., SRIVASTAVA, S., FLORENS, L., WASHBURN, M. P. & SKOWRONSKI, J. (2011) Vpx relieves inhibition of HIV-1 infection of macrophages mediated by the SAMHD1 protein. *Nature*, 474, 658-61.

- HSU, C. L., NEILSEN, C. V. & BRYCE, P. J. (2010) IL-33 is produced by mast cells and regulates IgE-dependent inflammation. *PLoS One*, 5, e11944.
- HUBBARD, A. K. & GIARDINA, C. (2000) Regulation of ICAM-1 expression in mouse macrophages. *Inflammation*, 24, 115-25.
- HUME, D. A. & GORDON, S. (1983) Optimal conditions for proliferation of bone marrow-derived mouse macrophages in culture: the roles of CSF-1, serum, Ca<sup>2+</sup>, and adherence. *J Cell Physiol*, 117, 189-94.
- HUME, D. A. & MACDONALD, K. P. (2012) Therapeutic applications of macrophage colony-stimulating factor-1 (CSF-1) and antagonists of CSF-1 receptor (CSF-1R) signaling. *Blood*, 119, 1810-20.
- HUME, D. A., PAVLI, P., DONAHUE, R. E. & FIDLER, I. J. (1988) The effect of human recombinant macrophage colony-stimulating factor (CSF-1) on the murine mononuclear phagocyte system in vivo. *J Immunol*, 141, 3405-9.
- HURST, S. M., WILKINSON, T. S., MCLOUGHLIN, R. M., JONES, S., HORIUCHI, S., YAMAMOTO, N., ROSE-JOHN, S., FULLER, G. M., TOPLEY, N. & JONES, S. A. (2001) Il-6 and its soluble receptor orchestrate a temporal switch in the pattern of leukocyte recruitment seen during acute inflammation. *Immunity*, 14, 705-14.
- IP, W. K. & LAU, Y. L. (2004) Role of mannose-binding lectin in the innate defense against *Candida albicans*: enhancement of complement activation, but lack of opsonic function, in phagocytosis by human dendritic cells. *J Infect Dis*, 190, 632-40.
- IWASAKI, A. & MEDZHITOV, R. (2004) Toll-like receptor control of the adaptive immune responses. *Nat Immunol*, 5, 987-95.
- JANSSEN, W. J., BARTHEL, L., MULDROW, A., OBERLEY-DEEGAN, R. E., KEARNS, M. T., JAKUBZICK, C. & HENSON, P. M. (2011) Fas determines differential fates of resident and recruited macrophages during resolution of acute lung injury. *Am J Respir Crit Care Med*, 184, 547-60.
- JENKINS, S. J., RUCKERL, D., COOK, P. C., JONES, L. H., FINKELMAN, F. D., VAN ROOIJEN, N., MACDONALD, A. S. & ALLEN, J. E. (2011) Local Macrophage Proliferation, Rather than Recruitment from the Blood, Is a Signature of TH2 Inflammation. *Science*.
- JENKINS, S. J., RUCKERL, D., THOMAS, G. D., HEWITSON, J. P., DUNCAN, S., BROMBACHER, F., MAIZELS, R. M., HUME, D. A. & ALLEN, J. E. (2013) IL-4 directly signals tissue-resident macrophages to proliferate beyond homeostatic levels controlled by CSF-1. *J Exp Med*.
- KAIKITA, K., HAYASAKI, T., OKUMA, T., KUZIEL, W. A., OGAWA, H. & TAKEYA, M. (2004) Targeted deletion of CC chemokine receptor 2 attenuates left ventricular remodeling after experimental myocardial infarction. *Am J Pathol*, 165, 439-47.
- KANITAKIS, J., PETRUZZO, P. & DUBERNARD, J. M. (2004) Turnover of epidermal Langerhans' cells. *N Engl J Med*, 351, 2661-2.
- KAPLAN, M. H., SCHINDLER, U., SMILEY, S. T. & GRUSBY, M. J. (1996) Stat6 is required for mediating responses to IL-4 and for development of Th2 cells. *Immunity*, 4, 313-9.
- KATO, S., YUZAWA, Y., TSUBOI, N., MARUYAMA, S., MORITA, Y., MATSUGUCHI, T. & MATSUO, S. (2004) Endotoxin-induced chemokine expression in murine peritoneal mesothelial cells: the role of toll-like receptor 4. *J Am Soc Nephrol*, 15, 1289-99.
- KIM, D. D., MIWA, T., KIMURA, Y., SCHWENDENER, R. A., VAN LOOKEREN CAMPAGNE, M. & SONG, W. C. (2008) Deficiency of decay-accelerating factor and complement receptor 1-related gene/protein  $\gamma$  on murine platelets leads to complement-dependent clearance by the macrophage phagocytic receptor CR1g. *Blood*, 112, 1109-19.
- KIM, J. M., RASMUSSEN, J. P. & RUDENSKY, A. Y. (2007) Regulatory T cells prevent catastrophic autoimmunity throughout the lifespan of mice. *Nat Immunol*, 8, 191-7.
- KING, P. D., SADRA, A., TENG, J. M., BELL, G. M. & DUPONT, B. (1998) CD2-mediated activation of the Tec-family tyrosine kinase ITK is controlled by proline-rich stretch-4 of the CD2 cytoplasmic tail. *Int Immunol*, 10, 1009-16.

- KOHYAMA, M., ISE, W., EDELSON, B. T., WILKER, P. R., HILDNER, K., MEJIA, C., FRAZIER, W. A., MURPHY, T. L. & MURPHY, K. M. (2009) Role for Spi-C in the development of red pulp macrophages and splenic iron homeostasis. *Nature*, 457, 318-21.
- KOMURO, K., ITAKURA, K., BOYSE, E. A. & JOHN, M. (1975) Ly-5: A new T-lymphocyte antigen system. *Immunogenetics*, 1, 452-456.
- KORESSAAR, T. & REMM, M. (2007) Enhancements and modifications of primer design programme Primer3. *Bioinformatics*, 23, 1289-91.
- KORKOSZ, M., BUKOWSKA-STRAKOVA, K., SADIS, S., GRODZICKI, T. & SIEDLAR, M. (2012) Monoclonal antibodies against macrophage colony-stimulating factor diminish the number of circulating intermediate and nonclassical (CD14(++)CD16(+)/CD14(+)CD16(++)) monocytes in rheumatoid arthritis patient. *Blood*, 119, 5329-30.
- KOZEL, T. R. (1996) Activation of the complement system by pathogenic fungi. *Clin Microbiol Rev*, 9, 34-46.
- KUBBUTAT, M. H., KEY, G., DUCHROW, M., SCHLUTER, C., FLAD, H. D. & GERDES, J. (1994) Epitope analysis of antibodies recognising the cell proliferation associated nuclear antigen previously defined by the antibody Ki-67 (Ki-67 protein). *J Clin Pathol*, 47, 524-8.
- KUNKEL, G. R., MASER, R. L., CALVET, J. P. & PEDERSON, T. (1986) U6 small nuclear RNA is transcribed by RNA polymerase III. *Proc Natl Acad Sci U S A*, 83, 8575-9.
- LAGUETTE, N., SOBHIAN, B., CASARTELLI, N., RINGEARD, M., CHABLE-BESSIA, C., SEGERAL, E., YATIM, A., EMILIANI, S., SCHWARTZ, O. & BENKIRANE, M. (2011) SAMHD1 is the dendritic- and myeloid-cell-specific HIV-1 restriction factor counteracted by Vpx. *Nature*, 474, 654-7.
- LANGERHANS, P. (1868) Über die Nerven der menschlichen Haut. *Virchows Archiv*, 44, 325-337.
- LATINI, S. & PEDATA, F. (2001) Adenosine in the central nervous system: release mechanisms and extracellular concentrations. *J Neurochem*, 79, 463-84.
- LAWSON, L. J., PERRY, V. H. & GORDON, S. (1992) Turnover of resident microglia in the normal adult mouse brain. *Neuroscience*, 48, 405-15.
- LEASK, A. & ABRAHAM, D. J. (2004) TGF-beta signaling and the fibrotic response. *FASEB J*, 18, 816-27.
- LEE, P. Y., WANG, J. X., PARISINI, E., DASCHER, C. C. & NIGROVIC, P. A. (2013) Ly6 family proteins in neutrophil biology. *J LeukOc Biol*.
- LEE, Y., AHN, C., HAN, J., CHOI, H., KIM, J., YIM, J., LEE, J., PROVOST, P., RADMARK, O., KIM, S. & KIM, V. N. (2003) The nuclear RNase III Drosha initiates microRNA processing. *Nature*, 425, 415-9.
- LEWIS, W. H. (1931) Pinocytosis. *Bull Johns Hopkins Hosp*, 29, 17-26.
- LICHANSKA, A. M. & HUME, D. A. (2000) Origins and functions of phagocytes in the embryo. *Exp Hematol*, 28, 601-11.
- LIVAK, K. J. & SCHMITTGEN, T. D. (2001) Analysis of relative gene expression data using real-time quantitative PCR and the 2(-Delta Delta C(T)) Method. *Methods*, 25, 402-8.
- LOKESHWAR, B. L. & LIN, H. S. (1988) Development and characterization of monoclonal antibodies to murine macrophage colony-stimulating factor. *J Immunol*, 141, 483-8.
- LONDON, A., COHEN, M. & SCHWARTZ, M. (2013) Microglia and monocyte-derived macrophages: functionally distinct populations that act in concert in CNS plasticity and repair. *Front Cell Neurosci*, 7, 34.
- LUCAS, T., WAISMAN, A., RANJAN, R., ROES, J., KRIEG, T., MULLER, W., ROERS, A. & EMING, S. A. (2010) Differential roles of macrophages in diverse phases of skin repair. *J Immunol*, 184, 3964-77.
- MACDONALD, K. P., PALMER, J. S., CRONAU, S., SEPPANEN, E., OLVER, S., RAFFELT, N. C., KUNS, R., PETTIT, A. R., CLOUSTON, A., WAINWRIGHT, B., BRANSTETTER, D., SMITH, J., PAXTON, R. J., CERRETTI, D. P., BONHAM, L., HILL, G. R. & HUME, D. A. (2010) An

- antibody against the colony-stimulating factor 1 receptor depletes the resident subset of monocytes and tissue- and tumor-associated macrophages but does not inhibit inflammation. *Blood*, 116, 3955-63.
- MAEDA, M., KUBO, K., NISHI, T. & FUTAI, M. (1996) Roles of gastric GATA DNA-binding proteins. *J Exp Biol*, 199, 513-20.
- MAEDA, M., OHASHI, K. & OHASHI-KOBAYASHI, A. (2005) Further extension of mammalian GATA-6. *Development, Growth and Differentiation*, 47, 591-600.
- MANTOVANI, A., SICA, A. & LOCATI, M. (2005) Macrophage polarization comes of age. *Immunity*, 23, 344-6.
- MANTOVANI, A., SICA, A., SOZZANI, S., ALLAVENA, P., VECCHI, A. & LOCATI, M. (2004) The chemokine system in diverse forms of macrophage activation and polarization. *Trends Immunol*, 25, 677-86.
- MATSUSHITA, M. (1996) The lectin pathway of the complement system. *Microbiol Immunol*, 40, 887-93.
- MCDONALD, J. U., ROSAS, M., BROWN, G. D., JONES, S. A. & TAYLOR, P. R. (2012) Differential dependencies of monocytes and neutrophils on dectin-1, dectin-2 and complement for the recognition of fungal particles in inflammation. *PLoS One*, 7, e45781.
- MCKNIGHT, A. J., MACFARLANE, A. J., DRI, P., TURLEY, L., WILLIS, A. C. & GORDON, S. (1996) Molecular cloning of F4/80, a murine macrophage-restricted cell surface glycoprotein with homology to the G-protein-linked transmembrane 7 hormone receptor family. *J Biol Chem*, 271, 486-9.
- MEISTER, G. & TUSCHL, T. (2004) Mechanisms of gene silencing by double-stranded RNA. *Nature*, 431, 343-9.
- MELNICOFF, M. J., HORAN, P. K., BRESLIN, E. W. & MORAHAN, P. S. (1988) Maintenance of peritoneal macrophages in the steady state. *J LeuKoc Biol*, 44, 367-75.
- MELNICOFF, M. J., HORAN, P. K. & MORAHAN, P. S. (1989) Kinetics of changes in peritoneal cell populations following acute inflammation. *Cell Immunol*, 118, 178-91.
- MERAD, M., GINHOUX, F. & COLLIN, M. (2008) Origin, homeostasis and function of Langerhans cells and other langerin-expressing dendritic cells. *Nat Rev Immunol*, 8, 935-47.
- MERAD, M., MANZ, M. G., KARSUNKY, H., WAGERS, A., PETERS, W., CHARO, I., WEISSMAN, I. L., CYSTER, J. G. & ENGLEMAN, E. G. (2002) Langerhans cells renew in the skin throughout life under steady-state conditions. *Nat Immunol*, 3, 1135-41.
- METCHNIKOFF, E. (1880) Über die intracelluläre Verdauung bei Coelenteraten. *Zoologischer Anzeiger*, 3, 261-263.
- METCHNIKOFF, E. (1883) Untersuchung über die mesodermalen Phagocyten einiger Wirbeltiere. *Biological Centralblatt*, 18, 560.
- METCHNIKOFF, E. (1892) Leçons sur la pathologie comparée de l'inflammation. *Paris, Masson*.
- MIETTINEN, M. & LASOTA, J. (2005) KIT (CD117): a review on expression in normal and neoplastic tissues, and mutations and their clinicopathologic correlation. *Appl Immunohistochem Mol Morphol*, 13, 205-20.
- MILDNER, A., SCHMIDT, H., NITSCHKE, M., MERKLER, D., HANISCH, U. K., MACK, M., HEIKENWALDER, M., BRUCK, W., PRILLER, J. & PRINZ, M. (2007) Microglia in the adult brain arise from Ly-6ChiCCR2+ monocytes only under defined host conditions. *Nat Neurosci*, 10, 1544-53.
- MILLER, J. C., BROWN, B. D., SHAY, T., GAUTIER, E. L., JOJIC, V., COHAIN, A., PANDEY, G., LEBOEUF, M., ELPEK, K. G., HELFT, J., HASHIMOTO, D., CHOW, A., PRICE, J., GRETER, M., BOGUNOVIC, M., BELLEMARE-PELLETIER, A., FRENETTE, P. S., RANDOLPH, G. J., TURLEY, S. J. & MERAD, M. (2012) Deciphering the transcriptional network of the dendritic cell lineage. *Nat Immunol*, 13, 888-99.
- MIYANISHI, M., TADA, K., KOIKE, M., UCHIYAMA, Y., KITAMURA, T. & NAGATA, S. (2007) Identification of Tim4 as a phosphatidylserine receptor. *Nature*, 450, 435-9.
- MOHRS, M., LEDERMANN, B., KOHLER, G., DORFMULLER, A., GESSNER, A. & BROMBACHER, F. (1999) Differences between IL-4- and IL-4 receptor alpha-deficient mice in chronic

- leishmaniasis reveal a protective role for IL-13 receptor signaling. *J Immunol*, 162, 7302-8.
- MOLKENTIN, J. D. (2000) The zinc finger-containing transcription factors GATA-4, -5, and -6. Ubiquitously expressed regulators of tissue-specific gene expression. *J Biol Chem*, 275, 38949-52.
- MORABITO, F., PRASTHOFER, E. F., DUNLAP, N. E., GROSSI, C. E. & TILDEN, A. B. (1987) Expression of myelomonocytic antigens on chronic lymphocytic leukemia B cells correlates with their ability to produce interleukin 1. *Blood*, 70, 1750-7.
- MORISE, H., SHIMOMURA, O., JOHNSON, F. H. & WINANT, J. (1974) Intermolecular energy transfer in the bioluminescent system of *Aequorea*. *Biochemistry*, 13, 2656-62.
- MORRISEY, E. E., IP, H. S., LU, M. M. & PARMACEK, M. S. (1996) GATA-6: A Zinc Finger Transcription Factor That Is Expressed in Multiple Cell Lineages Derived from Lateral Mesoderm. *Developmental Biology*, 177, 309-322.
- MULLALY, S. C. & KUBES, P. (2007) Mast cell-expressed complement receptor, not TLR2, is the main detector of zymosan in peritonitis. *Eur J Immunol*, 37, 224-34.
- MULLER-EBERHARD, H. J. (1988) Molecular organization and function of the complement system. *Annu Rev Biochem*, 57, 321-47.
- MUNRO, S. & PELHAM, H. R. (1986) An Hsp70-like protein in the ER: identity with the 78 kd glucose-regulated protein and immunoglobulin heavy chain binding protein. *Cell*, 46, 291-300.
- MURPHY, J., SUMMER, R., WILSON, A. A., KOTTON, D. N. & FINE, A. (2008) The prolonged life-span of alveolar macrophages. *Am J Respir Cell Mol Biol*, 38, 380-5.
- NAHRENDORF, M., SWIRSKI, F. K., AIKAWA, E., STANGENBERG, L., WURDINGER, T., FIGUEIREDO, J. L., LIBBY, P., WEISSELEDER, R. & PITTET, M. J. (2007) The healing myocardium sequentially mobilizes two monocyte subsets with divergent and complementary functions. *J Exp Med*, 204, 3037-47.
- NAITO, M., UMEDA, S., YAMAMOTO, T., MORIYAMA, H., UMEZU, H., HASEGAWA, G., USUDA, H., SHULTZ, L. D. & TAKAHASHI, K. (1996) Development, differentiation, and phenotypic heterogeneity of murine tissue macrophages. *J Leukoc Biol*, 59, 133-8.
- NALDINI, L. (1998) Lentiviruses as gene transfer agents for delivery to non-dividing cells. *Curr Opin Biotechnol*, 9, 457-63.
- NATHAN, C. (2006) Neutrophils and immunity: challenges and opportunities. *Nat Rev Immunol*, 6, 173-82.
- NATHAN, C. F., MURRAY, H. W., WIEBE, M. E. & RUBIN, B. Y. (1983) Identification of interferon-gamma as the lymphokine that activates human macrophage oxidative metabolism and antimicrobial activity. *J Exp Med*, 158, 670-89.
- NEGRINI, D., DEL FABBRO, M. & VENTUROLI, D. (1993) Fluid exchanges across the parietal peritoneal and pleural mesothelia. *J Appl Physiol* (1985), 74, 1779-84.
- NOBEN-TRAUTH, N., SHULTZ, L. D., BROMBACHER, F., URBAN, J. F., JR., GU, H. & PAUL, W. E. (1997) An interleukin 4 (IL-4)-independent pathway for CD4+ T cell IL-4 production is revealed in IL-4 receptor-deficient mice. *Proc Natl Acad Sci U S A*, 94, 10838-43.
- OBAYASHI, K., TAKADA, K., OHASHI, K., KOBAYASHI-OHASHI, A. & MAEDA, M. (2012) Role of the PEST sequence in the long-type GATA-6 DNA-binding protein expressed in human cancer cell lines. *Advances in Bioscience and Biotechnology*, 3, 314-320.
- OHARA, J. & PAUL, W. E. (1985) Production of a monoclonal antibody to and molecular characterization of B-cell stimulatory factor-1. *Nature*, 315, 333-6.
- OHNMACHT, C., PULLNER, A., VAN ROOIJEN, N. & VOEHRINGER, D. (2007) Analysis of eosinophil turnover in vivo reveals their active recruitment to and prolonged survival in the peritoneal cavity. *J Immunol*, 179, 4766-74.
- OVCHINNIKOV, D. A. (2008) Macrophages in the embryo and beyond: much more than just giant phagocytes. *Genesis*, 46, 447-62.
- PAOLICELLI, R. C., BOLASCO, G., PAGANI, F., MAGGI, L., SCIANNI, M., PANZANELLI, P., GIUSTETTO, M., FERREIRA, T. A., GUIDUCCI, E., DUMAS, L., RAGOZZINO, D. & GROSS, C.

- T. (2011) Synaptic pruning by microglia is necessary for normal brain development. *Science*, 333, 1456-8.
- PARWARESCH, M. R. & WACKER, H. H. (1984) Origin and kinetics of resident tissue macrophages. Parabiosis studies with radiolabelled leucocytes. *Cell Tissue Kinet*, 17, 25-39.
- PATRIOTIS, C., MAKRIS, A., BEAR, S. E. & TSICHLIS, P. N. (1993) Tumor progression locus 2 (Tpl-2) encodes a protein kinase involved in the progression of rodent T-cell lymphomas and in T-cell activation. *Proc Natl Acad Sci U S A*, 90, 2251-5.
- PEISER, L., MUKHOPADHYAY, S. & GORDON, S. (2002) Scavenger receptors in innate immunity. *Curr Opin Immunol*, 14, 123-8.
- PERLMAN, H., SUZUKI, E., SIMONSON, M., SMITH, R. C. & WALSH, K. (1998) GATA-6 induces p21(Cip1) expression and G1 cell cycle arrest. *J Biol Chem*, 273, 13713-8.
- PETROVIC-DJERGOVIC, D., HYMAN, M. C., RAY, J. J., BOUIS, D., VISOVATTI, S. H., HAYASAKI, T. & PINSKY, D. J. (2012) Tissue-resident ecto-5' nucleotidase (CD73) regulates leukocyte trafficking in the ischemic brain. *J Immunol*, 188, 2387-98.
- POLLARD, J. W. (2009) Trophic macrophages in development and disease. *Nat Rev Immunol*, 9, 259-70.
- PRINZ, M., PRILLER, J., SISODIA, S. S. & RANSOHOFF, R. M. (2011) Heterogeneity of CNS myeloid cells and their roles in neurodegeneration. *Nat Neurosci*, 14, 1227-35.
- RAO, S., LOBOV, I. B., VALLANCE, J. E., TSUJIKAWA, K., SHIOJIMA, I., AKUNURU, S., WALSH, K., BENJAMIN, L. E. & LANG, R. A. (2007) Obligatory participation of macrophages in an angiopoietin 2-mediated cell death switch. *Development*, 134, 4449-58.
- RIZZO, M. A., DAVIDSON, M. W. & PISTON, D. W. (2009) Fluorescent protein tracking and detection: fluorescent protein structure and color variants. *Cold Spring Harb Protoc*, 2009, pdb top63.
- ROGERS, S., WELLS, R. & RECHSTEINER, M. (1986) Amino acid sequences common to rapidly degraded proteins: the PEST hypothesis. *Science*, 234, 364-8.
- ROSAS, M., DAVIES, L. C., GILES, P. J., LIAO, C. T., KHARFAN, B., STONE, T. C., O'DONNELL, V. B., FRASER, D. J., JONES, S. A. & TAYLOR, P. R. (2014) Tissue Macrophage Phenotype is Intrinsically Linked to Proliferative Renewal *In Submission*.
- ROSAS, M., LIDDIARD, K., KIMBERG, M., FARO-TRINDADE, I., MCDONALD, J. U., WILLIAMS, D. L., BROWN, G. D. & TAYLOR, P. R. (2008) The induction of inflammation by dectin-1 in vivo is dependent on myeloid cell programming and the progression of phagocytosis. *J Immunol*, 181, 3549-57.
- ROSAS, M., OSORIO, F., ROBINSON, M. J., DAVIES, L. C., DIERKES, N., JONES, S. A., REIS, E. S. C. & TAYLOR, P. R. (2011) Hoxb8 conditionally immortalised macrophage lines model inflammatory monocytic cells with important similarity to dendritic cells. *Eur J Immunol*, 41, 356-365.
- ROSAS, M., THOMAS, B., STACEY, M., GORDON, S. & TAYLOR, P. R. (2010) The myeloid 7/4-antigen defines recently generated inflammatory macrophages and is synonymous with Ly-6B. *J LeuKoc Biol*, 88, 169-180.
- RYAN, M. D., KING, A. M. & THOMAS, G. P. (1991) Cleavage of foot-and-mouth disease virus polyprotein is mediated by residues located within a 19 amino acid sequence. *J Gen Virol*, 72 ( Pt 11), 2727-32.
- SABIN, F. R., DOAN, C. A., & CUNNINGHAM, R. S. (1925) Discrimination of two types of phagocytic cells in the connective tissues by the supravitral technique. *Contrib. Embryol. (Am)*, 16, 125-162.
- SACKS, S. H. (2010) Complement fragments C3a and C5a: the salt and pepper of the immune response. *Eur J Immunol*, 40, 668-70.
- SANCHEZ, I. & DYNLACHT, B. D. (2005) New insights into cyclins, CDKs, and cell cycle control. *Semin Cell Dev Biol*, 16, 311-21.

- SATOH, T., KIDOYA, H., NAITO, H., YAMAMOTO, M., TAKEMURA, N., NAKAGAWA, K., YOSHIOKA, Y., MORII, E., TAKAKURA, N., TAKEUCHI, O. & AKIRA, S. (2013) Critical role of Trib1 in differentiation of tissue-resident M2-like macrophages. *Nature*, 495, 524-8.
- SATPATHY, A. T., WU, X., ALBRING, J. C. & MURPHY, K. M. (2012) Re(de)fining the dendritic cell lineage. *Nat Immunol*, 13, 1145-54.
- SAWYER, R. T., STRAUSBAUCH, P. H. & VOLKMAN, A. (1982) Resident macrophage proliferation in mice depleted of blood monocytes by strontium-89. *Lab Invest*, 46, 165-70.
- SCHMIDT-SUPPRIAN, M. & RAJEWSKY, K. (2007) Vagaries of conditional gene targeting. *Nat Immunol*, 8, 665-8.
- SCHOLZEN, T. & GERDES, J. (2000) The Ki-67 protein: from the known and the unknown. *J Cell Physiol*, 182, 311-22.
- SCHULZ, C., GOMEZ PERDIGUERO, E., CHORRO, L., SZABO-ROGERS, H., CAGNARD, N., KIERDORF, K., PRINZ, M., WU, B., JACOBSEN, S. E., POLLARD, J. W., FRAMPTON, J., LIU, K. J. & GEISSMANN, F. (2012) A Lineage of Myeloid Cells Independent of Myb and Hematopoietic Stem Cells. *Science*, 336, 86-90.
- SCOTT, E. W., SIMON, M. C., ANASTASI, J. & SINGH, H. (1994) Requirement of transcription factor PU.1 in the development of multiple hematopoietic lineages. *Science*, 265, 1573-7.
- SHIBUYA-FUJIWARA, N., HIRAYAMA, F., OGATA, Y., IKEDA, H. & IKEBUCHI, K. (2001) Phagocytosis in vitro of polyethylene glycol-modified liposome-encapsulated hemoglobin by human peripheral blood monocytes plus macrophages through scavenger receptors. *Life Sci*, 70, 291-300.
- SHIMOMURA, O., JOHNSON, F. H. & SAIGA, Y. (1962) Extraction, purification and properties of aequorin, a bioluminescent protein from the luminous hydromedusan, Aequorea. *J Cell Comp Physiol*, 59, 223-39.
- SIEMERING, K. R., GOLBIK, R., SEVER, R. & HASELOFF, J. (1996) Mutations that suppress the thermosensitivity of green fluorescent protein. *Curr Biol*, 6, 1653-63.
- SODHI, C. P., LI, J. & DUNCAN, S. A. (2006) Generation of mice harbouring a conditional loss-of-function allele of Gata6. *BMC Dev Biol*, 6, 19.
- SOEHNLEIN, O. & LINDBOM, L. (2010) Phagocyte partnership during the onset and resolution of inflammation. *Nat Rev Immunol*, 10, 427-39.
- SPETH, C., RAMBACH, G., LASS-FLORL, C., DIERICH, M. P. & WURZNER, R. (2004) The role of complement in invasive fungal infections. *Mycoses*, 47, 93-103.
- ST JOHN, A. L. & ABRAHAM, S. N. (2013) Innate immunity and its regulation by mast cells. *J Immunol*, 190, 4458-63.
- STEIN, M., KESHAV, S., HARRIS, N. & GORDON, S. (1992) Interleukin 4 potently enhances murine macrophage mannose receptor activity: a marker of alternative immunologic macrophage activation. *J Exp Med*, 176, 287-92.
- STURN, A., QUACKENBUSH, J. & TRAJANOSKI, Z. (2002) Genesis: cluster analysis of microarray data. *Bioinformatics*, 18, 207-8.
- SZYMCZAK, A. L., WORKMAN, C. J., WANG, Y., VIGNALI, K. M., DILIOGLOU, S., VANIN, E. F. & VIGNALI, D. A. (2004) Correction of multi-gene deficiency in vivo using a single 'self-cleaving' 2A peptide-based retroviral vector. *Nat Biotechnol*, 22, 589-94.
- TAKAHASHI, K. (2000) Development and Differentiation of Macrophages and Related Cells: Historical Review and Current Concepts. *Journal of Clinical and Experimental Hematopathology*, 41, 1-31.
- TAKEDA, M., OBAYASHI, K., KOBAYASHI, A. & MAEDA, M. (2004) A unique role of an amino terminal 16-residue region of long-type GATA-6. *J Biochem*, 135, 639-50.
- TARLING, J. D., LIN, H. S. & HSU, S. (1987) Self-renewal of pulmonary alveolar macrophages: evidence from radiation chimera studies. *J LeuKoc Biol*, 42, 443-6.
- TAYLOR, P. R., BROWN, G. D., GELDHOF, A. B., MARTINEZ-POMARES, L. & GORDON, S. (2003) Pattern recognition receptors and differentiation antigens define murine myeloid cell heterogeneity ex vivo. *Eur J Immunol*, 33, 2090-7.



- TAYLOR, P. R., BROWN, G. D., HERRE, J., WILLIAMS, D. L., WILLMENT, J. A. & GORDON, S. (2004) The Role of SIGNR1 and the {beta}-Glucan Receptor (Dectin-1) in the Nonopsonic Recognition of Yeast by Specific Macrophages. *J Immunol*, 172, 1157-1162.
- TAYLOR, P. R., MARTINEZ-POMARES, L., STACEY, M., LIN, H. H., BROWN, G. D. & GORDON, S. (2005a) Macrophage receptors and immune recognition. *Annu Rev Immunol*, 23, 901-44.
- TAYLOR, P. R., REID, D. M., HEINSBROEK, S. E., BROWN, G. D., GORDON, S. & WONG, S. Y. (2005b) Dectin-2 is predominantly myeloid restricted and exhibits unique activation-dependent expression on maturing inflammatory monocytes elicited in vivo. *Eur J Immunol*, 35, 2163-74.
- TAYLOR, P. R., TSONI, S. V., WILLMENT, J. A., DENNEHY, K. M., ROSAS, M., FINDON, H., HAYNES, K., STEELE, C., BOTTO, M., GORDON, S. & BROWN, G. D. (2007) Dectin-1 is required for [beta]-glucan recognition and control of fungal infection. *Nat Immunol*, 8, 31-38.
- TSONI, S. V., KERRIGAN, A. M., MARAKALALA, M. J., SRINIVASAN, N., DUFFIELD, M., TAYLOR, P. R., BOTTO, M., STEELE, C. & BROWN, G. D. (2009) Complement C3 plays an essential role in the control of opportunistic fungal infections. *Infect Immun*, 77, 3679-85.
- UDERHARDT, S., HERRMANN, M., OSKOLKOVA, O. V., ASCHERMANN, S., BICKER, W., IPSEIZ, N., SARTER, K., FREY, B., ROTHE, T., VOLL, R., NIMMERJAHN, F., BOCHKOV, V. N., SCHETT, G. & KRONKE, G. (2012) 12/15-lipoxygenase orchestrates the clearance of apoptotic cells and maintains immunologic tolerance. *Immunity*, 36, 834-46.
- UNTERGASSER, A., CUTCUTACHE, I., KORESSAAR, T., YE, J., FAIRCLOTH, B. C., REMM, M. & ROZEN, S. G. (2012) Primer3--new capabilities and interfaces. *Nucleic Acids Res*, 40, e115.
- VAN DEN BERG, T. K. & KRAAL, G. (2005) A function for the macrophage F4/80 molecule in tolerance induction. *Trends Immunol*, 26, 506-9.
- VAN FURTH, R. & COHN, Z. A. (1968) The origin and kinetics of mononuclear phagocytes. *J Exp Med*, 128, 415-35.
- VAN FURTH, R., COHN, Z. A., HIRSCH, J. G., HUMPHREY, J. H., SPECTOR, W. G. & LANGEVOORT, H. L. (1972) The mononuclear phagocyte system: a new classification of macrophages, monocytes, and their precursor cells. *Bull World Health Organ*, 46, 845-52.
- VAN WESENBEECK, L., ODGREN, P. R., MACKAY, C. A., D'ANGELO, M., SAFADI, F. F., POPOFF, S. N., VAN HUL, W. & MARKS, S. C., JR. (2002) The osteopetrotic mutation toothless (tl) is a loss-of-function frameshift mutation in the rat Csf1 gene: Evidence of a crucial role for CSF-1 in osteoclastogenesis and endochondral ossification. *Proc Natl Acad Sci U S A*, 99, 14303-8.
- VOEHRINGER, D., SHINKAI, K. & LOCKSLEY, R. M. (2004) Type 2 immunity reflects orchestrated recruitment of cells committed to IL-4 production. *Immunity*, 20, 267-77.
- WANG, J. X., BAIR, A. M., KING, S. L., SHNAYDER, R., HUANG, Y. F., SHIEH, C. C., SOBERMAN, R. J., FUHLBRIGGE, R. C. & NIGROVIC, P. A. (2012a) Ly6G ligation blocks recruitment of neutrophils via a beta2-integrin-dependent mechanism. *Blood*, 120, 1489-98.
- WANG, Y., SZRETTER, K. J., VERMI, W., GILFILLAN, S., ROSSINI, C., CELLA, M., BARROW, A. D., DIAMOND, M. S. & COLONNA, M. (2012b) IL-34 is a tissue-restricted ligand of CSF1R required for the development of Langerhans cells and microglia. *Nat Immunol*, 13, 753-60.
- WEI, S., LIGHTWOOD, D., LADYMAN, H., CROSS, S., NEALE, H., GRIFFITHS, M., ADAMS, R., MARSHALL, D., LAWSON, A., MCKNIGHT, A. J. & STANLEY, E. R. (2005) Modulation of CSF-1-regulated post-natal development with anti-CSF-1 antibody. *Immunobiology*, 210, 109-19.
- WEISS, S. J. (1989) Tissue destruction by neutrophils. *N Engl J Med*, 320, 365-76.
- WIKTOR-JEDRZEJCZAK, W., BARTOCCI, A., FERRANTE, A. W., JR., AHMED-ANSARI, A., SELL, K. W., POLLARD, J. W. & STANLEY, E. R. (1990) Total absence of colony-stimulating factor 1 in the macrophage-deficient osteopetrotic (op/op) mouse. *Proc Natl Acad Sci U S A*, 87, 4828-32.

- WIKTOR-JEDRZEJCZAK, W., URBANOWSKA, E., AUKERMAN, S. L., POLLARD, J. W., STANLEY, E. R., RALPH, P., ANSARI, A. A., SELL, K. W. & SZPERL, M. (1991) Correction by CSF-1 of defects in the osteopetrotic op/op mouse suggests local, developmental, and humoral requirements for this growth factor. *Exp Hematol*, 19, 1049-54.
- WONG, K., VALDEZ, P. A., TAN, C., YEH, S., HONGO, J. A. & OUYANG, W. (2010) Phosphatidylserine receptor Tim-4 is essential for the maintenance of the homeostatic state of resident peritoneal macrophages. *Proc Natl Acad Sci U S A*, 107, 8712-7.
- YAGITA, H., OKUMURA, K. & NAKAUCHI, H. (1988) Molecular cloning of the murine homologue of CD2. Homology of the molecule to its human counterpart T11. *J Immunol*, 140, 1321-6.
- YONA, S., KIM, K. W., WOLF, Y., MILDNER, A., VAROL, D., BREKER, M., STRAUSS-AYALI, D., VIUKOV, S., GUILLIAMS, M., MISHARIN, A., HUME, D. A., PERLMAN, H., MALISSEN, B., ZELZER, E. & JUNG, S. (2012) Fate Mapping Reveals Origins and Dynamics of Monocytes and Tissue Macrophages under Homeostasis. *Immunity*, 38, 79-91.
- YOSHIDA, H., HAYASHI, S., KUNISADA, T., OGAWA, M., NISHIKAWA, S., OKAMURA, H., SUDO, T. & SHULTZ, L. D. (1990) The murine mutation osteopetrosis is in the coding region of the macrophage colony stimulating factor gene. *Nature*, 345, 442-4.
- ZHANG, D. E., HETHERINGTON, C. J., CHEN, H. M. & TENEN, D. G. (1994) The macrophage transcription factor PU.1 directs tissue-specific expression of the macrophage colony-stimulating factor receptor. *Mol Cell Biol*, 14, 373-81.
- ZHOU, X., CUI, Y., HUANG, X., YU, Z., THOMAS, A. M., YE, Z., PARDOLL, D. M., JAFFEE, E. M. & CHENG, L. (2003) Lentivirus-mediated gene transfer and expression in established human tumor antigen-specific cytotoxic T cells and primary unstimulated T cells. *Hum Gene Ther*, 14, 1089-105.
- ZUFFEREY, R., DONELLO, J. E., TRONO, D. & HOPE, T. J. (1999) Woodchuck hepatitis virus posttranscriptional regulatory element enhances expression of transgenes delivered by retroviral vectors. *J Virol*, 73, 2886-92.
- ZUFFEREY, R., NAGY, D., MANDEL, R. J., NALDINI, L. & TRONO, D. (1997) Multiply attenuated lentiviral vector achieves efficient gene delivery in vivo. *Nat Biotechnol*, 15, 871-5.